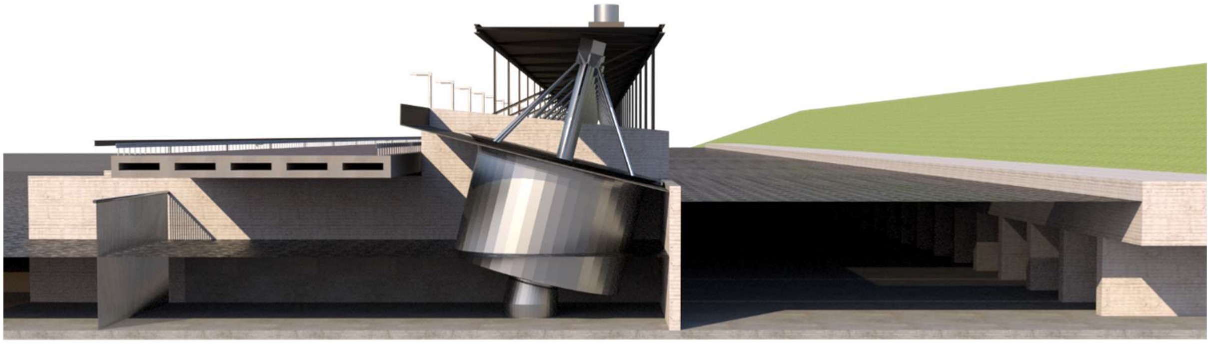

Case Study: **Deltapump**

On the civil design and cost estimate of a high-capacity enclosed-screw pumping station concept and its application to protect the Rhine-Meuse delta from flooding before the year 2100

by Tom Scheeper

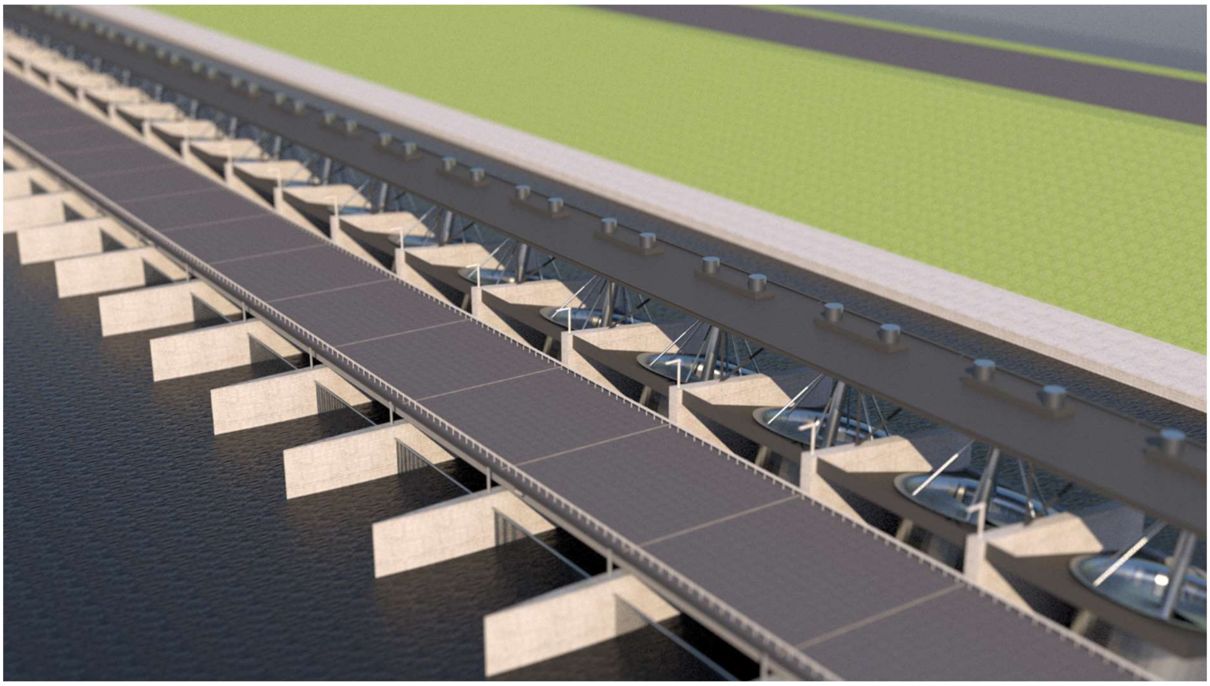

Case Study: Deltapump

On the civil design and cost estimate of a high-capacity enclosed-screw pumping station concept and its application to protect the Rhine-Meuse delta from flooding before the year 2100

by **Tom Scheeper**

22 June 2020

Als onderdeel ter verkrijging van de graad van

Bachelor of Science

in de Civiele Techniek

Technische Universiteit Delft

Faculteit Civiele Techniek en Aardwetenschappen

Afdeling Waterbouwkunde

Studentennummer: 4553055

Supervisors: dr.ir. J.D. Bricker

ir. W.F. Molenaar

> ” Men mag niet uit het oog verliezen, dat de mogelijkheid van overstroming nooit met volkomen zekerheid uitgesloten kan worden.
>
> *- Deltacommissie, 1960*

Preface

This bachelor's thesis is written in partial fulfilment to obtain the degree of Bachelor of Science in civil engineering at the Technische Universiteit Delft. In this thesis, the fluvial flood risks of the Rhine-Meuse delta are investigated and consequently the civil structure is designed of a high-capacity pumping station with an innovative pump concept called the „Deltapump". Its total capital and operational costs are compared with those of conventional designs to determine whether such a design is feasible.

Due to the jargon, this thesis is intended for those with a background in, or students of civil engineering. For those without a background in civil engineering, common terminology and symbols within this thesis are elucidated within the nomenclature section. NB the appendices are often referred to in the text, denoted as „App.".

Information about the Deltapump concept and large pumping stations is found in App. I and II. An extensive flood risk analysis simulation to quantify the necessity of a large pumping station, is found in App. III. Furthermore, the design of the pumping station can be found in chapter 5. I also want to inform non-Dutch speaking readers that almost all sources are in Dutch.

I would like to express my gratitude to dr.ir. J. D. Bricker and ir. W. F. Molenaar for their guidance and feedback during the last ten weeks, especially considering these special circumstances we have faced. I would also like to thank ir. J. Schut and his son G. Schut for inventing the Deltapump concept and providing me with information about it.

's-Gravenhage, 22 June 2020

Tom Scheeper

Abstract

According to the European Environment Agency (2016, pp. 137–140) annual mean river flow and the frequency of fluvial floods will have increased by 20% before the year 2100, in North-western Europe. It had been postulated in media in reports (De Ingenieur, 2014; „MIRT-verkenning Grevelingen", 2012; Slootjes et al., 2010; Slootjes, 2013; Lammers, 2014) that because of this, large pumping stations are required in the Rhine-Meuse delta in the Netherlands.

To investigate this postulation, a simulation model in Python was created that describes the Rhine-Meuse delta as four separate water basins with flow exchanges and boundary conditions (astronomical tides and river inflow). From this simulation model it was concluded that every 86–137 years, flood flow rates of the rivers are such, that the design maximum water level is compromised. The acceptable flooding risk is only once every 2.000 years, so this situation is unacceptable.

Dutch engineer answered to the postulation and invented a high-capacity pump called the „Deltapump", with a capacity ranging 170–200 m^3s^{-1}. Moreover, a conceptual design for a pumping station was created. After a conceptual design creation, verification calculations and a cost-to-merit evaluation, a pumping station with 28 Deltapumps in total, based on the conceptual design of Schut, was created. This pumping station is integrated within the Haringvlietdam and is covers an area of 420 × 190 m^2. Its capacity, dependent on water levels in the Haringvliet, ranges 4.900 to 5.250 m^3s^{-1}, making it by an extremely large margin, the biggest pumping station in the world. Its costs, expressed as Net Present Value, are estimated at € 915 million by the year 2100, 70% of which covers the mechanical components of the pumping station and 30% the civil components.

After the flood risk analysis and the pumping station design, it was posed that, whilst the pumping station itself has advantages—better capacity per unit width and less costs per unit capacity, it is not a cost-effective method to prevent flooding in the Rhine-Meuse delta. Calculations and the simulation show it only requires operation once every 92 years. It would therefore seem more cost-effective, and a permanent solution, to upgrade all dykes and dams along the Rhine-Meuse delta, so that more water can be stored. This should be investigated in future reports.

Contents

Nomenclature

Roman symbols

Symbol	Explanation	Appears in	Unit
A	Cross-sectional area or surface area	4, III, VIII	m^2
b	Cross-sectional width	VIII	m
b_t	Gaussian temporal mean	III	s
B	Storage width of a waterway	III	m
B_C	Conveyance width of a waterway	III	m
B_{WEIR}	Width of a weir	VIII	m
c_f	Friction slope	III	m/m
c_s	Gaussian spatial standard deviation	III	m
c_t	Gaussian temporal standard deviation	III	s
C_{FW}	Flood wave propagation velocity	III	ms^{-1}
C'_P	Primary consolidation coefficient	VIII	-
C_W	Wind set-up coefficient	VI	-
d	Depth of a waterway	III	m
e	Prestressing steel eccentricity	VIII	m
E	Young's Modulus	VIII	Nm^{-2}
f	Darcy-Weisbach friction coefficient	III	-
f_{CD}	Concrete design compressive strength	VIII	Nm^{-2}
F	Point load or force	VIII	N
g	Gravitational acceleration (9,81 ms^{-2})	I	ms^{-2}
G	Self-weight	VIII	Nm^{-1}
h	Hydraulic head or cross-sectional height	4, III, VIII	m
H	Energy head	VIII	m
i	Radius of gyration	VIII	m
i_B	Bed slope (- $-\partial z_B / \partial s$)	III	m/m
I_{YY} and I_{ZZ}	Second area moment	II	m^4
K_P	Passive earth pressure coefficient	VIII	-
ℓ_{buc}	Buckling length	VIII	m
L	Length	III	m
m'	Sharp-crested weir discharge coefficient	VIII	-
M	Bending moment	VIII	Nm
N	Normal force	VIII	N
$Ø$	Diameter	1, I, VIII	m

p	Exceedance probability	III	s^{-1}
P_{DP}	Deltapump power consumption	I	W
P_0	Prestressing steel initial compressive force	VIII	N
P_∞	Prestressing steel final compressive force	VIII	N
q	Distributed load	VIII	Nm^{-1}
q_C	Cone resistance	VIII	Nm^{-2}
Q	Flow rate or discharge	4, III	m^3s^{-1}
$\hat{Q}$	Maximum flood flow rate	III	m^3s^{-1}
$\tilde{Q}$	Decreased maximum flood flow rate	III	m^3s^{-1}
r	Radius	I	m
R	Resistance force or load	VIII	N
s	Pile shape coefficient	VIII	-
t_0	Theoretical pile length	VIII	m
t	Time	4, I, III	s
t_P	Practical pile length	VIII	m
t_{SS}	Storm surge duration	III	s
T	Return period of wave period	III	s
u	Flow velocity or wind velocity	I	ms^{-1}
w	Vertical deflection	VIII	m
W_{YY} and W_{ZZ}	Section modulus	VIII	m^3
x_u	Concrete compression zone height	VIII	m
z_B	Bed level	III	m

Greek symbols

Symbol	Explanation	Appears in	Unit
α	Buckling parameter or concrete shape factor	VIII	-
α_P	Pile type coefficient	VIII	-
β	Pile tip coefficient	VIII	-
γ'	Effective density	VIII	kgm^{-3}
Γ	dimensionless tidal basin parameter	III	-
δ	Pile wall friction	VIII	rad
ε	Strain	VIII	-
η_{DP}	Deltapump power consumption efficiency	I	-
λ	Slenderness	VIII	-
λ_e	Limit slenderness	VIII	-
$\bar{\lambda}$	Slenderness ratio	VIII	-

μ	Discharge contraction coefficient	I	
ρ_W	Density of water	I	kgm^{-3}
σ	Normal (bending) stress	VIII	Nm^{-2}
σ'	Effective vertical ground pressure	VIII	Nm^{-2}
σ_c	Concrete stress	VIII	Nm^{-2}
σ_P	Prestressing steel stress	VIII	Nm^{-2}
τ	Tidal basin relaxation time	III	s
φ	Internal friction	VIII	rad
χ	Buckling factor	VIII	-
ω	Rotational velocity	I	s^{-1}
ω_0	Natural frequency	III	s^{-1}

Acronyms

NAP	Normaal Amsterdams Peil.	The Dutch reference datum for heights and water levels.
rpm	Rounds Per Minute.	Common unit to describe velocities of rotating bodies.
capex	CAPital EXpenditures.	The total costs for initiating a project
opex	OPerational EXpenditures.	Yearly costs for maintaining and operating a project.
MSL	Mean Sea Level	

Terminology

Catchment area	All precipitation (rain, hail, snow) that falls within this area ends up in the same river
Conveyance width	The width of the river cross-section through which water flows.
Fluvial	Occurring on, in or caused by rivers
Gauging station	Stations along Dutch rivers, canals and lakes that measure, among other things, flow rates and water levels approximately every 10 minutes.
Storage width	The total width of the river cross-section: conveyance width and the width of the river in which water is still.

Chapter 1 // Introduction

It is widely known that climate change leads to a rise of the mean sea level. As a consequence, areas located below mean sea level are in danger of flooding from seas. Contrary to popular belief, dangers of flooding not always arise from sea, but more often from within the hinterland. According to the European Environment Agency (EEA, 2016, pp. 137–140), annual mean river flow as well as the frequency and severity of fluvial floods are projected to increase in North-western Europe before the year 2100. In the Rhine-Meuse delta in the Netherlands, these developments could prove disastrous: during a storm surge flood defences close and as a result river water can't discharge into the North Sea, thus making the delta „een badkuip die volloopt, terwijl de afvoer dicht zit" [a bathtub that fills, while the drain is closed] (De Ingenieur, 2014). The delta is inhabited by 1,8 million people, thus making it a potential severe problem (Centraal Bureau for Statistiek, 2020). It has therefore been postulated in media and reports (De Ingenieur, 2014; „MIRT-verkenning Grevelingen", 2012; Slootjes et al., 2010; Slootjes, 2013; Lammers, 2014;) that in the near future large pumping stations need to be constructed.

§1.1 The Deltapump concept: a solution to the flooding problem?

Dutch mechanical engineer J. Schut answered to this call and created his concept called the „Deltapump". Concerning the design of the Deltapump, Schut stated that his concept started with the question „how do you move a large body of water?" His answer is by creating a large (Ø 10 m) and rapidly rotating cylinder—60 rpm—with two helical blades inside, see Figure 1.1.

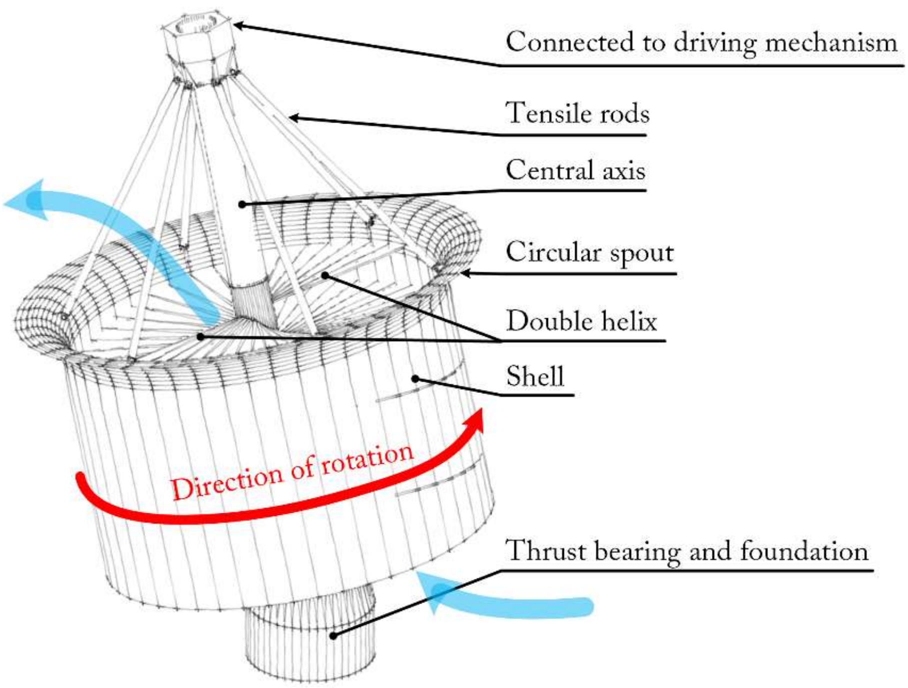

Figure 1.1
Digital sketch of the Deltapump concept. Direction of flow shown in blue.

A report on its estimated pumping curve can be found in App. I. For a head of difference of 4 m the pump capacity is approximately 200 m^3s^{-1}, it decreases for higher head differences. The maximum head is 108,1 m and the maximum pump capacity is 247 m^3s^{-1}.

The Deltapump can be described as an enclosed-screw rotary positive displacement pump (Garbus, 2008, p. 11.3, 11.38). In comparison with the Deltapump, conventional designs are usually rather long (~30 m vs. 7 m), have small diameters (~1 m vs. 10 m) and are orientated more horizontally (30–45° vs. 75°). Moreover, their masses are significantly smaller than that of the Deltapump, where the thrust bearing is subjected to forces in order of meganewtons. For these reasons, the Deltapump is special.

§1.2 Deltapump pumping station concept at Haringvlietdam

Schut created the Deltapump for the postulated flooding problem in the Rhine-Meuse delta. A pump, of course, requires a pumping station structure around it to properly operate. He therefore created a conceptual design for a pumping station with five Deltapumps—a total capacity of 1.000 m^3s^{-1} according to his calculations—to be constructed at the Haringvlietdam. A longitudinal cross section is shown in Figure 1.2.

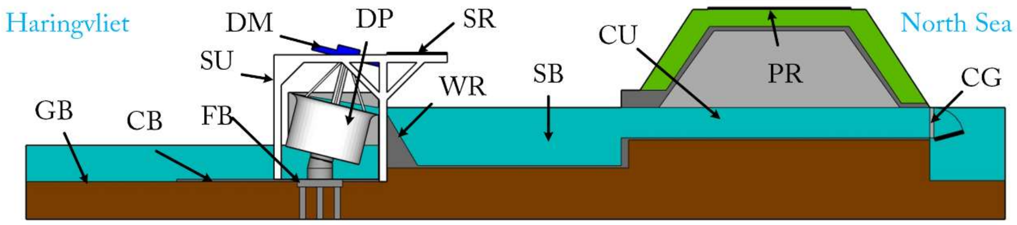

GB:	Gravel bed	DM:	Driving mechanism	SB:	Stilling basin
CB:	Concrete bed	DP:	Deltapump	CU:	Culvert
FB:	Foundation & bearing	SR:	Service road	PR:	Provincial road
SU:	Supporting structure	WR:	Weir	CG:	Closable gate

Figure 1.2 Longitudinal cross-section of the Deltapump pumping station concept at Haringvlietdam according to the design by Schut.

When it is in operation, water from the Haringvliet flows towards the North Sea. It encounters bed protection and enters the Deltapump in which it gains hydraulic head. Flow is then directed over a weir and ends up in a small stilling basin where the flow is stabilised. Through a culvert, flow reaches the North Sea. The service road serves as a temporary bypass during construction, so that traffic can continue on the Haringvlietdam. For this project, Schut estimated a total cost of about € 250 million.

The civil structure of this pumping station concept has not yet been verified and its costs are merely a rough estimate. Moreover, a proper flood risk analysis of the Rhine-Meuse delta has not been performed to determine whether a pumping station is even required at all.

§1.3 Research problem and scope

The scope of this thesis is to investigate the postulated flooding problem in the Rhine-Meuse delta and design a pumping station with the Deltapump, if it is required. The overarching research question is:

> In comparison with large conventional pumping stations, is the Deltapump cost-effective concept to prevent flooding in the Rhine-Meuse delta before 2100?

From this overarching research question, three sub-questions are derived:

> 1. What are large pumping stations? What do conventional designs of these entail and how much do they cost?
> 2. Is a large pumping station required in the Rhine-Meuse delta before the year 2100?
> 3. How to design a pumping station for the Deltapump concept, how much does it cost?

§1.4 Structure of the thesis

In order to get an understanding of what large pumping stations (and their pumps) entail and how much they cost (sub-question 1), first a short inquiry is done of them in the following chapter. Next, the civil engineering design cycle (Molenaar & Voorendt [lecture notes], 2020) will be iterated through for the design of the pumping station, see the box at bottom of the page.

In the problem analysis the location of this case study is analysed: The Rhine-Meuse delta in the Netherlands. Moreover, the second sub-question is addressed by performing a flood risk analysis in the fourth chapter. The definite design is presented in the main body, with the basis of design, the concepts, verification calculations and the evaluation in the appendices.

After the design cycle, chapter 6 presents the life-time costs and chapter 7 shows the sequence of construction. Based on these costs and those derived from the reference projects in chapter 2, the conclusions and recommendations are given in chapter 8.

	Design phase	Main body	Appendices
i	Problem analysis	Chapter 3 (Location analysis) Chapter 4 (Flood risk analysis)	III, IV, V
ii	*Basis of design*		*VI*
iii	*Design concepts*		*VII*
iv	*Design verification*		*VIII*
v	*Design evaluation*		*IX*
vi	Design integration	Chapter 5 (Pumping station design)	X

Chapter 2 // High-capacity pumps & large pumping stations

This chapter provides insight into conventional high-capacity pumps and large pumping stations. First, general workings of pumping and dewatering, and high-capacity pumps are presented. Then, the general characteristics of the reference projects (large pumping stations) are shown.

Pumping and dewatering

In general, two scenarios can be described for water exchange between two waterbodies with uneven water levels, shown in Figure 2.1. The first scenario is moving water from a higher location to a lower location. This process is called dewatering [in Dutch: „spuien"] and is naturally instigated by gravity. In order to control water levels, dewatering sluices contain gates which can be closed; the discharge through such a sluice is then proportional to the size of the opening. When the opposite is required, a pump is necessary to overcome the difference in water level.

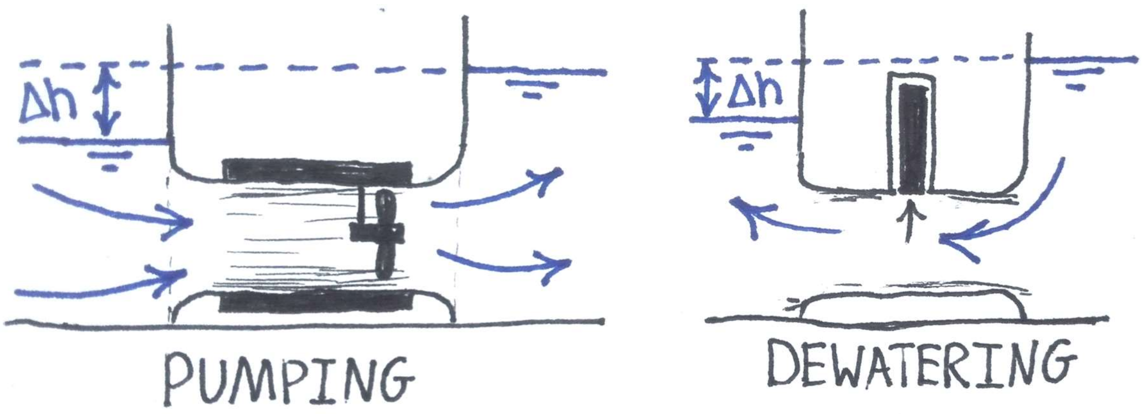

Figure 2.1 Difference between pumping and dewatering. The pump shown is a horizontally axial mounted pump

High-capacity pumps

Garbus (2008, p. 11.2) distinguishes two categories of pumps: positive displacement pumps and kinetic pumps. The former are pumps in which water is moved by means of a physical object. Common examples of these are the Archimedes screw or a medieval water wheel. The second category involves velocity or pressure changes to accelerate the water, caused by rotating impellers (Garbus, 2008, p. 11.1).

For low head-differences and high capacities—or in general, storm water applications, so-called „horizontally mounted, axial-flow pumps" are the most commonly used pump type (Garbus, 2008, p. 11.33). This pump type is shown in the sketch of Figure 2.1. Conventional designs have capacities up to 30 m^3s^{-1} and are customly engineered for higher capacities.

Pump performances

In order to quantify the performance of each pump type under varying circumstances, so-called „pump characteristics curves" are created. As a function of discharge, they show the total generated head, power consumption and efficiency (Cooper & Tchobanoglous, 2008, p. 10.8). Based on the required discharge and head of the project, the most fitting pump can be chosen. Figure i.8 in App. I shows such a performance curve, in this case for the Deltapump.

Large pumping stations

Three reference projects are analysed: the largest pumping station in the world (West Closure Complex (WCC), New Orleans), the largest pumping station in Europe (Rijksgemaal IJmuiden, the Netherlands) and project that, due to its integration within the flood defences, is similar to that of Schut's design: the currently under construction, Afsluitdijk pumping station. A full report with information about the projects, the pumps, images and all sources is found in App. II. A summary with the most important characteristics of the projects is presented in the table below.

Table 2.2 Summary of the features of the two large pumping stations. Values left out are unknown. From AAEES (2012), De Afsluitdijk (n.d.), European Commission (2019, p. 12), fxtop (2020), GWW (n.d.), Manyard (2013, p. 10), Mol (2019), NGS (n.d.), Schmit (1999), U.S. Army Corps of Engineers (2013, p. 1) & Zimmermann (2015).

	WCC	IJmuiden	Afsluitdijk
Station dimensions	140 m	50 m	~30 m
Total capacity	540 m^3s^{-1}	260 m^3s^{-1}	235 m^3s^{-1}
Number of pumps	11	6	6
Pump configuration	11×49 m^3s^{-1}	4×40 m^3s^{-1}, 2×50 m^3s^{-1}	6×39 m^3s^{-1}
Pump type	overhung impeller	horizontal axial flow	overhung impeller
Head	8	1,2	
Power consumption	41,2 MW	7,1 MW	11,7 MW
Capex	€ 270 million	€ 70 million	
Opex	~ € 0	€ 700 thousand	
Costs per m^3s^{-1}	€ 500 thousand	€ 270 thousand	
Capacity density	3,9 m^2s^{-1}	5,2 m^2s^{-1}	7,8 m^2s^{-1}

Chapter 3 // The Rhine-Meuse delta & the Delta Works

This chapter provides a background into the location that is considered within this case-study: The Rhine-Meuse delta, the river delta in the west of the Netherlands, see the figure below. The following components of this system are described: The rivers the Rhine and the Meuse and its flood protection (Delta Works).

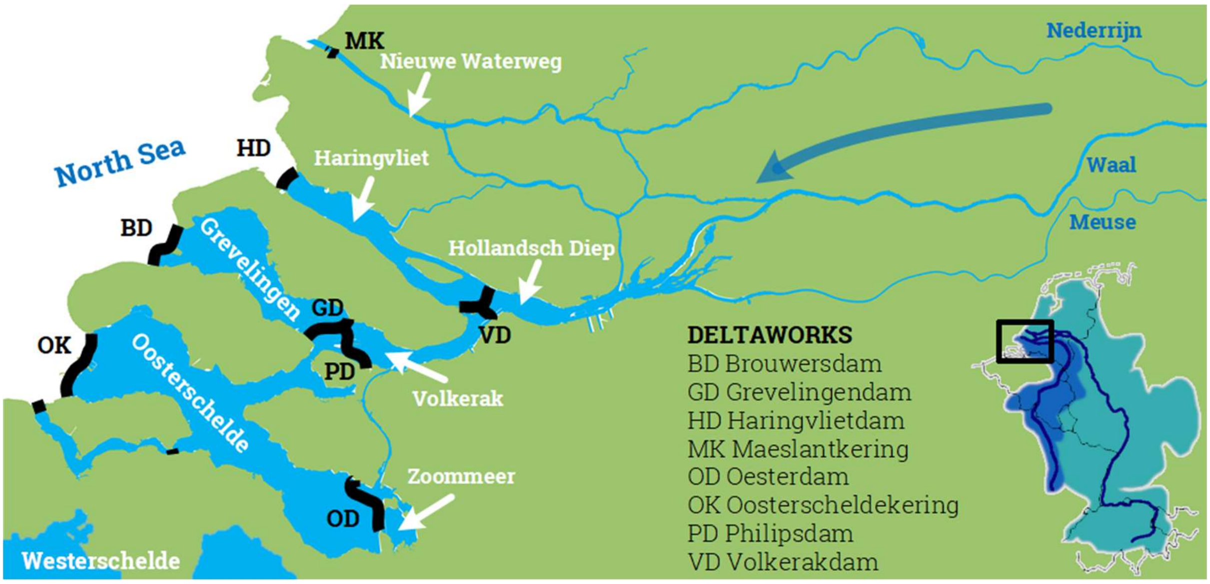

Figure 3.1 The Rhine-Delta: rivers, estuaries, Delta Works and the catchment areas of the Rhine and Meuse. Map created with open-soure data from Openstreetmap (2020), the catchment areas adapted from LeBret (2018), Schulte et al. (2018) and Demarée et al. (2006).

§3.1 The rivers Rhine and Meuse

Present situation

The Rhine and the Meuse are the two major rivers that flow through the Netherlands. The former is the largest of the two in terms of flow rate and catchment area and originates out of the Swiss Alps. It flows from Switzerland through Western Germany and crosses the Dutch border at Lobith. Its catchment area spans five countries and is found in Figure 3.1. Downstream of Lobith, the Rhine and the Meuse form an extensive delta spanning the entire width of the Netherlands (Jülich & Lindner, 2005, p. 5-17). In this delta, the Rhine splits into the Nederrijn and the Waal. During the winter, the flow is about 2.350 m^3s^{-1} and mainly comprises of rainwater. During summer, the flow is about 1.800 m^3s^{-1} comprises of snowmelt (Jülich & Lindner, p. 7, p. 31). The annual mean flow is 2.200 m^3s^{-1} (Ministerie van Verkeer en Waterstaat (V&W), p. 36).

The Meuse springs from North Eastern France and flows through the Ardennes before entering the Netherlands at Borgharen. The average winter flow is approximately 500 m^3s^{-1} (V&W, 2007, p. 38).

The majority of the Rhine flow is distributed over two estuaries: the Nieuwe Waterweg and the Haringvliet. At the Hollandsch Diep, a wide river upstream of the Haringvliet, the Meuse enters the Delta. Water from both of these estuaries flows out into the North Sea (Jülich & Lindner, p. 23).

Prospects

According to the European Environment Agency (EEA, 2016), annual river flow in northern Europe is projected to increase this century due to seasonal shifts (p. 138). Moreover, fluvial floods—phenomena where extreme local precipitation causes a temporary rise in flow rate—are projected to become more extreme in certain parts of Europe (p. 140). Both of these events lead to an increase in flow rate and water height. The former ministry of Water Management (V&W, 2007, p. 32) reports that before 2100, the design maximum flood flow rate is 18.000 m^3s^{-1} for the Rhine at Lobith and 4.600 m^3s^{-1} for the Meuse at Borgharen.

§3.2 Flood protection and the Delta Works

A total of 1,8 million people resides within the municipalities surrounding the Rhine-Meuse delta, about 10% of the Dutch population (Centraal Bureau voor Statistiek, 2020). Moreover, the Rotterdam Harbour, the largest harbour in Europe, is located at the Nieuwe Waterweg. It is therefore imperative this area is protected against storm surges and/or fluvial floods. Yet, this has not always been the case.

Watersnoodramp 1953 and the Delta Works

In 1953 a large storm surge coinciding with spring tide hit the Rhine-Meuse delta. As a result, 1.800 people died and 72.000 were displaced (Rijkswaterstaat, n.d.-b). As a direct consequence of this, the Delta Works were commissioned. Work finished 46 years later in 1997 with the completion of the Maeslantkering, with 237 meter the biggest moving structure in the world (SteenhuisMeurs, 2015, p. 78). According to the Rijkswaterstaat (n.d.-c) the Delta Works includes „5 storm surge barriers, 2 sluices and 6 dams”. The locations of the Delta Works are shown in **Figure 3.1**. NB only the Delta Works that are most important in general, and relevant to this study are shown. From the figure it can be seen that the Delta Works, from Oosterscheldekering to the Maeslantkering, span the entire coast of the delta.

Dyke rings and acceptable flood risks

In order to quantify flood risks, so-called „dijkringgebieden” [dyke rings] have been created for areas that require flood protection—approximately 60% of the Dutch surface area is covered by dyke rings (V&W, 2006, p. 12). To each of these dyke rings an exceedance frequency (EF) is assigned in terms of reciprocal years. This EF implies the acceptable flooding risk, the theoretical frequency the area is allowed to flood. Most of these range 1.000–10.000 years so that the risk of flooding during a single human life is about 1–10%. In coherence with this EF, the highest design water level for the waterbody is prescribed: lower EF means relatively higher water level. The flood protection structures are then calculated based on the values corresponding to the local dyke ring.

Operation during storm surges

The Maeslantkering is always opened and rarely closes to keep the Rotterdam Harbour in operation. It only closes once water levels at Rotterdam have reached +3,00 m NAP (Bol, 2005, p. 314). The operation of the Haringvliet sluices, shown in the figure below, is different. Leeuwen et al. (2004, p.9) report that it fully closes during storm surges, partly closes under high tide and is fully opened under low tide, to discharge river water into the North Sea. The latter is not true when the flow rate at Lobith has dropped below 1.200 m^3s^{-1}, to prevent brackish water entering the Haringvliet.

Figure 3.2 The Haringvliet sluices. From Rijkswaterstaat (2011a)

Operation during fluvial floods

During fluvial floods on the Rhine and Meuse, the Haringvlietdam is fully opened. However, when a storm surge coincides with a fluvial flood, the storm surge barriers close which prevents water discharge. Current procedures (Rijkswaterstaat, 2011b, p. 7) are to store water in the Volkerak-Zoommeer to prevent the delta from filling „like a bathtub". This water storage is possible by opening dewatering sluices in the Volkerakdam so that water can enter from the Hollandsch Diep. It is however not known whether this water storage will be sufficient before the year 2100, when fluvial floods will have increased to 18.000 and 4.600 m^3s^{-1} in the Rhine and Meuse, and mean sea level will have risen.

The next chapter investigates the probabilities of this.

Chapter 4 // Flood risk analysis of the Rhine-Meuse delta

In order to quantify the necessity of a pumping station, a storage basin model with probability-based Rhine and Meuse flow is created. With this storage basin model, it is also possible to determine what pumping station capacity is required for the delta to not flood. The full report on the storage basin model and flood risk analysis, is found in App. III. A summary is presented here.

§4.1 The storage basin model

In the figure below, the storage basin is presented in the Rhine-Meuse delta. In this model, water is stored in Zoommeer and the Volkerak, and optionally in the Grevelingen. This is in accordance with current procedures and future expansions (Slootjes et al., 2010, pp. 6–8; Projectorganisatie Ruimte voor de Rivier 2006, p. 53; Lammers, 2014, p. 64). The Haringvliet and Hollandsch Diep estuaries form part of the calculation model, but not of the storage model; the estuaries can't be fully closed off with sluices, in contrary to the three lakes.

Figure 4.1 Overview of the storage basin model. Created with open-source data from Openstreetmap (2020).

In earlier reports (Slootjes, 2010, pp. 47–48; Slootjes, 2013, pp. D-1–D-5), three upgrades have been presented for sluices in the Volkerakdam, to increase its effective area from 570 m^2 to 1.200, 1.350 or 2.000 m^2. Moreover, for the construction of currently non-existent Grevelingendam sluices, two concepts are presented: 540 and 1.350 m^2. In total twelve storage basin configurations are possible, if the option to not construct Grevelingen sluices is included (this means no water storage in Grevelingen).

§4.2 Flow exchange within the storage basin model

A system of four coupled equations describes exchange of water between the four basins from Figure 4.1 and the boundary conditions. These basins are: Grevelingen, Volkerak, Zoommeer and Haringvliet-Hollandsch Diep. These equations correspond to the „small-basin approximation", an approximation meaning that water levels can be assumed equal at all times in spatial, but not temporal, dimensions (Battjes & Labeur, 2017, p. 93). The equation corresponding to this approximation is:

$$\Delta Q_{SB,IN} = A_{SB}\frac{dh_{SB}}{dt} \qquad \textit{Equation (4.1)}$$

To put this equation into words: the net inflow into a storage basin $\Delta Q_{SB,IN}$ is equal to its change in water level multiplied with its surface area. The net inflow into a basin depends on a number of boundary conditions: operation of dewatering sluices, astronomical tides and river inflow. The discharge through dewatering sluices with an effective area A_{SL} can be calculated with Torricelli's law:

$$Q(t) = \pm A_{SL}\sqrt{2g\left|h_1(t)-h_2(t)\right|} \qquad \textit{Equation (4.2)}$$

The equation is either positive or negative, depending on the water level difference and the positive flow direction. The figure below shows a schematic model of the flow exchange between the basins. The boundary conditions are shown dashed.

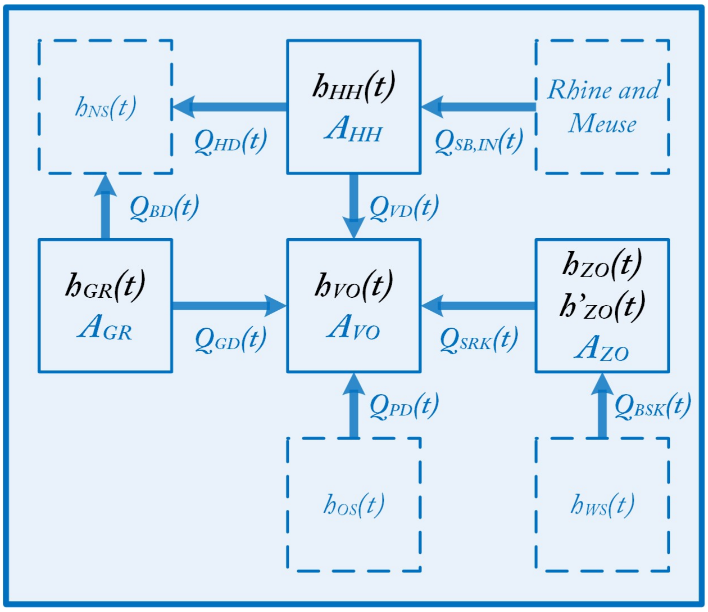

Figure 4.2 Schematic model of the storage basin with flow exchanges and boundary conditions (dashed).

The subscripts $_{BD}$, $_{GD}$, $_{HD}$, $_{PD}$ and $_{VD}$ correspond to the sluices in the Brouwersdam, Grevelingendam, Haringvlietdam, Philipsdam and Volkerakdam. The subscripts $_{NS}$, $_{HH}$, $_{GR}$, $_{VO}$, $_{ZO}$, $_{OS}$ and $_{WS}$ correspond to the North Sea, Haringvliet-Hollandsch Diep, Grevelingen, Volkerak, Zoommeer, Oosterschelde and the Westerschelde. The subscripts $_{SRK}$, $_{BSK}$ and $_{SB,IN}$ correspond to flow in the Schelde-Rijnkanaal and

Bathse spuikanaal, and the river inflow. The latter is complicated because it is a function of upstream river characteristics and flood probabilities.

§4.3 Fluvial flood probabilities

As mentioned in the introduction, a critical situation occurs when storm surges cause flood defences to close, creating an ever-filling „bathtub" (De Ingenieur, 2014). The bathtub, this storage basin, overflows at the critical water level of +2,5 m NAP (Ministerie van Verkeer en Rijkswaterstaat, 2006, pp. 128–165)—if the storm surge exceeds this water level, flood defences need to be closed. The lowest acceptable flood risk along the entire basin is 1/2.000 annum^{-1}, namely the Hoeksche Waard (p. 165). This means that theoretically-speaking, this area is allowed to flood every 2.000 years.

The decisive flood scenario, the scenario conveying the most water with a total probability equal to this acceptable flood risk, is a Rhine flood flow rate $\hat{Q}_{Lobith}$ of 12.900 m^{3}s^{-1} and Meuse mean flow coinciding with a 40-hour storm surge. With this decisive scenario two things are calculated: 1) whether a pumping station necessary and 2) if a pumping station is necessary, what minimum pumping capacity it should have so that the design water level of +2,5 m NAP is not exceeded during the 40-hour storm surge.

§4.4 Flood flow rate of the rivers

Fluvial floods on the Rhine and Meuse can be described with a time-dependent Gaussian according to Ministerie van Verkeer en Waterstaat (2007, p. 35). The equation that is defined to describe this, is shown below. Mean flow and flood flow are separated as the former is a constant and the latter is time-dependent. Figure 4.3 (left) illustrates this.

$$Q_{SB,IN}(t) \equiv \underbrace{\tilde{Q} e^{-\left(\frac{t-b_t}{c_{t,init}+\Delta c_t}\right)^2}}_{\text{Flood wave}} + \underbrace{Q_{MEAN}}_{\text{Mean flow}} \qquad \textit{Equation (4.3)}$$

In this equation, $c_{t,init}$ represents the initial temporal standard deviation at Lobith or Borgharen and b_t the time t at which the maximum flow rate occurs. Battjes & Labeur (2017, p. 149) state that „*the flood wave decreases in height and (consequently) increases in length as it propagates downriver*". This effect is introduced into the equation above by defining the reduced maximum flow rate $\tilde{Q}$ and the change in temporal standard deviation Δc_t. Figure 4.3 (right) illustrates this effect for the both the Rhine and the Meuse by plotting the flood wave at the inlet of the storage basin (Hollandsch Diep) relative to that at either Lobith or Borgharen. Both effects are stronger for the Rhine as it bifurcates into multiple rivers along its course from Lobith the Hollandsch Diep and because the flood wave velocities are lower in comparison with the Meuse.

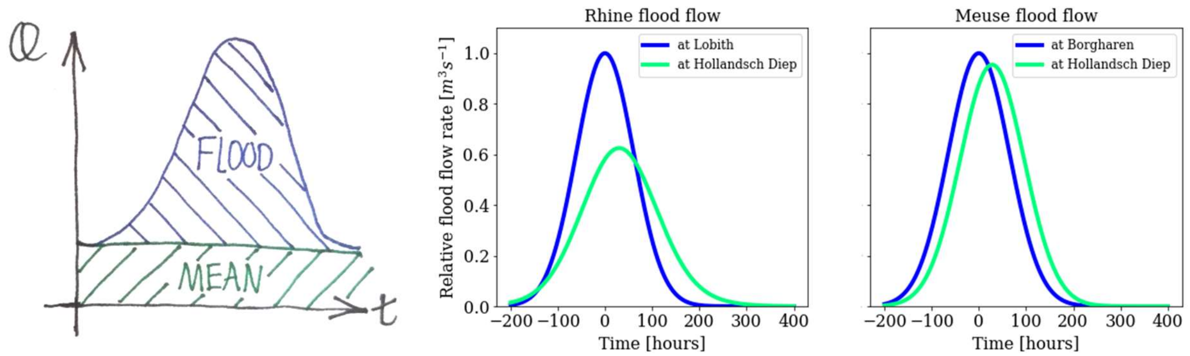

Figure 4.3 Left: separation of constant mean flow and time-dependent flood flow. Right: the effects of flood waves travelling downstream illustrated for the Rhine and Meuse: wavelength increases and flow rate decreases.

§4.5 Is the Rhine-Meuse delta at risk of flooding?

To simulate the effects of river inflow $Q_{SB,IN}(t)$ on the storage basin model of **Figure 4.2**, a numerical python program is written that iterates through all flow exchanges in the basin with a time interval of 10 seconds. To find the critical inflow, the flood flow rate at Lobith was gradually increased with steps of 50 m^3s^{-1} until the critical water level of +2,50 m NAP was exceeded during the 40-hour storm surge.

For the current situation, that is, water storage in the Volkerak-Zoommeer only and Volkerakdam sluices of 570 m^2, the simulation resulted in a critical Lobith flood flow rate of 4.450 m^3s^{-1}. This flow, in coincidence with a 40-hour storm surge of +2,5 m NAP-high, occurs **every 86 years**. This flooding risk is larger than the acceptable limit of once every 2.000 years. Even when including water storage in Grevelingen and the largest sluice upgrades, the flooding risk only decreased to once every 137 years.

With that concluded, the design problem can now be formulated:

→ Before the year 2100, fluvial flood events on the Rhine and Meuse are projected to have become more extreme and frequent, which, in combination with a storm surge on the North Sea, results that, without a pumping station facility, river water can't be discharged into the North Sea, posing an unacceptable flooding risk for the Rhine-Meuse delta

In addition to the reference projects analysis, the location analysis and this flood risk analysis, a stakeholder analysis is performed as well to gain insight in the parties that are interested in the project and/or have significant influence. This is presented in **App. IV**. Moreover, in **App. V** process, functional and operational analyses are presented to gain overview and insight in the desired performance of the system.

Chapter 5 // The Haringvlietdam Deltapump pumping station

This chapter presents the definite pumping station design at the Haringvlietdam. This concerns „phase six" of the civil engineering design cycle: the design integration, as presented within the introduction. The preceding four design phases—basis of design, creation of concepts, verification of the concepts and the evaluation—are left out of the main body. The basis of design is found in App. VI, the creation of concepts in App. VII, the verification of the concepts—the engineering calculations, in App. VIII and the evaluation of the concepts in App. IX.

§5.1 Overview of civil works in the Rhine-Meuse delta

A total of twenty different storage basin configurations were presented within the creation of concepts. These configurations depend on the location of the pumping station, the sluices of the Volkerakdam and Grevelingendam, and the inclusion of the Grevelingen for storage. Each of these configurations has its own advantages and each will require a different pumping station capacity. From the evaluation, the configuration with the best merit-to-cost ratio was chosen. This configuration is presented in the figure below.

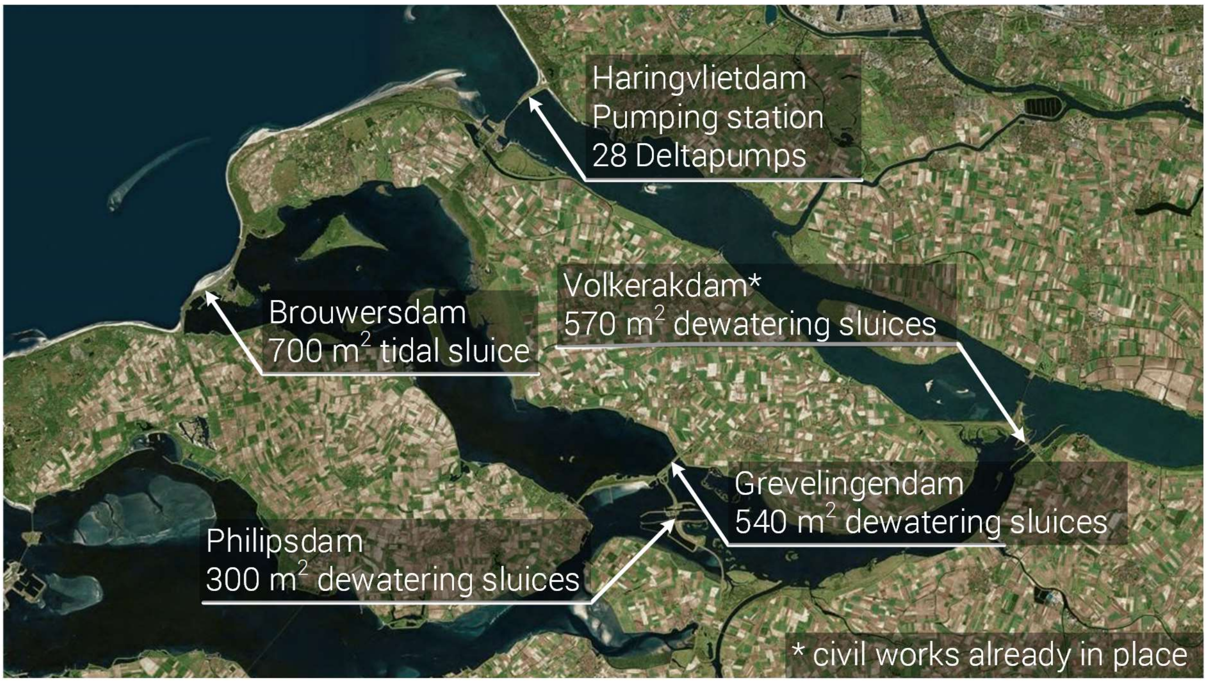

Figure 5.1 Overview of all civil works corresponding to the chosen storage basin configuration. Adapted from Zoom Earth (2020).

§5.2 Modular Haringvlietdam pumping station design

The design and the calculations of the pumping station were considered modularly, that is, a 15-meters-wide section that includes only one Deltapump. The figure below shows the design of the module.

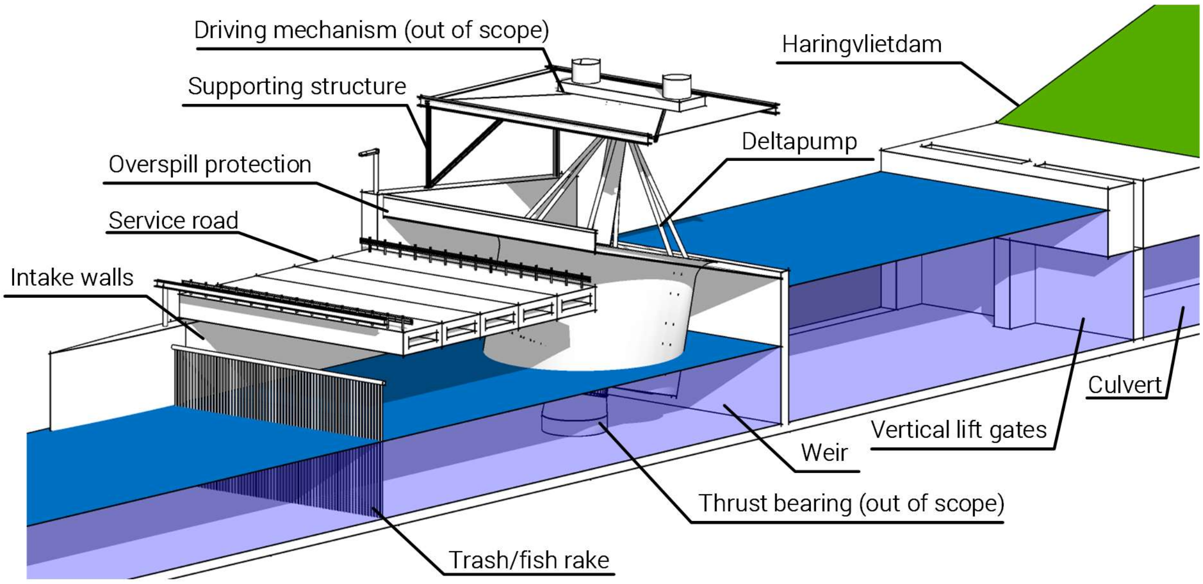

Figure 5.2 Overview of all components of a Deltapump pumping station module

The Deltapump transfers all vertical loads and half of the horizontal loads towards the thrust bearing. The thrust bearing is a mechanical component and is subsequently left out of scope. The other half of the horizontal loads is transferred to the supporting structure, which is a steel truss made out of HE-beams ranging from 160 to 450 mm width. The steel class is S355.

The rest of the pumping station design is made out of concrete. Certain parts like the intake walls, the weir, the beds and the culvert walls are only subjected to normal forces and small bending moments, and are therefore designed without reinforcement. As the culvert is integrated within the Haringvlietdam, see **Figure 5.3**, its roof slab has to resist loads of 14-meter-high soil layer. It was found that large tensile stresses develop and therefore reinforcement is required.

The service road will serve as a temporary bypass for traffic when the culvert is constructed, as its construction requires excavation works on the Haringvlietdam. Moreover, during construction and in the future during large maintenance works, this service road is required to withstand the loads of a 500-ton crane that is lifting a Deltapump. Due to the enormous bending moments this produces, in the order of 10.000 kNm, it was found that pre-stressed hollow concrete slabs of 1,2 meter high, are required. Five separate slabs, each 3 meters wide, cover a total road width of 15 meter.

The concrete class is C20/25 for all parts but the service road. The service road, due to its large bending moments, is made of C50/60 and its pre-stressing steel of Y1860C.

Figure 5.3 Longitudinal cross-section of the Deltapump pumping station at Haringvlietdam.

§5.3 Haringvlietdam pumping station: integration

The chosen configuration requires a total of 28 Deltapumps, or modules, to be put into the pumping station. With the module-width of 15 meters, this amounts to 420 meters. The length of each module is about 190 meters, of which 120 meter spanning the culvert.

The bed in the pumping station is a 50 cm thick concrete layer at -4,5 m NAP. A quick survey with Navionics (2020) reveals that along the entire shore of the Haringvlietdam, this depth is available. This is good because it decreases excavating and dredging works. However, for excavation work above ground, survey with Zoom Earth (2020) shows that the Haringvlietdam is about 180 m wide at the head of the sluices and increases up to 320 meters near the shore. It would therefore be desired to place the pumping station as close to the sluices as possible. As the service road also needs to be (temporarily) connected to the provincial road, the integration shown below is proposed.

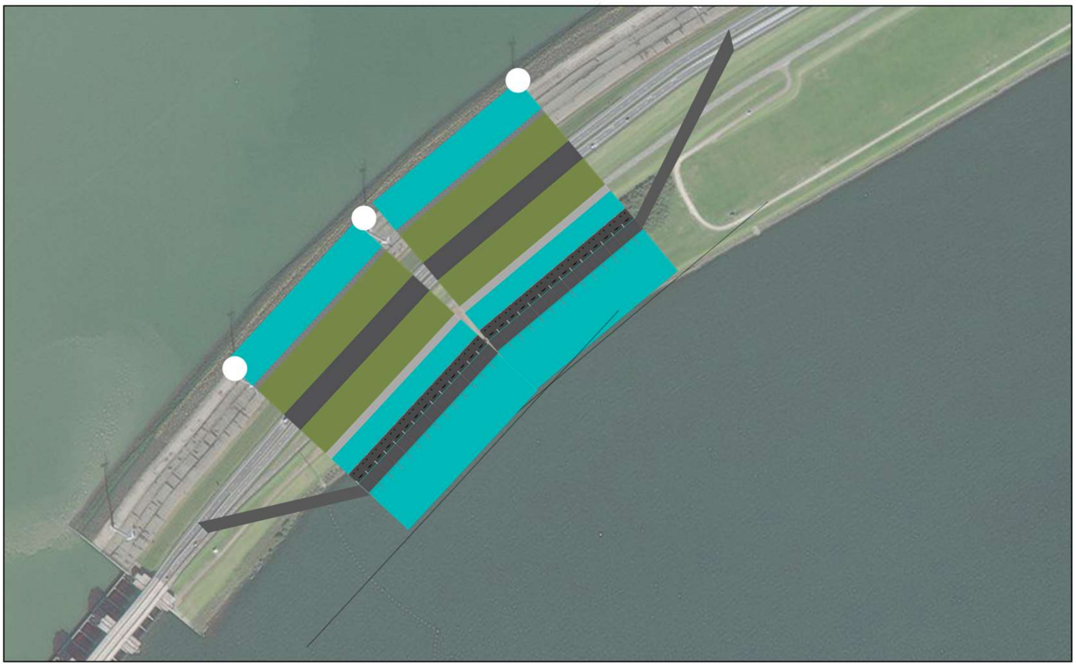

Figure 5.4 Integration proposal of the pumping station into the Haringvlietdam. Bypasses shown in grey lines and windmills with white circles.

As of now, three wind turbines are located within this proposed construction area. It should be investigated whether these can be preserved. It could be possible that, due to the high discharge, local scour causes instabilities in the soils surround the turbines.

§5.4 Haringvlietdam pumping station: operational simulations

This section shows how the pumping station operates during storm surge and fluvial flood conditions. With this storage basin configuration, the pumping station requires operation every 92 years, or when flow at Lobith has surpassed 4.500 m^3s^{-1} during a storm surge (see **Table iii.6.4**).

For the simulation, the decisive flood scenario (12.900 m^3s^{-1} flow at Lobith and Meuse mean flow) is presented, as this scenario gives the highest water levels once every 2.000 years. The figure below shows a graph created with the simulation program, displaying water levels, flow rates and power consumption.

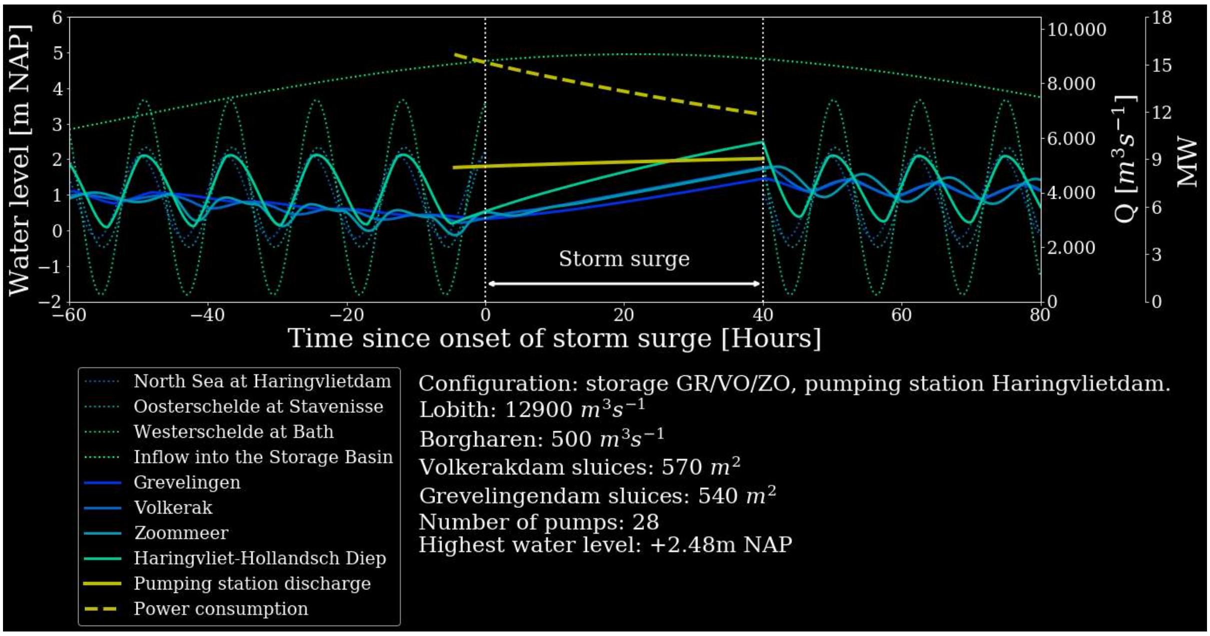

Figure 5.5 Graph displaying all water levels, pumping station discharge, river inflow and power consumption, before, during and after the storm surge, which is present between *t* = 0 and *t* = 40 hours.

From 48 hours before the storm surge, predictions are accurate enough for coming storm surges. For that reason, from *t* = -48 hours, pre-drainage commences from the Grevelingen, Volkerak and Zoommeer into the Westerschelde and Oosterschelde respectively, during low tides. During these 48 hours, water levels in these three waterbodies drop about 70 cm. The water levels in the Grevelingen and Volkerak decrease almost linearly, whilst the Zoommeer, due to the tidal channels, displays oscillatory behaviour.

During the last low tide, 12 to 0 hours before the storm surge commences, the Haringvlietdam closes so that the initial water level is at its lowest. As of that moment, water can't be discharged into the North Sea anymore, so the Volkerakdam sluices open so that water storage can commence. Furthermore, the pumping station is turned on simultaneously. The graph displays a pumping station capacity ranging from 4.920 to 5.240 m^3s^{-1}. During its operation, power consumption ranges 11,8 to 15,6 MW per Deltapump.

Chapter 6 // Life-time cost estimates of the pumping station

In this section, the life-time cost estimates of the Haringvlietdam pumping station are calculated. These costs are expressed in the so-called Net Present Value (NPV), so that the future costs can be expressed by today's relative values. The NPV is calculated with the following equation:

$$NPV(n) = F_0 + \sum_{1}^{n} \frac{F_n}{(1+r)^n} \qquad \textit{Equation (6.1)}$$

In this equation F_0 are the initial costs, F_n are the investments in year n and r is the discount rate, assumed to be 5,5%, as in the reports of Lammers (2014) and Slootjes (2013). Furthermore, the following investments are assumed:

- → Civil works:
  - Every year: opex, 1% of initial costs
  - Every 10 years: large maintenance, 5% of initial costs
  - After lifetime of 40 years: complete re-investment of initial costs
- → Mechanical works:
  - Every year: opex, 10% of initial costs
  - Every 5 years: large maintenance, 20% of initial costs
  - After lifetime of 20 years: complete re-investment of initial costs

As this thesis considers up to the year 2100, the NPV is calculated up to n = 80. The initial costs per module are calculated and presented in App. X. The figure below shows the life-time cost estimates over the period of 80 years. For a life-time of 80 years, the civil works are € 294 million and the mechanical works are € 621 million. In total, this is € 915 million.

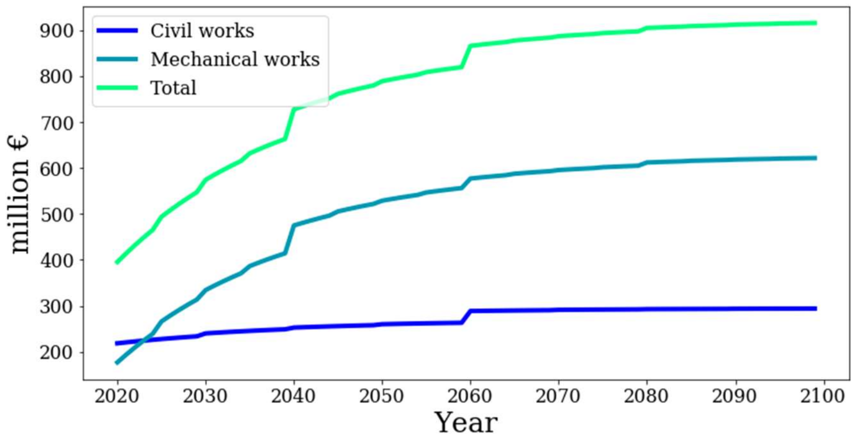

Figure 5.6 Life-time cost estimates of the civil and mechanical works up to the year 2100.

Chapter 7 //

Sequence of construction

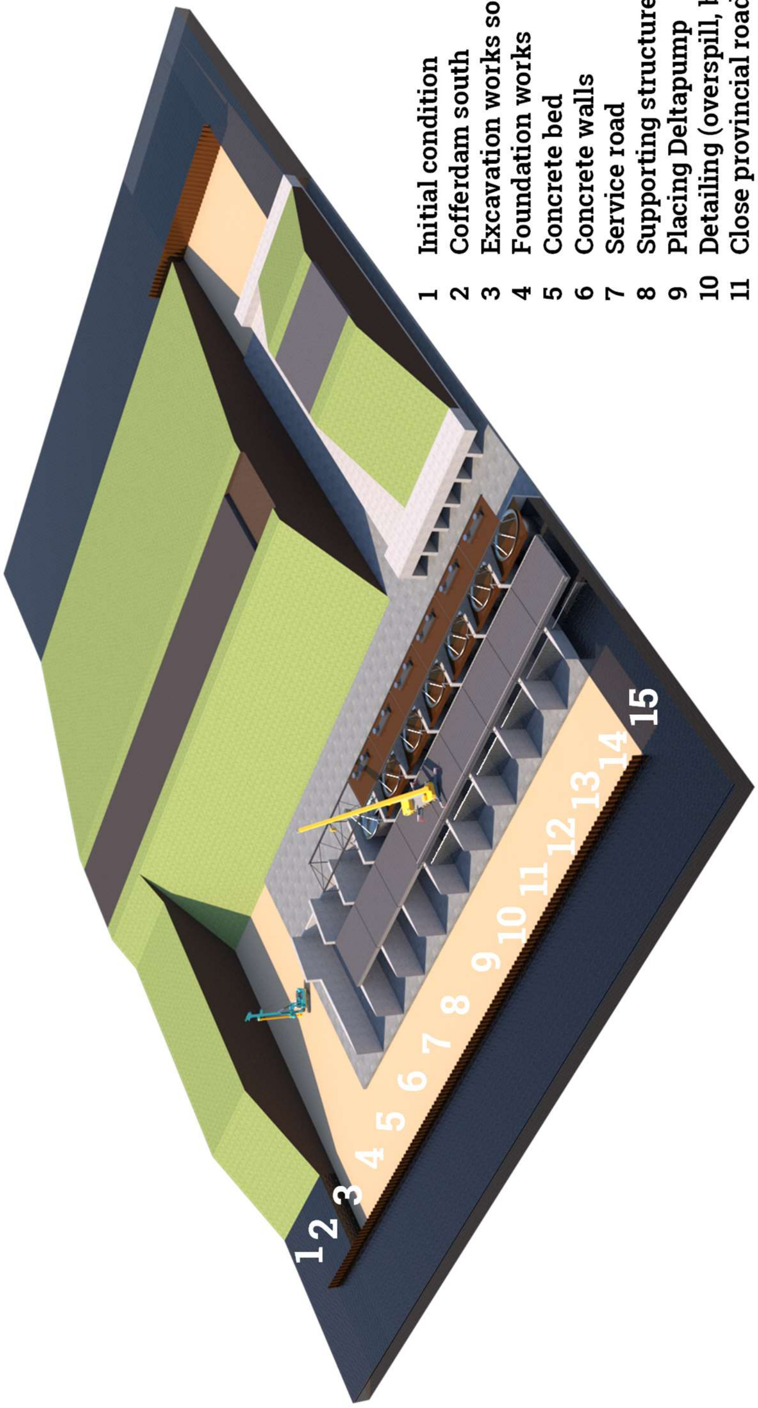

1 Initial condition
2 Cofferdam south
3 Excavation works south shore
4 Foundation works
5 Concrete bed
6 Concrete walls
7 Service road
8 Supporting structure
9 Placing Deltapump
10 Detailing (overspill, barriers, lamps etc)
11 Close provincial road, open bypass
12 Excavation works Haringvlietdam
13 Concrete culvert
14 Replace earthen dam and road
15 Remove cofferdams

Chapter 8 // Conclusions & recommendations

Conclusions

The main scope of this thesis was to investigate whether the Deltapump is a cost-effective concept, in comparison with large conventional pumping stations, to prevent flooding in the Rhine-Meuse delta before 2100. Three sub-questions were formulated, each is now elaborated.

” *What are large pumping stations? What do conventional designs of these entail and how much do they cost?*

From the analysis of the reference projects it was found that large pumping station are pumping station with a total capacities ranging 200–550 m^3s^{-1}. All of these projects pump excess water towards the sea to prevent flooding of the hinterland. Pumps in these pumping stations have capacities ranging from 40–50 m^3s^{-1}, these are the biggest pumps in the world and are exclusively kinetic pumps, where the Deltapump is a positive displacement pump. Because of their size, they are exclusively customly engineered. Per m^3s^{-1} capacity, pumping station costs are about € 250.000 to € 500.000 and their capacity densities range 4 to 8 m^2s^{-1}.

” *Is a large pumping station required in the Rhine-Meuse delta before the year 2100?*

From the simulations of the Rhine-Meuse delta it was derived that, depending on sizes of sluices within the storage basin, a Lobith flood flow rate ranging from 4.450–6.600 m^3s^{-1} the delta is at risk of flooding, as the design maximum water level has been reached. These Lobith flood flow rates coinciding with a storm surge occur every 86 to 137 years. With an acceptable flood risk of once every 2.000 years, the answer to the question above is: yes, if the design maximum water levels are left unchanged.

” *How to design a pumping station for the Deltapump concept, how much does it cost?*

The civil works of the pumping station are relatively straightforward. The crucial part of the design is the weir: it is the component the Deltapump has to transfer water past. The rest of the structure is subsequently built around the Deltapump and the weir. Unfortunately, due to the width of the Haringvlietdam, a lot of earth excavation is required. The costs, consisting of mechanical and civil costs, expressed as Net Present Value by the year 2100 are € 613 and € 294 million respectively. In total this is € 915 million.

Now the main question is addressed:

> ” *In comparison with large conventional pumping stations, is the Deltapump cost-effective concept to prevent flooding in the Rhine-Meuse delta before 2100?*

The answer to the first part of the question, „*In comparison…concept*”, is yes, the Deltapump is a cost-effective concept in comparison with large conventional pumping stations. With an average capacity of 5.000 m^3s^{-1}, the relative costs are € 183.000 per m^3s^{-1}. This is 1,5 to 3 times more cost-effective than the large conventional pumping stations that were analysed. Moreover, the space it requires is smaller: the density capacity is 12 m^2s^{-1} where the reference projects range 4–8 m^2s^{-1}.

However, when addressing the full question, the answer is no. It was found with the simulations that the pumping station would only need to be turned on every 92 years. Its full capacity, all 28 Deltapumps in operation, is only required every 2.000 years. With total costs of € 915 million, the construction and maintenance of the pumping station would be like, pun intended, *water naar de zee dragen* [carrying water to the sea].

Recommendations

This brings us to the recommendations. Although the Deltapump is relatively cost-effective, a better solution to the flooding problem would be to upgrade the dykes and dams along the Rhine-Meuse delta. Intuitively, the upgrade and maintenance of dykes seems more cost-effective, environmental friendlier and less labour intensive than the construction of a large pumping station. The Haringvlietdam pumping station would require staff, additional maintenance crew and must be actively inspected, whilst larger dykes and dams can be left relatively unattended after upgrades. It should be investigated in future reports whether this alternative, upgrading the dykes and dams in the Rhine-Meuse delta to withstand higher design water levels, is a more cost-effective method than the construction of a large pumping station.

Secondly, the workings of the Deltapump are not yet proved. A mechanical study should be performed with Computational Fluid Dynamics to see whether it works and if it can be further optimised.

Thirdly and lastly, a study should be performed into the forces and vibrations caused by the Deltapump when it is in operation. As these are yet unknown, these were left out of this study. Due to the cyclic loading, it is possible that large soil settlements will occur and/or that the supporting structure will fatigue.

Bibliography

Literature

AHN. (2020). AHN-viewer [Online elevation map]. Retrieved from https://ahn.arcgisonline.nl/ahnviewer/

American Acadamy of Environmental Engineers & Scientists. (2012). 2012 Excellence in Environmental Engineering and Science™ Awards Competition Winner. Retrieved 6 May 2020, from https://www.aaees.org/e3scompetition/2012honor-design1.php

Anonymous. (1976). *Onderzoek naar de mogelijkheid van afsluiting van de Oosterschelde met een gedeeltelijk geprefabriceerde stormvloedkering*. Retrieved from http://resolver.tudelft.nl/uuid:efb88c5f-9af4-4be2-b6d9-36da46b51648

ArcelorMittal. (2018). Prijslijst nr 89. Retrieved 20 June from https://ds.arcelormittal.com/repository/ArcelorMittal%20Staalhandel%20vanaf%202017/Prijslijst%2089.pdf

Bansal, R.K. (2005). *A textbook of fluid mechanics and hydraulic machines*. New Delhi, India: Laxmi publications ltd.

Battjes J. & Labeur R. J. (2017). *Unsteady flow in open channels*. Cambridge, England: Cambridge university press

Bol, R. (2005). Operation of the 'Maeslant Barrier' (storm surge barrier in the Rotterdan New Waterway). In C. A. Fletcher & T. Spencer (Eds.), *Flooding and Environmental Challenges for Venice and Its Lagoon: state of knowledge* (pages 311-316). Cambridge, England: Cambridge University Press

Braam, C.R. & Lagendijk, P. (2011). *Constructieleer gewapend beton*. Boxtel, the Netherlands: Æneas

BROLoket. (n.d.). [Cone penetration tests]. Retrieved from https://www.broloket.nl/ondergrondgegevens

Centraal Bureau voor Statistiek. (2020, 20 March). *Regionale kerncijfers Nederland* [Data set]. Retrieved from https://opendata.cbs.nl/statline/#/CBS/nl/dataset/70072ned/table?ts=1588920533714

Chbab, H. (2016). *Waterstandsverlopen Rijntakken en Maas: wettelijk toetsinstrumentarium WTI-2017*. Retrieved from http://publicaties.minienm.nl/documenten/waterstandsverlopen-rijntakken-en-maasb

Cooper, P. & Tchobanoglous, G. (2008). Performance of Centrifugal Pumps. In G.M. Jones (Ed), *Pumping Station Design.* (pp. 10.1-10.10). Oxford, England: Elsevier

De Afsluitdijk. (n.d.). Vergroten waterafvoer. Retrieved from https://deafsluitdijk.nl/projecten/vergroten-waterafvoer/hoe/

De Ingenieur. (2014, 10 September). *Sluit de nieuwe waterweg af*. Retrieved from https://www.deingenieur.nl/artikel/sluit-de-nieuwe-waterweg-af

Deltcommissie. (1960). *Eindverslag en interimadviezen*. [Quote on page iii, source: p. 104]. Retrieved from http://resolver.tudelft.nl/uuid:0e28dfd8-4e67-4267-a443-54b74a062bcb

Deltacommissaris. (n.d.). Wat is de rol van de deltacommissaris? Retrieved 29 April 2020, from https://www.deltacommissaris.nl/organisatie/vraag-en-antwoord/wat-is-de-rol-van-de-deltacommissaris

Demarée, Gaston. (2006). The catastrophic floods of February 1784 in and around Belgium—a Little Ice Age event of frost, snow, river ice… and floods. Hydrological Sciences–Journal–des Sciences Hydrologiques. 51. 10.1623/hysj.51.5.878.

DINOLoket. (n.d.). [Lithostratigraph and lithograph]. Retrieved from https://www.dinoloket.nl/ondergrondgegevens

Dukers, J. (2003). Kostenramingsmethode paalfunderingen. Retrieved from https://www.dace.nl/download/?id=17694458

European Environment Agency. (2017). *Climate change, impacts and vulnerability in Europe 2016: An indicator-based report* (EEA Report No 1/2017). Retrieved from doi:10.2800/534806

European Commission. (2019). *Energy prices and costs in Europe*. Retrieved from https://eur-lex.europa.eu/legal-content/EN/TXT/?qid=1548155579433&uri=CELEX:52019DC0001

Fxtop. (2020). Historical currency converter with official exchange rates from 1953. Retrieved 5 May 2020, from https://fxtop.com/

Garbus, R.O. (2008). Types of pumps. In G.M. Jones (Ed), *Pumping Station Design* (pages 11.1-11.41). Oxford, England: Elsevier

Grondverzet. (n.d.). Kosten grondverzet per M3. Retrieved 20 June 2020 from https://grondverzet.nu/kosten-grondverzet-per-m3/

Gumbel, E. J. (1941). The return period of flood flows. *Annals of Mathematical Statistics* (Vol. 12, Number 2), pp. 163–190.

Guinness World Records. (2004). Most powerful water pump. Retrieved 6 May 2020, from https://www.guinnessworldrecords.com/world-records/most-powerful-water-pump

GWW. (n.d.). *Het grootste en energiezuinigste gemaal van Europa*. Retrieved from https://datachallenge.nl/files/Energie%20RWS%20-%20Artikel%20het-grootste-en-zuinigste-gemaal-van-europa.pdf

Heemskerk, P.W.M. (2016). *Technical feasibility of the Tilting Lock* [Master's thesis]. Retrieved from http://resolver.tudelft.nl/uuid:5162a060-b798-4165-ae24-5238cba1f63e

Jülich, W. & Lindner, K. (2005). Hydrology of the Rhine. In T. P. Knepper (Ed.), *The Handbook of Environmental Chemistry* (volume 5L, pages 3-46). Berlin, Germany: Springer.

Julien, P. Y., Klaassen, G. J., Ten Brinke, W. B. M. & Wilbers, A. W. E. (2002). Case Study: Bed Resistance of Rhine River during 1998 Flood. *Journal of hydraulic engineering* (Vol. 128, issue 12), pp. 1042–1050.

KNMI. (2020). *330 Hoek van Holland*. [Dataset]. Retrieved from http://projects.knmi.nl/klimatologie/daggegevens/selectie.cgi

Lammers, J. (2014). *Ontwerp-rijksstructuurvisie Grevelingen en Volkerak-Zoommeer*. Retrieved from https://www.zwdelta.nl/publicaties-rijksstructuurvisie-grevelingen-en-volkerak-zoommeer

LeBret. (2018). Blank map Western Europe with rivers [Illustration]. Wikipedia Commons. https://commons.wikimedia.org/wiki/File:Blank_map_Western_Europe_with_rivers.svg

Maynord, S.T. (2013). *Physical Model Study of Flowerpot Discharge Outlet, West Closure Complex, New Orleans, Louisiana*. Retrieved from https://apps.dtic.mil/dtic/tr/fulltext/u2/a583046.pdf

Ministerie van Verkeer en Waterstaat. (2006). *Hydraulische randvoorwaarden 2006 voor het toetsen van primaire waterkringen*. Retrieved from http://publicaties.minienm.nl/documenten/hydraulische-randvoorwaarden-primaire-waterkeringen-voor-de-derd

Ministerie van Verkeer en Waterstaat. (2007). *Leidraad rivieren*. Retrieved from http://publicaties.minienm.nl/documenten/leidraad-rivieren-2007

„MIRT-VERKENNING GREVELINGEN". (2012). Retrieved from https://www.deltaexpertise.nl/wiki/index.php/GVZM_Uitvoeren_MIRT-verkenning_Grevelingen_VN

Mol, J. (2019). *Meer afvoercapaciteit dankzij specialistisch maatwerk in pompen*. GWW-Bouw. Retrieved from https://www.gww-bouw.nl/artikel/meer-afvoercapaciteit-dankzij-specialistisch-maatwerk-in-pompen/

Natura 2000. (n.d.). Haringvliet. Retrieved 29 April 2020, from https://www.natura2000.nl/gebieden/zuid-holland/Haringvliet

Navionics. (2020). Navionics CharViewer [Online bed level map]. Retrieved from https://webapp.navionics.com/?lang=en#boating@12&key=ohj%7BHm~wW

Nederhoff. (n.d.). 500 tons hydraulische autokraan. Retrieved from https://www.nederhoff.nl/verhuur/weg-terreinkranen/

NEN 9997-1+C2 (nl). (2017). Retrieved 29 April 2020, from https://connect.nen.nl/Standard/PopUpHtml?RNR=3535337&search=&Native=1&token=a1268ecc-112f-4013-9eef-3c429da36691

NewOrleansIsPumped. (2010). *GIWW West Closure Complex* [Screenshot of YouTube video at 2:55]. Retrieved fro m https://youtu.be/sdJ7BUSipH4

NGS. (n.d.). Rijksgemaal IJmuiden. Retrieved 6 May 2020, from https://www.gemalen.nl/gemaal_detail.asp?gem_id=264

NGS. (2004). Rijksgemaal IJmuiden [Photograph]. Retrieved from https://www.gemalen.nl/gemaal_detail.asp?gem_id=264

Openstreetmap. (2020). [Topographic map and open-source cartographic database]. Retrieved from http://Openstreetmap.orgo

Pieters, T. & Verpuy, C. (1997). Getijanalyse Schelde-estuarium, Invloed plaatselijke veranderingen bergende oppervlakte op getij voortplanting. Een analyse met TRECOS-Westerschelde 1997. Vlissingen, Delft. Rapport BGW-97.6

Projectorganisatie Ruimte voor de Rivier. (2006). *Planologische Kernbeslissing Ruimte voor de Rivier Deel 4*. Retrieved from http://publicaties.minienm.nl/documenten/planologische-kernbeslissing-ruimte-voor-de-rivier-dl-4-vastgest

Reformatisch Dagblad. (1975). *Grootste gemaal in ons land gereed*. Retrieved 5 May 2020, from https://www.digibron.nl/viewer/collectie/Digibron/id/dff78a46ec9ae1640456e5ffa2f8c764

Rijkswaterstaat. (1972). Gemaal en spuisluizen IJmuiden ID396699 [Photograph]. Retrieved from https://beeldbank.rws.nl/MediaObject/Details/396699

Rijkswaterstaat. (2011a). *Beschrijving huidige situatie Haringvliet: achtergrondrapportage voor onderzoek naar alternatief voor het Kierbesluit*. Retrieved from http://publicaties.minienm.nl/documenten/documenten-kier-haringvlietsluizen

Ruhjswaterstaat. (2011b). *Waterbergingsplan Volkerak-Zoommeer*. Retrieved from http://www.commissiemer.nl/docs/mer/p22/p2224/2224-048waterbergingsplan.pdf

Rijkswaterstaat. (2015). *Inzetprotocol Waterberging Volkerak-Zoommeer*. Retrieved from https://www.deltaexpertise.nl/images/f/f4/Inzetprotocol_waterberging_VZM_2015.pdf

Rijkswaterstaat. (2019). *Haringvlietsluizen hoog- en laagwaterstanden en -tijdstippen* [Data set]. Retrieved from https://getij.rws.nl/

Rijkswaterstaat. (n.d.-a). Vaarwegenoverzicht. Retrieved 5 May 2020, from https://www.rijkswaterstaat.nl/water/vaarwegenoverzicht/index.aspx

Rijkswaterstaat. (n.d.-b). Deltawerken. Retrieved 4 May 2020, from https://www.rijkswaterstaat.nl/water/waterbeheer/bescherming-tegen-het-water/waterkeringen/deltawerken/

Rijkswaterstaat. (n.d.-c). Watersnoodramp 1953. Retrieved 4 May 2020, from https://www.rijkswaterstaat.nl/water/waterbeheer/bescherming-tegen-het-water/watersnoodramp-1953/index.aspx

Rijkswaterstaat. (2020). Rijkswaterstaat Waterinfo [Online water information database]. Retrieved 6 June 2020, from https://waterinfo.rws.nl/

Rijkswaterstaat Oost-Nederland. (2017). *Watersysteem rapportage rijntakken 1990-2015: ontwikkelingen waterkwaliteit en ecologie*. Retrieved from https://www.stroming.nl/overzicht/watersysteemrapportage-rijntakken-1995-2010

Rorres, C. (2000). The Turn of the Screw: Optimal Design of an Archimedes Screw. *Journal of Hydraulic Engineering* (Vol. 126, issue 1), pp. 72-80.

Schmit, H. (1999, 11 februari). Capaciteit van gemalen vergroot. *Trouw*. Retrieved from https://www.trouw.nl/nieuws/capaciteit-van-gemalen-vergroot~b820c6a5/

Schulte-Wülwer-Leidig, Anne & Gangi, Laura & Stötter, Tabea & Braun, Marc & Schmid-Breton, Adrian. (2018). Transboundary Cooperation and Sustainable Development in the Rhine Basin. 10.5772/intechopen.73260.

Slootjes, N., Kruchten, Y.J.G. van, Bulthuis, J. & Slager, J.W. (2010). *Gevoeligheidsanalyse Waterberging Zuidwestelijke Delta* [Case study]. Retrieved from https://www.deltaexpertise.nl/wiki/index.php/GVZM_Waterberging_in_Volkerak-Zoommeer_VN

Slootjes, N. (2013). *Kosten en effecten van waterberging Grevelingen* [Case study]. Retrevied from https://www.deltaexpertise.nl/wiki/index.php/Bestand:Kosten_en_effecten_van_waterberging_Grevelingen_2013.pdf

SteenhuisMeurs. (2015). *De Deltawerken - Cultuurhistorie en ontwerpgeschiedenis*. Retrieved from http://resolver.tudelft.nl/uuid:bedc2a9a-8b5e-422b-9124-be83a987a621

Technische Adviescommissie voor de Waterkeringen. (2002). *Leidraad Zandige Kust*. Retrieved from http://publicaties.minienm.nl/documenten/leidraad-zandige-kust-1

TidesChart. (2020). Eb en vloed tijden en getijgrafieken voor Netherlands [Tidal charts]. Retrieved on 12 June 2020, from https://nl.tideschart.com/Netherlands/

Tosserams M., Lammers E.H.R.R. & Platteeuw M. (2000). *Het Volkerak-Zoommeer*. Lelystad, the Netherlands: Ministerie van Verkeer en Waterstaat

U.S. Army Corps of Engineers. (2013). *West Closure Complex*. Retrieved from https://www.mvn.usace.army.mil/Portals/56/docs/PAO/FactSheets/WCC.pdf

Van Vuren, B.G. (2005). *Stochastic modelling of river morphodynamics* [Doctoral thesis]. Retrieved from http://resolver.tudelft.nl/uuid:d2723fe3-f822-4e87-a7cd-d81fcd50a934

Vellinga, P., Katsman, C., Sterl, A. & Beersma, J. (2008). *Onderzoek naar bovengrensscenario's voor kliamatverandering voor overstromingsbescherming van Nederland*. Retrieved from https://edepot.wur.nl/30314

Vuik, C., Vermolen, F.J., Van Gijzen, M.B. & Vuik, M.J. (2017). *Numerical Methods for Ordinary Differential Equations*. Delft, the Netherlands: Delft Academic Press

Waterschappen. (n.d.). Mijn waterschap [Web page]. Retrieved 15 June 2020 from https://www.waterschappen.nl/mijn-waterschap/

Winkelhorst, J. (2013). *Hydraulic analysis of a flood channel from the Afgedamde Maas to the Biesbosch and Bergse Maas* [Master thesis]. Retrieved from http://resolver.tudelft.nl/uuid:05da335c-f54d-4f98-ba39-d6861f74c5fe

Zimmerman, K.A. (2015, 27 August). Hurricane Katrina: Facts, Damage & Aftermath. Retrieved 5 May 2020, from https://www.livescience.com/22522-hurricane-katrina-facts.html

Zoom Earth. (2020). [Satellite map]. Retrieved from http://zoom.earth

Table of appendices

Appendix I // The Deltapump and its pumping station concept

This appendix is an extension to the introduction, where the Deltapump concept is presented.

The first two section presents a hydromechanical description of the Deltapump and is based on personal communications with and an information package sent by J. Schut (2020). As the pumping curve for the Deltapump is not yet derived, an approximation is presented next. Lastly, Schut's design for the Haringvlietdam pumping station with the Deltapump concept is presented.

§I.1 Deltapump description and characterisation

See Figure i.1, the concept of the Deltapump is derived from the Archimedes screw pump. Its deviation is that it's thicker (diameter > height) and it's encased by a shell. The inner screw consists of a double helix and is welded to both the central axis and shell, so that the shell rotates along. Its material is yet to be determined, which most likely will be a high-grade alloy. At the top of the shell there is a circular spout that stimulates flow out of the Deltapump. Six rods provide a tensile connection between the top of the shell and the central axis. The top of the central axis is connected to the driving mechanism which causes the Deltapump to rotate. The central axis is mounted at the bottom to a thrust bearing which allows for rotation. The Deltapump is designed to work in non-submerged conditions.

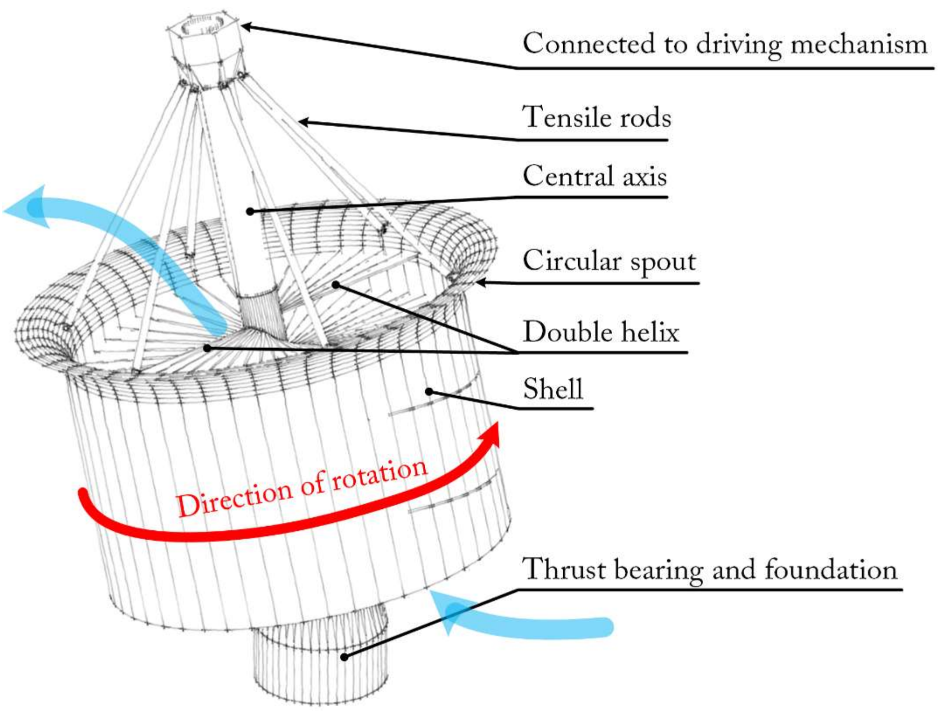

Figure i.1 Digital sketch of the Deltapump concept. Direction of flow shown in blue.

These thrust bearings are yet to be designed, as the enormous forces and rotational velocity impose a rather difficult challenge. It was suggested to employ hydrodynamic lubrication bearings with glycol at a pressure of about 10–20 bar. Concerning the driving mechanism, power is supplied by two 6kV electrical engines per Deltapump. These electrical engines have a revolution speed of 1500 rpm and are reduced to 60 rpm by two *5-to-1* gears.

According to Garbus (2008, p. 11.3, 11.38) the Deltapump can be characterised as an enclosed-screw rotary positive displacement pump. He further states these pumps types have a very high efficiency due to the absence of slippage. For screw pumps, slippage is the phenomenon where water spills over the screws and falls back down. This is prevented by the shell. Conventional designs of this pump type are, however, rather long (>10 m), have small diameters (<1 m) and have an angle of about 30–45° to the horizontal.

§I.2 Deltapump specifications

In his design of the pumping station at the Haringvlietdam, the Deltapump has the following specifications:

> diameter: 10 m
> height: 6 m
> central axis diameter: 120 cm
> helical slope (at the circumference): 10%
> angle of inclination: 25%
> spout width: 1 m
> spout height: 1 m
> rotational velocity: 60 rpm

The height of the central axis sticking out of the Deltapump was not defined. In this thesis this is assumed to be 7 m, equal to the height of the cylinder. See the figure to the right for a schematic cross-section showing the dimensions.

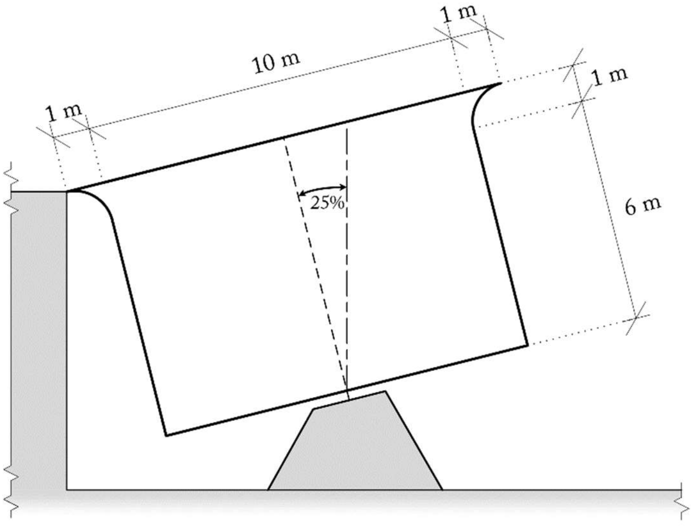

Figure i.2 Dimensions of the Deltapump

In the information package by Schut, no pumping curve was present as it is yet to be accurately derived from Computational Fluid Dynamics (CFD) or experiments. Instead, Schut estimated the pump capacity as 200 m^3s^{-1} for his design of the Haringvlietdam, independent of head. The following calculation method was used.

The rotational velocity of 60 rpm or 1 rev/s results in a tangential velocity at the circumference:

$$u_t = \omega \times r = 1 \times 2\pi \times 5 = 10\pi \text{ ms}^{-1} \qquad \textit{equation i.1}$$

The helical slope is 10% so that the axial velocity amounts to π or 3,14 ms^{-1}. Schut calculated the capacity by multiplying the surface area of the Deltapump with the axial velocity:

$$Q_{DP} = u_a \times A_{DP} = \pi \times (\pi \times 5^2 - \pi \times 0,6^2) = 24,64\pi^2 = 243,2 \text{ m}^3\text{s}^{-1} \qquad \textit{equation i.2}$$

To account for potential losses, he rounded this down to 200 m^3s^{-1}—a loss of 20%. This method is however wrong. The inclination of the Deltapump is very small, so only a small volume of water is retained at all times. This is about 10%, see the red volume in Figure i.3.

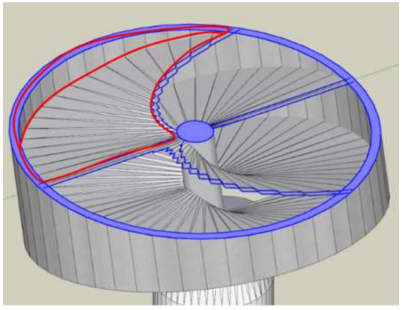

Figure i.3 Vertical cross-section of the Deltapump. The volume within the red lines is the retained volume.

The rest of the water is free to flow down. This is the phenomenon called slippage or backflow. Rorres (2000, pp. 75–76) states that for normal enclosed-screw pumps, the dimensions of the inner radius, the number of blades and the helical slopes are adjusted such, that this retained volume is maximised. Moreover, he defined three parameters: the optimal radius ratio $\rho *$, the optimal pitch ratio $\lambda *$ and the optimal volume ratio ν. The table below shows a comparison between the optimal values and the values according to the Deltapump specifications. From these values it can be concluded that, to maximise the retained volume, the inner radius has to be increased from 120 to 540 cm.

Table i.4 Comparison between three ratios of the Deltapump and optimal Archimedes screw designs, from Rorres (2000, p. 76).

	Radius ratio	Pitch ratio	Volume ratio
Deltapump	0,12	-0,45	~10%a
Optimal Archimedes	0,5369	0,1863	27,5%

§I.3 Deltapump pumping curve approximation

In order to conclude whether this backflow is significant, an approximation for the pumping curve is presented here. Let's investigate the effects of gravity on the non-retained volume of water, as gravity affects 90% of the volume. Let's start with the following equation:

$$\frac{dh}{dt} = u_a \qquad \textit{equation i.3}$$

It represents the rise in water level, *dh/dt*, of a water column undergoing an axial velocity u_a caused by being pushed upwards by the Deltapump. At the same time, water is leaking out of the bottom due to the backflow as a function of height *h*, approximated with Torricelli's law:

$$Q_{LEAK}(h) = \mu A_{DP,IN}\sqrt{2 \times g \times h} \qquad \textit{equation i.4}$$

If divided by the Deltapump cross-sectional area, this backflow causes a decrease in water level:

$$\frac{dh}{dt} = -\frac{Q_{LEAK}(h)}{A_{DP}} = -\mu\frac{A_{DP,IN}}{A_{DP}}\sqrt{2 \times g \times h} \qquad \textit{equation i.5}$$

Combining the two yields an ordinary non-linear first order differential equation:

$$\frac{dh}{dt} = u_a - \mu\frac{A_{DP,IN}}{A_{DP}}\sqrt{2 \times g \times h} \qquad \textit{equation i.6}$$

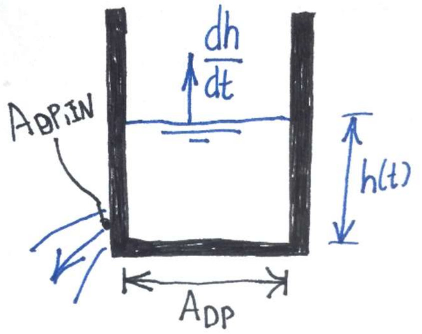

Figure i.5 Cross-section of the calculation model

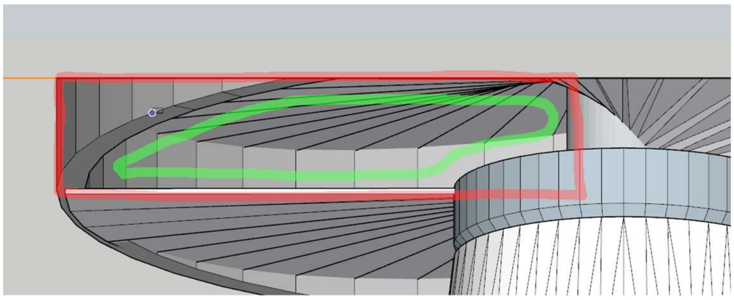

Figure i.6 Horizontal front view of the inlet at the bottom of the Deltapump.

Now unto the constants from equation i.6. See Figure i.5 for a cross-section corresponding to the model. In the equation, μ is the contraction coefficient, $A_{DP,IN}$ is the surface area of the Deltapump inlet, A_{DP} is the surface area of the Deltapump and g is the gravitational acceleration. The surface area of the pump A_{DP} is 24,64π m^2. For the surface area of the inlet, $A_{DP,IN}$, see the red box in Figure i.6. The height of this box is 0,5π or 1,57 m: the pitch between two blades. Because the helical blades have a certain thickness, this gap decreases to 1,50 m. With a central axis diameter of 1,2 meter, the width of the inlet is 5 – 0,5 × 1,2 = 4,4 m. There are two helical blades, so the area has to multiplied by two. This yields 2 × 1,5 × 4,4 = 13,2 m^2.

An assumed effective area, the green box in Figure i.6, yields a contraction coefficient of 0,4 after image analysis with GIMP (version 2.10). For the calculations of the contraction coefficient the horizontal view was chosen of the model, as it is expected that water in the intake canal will flow horizontally. The resulting equation:

$$\frac{dh}{dt} = \pi - 0,4 \times \frac{13,2}{24,64\pi}\sqrt{2 \times 9,81 \times h} \qquad \textit{equation i.7}$$

Solving this non-linear equation for *h(t)* will yield some exponential relation between the height of the water column and time, in an infinitely-high Deltapump. This rise however stops once the right side of the equation is zero. Let this be known as the maximum head $H_{DP,MAX}$, the height this Deltapump specification can raise the water level to. By solving equation i.7 for *h*, this yields 108,1 m. At this height, the velocity caused by the Deltapump equals that instigated by gravity. Equation i.7 is realistic, as it converges at $H_{DP,MAX}$: for water levels higher than the maximum, it goes back to equilibrium by discharging water through the inlet at the bottom of the Deltapump.

Now unto the reason for this application: the capacity as a function of height. If the walls from Figure i.5 end at any height *h* lower than the maximum head, water will pour out of the box with a velocity $\frac{dh}{dt}(h)$. If this is multiplied by the surface area, it yields the pump capacity for that height. By doing so, the assumption is made that the full volume of the Deltapump, up to a height *h* is occupied by water. In other words, there are no cavities present just as assumed by Schut.

$$Q_{DP} = A_{DP}\frac{dh}{dt} = 24,64\pi^2 - 5,28\sqrt{19,62 \times h} \qquad \textit{equation i.8}$$

As it was estimated that 10% of the water volume is retained, always, this equation should be rewritten to account for that fact:

$$Q_{DP} = \begin{cases} h \le H_{DP,MAX}, & 0,9 \times (24,64\pi^2 - 5,28\sqrt{19,62 \times h}) \times \left(1 - \frac{h}{H_{DP,MAX}}\right) + 0,1 \times (24,64\pi^2) \\ h > H_{DP,MAX}, & 0,1 \times 24,64\pi^2 \end{cases}$$

equation i.9

It can be calculated that the assumed 200 m^3s^{-1} is reached if the head is 3,2 m. Table i.7 shows the capacities for ranges 1 to 10 meter.

Table i.7 Pump capacities for head differences from 1 to 10 m.

Head [m]	1	2	3	4	5	6	7	8	9	10
Capacity [m^3s^{-1}]	220,3	209,9	201,7	194,5	188,2	182,3	176,9	171,9	167,1	162,5

To answer the question stated at the beginning of this section: yes, backflow is significant. Now pump characteristics curves for $H(Q)$ and $P(Q)$ can be found, see Figure i.8. Power can be calculated with:

$$P_{DP} = \frac{\rho_W g Q_{DP} \Delta H_{DP}}{\eta} \qquad \textit{equation i.10}$$

Where ρ_W is the density of water and η is the efficiency of the driving mechanism, assumed to be 80%.

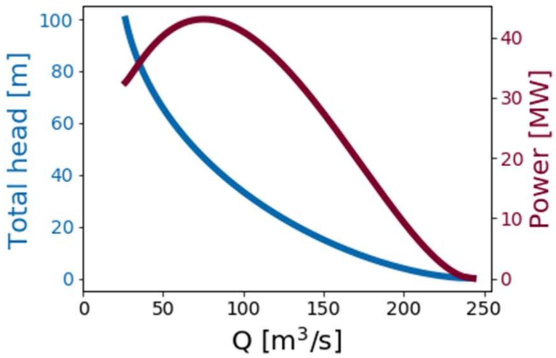

Figure i.8 H-Q and P-Q curves of the Deltapump.

A few remarks are now made discussing the validity and application of this model.

1. From this pumping curve analysis, it is concluded that, for the Deltapump to work, the intakes should be fully submerged. Without the effect of contraction, backflow is equal to the axial velocity. This requirement is translated into the boundary conditions, in App. VI.
2. Torricelli's law is applicable when the surface area of the leak is relatively small in comparison to the surface area of the water column: this ratio is: 0,4 × 13,2/77,4 = 0,068. This is small enough for this approximation to be valid.
3. It was assumed that the full volume of the Deltapump is occupied by water. It is more likely that cavities will be formed, yielding even lower capacities. This cannot be described with model and requires Computational Fluid Dynamics (CFD).
4. There might be other factors at play so this model isn't entirely accurate, like 1) friction caused by Deltapump irregularities or 2) water pushed to the outside due to centrifugal forces causing cavities in the middle. This model does however show the effect of head difference on the capacity. Without this model, the Deltapump would have a constant capacity even for infinitely high head differences—which is impossible. The accurate workings can only be derived with CFD analysis.

§I.4 Deltapump pumping station concept at the Haringvlietdam

Schut created a conceptual design for a pumping station on the north abutment of Haringvlietdam, to pump water from the Haringvliet to the North Sea. A longitudinal cross-section is shown in **Figure i.9**.

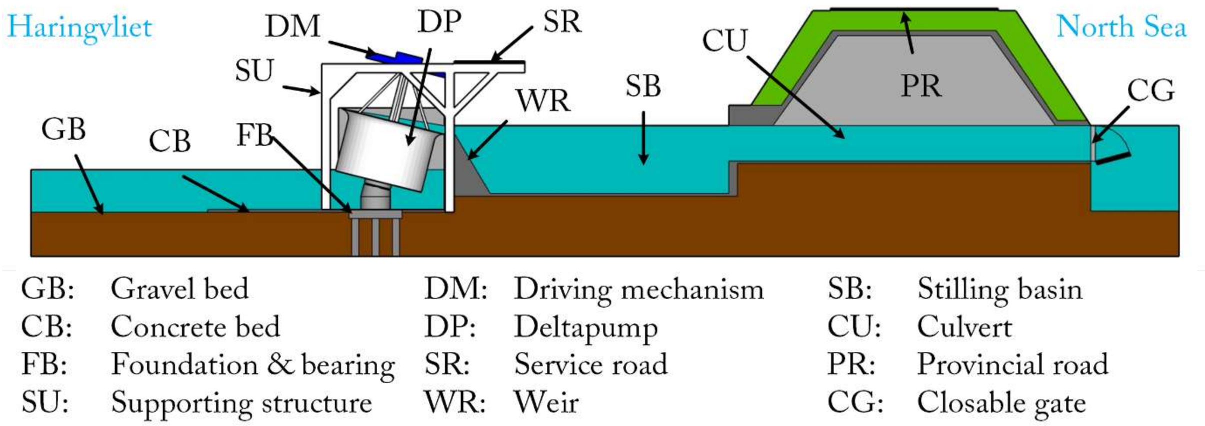

Figure i.9 Cross-section of the Deltapump pumping station concept at Haringvlietdam

With his assumed 200 m^3s^{-1} pump capacity, the complete pumping station has a capacity of 1.000 m^3s^{-1}—five Deltapumps. So, five of these longitudinal cross-sections make up the pumping station. In his concept the longitudinal dimensions are, among other things, already given. All given parameters are:

Gravel bed	20 m long, 20 cm layer of coarse gravel and above a 30 cm layer of fine gravel
Concrete bed	25 m long, 30 cm thick concrete floor at -4,50 m NAP
Weir	1,2 m long and at +3,0 m NAP, bottom; 5,2 m long and at -4,5 m NAP.
Stilling basin:	30 m long, 30 cm thick concrete floor at -2,70 m NAP
Service road	8 m wide, 40 cm thick, supported by 1×1 m2 concrete beams.
Culvert	40 m long and varying height (in the shape of a trapezium) from 4 to 12 m.
Foundation	a Ø 6 m and 1 m thick slab with eight 100-ton compression piles underneath

In this design water flows over a gravel and concrete bed before entering the Deltapump. Water then flows over a weir and enters a stilling basin in which the flow is stabilised. Consequently, water flows underneath the provincial road in a tunnel and enters the North Sea.

Appendix II // Inquiry into large pumping stations (reference projects)

This appendix is the background of **Chapter 2**.

In this short inquiry, three large pumping stations are analysed. These are listed below with their relevance to the project in parenthesis.

→ Rijksgemaal IJmuiden (largest in Europe)
→ West Closure Complex New Orleans (largest in the world)
→ Gemaal Afsluitdijk (integrated within flood defences)

In this case, „large" doesn't necessarily imply size but rather pump capacity [m^3s^{-1}]. Following from these projects, a short description of the pumps used in these projects is given.

§II.1 Rijksgemaal IJmuiden

The Rijksgemaal IJmuiden is located at the interface of the North Sea channel and the North Sea, in the province of North Holland. With a capacity of 260 m^3s^{-1} it is the biggest pumping station in Europe (GWW, n.d.). It serves an area (bemalingsgebied) of about 4.000 km^2, one-tenth of the Netherlands. Moreover, its function is to keep the water level in the North Sea Channel between -0,55 and -0,30 m NAP and it keeps the salinity of the Amsterdam-Rhine Canal and the Markermeer, the second largest lake in the Netherlands, low (GWW, n.d.). Under normal circumstances on the North Sea, the pumping station is shut off and water is naturally discharged through dewatering sluices, just like at the Haringvlietdam. Power consumption is, for an energy head of 1,2 m, 7,1 MW (NGS, n.d.).

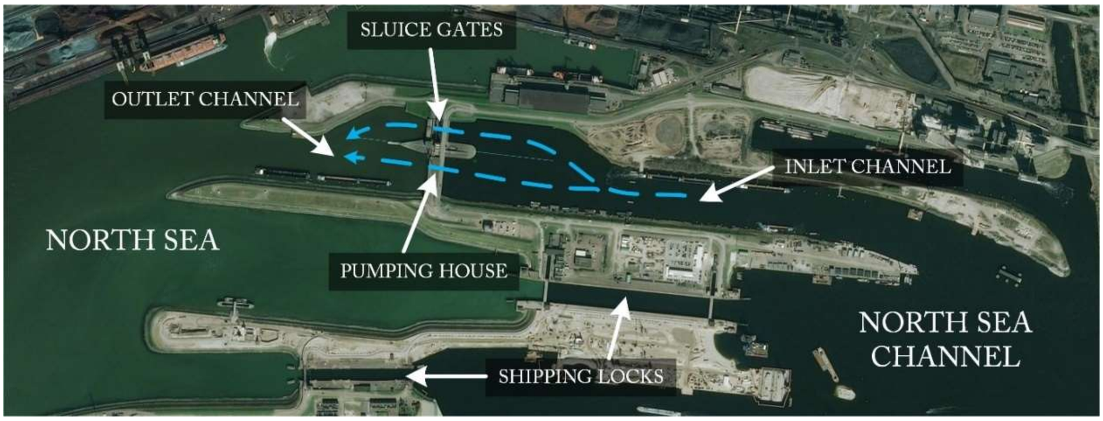

Figure ii.1 Overview of the IJmuiden gemaal with the components. Adapted from (Zoom Earth, 2020).

The components that make up this pumping station are the in- and outlet channels, the sluice gates, the pumping house and a service road. The pumping house is made of reinforced concrete and contains the pumps, the pump shafts, technical installations, maintenance room and a control room (NGS, n.d.). Adjacent to the pumping station there are two shipping locks that allow ships from the Amsterdam harbour to enter the North Sea. See the figure below for an overview of the project.

When the Rijksgemaal IJmuiden was built in 1975, its initial costs were *ƒ* 35 million (Reformatisch Dagblad). In 2004 upgrades to the pumping station were completed which increased the pumps from four to six and it costed *ƒ* 125 million (Schmit, 1999). Adjusted for inflation, the CapEx (Capital Expenditures) would have been € 70 million today (fxtop, 2020). The pumping station uses about 9 million kWh per annum (GWW, n.d.), corresponding to an OpEx (Operational Expenditures) of € 700.000 (European commission, 2019, p. 12).

§II.2 West Closure Complex

In 2005, Hurricane Katrina devastated the southern coast of the United States. The city of New Orleans, in the state of Louisiana, suffered the worst of all. In total 1.833 people were killed and the damages were up to $ 108 thousand million (Zimmermann, 2015). The resulting storm surge broke through the floodwalls and flooded about 80% of New Orleans. This catastrophe commissioned the project Hurricane and Storm Damage Risk Reduction System (HSDRRS) in the state of Louisiana costing $ 14,5 thousand million. The project „…consists of 350 miles [560 kilometres] of levees and floodwalls; 73 non-Federal pumping stations; 3 canal closure structures with pumps; and 4 gated outlets" (U.S. Army Corps of Engineers, 2013, p.1).

Figure ii.2 Overview of the West Closure Complex project. From U.S. Army Corps of Engineers (2013, p. 2).

The West Closure Complex (WCC) is the main structure of the project. It is a pumping station with a capacity of about 540 m^3s^{-1} and a power consumption of 41 MW (AAEES, 2012). The energy head is 26,5 feet, or 8 m (Manyard, 2013, p. 10), and the exceedance frequency used in the design is 1/100 years. Moreover, the costs of the project are € 770 million (U.S Army Corps of Engineers, 2013), of which the pumping station is estimated at € 270 million (AAEES, 2012). See **Figure ii.2** for an overview.

§II.3 Gemaal Afsluitdijk

The gemaal Afsluitdijk is, as of June 2020, still under construction. De Afsluitdijk (n.d.) gives two reasons for the construction of this pumping station: the dewatering sluices can't be used during 1) high-water on the Wadden Sea and 2) during wind-setup or storm surges on the Wadden Sea. The total capacity of the pumping station will be 235 m^3s^{-1} with a power consumption of 11,7 MW (Mol, 2019). A cross-section of the project is shown in the figure below. Before entering the pump, water first flows through a trash rack. Then, water flows through a culvert that runs underneath the Afsluitdijk, towards the Wadden Sea. In the tunnel, to vertical lift gates can be lowered to stop water flow.

Figure ii.3 Overview of the Afsluitdijk gemaal project. From Mol (2019).

§II.4 Pump installations of large pumping stations

General description of pumps

Garbus (2008, p. 11.2) categorises pumps into two main groups: positive displacement pumps and kinetic pumps. Positive displacement pumps involve an object physically moving the liquid from one place to another, e.g. an Archimedes' screw or water wheel. As a result of this displacement, the hydraulic head is affected. The kinetic pumps involve displacements due to pressure and velocity changes in the system, e.g. due to impellers, and can be categorised into two subgroups: vertical and centrifugal (Garbus, p. 11.1). In the latter, flow is rotationally accelerated in a volute—a shell-like shape, whereas in the former liquid is accelerated in the direction of the pipes.

The performance of a specific pump can be summarised in so-called „pump characteristics" graphs. For a given pump type and operational speed these characteristics show the relation between head difference and pump capacity. In practice this means that with the knowledge of required head difference and pump capacity, appropriate pumps can be found with these characteristics (Cooper & Tchobanoglous, 2008, p. 10.8).

Rijksgemaal IJmuiden

The pumps of the Rijksgemaal IJmuiden are about 4 m in diameter and are horizontal axial-flow pumps, which, contrary to its name, are categorised as vertical pumps by Garbus (2008, p.11.9). For a head difference of 1,2 m, four pumps have a capacity of 40 m^3s^{-1} and two a capacity of 50 m^3s^{-1} (NGS, n.d.). In addition, the installed pumps have, in pairs, different pump characteristics; dependent on conditions, the most energy efficient configuration is chosen (GWW, n.d.). These 50 m^3s^{-1} pumps, shown in **Figure ii.4**, are the most powerful pumps in the world (Guinness World Records, 2004)

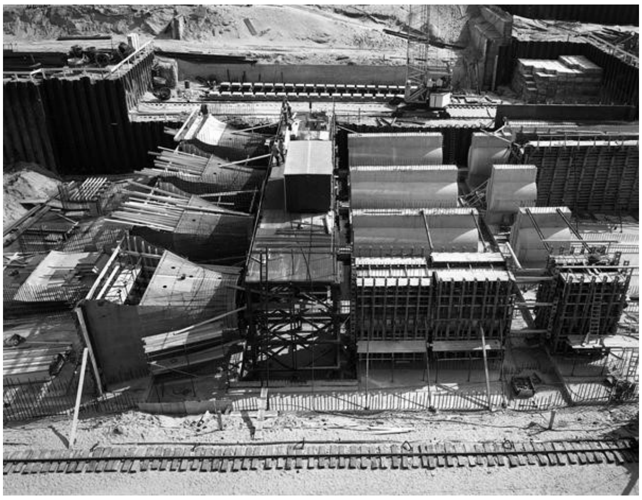

Figure ii.4 (left) Front view of one of the newer axial-flow pumps of IJmuiden (NGS, n.d.).
Figure ii.5 (right) Side view of the in- and outtake channels during construction (Rijkswaterstaat, 1972).

According to Garbus (2008, p. 11.9), these horizontal axial-flow pumps are most suitable for applications with very high discharges and very low head differences; these are the only suitable pumps with a capacity in the range of 6 to 30 m^3s^{-1} (pp. 11.40–41). In addition, he states they often require a bearing frame to resist against radial and thrusting forces. In IJmuiden, this bearing frame is submerged together with the pump and the driving mechanism (NGS, n.d.). These are placed between concrete the in- and outtake ducts—shown in **Figure ii.5**. These ducts are approximately 12 m apart.

West Closure Complex

In the West Closure Complex (WCC), the pumping concept is denoted as Flowerpot Discharge Outlets (FPDO) (Maynord, 2013, pp. 2-6). Manyard states that in this concept horizontal flow enters the FPDO at the bottom, in a 12,5 m wide intake, and is subsequently propelled by the pump into a discharge chamber. From this discharge chamber, water flows out of the system. He further states that the name flowerpot comes from the shape of the pipe above the pump: the increases in diameter to cause deceleration. Figure ii.6 shows a cross-section of the FPDO concept.

Figure ii.6 (left) Model of the Flowerpot Discharge Outlet concept. From NewOrleansIsPumped (2010).
Figure ii.7 (right) The overhung-impeller pump used in the WCC (AAEES, 2012).

In the WCC the impellers have a diameter of 3,5 m, or 140 inches (NewOrleansIsPumped, 2010). Eleven of these pumps are used with a capacity of 49 m^3s^{-1} each (Manyard, 2013, p. 1), see Figure ii.7. The pumps used in this concept can be described as overhung-impeller pumps, where „the impeller is mounted at the end of the pump shaft in a cantilever fashion." (Garbus, 2008, p. 11.6). In addition, he states they are the most used pumps in water management structures (p. 11.17) and, conventional designs, are capable of a capacity up to 3 m^3s^{-1} (Garbus, 2008, p. 11.40). Due to the dimensions of the WCC pumps, computational fluid dynamics were deployed to validate this concept (AAEES, 2012).

Gemaal Afsluitdijk

The pumps in the gemaal Afsluitdijk are, just like the WCC, overhung impeller pumps (Mol, 2019). Furthermore, they have a capacity of 39 m^3s^{-1} each and a diameter of 4,6 meters. Mol (2019) also states that its weight is around 120 tons and it's 12 meters high.

Appendix III // Flood risk analysis of the Rhine-Meuse delta

In this appendix chapter a flood risk analysis is performed. In this analysis, the Rhine-Meuse delta is modelled as a storage basin with flow entering from the Rhine and Meuse. First, this storage model is described in section 1 and 2. Fluvial flood scenarios and their probabilities are described in the third section. Then, in section 4, the characteristics of all relevant rivers in the Rhine-Meuse delta are presented. Next, a mathematical model is formulated for the inflow of fluvial floods from the Rhine and Meuse. In section 6, this mathematical model is then used to determine whether the Rhine-Meuse delta is at risk of flooding—and if it requires a large pumping station. Section 7 discusses the validity of the model. Summarising and concluding remarks are found in §III.6.3 and §III.6.4.

§III.1 The storage of water in the Rhine-Meuse delta

To investigate the effects of fluvial floods events in the Rhine-Meuse delta, a storage basin model is formulated. First the extent of this model is described and secondly the hydraulic limits are described. Lastly, all possible configurations for the storage basin model are described with their capex.

§III.1.1 The extent storage basin model

According to Slootjes et al. (2010, pp. 6–8) and Projectorganisatie Ruimte voor de Rivier (2006, p. 53), it is currently procedure to store water in the Volkerak-Zoommeer. Moreover, plans have been made to expand this storage basin to the Grevelingen. The Volkerak and Zoommeer have a surface area of respectively 63,1 and 18,0 km^2 (Tosserams et al. 2000, p. 25) and Grevelingen 140 km^2 (Rijkswaterstaat, n.d.-a). See Figure iii.1.1 for an overview of the model. NB While the Haringvliet and Hollandsch Diep are part of the calculation model, they are not necessarily the „storage" part of the model: they can't be fully closed off so that water enters nor leaves. The area of the Haringvliet is 110 km^2 and that of Hollandsch Diep 40 km^2 (Rijkswaterstaat, n.d.-a; Zoom Earth, 2020).

Slootjes concluded that water storage is not viable on the Oosterschelde (pp. 25–28). This is rather unfortunate, as the area of the Oosterschelde is 350 km^2 (Rijkswaterstaat, n.d.-a) whilst the combined area of the other four is 221,1 km^2. The inclusion of the Oosterschelde would almost have tripled the storage basin area—its volume likewise. Another suggestion presented by Rijkswaterstaat (2011b, p. 10) is pre-draining the Volkerak-Zoommeer into the Ooster- and Westerschelde. According to current procedures, during ebb tides 48 hours before the storm surge, pre-draining takes place (Rijkswaterstaat, 2015, p. 4). Before that, a storm surge can't be predicted accurately.

Rijkswaterstaat gives the average water levels of the Grevelingen and Volkerak-Zoomeer: +0,03 (2020) and +0,15 m NAP (2011b, p. 52). Before 2100, the Haringvliet-Hollandsch Diep has an average water level of +0,93 m NAP, the MSL (Leeuwen et al., 2004, p. 14; Technische Adviescommissie voor de Waterkeringen, 2002, p. 142). The largest dimension of the storage basin is 56 km: from the Brouwersdam to Moerdijk (Zoom Earth, 2020).

Figure iii.1.1 Overview of the storage model of in the Rhine-Meuse Delta. Names of dike rings shown in black. Created with open-source data from Openstreetmap (2020).

§III.1.2 Acceptable flooding risk and design water levels

Of all dyke rings along the storage model, see **Figure iii.1.1**, the Hoeksche Waard has the lowest exceedance frequency: 1/2.000 annum^{-1} (Ministerie van Verkeer en Rijkswaterstaat, 2006, p. 37). In other words, it is acceptable that this area theoretically floods every 2.000 years. The other five dike rings have an exceedance frequency of 1/4.000 annum^{-1}. The dykes along the Hoeksche Waard are designed to withstand a water level of +2,5 m NAP; this is the lowest design water level in the entire storage basin (pp. 128–165). The highest design water level is at the West-Brabant dyke ring, with a water level of +2,8 m NAP (p. 165). In conclusion, this means that, for the water levels caused by a fluvial events, it is acceptable that they exceed +2,5 m NAP every 2.000 years.

Naturally, it is optional to increase the heights of the dykes so that they can withstand higher water levels. This intervention will be beneficial for the capex of the pumping station, as a smaller pumping station will be required. It is however unsure if this option is beneficial for the total costs; it might be more cost-effective to build a bigger pumping station than strengthening the dykes. This should therefore be examined. Let's propose three interventions:

1. No intervention: keep the dykes as they are; +2,5 m NAP design water level
2. Slight strengthening: increase all dykes to the current maximum of +2,8 m NAP.
3. Radical strengthening: increase all dykes to withstand +3,1 m NAP.

The second and third intervention are not presented in the calculations here. They are separately elaborated later in the evaluation phase.

§III.1.3 Flow within the storage basin

Water can enter the Volkerak from the Hollandsch Diep through dewatering sluices located in the Volkerakdam, see Figure iii.1.1. These dewatering sluices have an effective area of 570 m^2 (Slootjes et al., 2010, p.29). However, plans have been presented for three upgrades. See the table below.

Table iii.1.2 Four concepts for upgrading the dewatering sluices in the Volkerakdam with their capex and opex. The opex of the „no-upgrade"-concept are guesstimated (Slootjes, 2013, p. D-1–D-2).

	capex [million €]	opex [thousand € $annum^{-1}$]	concept
570 m^2	0	~500	no upgrade
1.350 m^2	134	1.062	upgrade of sluices
1.200 m^2	150	2.102	addition of sluices
2.000 m^2	284	3.164	concept 1 and 2 combined

Water storage in the Grevelingen

If water storage is expanded to the Grevelingen, dewatering sluices will have to be constructed in the Grevelingendam, as there is currently no means to directly discharge water from the Volkerak into the Grevelingen (Lammers, 2014, p. 11). For the Grevelingendam, Slootjes (2013, pp. D-3–D-5) presents four concepts, shown in Table iii.1.3.

Table iii.1.3 Four concepts for dewatering sluices in the Grevelingendam with their capex and opex (Slootjes, 2013, p. D-5).

	capex [million €]	opex [thousand € $annum^{-1}$]	connection between Grevelingen and Volkerak
540 m^2	56	170	open
1.350 m^2	92	280	open
540 m^2	83	750	closed
1.350 m^2	143	1.290	closed

Slootjes (2010, p. 10) states that an open connection between the Volkerak and the Grevelingen results in salinification of the Volkerak-Zoommeer and it requires tides to be re-introduced in the Grevelingen. Notwithstanding, the Rijkswaterstaat (Lammers., 2014, pp. 61–66) concluded that an open connection is the best concept. The full concept of Lammers (p. 49) includes the following two measures:

- → Brouwersdam: closable sluice of 700 m^2 to allow water flow between Grevelingen and the North Sea, € 130 million (p. 21; p. 32)
- → Philipsdam: closable sluice of 300 m^2 for the benefit of tidal dynamics and salinity, € 47,4 million (p. 32; p. 66)

Furthermore, expansion to the Grevelingen requires additional flood protection measures along the shore of the Grevelingen. These works include upgrades to existing dykes and flood protection measures to marinas and buildings outside dyke rings. Slootjes gives the capex and opex, as a function of highest water level, of these works: up to respectively € 57 million and € 79 thousand annum^{-1} (2013, p. D-10).

§III.1.4 Storage basin configurations and their initial costs

Within the storage basin concepts, we have thus far created the following permutations:1) inclusion of Grevelingen, 2) effective area of Volkerakdam sluices and 3) if Grevelingen included, the effective area of Grevelingendam sluices. In the table below, all twelve configurations are shown with the total initial capex based on the sluices and Grevelingen storage. The costs of upgrading flood protection in the Grevelingen are excluded, as these depend on the highest water level. These costs can only be estimated when the calculations have been performed.

Table iii.1.4 Initial capex for twenty storage basin configurations expressed in million €. All configurations can be combined with design water levels of +2,5, +2,8 or +3,1 m NAP. Costs of flood protection measures on the Grevelingen are excluded. Value in italics is the current situation.

		Volkerak sluices			
		570 m^2	1.200 m^2	1.350 m^2	2.000 m^2
No storage in Grevelingen		*0*	150	134	284
Storage in Grevelingen,	540 m^2	233,7	383,7	367,7	517,7
Grevelingen sluices	1.350 m^2	269,7	419,7	403,7	553,7

§III.2 Numerical formulation of the storage basin model

In this section, the numerical formulation for the storage basin is presented. First the numerical method is presented, then the equations for water levels and then the equations for flow exchange between basins. Consequently, the hydraulic boundary conditions and initial conditions are presented. Lastly, it is shown how the numerical method is iterated through.

§III.2.1 Numerical solution method: Euler forward

The solution method for the systems of equations that will be derived later, is the Euler forward method. A numerical method is chosen because, due to the nature of the equations—non-linearity and absolute values, no analytical solution is possible. Moreover, some constants (like the effective area A_{SL} of sluices) are step functions: they are either $1\times A_{SL}$ or $0\times A_{SL}$. Furthermore, due to the complexity of the systems of equations, it is easier for computation. The Euler forward method is (Vuik et al., 2016, p. 67):

$$w_n = w_{n+1} + \Delta t \times f\left(t_n, w_n\right) \qquad \textit{equation iii.1}$$

The time interval Δt that will be used is 10 seconds. Furthermore, the Euler forward method can be written for a system of equations (Vuik, p. 81):

$$\begin{cases} \vec{y}' &= \vec{f}(t,\vec{y}), \\ \vec{y}(t_0) &= y_0 \end{cases} \forall\ t > t_0$$
$$\vec{f} = \left(t, y_1 \ldots y_m\right)^T \qquad \textit{equation iii.2}$$
$$\vec{y} = \left(y_1 \ldots y_m\right)^T$$

§III.2.2 The small-basin approximation

For the storage basin, let's consider the „small-basin approximation", meaning that „the water level in the basin can be assumed to be horizontal at all times" (Battjes & Labeur, 2017, p. 93). The small-basin approximation is valid when the wavelength of the flood wave is much larger than the largest horizontal dimension of the basin (p. 91). In practice, a ratio of approximately twenty is the criterium. The smallest wavelength is later found to be 1.169 km (§III.7) and the largest dimension 56 km: the ratio is approximately 20 so that criterium is satisfied. The equation corresponding to this approximation is:

$$\Delta Q_{SB} = A_{SB}\frac{dh_{SB}}{dt} \qquad \textit{equation iii.3}$$

Where ΔQ_{SB} is the net inflow into the storage basin, A_{SB} is the surface area of the basin and h_{SB} is the water level in the basin. As seen in Figure iii.1.1, the storage model consists of up to five lakes: Grevelingen, Volkerak, Zoommeer, Haringvliet and Hollandsch Diep. The Hollandsch Diep transitions into the Haringvliet at the Volkerakdam, over the full width (no dewatering sluice).

Therefore, the water levels in these lakes can be assumed equal at all times. This is not the case for the Grevelingen and Volkerak, and Zoommeer and Volkerak, as these are connected with sluices respectively Schelde-Rijnkanaal with an effective area that is very small (~1000 m^2) relative to the cross-sections of the lakes (~100.000 m^2). Therefore, let's model equation iii.3 for following four basins:

1. Haringvliet-Hollandsch Diep
2. Volkerak
3. Zoommeer
4. Grevelingen

This model is schematically represented with boundary conditions and flow exchanges below.

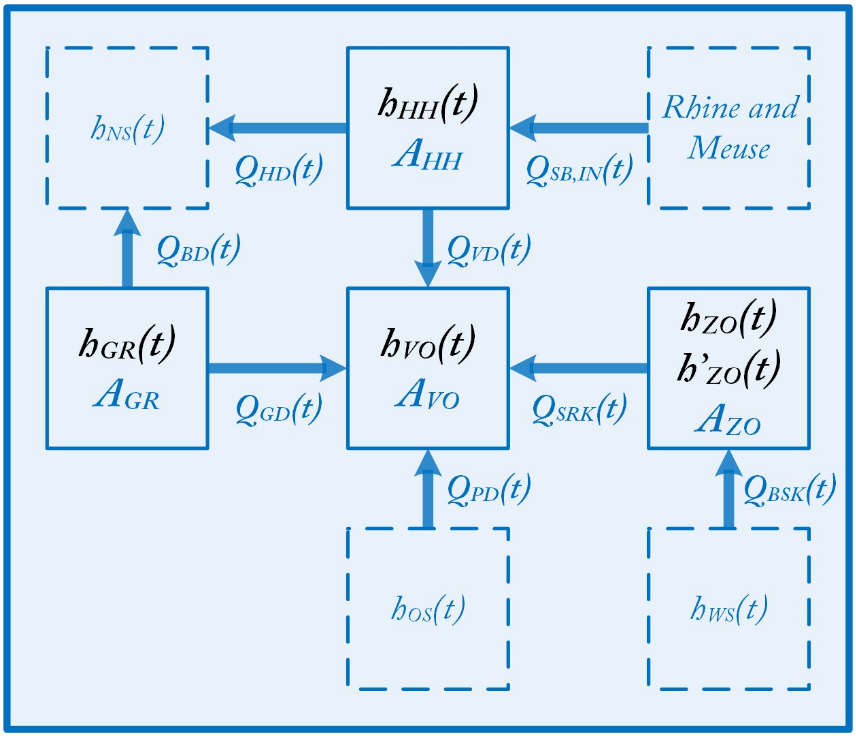

Figure iii.2.1 Schematic model of the storage basin with flow exchanges and boundary conditions.

The figure shows all possible flow exchanges in the model. The subscripts $_{BD}$, $_{GD}$, $_{HD}$, $_{PD}$ and $_{VD}$ mean Brouwersdam, Grevelingendam, Haringvlietdam, Philipsdam and Volkerakdam. The subscripts $_{BSK}$, $_{SRK}$ and $_{SB,IN}$ mean Bathse Spuikanaal, Schelde-Rijnkanaal and storage basin inflow respectively. The storage basin inflow $Q_{SB,IN}(t)$ is a rather complex equation which depends on a multitude of factors. Therefore, sections §III.3 to §III.5 are dedicated to formulating a mathematical model for the inflow based on probabilities, river characteristics and conditions at Lobith and Borgharen.

Next, all other flow interactions between the basins are mathematically formulated.

§III.2.3 Flow through discharge sluices

The discharge through the five sluices (Grevelingendam, Volkerakdam, Haringvlietdam, Philipsdam and Brouwersdam) depends on the difference between water levels on both sides of the sluices. Because the Bathse spuisluis is connect to a tidal channel, another equation is applicable, see next section. The discharge is described by Torricelli's law:

$$Q = A_{SL}\sqrt{2g\left(h_1 - h_2\right)} \qquad \textit{equation iii.4}$$

Note that, due to the square root, this equation requires the water level difference to be positive. In equation iii.4, this will cause a flow Q from location 1 to location 2. As both directions are possible in the storage basin, both cases are modelled for every dam. Therefore, Torricelli's law is from now on written with a modulus in the root and a plus-minus.

§III.2.4 Flow through the Schelde-Rijnkanaal and Bathse spuikanaal

Interaction between the Volkerak and Zoommeer, and the Zoommeer and Westerschelde takes places through the Schelde-Rijnkanaal and Bathse spuikanaal respectively. These interactions don't adhere equation iii.4 because, as proven later, inertia is significant. This is further elaborated on in §III.7. The set of equations are now presented for the Schelde-Rijnkanaal. Battjes & Labeur (2017, pp. 105–108) present the solution for this problem. The following second-order ordinary differential equation is applicable:

$$\frac{1}{\omega_0^2}\frac{d^2 h_{ZO}}{dt^2} + \tau\frac{dh_{ZO}}{dt} + h_{ZO}(t) = h_{VO}(t) \qquad \textit{equation iii.5}$$

The subscripts $_{ZO}$ and $_{VO}$ mean Zoommeer en Volkerak respectively, τ is the relaxation time and ω_0 is the natural frequency of the basin (Zoommeer):

$$\omega_{0,SRK} \equiv \sqrt{\frac{g}{L_{SRK}}\frac{d_{C,SRK} \times B_{C,SRK}}{A_{ZO}}} \qquad \textit{equation iii.6}$$

L means channel length, d_C means conveyance depth, B_C means conveyance width and A_{ZO} is the surface area of the Zoommeer. The length of the Schelde-Rijnkanaal is approximately 15 km (Zoom Earth, 2020), the conveyance depth is approximately 6 m (Navionics, 2020) and its width 270 m (Zoom Earth, n.d.-a).

The relaxation time τ can be calculated with the following equations:

$$\tau_{SRK} \equiv \frac{1}{\omega_{M_2}}\frac{1}{\sqrt{2}}\sqrt{-(1-\left(\frac{\omega_{M_2}}{\omega_{0,SRK}}\right)^2)^2+\sqrt{\left(1-\left(\frac{\omega_{M_2}}{\omega_{0,SRK}}\right)^2\right)^4+4\Gamma^2}}$$

$$\Gamma \equiv \left(\frac{\omega_{M_2}}{\omega_{0,SRK}}\right)^2 \times \left(\frac{8}{3\pi}\left(\frac{1}{2}+\frac{c_f L_{SRK}}{d_{SRK}}\right)\frac{A_{ZO}\hat{h}_{VO}}{d_{SRK}B_{C,SRK}L_{SRK}}\right)$$

equation iii.7

In this rather long equation, ω_{M_2} is the frequency of the semi-diurnal tide, c_f is the friction slope of the canal and $\hat{h}_{VO}$ is the amplitude of the tide in the Volkerak. The latter can only be determined from iteration, assuming any non-zero value initially (for an initial zero value, equation iii.7 is zero as well). The friction slope is 0,005, see §III.4.2 and the frequency of the semi-diurnal tide is 1,406 × 10^{-4} s (Battjes, p. 17). For the Bathse spuikanaal, the only different values are the length and the width: 8 km and 180 m (Zoom Earth, 2020).

§III.2.5 Time periods of interest

For this mathematical model, the flood defences close at t = 0 hours and open again at t_{SS} = 40 hours, see next section §III.3.1. At t = 20 hours, the peak of the fluvial flood arrives at the storage basin, so that the total water conveyed is maximal. In §III.5.6 the practical time T_{PRAC} period is defined, during which the influence of the fluvial flood is significant. At t = (-0,5×T + 20 hours) the water levels can be assumed to be mean water levels, as the conveyed fluvial volume is insignificant outside this period. The study period lasts until t = (0,5×T + 20 hours) as by then, the influence of the fluvial flood has vanished. During this study time, we can derive four consequent periods of interest:

1.	Before pre-draining: from	$t \in \left[-\frac{T_{PRAC}}{2}+20,-48\right]$
2.	During pre-draining	$t \in [-48,0]$
3.	Storm surge	$t \in [0,40]$
4.	Draining the basin	$t \in \left[0,\frac{T_{PRAC}}{2}+20\right]$

§III.2.6 Hydraulic boundary conditions

Maximum water level

During the study period, the water levels h in the storage basin must not exceed the design water levels of +2,5 m NAP:

$$h_{HH}(t),\ h_{VO}(t),\ h_{ZO}(t),\ h_{GR}(t) \leq +2{,}5 \text{ m NAP } \forall \text{ t} \in \left[-\frac{T_{PRAC}}{2}+20, \frac{T_{PRAC}}{2}+20\right] \quad \textit{equation iii.8}$$

The subscripts $_{HH}$ and $_{GR}$ mean Haringvliet-Hollandsch Diep and Grevelingen respectively.

North Sea tide

Due to astronomical tides, the water level of the North Sea $h_{NS}(t)$ will oscillate. Before 2100, the MSL is +0,93 m NAP and the mean tide range is 2,29 m (Leeuwen et al., 2004, p. 14; Technische Adviescommissie voor de Waterkeringen, 2002, p. 142). We can therefore model the North Sea water level with the following equation:

$$h_{NS}(t) = 0{,}93 + \frac{2{,}29}{2}\cos(\omega_{M_2} t) \quad \textit{equation iii.9}$$

No phase shift is added to the equation so that its maximum occurs at t = 0 hours, the time when the flood defences close. As a result, the storage basin will have the highest initial water level.

Oosterschelde tide

The tide in the Oosterschelde $h_{OS}(t)$ can be modelled equally as equation iii.9, but with a phase shift as the high tide at Stavenisse, near the Grevelingendam, occurs approximately 46 minutes (ΔT_{OS}) later than at Haringvlietdam (TidesCharts, 2020). The tidal range is 2,80 m (Anonymous, 1976, p. 18).

$$h_{OS}(t) = 0{,}93 + \frac{2{,}80}{2}\cos(\omega_{M_2} t - \Delta T_{OS}) \quad \textit{equation iii.10}$$

Westerschelde tide

The water level in the Westerschelde $h_{WS}(t)$ at Bath is:

$$h_{WS}(t) = 0{,}93 + \frac{5{,}48}{2}\cos(\omega_{M_2} t - \Delta T_{WS}) \quad \textit{equation iii.11}$$

The phase shift ΔT_{OS} is 30 minutes (TidalCharts, 2020) and the tidal range is 5,48 m (Pieters & Verspuy, 1997).

§III.2.7 Initial conditions

The numerical solution, described in the next section, requires initial conditions to work. From **Figure iii.2.1**, the required initial conditions can be derived. These are shown in the table below.

Table iii.2.2 Initial conditions for the numerical method

	No Grevelingen storage	Grevelingen storage	Unit
$h_{HH,0}$	+0,93	+0,93	m NAP
$h_{VO,0}$	+0,15	+0,93	m NAP
$h_{GR,0}$	not necessary	+0,93	m NAP
$h_{ZO,0}$	+0,15	+0,93	m NAP
$h'_{ZO,0}$	0	0	ms^{-1}

§III.2.8 Numerical method for the system of equations

With the equations, the boundary conditions and the initial conditions determined, the system of equations can be formulated. With the positive directions from Figure iii.2.1, the discharges through the five sluices are as follows:

$$\begin{aligned}
Q_{BD,N} &= \pm A_{SL,BD}\sqrt{2g\left|h_{GR,N}-h_{NS,N}\right|}\\
Q_{GD,N} &= \pm A_{SL,GD}\sqrt{2g\left|h_{GR,N}-h_{VO,N}\right|}\\
Q_{HD,N} &= \pm A_{SL,BH}\sqrt{2g\left|h_{HH,N}-h_{NS,N}\right|}\\
Q_{PD,N} &= \pm A_{SL,PD}\sqrt{2g\left|h_{OS,N}-h_{VO,N}\right|}\\
Q_{VD,N} &= \pm A_{SL,VD}\sqrt{2g\left|h_{HH,N}-h_{VO,N}\right|}
\end{aligned}$$

equation iii.12

As the equations for the Schelde-Rijnkanaal and Bathse Spuikanaal are second-order ordinary differential equations, the method is a little different. Due to the second-order, forward Euler yields the first-order derivative, as also shown Figure iii.2.1. The corresponding equations with help from equation iii.2 are:

$$\begin{aligned}
\frac{dh_{ZO,SRK,N}}{dt} &= \frac{dh_{ZO,SRK,N-1}}{dt} + \Delta t \times \omega_{0,SRK}^{2} \times \left(-h_{ZO,N-1} - \tau_{SRK} \times \frac{dh_{ZO,SRK,N-1}}{dt} + h_{VO,N-1}\right)\\
\frac{dh_{ZO,BSK,N}}{dt} &= \frac{dh_{ZO,BSK,N-1}}{dt} + \Delta t \times \omega_{0,BSK}^{2} \times \left(-h_{ZO,N-1} - \tau_{BSK} \times \frac{dh_{ZO,BSK,N-1}}{dt} + h_{WS,N-1}\right)
\end{aligned}$$

equation iii.13

NB because the equations are of second-order, the numerical method requires values of $_{N-1}$ instead of $_{N}$. If these are multiplied with the surface area of the Zoommeer, the discharge through the Schelde-Rijnkanaal, in direction of the Volkerak, and the discharge through the Bathse-Spuikanaal, in the direction of the Zoommeer, are obtained:

$$Q_{SRK,N} = -A_{ZO} \frac{dh_{ZO,SRK,N}}{dt}$$
$$Q_{BSK,N} = A_{ZO} \frac{dh_{ZO,BSK,N}}{dt}$$

equation iii.14

Then, with all flows between the basins determined, the rise in water level for each basin can be calculated. According to the positive directions from Figure iii.2.1, this is:

$$\frac{dh_{GR,N}}{dt} = \frac{1}{A_{GR}}\left(-\underbrace{Q_{BD,N}}_{\text{If Brouwersdam == Open}} - \underbrace{Q_{GD,N}}_{\text{If Grevelingendam == Open}} \right)$$
$$\frac{dh_{HH,N}}{dt} = \frac{1}{A_{HH}}\left(Q_{SB\_IN,N} - \underbrace{Q_{HD,N}}_{\text{If Haringvlietdam == Open}} - \underbrace{Q_{VD,N}}_{\text{If Volkerakdam == Open}} \right)$$
$$\frac{dh_{VO,N}}{dt} = \frac{1}{A_{VO}}\left(\underbrace{Q_{GD,N}}_{\text{If Grevelingendam == Open}} + \underbrace{Q_{PD,N}}_{\text{If Philipsdam == True}} + \underbrace{Q_{VD,N}}_{\text{If Volkerakdam == Open}} + Q_{SRK,N} \right)$$
$$\frac{dh_{ZO,N}}{dt} = \frac{1}{A_{ZO}}\left(\underbrace{Q_{BSK,N}}_{\text{If Bathse spuisluis == Open}} - Q_{SRK,N} \right)$$

equation iii.15

NB the Oosterschelde, Westerschelde and North Sea are excluded from the equations above, as, due to their large surface areas and this surface area being reciprocal, it would yield close to zero. In other words, discharge doesn't affect those water levels; only the astronomical tide does.

Now, with the rise in water levels determined, the new water levels h_{N+1} can be determined with the forward Euler method from equation iii.1:

$$h_{GR,N+1} = h_{GR,N} + \Delta t \frac{dh_{GR,N}}{dt}$$
$$h_{HH,N+1} = h_{HH,N} + \Delta t \frac{dh_{HH,N}}{dt}$$
$$h_{VO,N+1} = h_{VO,N} + \Delta t \frac{dh_{VO,N}}{dt}$$
$$h_{ZO,N+1} = h_{ZO,N} + \Delta t \frac{dh_{ZO,N}}{dt}$$

equation iii.16

With these new water levels h_{N+1}, the process can be repeated infinitely for $t + \Delta t$ by performing equations iii.12 to iii.16 in order. However, as noted in §III.2.5 for certain periods, the sluices need to be closed. The following section discusses this.

§III.2.9 Storage basin operation pseudo-code

The aforementioned is implemented in equation iii.15 by showing pseudo-code beneath the flow interactions through the sluices. This pseudo-code describes the operations within the numerical program, but then simplified. The controls for each of the six dams/sluices are now elaborated. All times are shown in *hours*.

Brouwersdam

For concepts without Grevelingen storage, the following is always true, as the Brouwersdam doesn't exist then: `Brouwersdam = closed`.

For concepts including Grevelingen storage, we can denote the following operation:

t < -48	Wait for prediction: „storm surge within 48 hours"	Open
-48 < t < +40	48 hours before storm surge, close Brouwersdam so that pre-draining can commence	Closed
t > +40	Storm surge over, drain the storage basin into the North Sea and return to normal tidal conditions	Open

Haringvlietdam

The following operation applies to the Haringvlietdam:

t < {last low tide}	Normal tidal conditions on the Haringvliet and Hollandsch Diep	Open
{last low tide} < t < +40	Last low tide before the predicted start of storm surge	Closed
t > +40	Storm surge over, drain the storage basin into the North Sea and return to normal tidal conditions	Open

When the Haringvlietdam is opened, the tidal range is almost equal to that of the North Sea: ~2 meter. It is then beneficial to prematurely close the Haringvlietdam at low tide so that the total water storage increases significantly: $2 \times 150{\times}10^6 / (40{\times}3.600) = 2.100\ m^3s^{-1}$ increase in allowed average storage basin inflow.

Volkerakdam

For the Volkerakdam, the following operations can be applied:

t < {last low tide}	Wait for storage to commence	Closed
t > {last low tide}	Commence water storage	Open

As soon as the Haringvlietdam closes, the Volkerakdam opens because at that moment, the water storage is required. After a certain period of time, the Volkerdam will close again to return to the initial situation. This is not included as this is irrelevant to the study.

Grevelingendam

The Grevelingen is always opened for concepts with storage in Grevelingen. For concepts without Grevelingen storage, the Grevelingendam doesn't exist. For the numerical iteration this means it is always closed.

Philipsdam

The Philipsdam is used for pre-draining into the Oosterschelde from t = 48 hours until the storm surge. The following operation applies to the Philipsdam:

t < -48	Wait for prediction: „storm surge within 48 hours"	Closed
-48 < t < 0 AND h_{VO}(t) > h_{OS}(t)	pre-draining	Open
t > 0	return to initial condition	Closed

Bathse spuisluis

t < -48	Wait for prediction: „storm surge within 48 hours"	Closed
-48 < t < 0 AND h_{ZO}(t) > h_{WS}(t)	pre-draining	Open
t > 0	return to initial condition	Closed

§III.2.10 Storage basin inflow

The only undefined variable in equations iii.12 to iii.16 is the storage basin inflow $Q_{SB,iN}(t)$. The next three chapters are dedicated to quantifying this variable. First, a flood risk analysis is performed to determine the probabilities of certain flood scenarios. From this flood risk analysis, the decisive flood scenario is the determined. Then, all relevant parameters of the rivers between Lobith/Borgharen and the storage basin are inventoried in §III.4. In the fifth section, the mathematical model is then formulated.

§III.3 Fluvial flood scenarios and probabilities

§III.3.1 Descriptions of scenarios

According to the Rijkswaterstaat (2011b, p. 87), the current design duration of a storm surge (stormopzetduur) is 29 hours. In addition, they state this will increase to 40 hours in the future. As this thesis describes the situation before the year 2100, a storm duration t_{SS} of 40 hours is considered. During this 40-hour period, flood defences close and the Rhine-Meuse delta slowly fills because water can't discharge into the North Sea. This is accelerated by fluvial floods on the Rhine and/or Meuse as the flow rate is significantly increased, e.g. at Lobith it increases from 2.200 up to 18.000 m^3s^{-1}.

Let's denote four fluvial flood scenarios, all coinciding with a 40-hour storm surge:

1. No fluvial flood
2. Rhine fluvial flood and Meuse mean flow
3. Meuse fluvial flood and Rhine mean flow
4. Rhine and Meuse fluvial flood

The summary of these four scenarios with their probabilities are given in Table iii.3.6.

§III.3.2 Inventory of probabilities

For the fluvial flood scenarios 2 to 4, an infinite number of permutations is possible as the flood flow rates at Lobith and Borgharen continuously range 2.200–18.000 m^3s^{-1} and 500–4.600 m^3s^{-1} respectively. Moreover, not every permutation is equally likely to happen; larger flood flow rates have lower probabilities. Therefore, the probabilities of a discrete range of permutations should be investigated to determine which flood scenario yields the highest rise in water level. As described in §III.1.2, for the storage basin a flooding risk of 1/2.000 $annum^{-1}$ is acceptable. The permutation that gives the highest rise in water level with a total probability of 1/2.000 $annum^{-1}$, is the decisive scenario from which the required pumping capacity is calculated. There will be permutations that yield higher rise in water levels, but the corresponding probabilities are lower than the acceptable flooding risk of 1/2.000 $annum^{-1}$. E.g. it would not be cost-effective to protect against a one in a million yearly chance of flooding.

To investigate this, the probabilities or return periods of the following events are required:

→ Probability of a +2,5 m NAP storm surge

→ Probability of fluvial flood on the Rhine with maximum flood flow rate X at Lobith

→ Probability of fluvial flood on the Meuse with maximum flood flow rate Y at Borgharen

→ Probability of fluvial flood occurring on the Rhine and Meuse simultaneously

→ Probability that fluvial flood on the Rhine coincides with a 40-hour storm surge

→ Probability that fluvial flood on the Meuse coincides with a 40-hour storm surge

→ Probability that fluvial flood on the Rhine and Meuse simultaneously coincides with a 40-hour storm surge

Probability of a +2,5 m NAP storm surge

For the probability of a storm surge the storm surge level of +2,5 is investigated. This is the highest allowable water level in the storage basin (§III.1.2). For storm surges below this level, it is not necessarily required to close the storm surge barriers as the hinterland is not in immediate danger of flooding.

Vellinga (2008, p. 114) reports the return periods of storm surges as a function of storm surge water level at Hoek van Holland, based on 118 years of measurements. See Figure iii.3.1 for the graph. Before the year 2100, sea level will have risen by 0,85 m (Technische Adviescommissie voor de Waterkeringen, 2002, p. 142). When finding the return period corresponding to a water level h, instead the return period for h – 0,85 should be found from the graph. For the storm surge height of +2,5 m NAP this return period is 3.

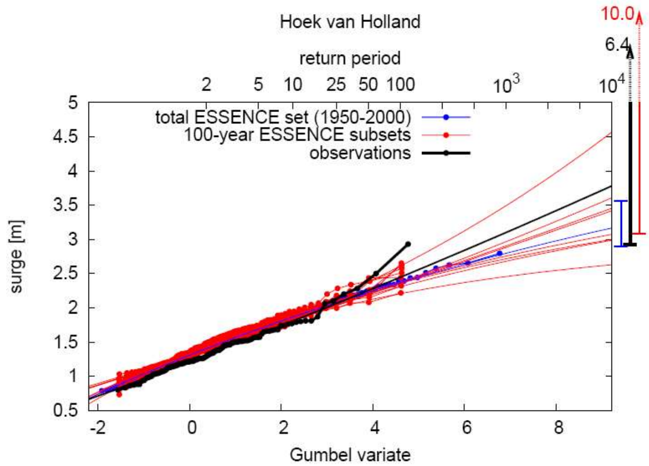

Figure iii.3.1 Hoek van Holland storm surge water levels as a function of return period T. From Vellinga (2008, p. 114)

Probability of fluvial floods on the Rhine or the Meuse

Chbab (2016, p. 16 & p. 50) gives Gumbel plots for flood flow rates of the Rhine and Meuse at Lobith and Borgharen, shown in Figures iii.3.2 and iii.3.3. These are based on measurements from the period 1901–2006 and 1911–2003 respectively, so are not accurate when including the effects of climate change. According to the European Environment Agency, climate change brings more frequent and severe periods of rainfall (2016, pp. 82–84). Specifically, for the Rhine and Meuse catchment area this increase is approximately 20%. This increase should be considered when analysing the Gumbel plots: finding the return period of for example 2.000 m^3s^{-1}, the return period corresponding to 2.000 × 80% = 1.600 m^3s^{-1} should be used.

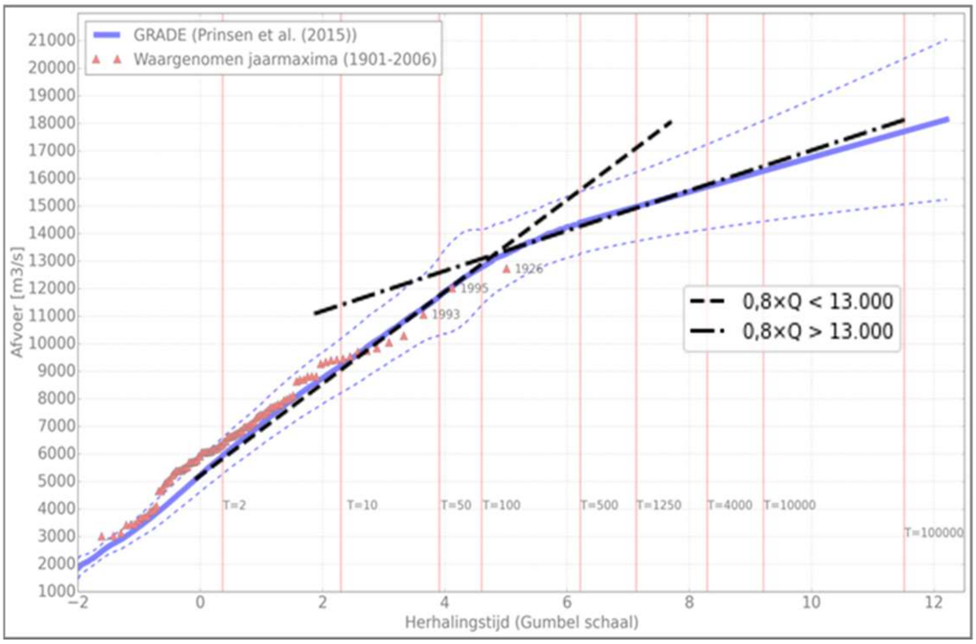

Figure iii.3.2 Return periods T of initial flood flow rates of the Rhine at Lobith with linear fit in black. Adapted from Chbab (2016, p. 16).

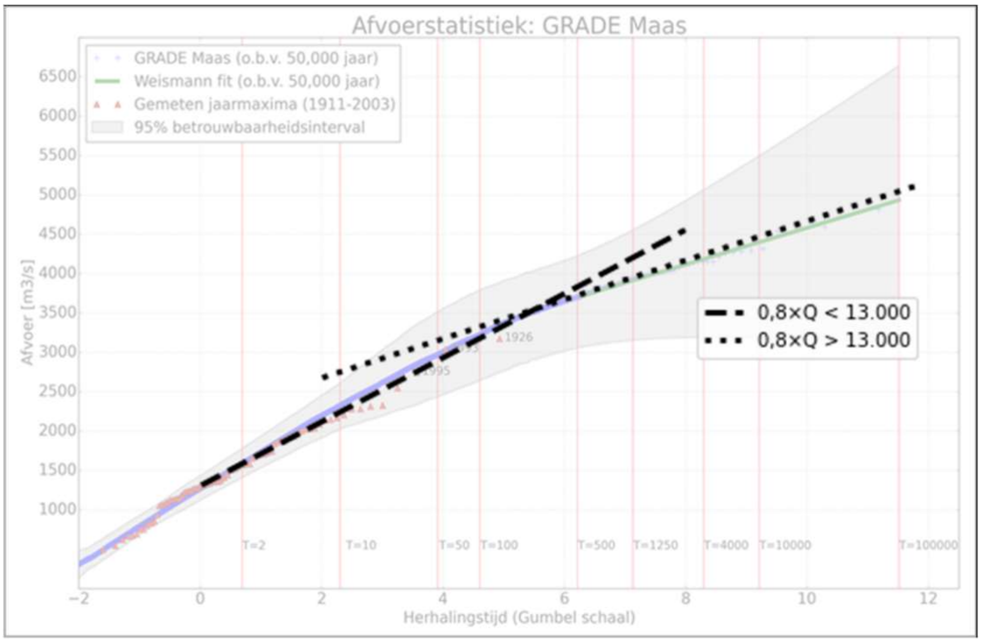

Figure iii.3.3 Return periods T of initial flood flow rates of the Meuse at Borgharen with linear fit in black. Adapted from Chbab (2016, p. 50).

Keeping in mind this increase in severity and frequency of fluvial floods, the return periods for the Rhine and Meuse are calculated with the following method. The values are not read off of the graphs as return periods are hard to determine due to the semi-logarithmic axes. In accordance with the graphs, a linear fit is introduced with the method from Gumbel (1941, pp. 165–176). This linear fit is shown in black in Figures iii.3.2 and iii.3.3.

$$\text{Gumbel return period: } y = -\ln\left(-\ln\left(1-\frac{1}{T}\right)\right) \qquad \textit{equation iii.17}$$

$$\text{Linear fit: } 0{,}8\times\hat{Q} = Ay + B \qquad \textit{equation iii.18}$$

The constants A and B from equation iii.18 are determined from Figures iii.3.2 and iii.3.3 by taking two points T, calculating the corresponding Gumbel return period y with equation iii.17, finding the slope between these two points and then finding the flow rate at y = 0. These constants are determined for two segments, as both graphs are kinked. See Table iii.3.4 for the constants. The return periods T corresponding to a maximum flood flow rate $\hat{Q}$ can be evaluated with the equation below, by rewriting equations iii.17 and iii.18 as a function of T. See Table iii.3.5 for the results.

$$T = \left(1-\exp(-\exp(-\frac{0{,}8\times\hat{Q}-B}{A}))\right)^{-1} \qquad \textit{equation iii.19}$$

Table iii.3.4 Constants for the linear Gumbel fit, equation iii.2.

	Rhine		Meuse	
	$0{,}8\times\hat{Q} < 13.000$	$0{,}8\times\hat{Q} > 13.000$	$0{,}8\times\hat{Q} < 3.250$	$0{,}8\times\hat{Q} > 3.250$
Constant *A*	1.653	723	413	253
Constant *B*	5.000	9.674	1.200	2.085

Table iii.3.5 Maximum Rhine and Meuse flood flow rates and their return periods, from Chbab (2016, p. 16 & p. 50).

Rhine		Meuse	
Lobith maximum flood flow rate $\hat{Q}_{R,FLOOD}$ [m^{3}s^{-1}]	Return period T [annum]	Borgharen maximum flood flow rate $\hat{Q}_{M,FLOOD}$ [m^{3}s^{-1}]	Return period T [annum]
4.000	1,1	1.000	1,1
6.000	1,5	1.500	1,6
8.000	2,9	2.000	3,2
10.000	6,7	2.500	7,5
12.000	16,7	3.000	18,8
14.000	43	3.500	48,6
16.000	112	4.000	127
18.000	690	4.600	547

Probability of fluvial flood on the Rhine and Meuse simultaneously

The worst-case scenario would be fluvial floods occurring on both the Rhine and Meuse simultaneously; is this probable? Jülich & Lindner state that the Meuse is a rainfall river (2005, p. 25) whilst the Rhine is both a rainfall and snowmelt river (pp. 30–31). Therefore, this scenario would only be possible for rainfall in the catchment areas of both rivers. Historical data confirms this has indeed occurred in the past: in the period 1824–2005 the occurrence of fluvial floods on both the Rhine and Meuse simultaneously was recorded 8 times (Jülich & Lindner, pp. 43–44). This roughly gives a probability of 1/23 annum^{-1}. With the 20% increase in frequency of extreme precipitation due to climate change, this probability increases to 1/18 annum^{-1}.

Probability that fluvial floods coincide with a 40-hour-storm surge

In section §III.6 the practical time period T_{PRAC} of fluvial flood waves is calculated for scenarios 2, 3 and 4. These are 14, 11 and 12,5 days respectively—independent of maximum flood flow rate.

Given a year with a storm surge and a fluvial flood, the probability of these coinciding would be to find the time period these can overlap. This is 14/365, 11/365 and 12,5/365 annum^{-1} respectively for the scenarios specified above.

§III.3.3 Probabilities of the fluvial flood scenarios

With all probabilities of events inventoried, the probabilities of the flood scenarios can be calculated. A calculation example is given for each of the four scenarios. A summary with return periods of all the discretised permutations is shown in Table iii.3.6 on the next page. NB this table only shows the return periods of the storage basin configuration with a +2,5 m NAP design water level.

Probability of the first scenario

The probability of the first scenario, a 40-hour +2,5 m NAP-high storm surge without fluvial floods, is 1/3 annum^{-1} as determined earlier.

Probability of the second scenario

The second scenario is a 40-hour storm surge coinciding with Rhine fluvial flood. This probability is calculated with the following multiplication: (probability of a 40-hour +2,5 m NAP-high storm surge) × (probability of fluvial flood on the Rhine with maximum flood flow rate Y at Lobith) × (probability that fluvial flood on the Rhine coincides with a 40-hour storm surge). For example, the probability of a 12.000 m^{3}s^{-1} flood flow rate at Lobith coinciding with +2,5 m NAP-high storm surge is: 1/3 × 1/16,7 × 14/365 = 1/1.310 annum^{-1}.

Probability of the third scenario

The third scenario is a 40-hour storm surge coinciding with Meuse fluvial flood. The calculation is the same as for the second scenario, except then for the Meuse instead of the Rhine. For example, the probability of a 3.500 m^{3}s^{-1} flood flow rate at Borgharen coinciding with a +2,5 m NAP-high storm surge is: 1/3 × 1/48,6 × 11/365 = 1/4.840 annum^{-1}.

Probability of the fourth scenario

The fourth scenario is a 40-hour storm surge coinciding with Rhine and Meuse fluvial flood. This probability is calculated with the following multiplication: (a 40-hour +2,5 m NAP-high storm surge) × (probability of fluvial flood on the Rhine with maximum flood flow rate Y at Lobith) × (probability of fluvial flood on the Meuse with maximum flood flow rate Z at Borgharen)× (probability that fluvial flood on the Rhine and Meuse simultaneously, coincides with a 40-hour storm surge) × (probability of fluvial flood occurring on the Rhine and Meuse simultaneously). For example, the probability of an 8.000 m^{3}s^{-1} flood flow rate at Lobith and a 2.500 m^{3}s^{-1} flood flow rate at Borgharen coinciding with a +2,5 m NAP-high storm surge is: 1/3 × 1/2,9 × 1/7,5 × 1/18 × 12,5/365 = 1/34.300 annum^{-1}.

From the discrete set presented in Table iii.3.5, all the possible permutations of the four scenarios are calculated. See the table on the next page.

Table iii.3.6 Return periods [annum] of the scenarios: a 40-hour +2,5 m NAP-high storm surge coinciding with 1) no fluvial flood, 2) Rhine flood, 3) Meuse flood and 4) Rhine and Meuse flood. Values rounded to two significant digits.

River		Meuse								
	Flow type	Mean	Fluvial flood							
River	Flow rate [m^3s^{-1}]	500	1.000	1.500	2.000	2.500	3.000	3.500	4.000	4.600
	Mean 2.200	3	100	150	290	680	1.700	4.400	12.000	50.000
	Fluvial flood 4.000	90	1.900	2.800	5.600	13.000	33.000	84.000	220.000	950.000
	6.000	120	2.600	3.800	7.600	18.000	44.000	110.000	300.000	1.300.000
	8.000	240	5.000	7.300	15.000	34.000	86.000	220.000	580.000	2.500.000
	10.000	540	12.000	17.000	34.000	79.000	200.000	510.000	1.300.000	5.800.000
	12.000	1.400	29.000	42.000	84.000	200.000	500.000	1.300.000	3.300.000	14.000.000
	14.000	3.500	75.000	110.000	220.000	510.000	1.300.000	3.300.000	8.600.000	37.000.000
	16.000	9.100	190.000	280.000	570.000	1.300.000	3.300.000	8.600.000	22.000.000	97.000.000
	18.000	56.000	1.200.000	1.700.000	3.500.000	8.200.000	20.000.000	53.000.000	140.000.000	600.000.000

Scenario 1	Scenario 2
Scenario 3	Scenario 4

§III.3.4 The decisive fluvial flood scenario

It is to no surprise that the worst-case scenario has an incredibly low probability: once every 600 million years. Everything has to line up for this to happen: a once in three year storm needs to occur simultaneously (to the day) with a once in 690 years Rhine flood and a once in 547 years Meuse flood.

As stated in §III.1.2 the acceptable flooding risk is 1/2.000 annum^{-1} for the storage basin in this calculation model. From Table iii.3.6 it can be seen that the majority of the permutations pose lower probabilities than the acceptable risk. These can therefore be discarded.

Intuitively, from this discrete set, the flood scenario of 12.000 m^3s^{-1} Rhine flood and Meuse mean flow, with a probability of 1/1.400 annum^{-1}, seems to be the decisive permutation as its combined flow rate (12.500 m^3s^{-1}) is relatively the largest. The exact flood flow rate at Lobith corresponding to a probability of 1/2.000 annum^{-1} is 12.900 m^3s^{-1}; **this is the decisive flood scenario for a storm surge of +2,5 m NAP.**

This is the most extreme scenario that occurs every 2.000 years and for this scenario it should be calculated whether the acceptable flood risk of 1/2.000 annum^{-1} is preserved. The answer to this is found in §III.6.4.

For the third scenario, the exact flood flow rate at Borgharen corresponding to a probability of 1/2.000 annum^{-1} is 3.036 m^3s^{-1}.

§III.4 Flow trajectories and river characteristics

As all flood defences are closed due to storm surges, water collects at the storage basin from Figure iii.1.1. The question now is: what trajectory does water from Lobith and Borgharen follow to reach this basin? These trajectories and their characteristics are defined here.

§III.4.1 Flow trajectories from Lobith and Borgharen to the storage basin

First, let's investigate the Rhine. The Rhine bifurcates into three rivers near Lobith: Nederrijn, Waal and IJssel. Flow in the former two meet downstream whilst the IJssel continues as a separate river and enters the North Sea via the IJsselmeer and the Wadden Sea. Winkelhorst (2013, p. 73) reports the distribution of flow for the bifurcation point at Lobith. The relative flow distribution is shown in the figure below. With flow entering the Nederrijn and the Waal, already two trajectories are defined towards the basin.

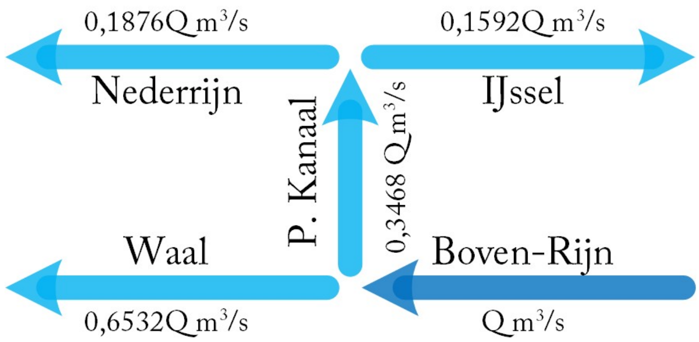

Figure iii.4.1 Schematisation of Rhine bifurcation at Lobith, P. Kanaal: Pannerdensch Kanaal. Tributaries and their relative flow rates shown. Data from Winkelhorst (2013, p. 73).

Now a textual description is given of four trajectories in total. An overview of the trajectories, to scale, is shown in Figure iii.4.3 and a schematisation with relative flow rates is shown in Figure iii.4.4. In reality, the course of flow towards this basin would be more complicated than presented here. To keep it simple yet realistic, the four most likely trajectories are modelled; these are the shortest trajectories.

Flow entering the Waal

From Figure iii.4.1, for flow entering the Waal the following trajectory (1) is defined: *Lobith* → Boven-Rijn (6,0 km) → *Millingen* → Waal (85 km) → *Woudrichem* → Boven-Merwede (8,8 km) → *Werkendam* → Nieuwe Merwede (21 km) → *Hollandsch Diep* (lengths: Rijkswaterstaat, n.d.-a; Zoom Earth, 2020). This is the shortest distance between Lobith and the basin and is in total 120,8 km. It is not the only possible connection: at Werkendam the Boven-Merwede bifurcates into the Nieuwe Merwede and the Beneden-Merwede, see Figure iii.4.2 for a schematisation. The distribution of flow at the bifurcation point can be approximated by relative conveyance width of the rivers. Visual inspection with Zoom Earth (2020) measures a conveyance width of 200 m for the Beneden-Merwede and 400 m for the Nieuwe Merwede at the bifurcation point. Therefore, 2/3 of flow in the Boven-Merwede takes the first trajectory and 1/3 of flow the second trajectory.

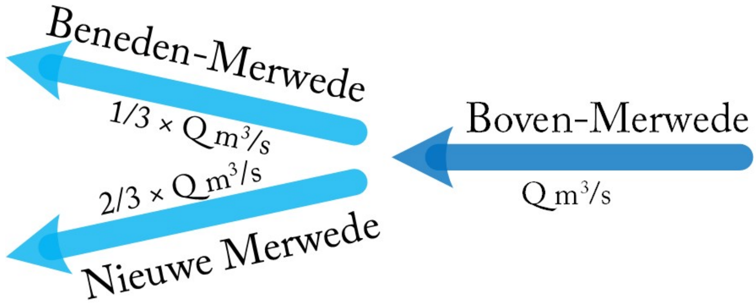

Figure iii.4.2 Schematisation of Boven-Merwede bifurcation at Werkendam

Water from the Beneden-Merwede can then flow via the Oude Maas and the Dordtsche Kil into the basin. The second trajectory summarised: *Lobith* → Boven-Rijn (6,0 km) → *Millingen* → Waal (85 km) → *Woudrichem* → Boven-Merwede (8,8 km) → *Werkendam* → Beneden-Merwede (14,8 km) → *Dordrecht* → Oude Maas (4,2 km) → *Dordrecht* → Dordtsche Kil (9 km) → *Hollandsch Diep*. This is 140 km in total (lengths: Rijkswaterstaat, n.d.-a; Zoom Earth, 2020).

Flow entering the Nederrijn

From Figure iii.4.1, for flow via the Nederrijn can enter the basin via multiple trajectories. Here, only one trajectory is modelled; the shortest trajectory. For longer trajectories, flow takes longer to reach the basin. The consequence of disregarding these longer trajectories is that the total flow from trajectory 3 into the storage basin during the storm surge is an overestimate—which is always better than an underestimate. However, as flow in the Nederrijn (0,1876×Q) is relatively lower than that of the Waal (0,6532×Q), this effect is assumed negligible. The shortest trajectory (3) is: *Lobith* → Boven-Rijn (6,0 km) → *Millingen* → Pannerdensch Kanaal (11,0 km) → *IJsselkop* → Nederrijn (54 km) → *Wijk bij Duurstede* → Lek (62 km) → *Krimpen aan de Lek* → Noord (8,6 km) → *Dordrecht* → Oude Maas (4,2 km) → *Dordrecht* → Dordtsche Kil (9 km) → *Hollandsch Diep* (lengths: Rijkswaterstaat, n.d.-a; Zoom Earth, 2020). This is 154,8 km in total.

Flow from the Meuse

For the Meuse, only a single trajectory is possible. This trajectory (4) is: *Borgharen* → Maas (196 km) → *Well* → Bersche Maas (24,5 km) → *Geertruidenberg* → Amer (12 km) → *Hollandsch Diep* (lengths: Rijkswaterstaat, n.d.-a). In total this is 232,5 km.

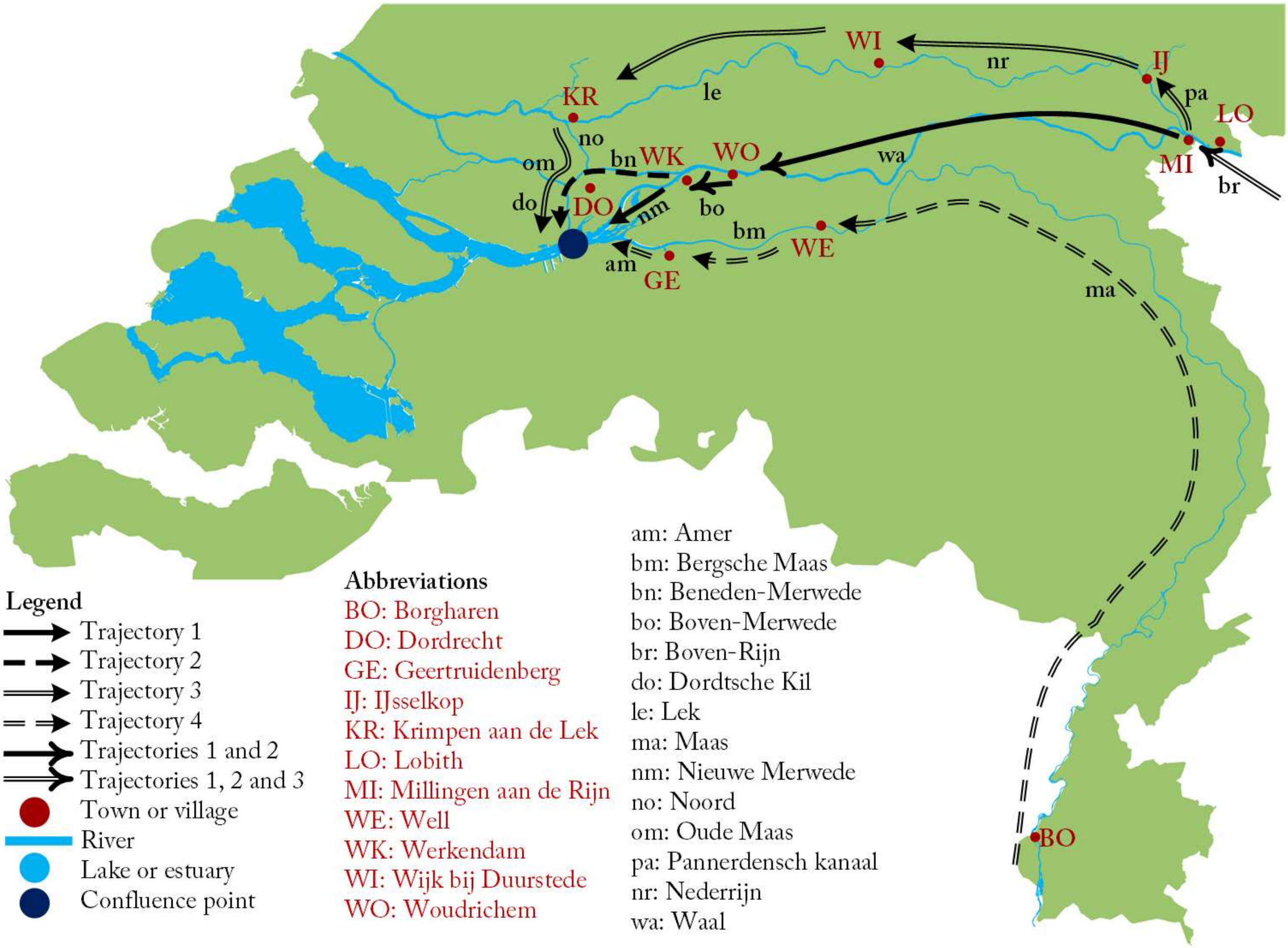

Figure iii.4.3 The four flow trajectories of the calculation model. Created with open-source data from Openstreetmap (2020).

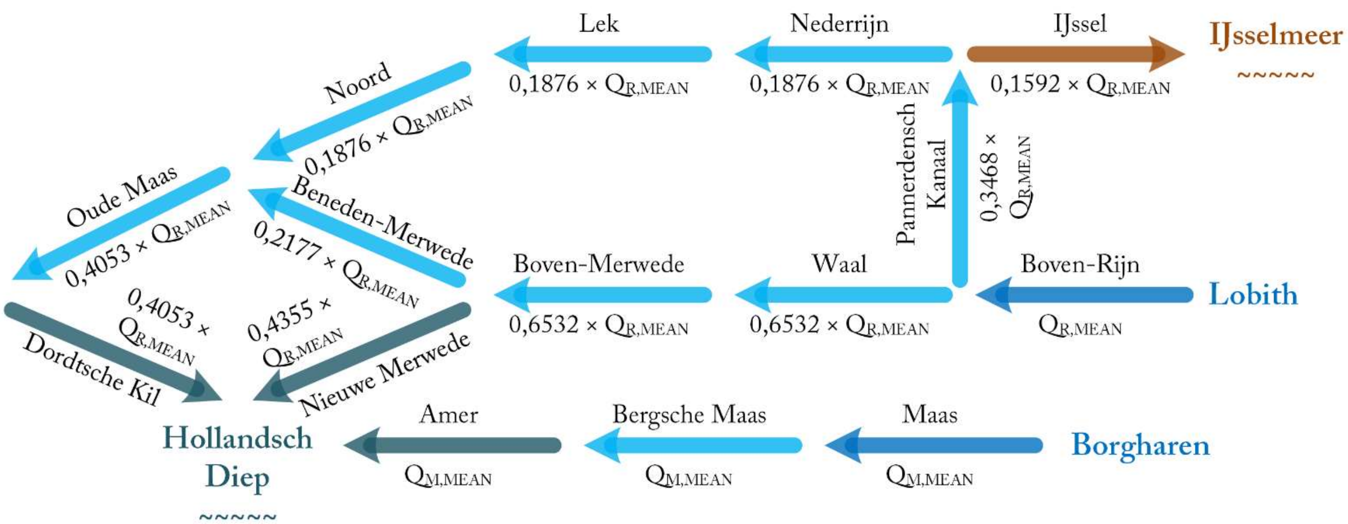

Figure iii.4.4 Schematisation of the flow trajectories used in this calculation model with distributions of mean flow rates.

§III.4.2 River characteristics

In this section, the relevant characteristics of the rivers and canals from **Figure iii.4.4** are presented. These characteristics are the lengths L, the conveyance widths B_C, the storage widths B, the depths d, the bed slopes i_B and the flood wave velocities C_{FW}. All characteristics are summarised in **Table iii.4.8**.

River dimensions

The lengths L from the rivers is from data from Rijkswaterstaat (n.d.-a) and, if data is missing, measured with satellite imagery of Zoom Earth (2020).

The conveyance widths B_C and the storage width B are determined from satellite imagery of Zoom Earth (2020). For every river, at four evenly-spaced points along the river course, these widths are measured with the built-in distance measuring tool. For smaller rivers, like the Amer, only two points were measured. At the same random points, the depths d are calculated with Navionics (2020) so that the depth can be averaged over the entire course.

Riverbed slopes

The bed slopes i_b are found with the following method. In the Waterinfo database of Rijkswaterstaat, gauging stations are located at every bifurcation and confluence point, see **Figure iii.4.5**. The average water level at every gauging station is calculated with data from Rijkswaterstaat (2020): from 01-01-2019 00:00 up to, and including 31-12-2019 23:50. With Navionics (2020) the average depth along the conveyance width at every gauging station is determined. Subtracting the average depth by the average water level yields the depth of the bed with respect to NAP. **Table iii.4.6** on the next page shows the parameters for the gauging stations.

With the bed levels at the gauging stations in **Table iii.4.6**, the bed slopes can be calculated for the rivers. This is done by dividing the difference in bed depth of two gauging stations by their distance, see **Table iii.4.7**. The bed slope value is positive if the bed level decreases.

NB that for the Bergsche Maas and the Boven-Merwede the bed slope is negative; an adverse slope. Water travelling downstream will experience a rising bed level; like climbing a shallow hill. Moreover, no gauging station is present at the intersection of the Oude Maas and the Dordtsche Kil. Therefore, the bed slope is presented for both rivers combined.

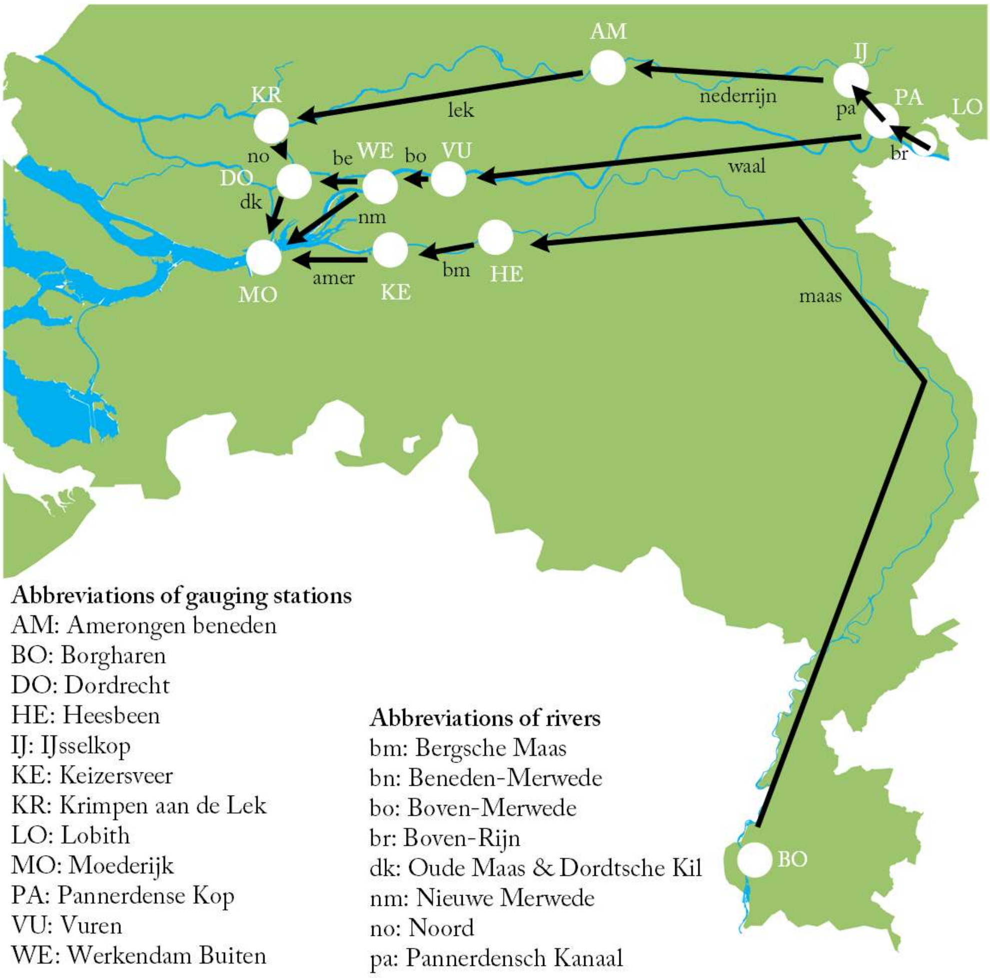

Figure iii.4.5 Locations of gauging stations and rivers between them (Rijkswaterstaat, 2020). Created with open-source data from Openstreetmap (2020)

Table iii.4.6 Bed levels at gauging stations calculated with average water levels and average depth. Average water levels from data between 01-01-2019 00:00 and 31-12-2019 23:50 of Rijkswaterstaat (2020) and average depth from Navionics (2020).

Gauging station	Abbreviation	Average water level [m NAP]		Average depth [m]		Bed level [m NAP]
Amerongen beneden	AM	+3,78	-	4,0	=	-0,22
Borgharen	BO	+38,78	-	5,0	=	+33,78
Dordrecht	DO	+0,47	-	6,5	=	-6,03
Heesbeen	HE	+0,65	-	5,9	=	-5,25
IJsselkop	IJ	+8,23	-	4,5	=	+3,73
Keizersveer	KE	+0,56	-	4,5	=	-3,94
Krimpen aan de Lek	KR	+0,36	-	5,8	=	-5,44
Lobith	LO	+8,93	-	4,5	=	+4,43

Gauging station	Abbreviation	Average water level [m NAP]		Average depth [m]		Bed level [m NAP]
Moerdijk	MO	+0,52	-	7,0	=	-6,48
Pannerdense Kop	PA	+8,61	-	4,6	=	+4,01
Vuren	VU	+0,86	-	5,1	=	-4,24
Werkendam buiten	WE	+0,67	-	4,3	=	-3,63

Table iii.4.7 Bed slopes of the rivers calculated with bed level differences and distance between gauging stations. Distances measured with satellite imagery from Zoom Earth (2020).

River	Gauging stations	Bed level difference [m]	Distance [km]	Bed slope [m/km]
Amer	KE to MO	-2,54	20,2	+0,126
Beneden-Merwede	WE to DO	-2,40	15,6	+0,154
Bergsche Maas	HE to KE	+1,31	17,1	-0,077
Boven-Merwede	VU to WE	+0,61	10,6	-0,058
Boven-Rijn	LO to PA	-0,42	5,4	+0,078
Dordtsche Kil & Oude Maas	DO to MO	-0,45	14,9	+0,030
Lek	AM to KR	-5,22	64,1	+0,081
Maas	BO to HE	-39,03	210,2	+0,186
Nieuwe Merwede	WE to MO	-2,4	23,1	+0,104
Noord	KR to DO	-0,59	9,4	+0,063
Nederrijn	IJ to AM	-3,95	43,8	+0,090
Pannerdensch Kanaal	PA to IJ	-0,28	11,1	+0,025
Waal	PA to VU	-8,25	82,5	+0,100

Flood wave velocities

The flood wave propagation velocity can be calculated with the following equation from Battjes & Labeur (2017, p. 147):

$$C_{FW} = \frac{3}{2}\frac{B_C}{B}\sqrt{\frac{g \times d \times i_B}{c_f}} \qquad \textit{equation iii.20}$$

In this equation B_C is the conveyance width of the river, B is the storage width of the river, g is the gravitational acceleration (9,81 ms^{-12}), d is the water depth, i_B is the bed slope and c_f is the friction slope. Julien et al. (2002, p. 1046) have calculated the dimensionless Darcy-Wesibach friction coefficient f during the 1998 Rhine flood. They determined this coefficient at 0,04 during the peak of the flood. Moreover, this coefficient was determined for both the Nederrijn and the Waal. Flood friction coefficients for the distributaries of the Waal and the Nederrijn (Lek, Noord, Boven-Merwede etc.), as well as the Meuse and its distributaries (Amer and Bergsche Maas) could not be found in literature. As these distributaries are all part of the same Delta, it is deemed unlikely that geomorphological characteristics of these rivers differ greatly. Therefore, for all rivers, the Darcy-Weisbach friction coefficient of 0,04 is used. According to Battjes & Labeur (2017, p. 178), the Darcy-Weisbach friction coefficient f and the friction slope c_f are related with the following equation:

$$c_f = \frac{f}{8} \qquad \textit{equation iii.21}$$

All resulting parameters and the flood wave propagation velocity C_{FW} are shown in Table iii.4.8.

Table iii.4.8 River and canal characteristics. Lengths from Rijkswaterstaat (n.d.-a) and Zoom Earth (2020). Conveyance and storage width measured from satellite imagery of Zoom Earth (2020). Depths from Navionics (2020).

River	Length L [km]	Conveyance width B_C [m]	Storage width B [m]	Depth d [m]	Bed slope i_B [m/km]	Flood wave velocity C_{FW} [ms^{-1}]
Amer	12	380	480	4,5	+0,126	1,25
Beneden-Merwede	14,8	200	300	5,0	+0,154	1,23
Bergsche Maas	24,5	200	200	6,0	-0,077	2,40
Boven-Merwede	8,8	360	400	5,5	-0,058	1,14
Boven-Rijn	6,0	320	400	4,5	+0,078	1,00
D. Kil & Oude Maas	13,2	280	280	6,5	+0,030	0,93
Lek	62	200	250	5,0	+0,081	1,07
Maas	196	140	140	7,0	+0,186	2,40
Nederrijn	54	100	150	5,5	+0,090	0,99
Nieuwe Merwede	21	500	650	4,3	+0,104	1,08
Noord	8,6	260	260	6,0	+0,063	1,29
Pannerdensch Kanaal	11,0	130	160	5,0	+0,025	0,60
Waal	85	300	350	4,0	+0,100	1,14

Note that due to the adverse slopes of the Bergsche Maas and the Boven-Merwede, equation iii.20 can't be solved. It is certainly not the case that the flood wave simply turns backwards and reflection is also unlikely as height profile of the wave is rather gradual. To circumvent this, the flood wave propagation velocities of the upstream river are assumed for the Bergsche Maas and Boven-Merwede: 2,40 ms^{-1} (Meuse) and 1,14 ms^{-1} (Waal) respectively. The effect of the adverse slope is elaborated in §III.5.3.

§III.5 Mathematical formulation of storage basin inflow

The factor $Q_{SB,IN}$ from equation iii.15 is by far the most complicated. Although we know the maximum flood flow rates at Lobith and Borgharen, Battjes (2017, pp. 151–152) states that as the flood wave propagates, the maximum flow rate decreases and the wavelength increases. To accurately model the conditions at the inlet of the storage basin (shown as „confluence point" in Figure iii.4.3), first a suitable mathematical description needs to be given for the inflow $Q_{SB,IN}$, secondly the wavelength of the flood waves need to be determined at the origin of the trajectories, then the increase in wavelength should be calculated over the trajectories and consequently the decreased maximum flow rate can be obtained. Finally, the travel times and time periods of the flood waves are presented.

§III.5.1 Mathematical description of the inflow

According to Ministerie van Verkeer en Waterstaat (2006, p. 35), flow rate functions of flood waves at Lobith and Borgharen can be modelled as a time-dependent gaussian function, see Figures iii.5.1 and iii.5.2. So, let's model the inflow of the basin with the following equation:

$$Q_{SB,IN}(t) \equiv \underbrace{\tilde{Q} e^{-\left(\frac{t-b_t}{c_{t,init}+\Delta c_t}\right)^2}}_{\text{Flood wave}} + \underbrace{Q_{MEAN}}_{\text{Mean flow}} \qquad \textit{equation iii.22}$$

In this equation $\tilde{Q}$ is the maximum flood flow rate of a river entering the described basin, b_t is the gaussian temporal mean (timestamp when maximum flow rate occurs), $c_{t,init}$ is the initial temporal standard deviation, Δc_t is the change in temporal standard deviation and Q_{MEAN} is the constant mean flow. As there are four trajectories defined, let's construct equation iii.5 for each of the four trajectories:

$$Q_{SB,IN}(t) = \left(\sum_{i}^{4} \underbrace{\tilde{Q}_i e^{-\left(\frac{t-b_{t,i}}{c_{t,init,i}+\Delta c_{t,i}}\right)^2}}_{\text{Trajectory } i} \right) + \underbrace{Q_{MEAN}}_{\text{Mean flow}} \qquad \textit{equation iii.23}$$

Mean flow of the Rhine at Lobith is 2.200 m^3s^{-1} (Ministerie van Verkeer en Waterstaat [V&W], 2007, p. 36). With help of Figure iii.4.4 it follows that 350 m^3s^{-1} of the mean flow enters the IJssel and 1.850 m^3s^{-1} flows towards the basin. Mean flow of the Meuse at Borgharen is 500 m^3s^{-1} and flows fully towards the basin (V&W, 2007, p. 38). Therefore, in this model the constant mean flow Q_{MEAN} is 1.850 + 500 = 2.350 m^3s^{-1}.

The parameters from equation iii.23 are elaborated in the next sections. First, $c_{t,init}$ is calculated for both Rhine and Meuse at Lobith and Borgharen. Then, Δc_t is calculated and in the fourth section $\tilde{Q}$ is calculated. Next, b_t is elaborated in the fifth section and the sixth section presents the result and the practical wave period T_{PRAC}.

§III.5.2 Flood wave initial temporal standard deviation

The standard flow rate distributions at Lobith and Borgharen are shown in the figure below.

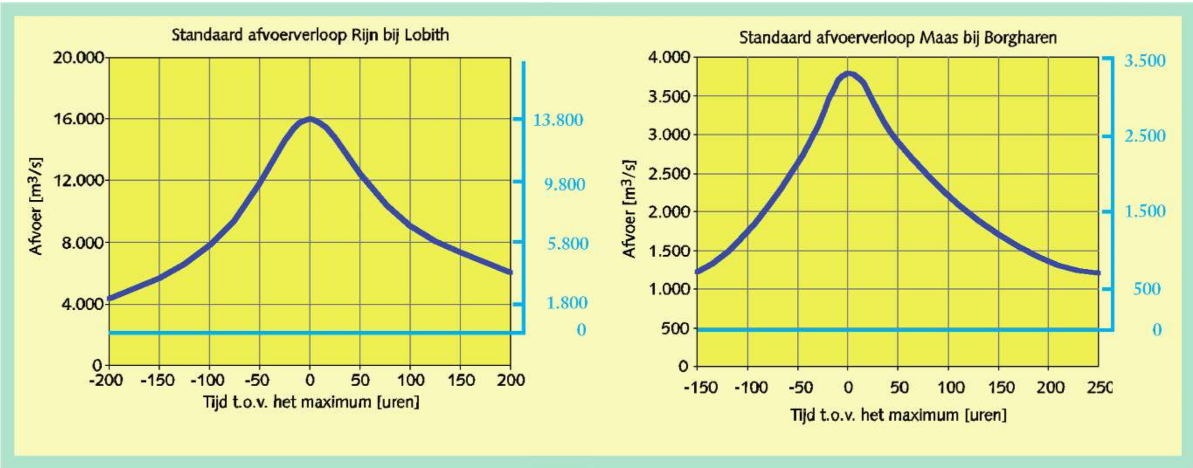

Figure iii.5.1 Graphs of the standard flow rate distribution at Lobith (left) and Borgharen (right) as a function of time. The light blue axes show the flow rate as a consequence of flood wave only. Adapted from Ministerie van Verkeer en Waterstaat (2007, p. 35).

The gaussian functions in the figures above are asymmetrical. See for example the left graph: for -200 hours and 200 hours, the flow rates are 4.000 and 6.500 m^3s^{-1} respectively. This is caused by the phenomenon of hysterises (Battjes, 2017, pp. 148–149). If Figure iii.5.1 is examined again, it can be derived that flow rates are symmetrical between the domain of [-50 hours, 50 hours]. This 100-hour-period is longer than the storm duration of 40 hours, so the hysterises can be ignored.

Now, we need to find the initial temporal standard deviation $c_{t,init}$ of both standard flow rate distributions. In the mathematical model described in step 1, the mean flow is separated from the flood wave. However, Figure iii.5.1 shows them combined. This is easily circumvented: new vertical axes (the light blue axes in Figure iii.5.1) are introduced. These new vertical axes are obtained by vertically transforming the graphs with the mean flow of the Rhine at Lobith (2.200 m^3s^{-1}) and the Meuse at Borgharen (500 m^3s^{-1}) respectively.

Now with these new vertical axes, the initial temporal standard deviation $c_{t,init}$ of the flood wave can be calculated. In **Figure iii.5.1**, the peak of the Rhine flood wave at Lobith is 13.800 m^{3}s^{-1} and occurs at t = 0 hours. It can be modelled with the following gaussian equation:

$$Q_{R,FLOOD}(t) = 13.800e^{-\left(\frac{t}{c_{t,init}}\right)^2} \qquad \textit{equation iii.24}$$

For t = 50 hours, the flow rate Q is 9.800 m^{3}s^{-1}. The only unknown is now $c_{t,init}$ which can be solved:

$$c_{t,init} = \frac{t}{\sqrt{-\ln\left(\frac{Q_{R,FLOOD}(t)}{13.800}\right)}} = \frac{50}{\sqrt{-\ln\left(\frac{9.800}{13.800}\right)}} \approx 3{,}1\times10^5 \text{ s} \qquad \textit{equation iii.25}$$

The same process can be repeated for the standard flow rate distribution graph of Borgharen where the flow rate is 3.250 m^{3}s^{-1} at t = 0 hours and 2.400 m^{3}s^{-1} at t = 50 hours.

$$c_{t,init} = \frac{t}{\sqrt{-\ln\left(\frac{Q_{M,FLOOD}(t)}{13.800}\right)}} = \frac{50}{\sqrt{-\ln\left(\frac{2.400}{3.250}\right)}} \approx 3{,}3\times10^5 \text{ s} \qquad \textit{equation iii.26}$$

Equation iii.24 with the obtained initial temporal standard deviations are overlaid on the standard flow rate distribution graphs in **Figure iii.5.2**.

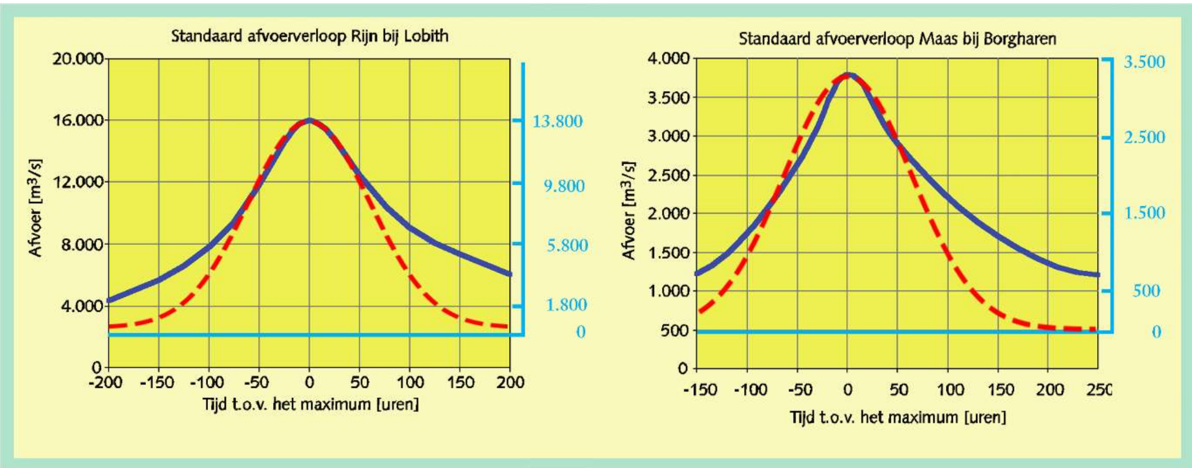

Figure iii.5.2 Graphs of the standard flow rate distribution at Lobith (left) and Borgharen (right) as a function of time. The light blue axes show the flow rate as a consequence of flood wave only. The red lines show the modelled gaussian equation. Adapted from Ministerie van Verkeer en Waterstaat (2007, p. 35).

In **Figure iii.5.2**, both modelled Gaussian equations are extremely accurate for the domain [-50 hours, 50 hours]. Timestamps outside this domain are extremely inaccurate and should not be used for the calculation model. However, in §III.5.5 it is derived that the largest offset to the mean is 33,9 hours, thus this gaussian model can be used for the flood waves.

It should be noted that standard flow rate distribution graphs show a maximum flow rate of 16.000 and 3.750 m^3s^{-1} for Lobith and Borgharen respectively. In this calculation model, however, a variety of maximum flow rates up to 18.000 and 4.600 m^3s^{-1} is used. It could not be concluded from literature review whether the standard distribution graphs show larger or smaller initial temporal standard deviations $c_{t,init}$ for higher or lower maximum flow rates. It is therefore assumed that the initial temporal standard deviations $c_{t,init}$ at Lobith and Borgharen remain constant, regardless of the maximum flow rate.

To summarise, the initial temporal standard deviations $c_{t,init}$ of flood waves modelled with a gaussian function are 3,1 × 10^5 s and 3,3 × 10^5 s for the Rhine at Lobith and Meuse at Borgharen respectively.

§III.5.3 Increase in flood wave temporal standard deviation

In this third step, the change in the temporal standard deviation Δc_t is calculated between Lobith or Borgharen and the basin. This is done for all four trajectories that were formulated in section §III.4.

According to Battjes (pp. 151–152), the change in spatial standard deviation Δc_s of the gaussian function describing a flood wave is:

$$\Delta c_s = \sqrt{\frac{Q_0}{i_b B}\Delta t} \qquad \textit{equation iii.27}$$

Where Q_0 is the initial mean flow rate (before the flood wave), i_b is the bed slope along the trajectory, B is the storage width along the trajectory and Δt is the time difference. The time difference can be calculated by dividing the total trajectory length ΔL by the flood wave propagation velocity C_{FW}. The change in standard deviation Δc_s is however expressed in units of length, whilst equation iii.23 requires a temporal standard deviation c_t, i.e. in units of time. The spatial standard deviation can be converted into temporal standard deviation if the spatial standard deviation is divided by the flood wave propagation velocity. Rewriting the equation yields:

$$\Delta c_t = \frac{\sqrt{\frac{Q_0}{i_b B}\Delta t}}{C_{FW}} = \frac{\sqrt{\frac{Q_0}{i_b B}\frac{\Delta L}{C_{FW}}}}{C_{FW}} = \frac{\sqrt{\frac{Q_0}{i_b B}\Delta L}}{C_{FW}^{\frac{3}{2}}} \qquad \textit{equation iii.28}$$

With the initial mean flow rate Q_0 distribution from Figure iii.4.4 and river characteristics from Table iii.4.8, the change in temporal standard deviation can be calculated for all rivers with equation iii.28.

See the table below. For rivers with an adverse slope, the change in temporal standard deviation is negative: the wavelength decreases.

Table iii.5.3 Change in temporal standard deviation for all rivers and trajectories, and the parameters used to calculate the temporal standard deviation with equation iii.15.

	River	ΔL [km] Length	B [m] Width	i_B [m/km] Bed Slope	Q_0 [m^{3}s^{-1}] Initial mean flow rate	C_{FW} [ms^{-1}] Flood wave propagation velocity	Δc_t [× 10^3 s] Change in temporal standard deviation
Meuse	Amer	12	480	+0,126	500	1,25	+7,13
	Bergsche Maas	24,5	200	-0,077	500	2,40	-7,59
	Meuse	196	140	+0,186	500	2,40	+16,50
Rhine	Beneden-Merwede	14,8	300	+0,154	479	1,23	+9,08
	Boven-Merwede	8,8	400	-0,058	1.437	1,14	-19,18
	Boven-Rijn	6,0	400	+0,078	2.200	1,00	+20,57
	D. Kil & Oude Maas	13,2	280	+0,030	892	0,93	+41,75
	Lek	62	250	+0,081	413	1,07	+32,13
	Nederrijn	54	150	+0,090	413	0,99	+41,26
	Nieuwe Merwede	21	650	+0,104	958	1,08	+15,37
	Noord	8,6	260	+0,063	413	1,29	+10,05
	Pannerdensch Kanaal	11,0	160	+0,025	763	0,60	+98,56
	Waal	85	350	+0,100	1.437	1,14	+48,53

Trajectory 1	+65,29
Trajectory 2	+100,75
Trajectory 3	+244,32
Trajectory 4	+16,04

§III.5.4 Decrease in maximum flood flow rate at the storage basin inlet

To determine the decrease in maximum flood flow rate, we take a look at the gaussian flood wave model from equation iii.24 but then with mean at t = 0:

$$Q_{SB,IN}(t) = \hat{Q}e^{-\left(\frac{t}{c_{t,init}}\right)^2} \qquad \textit{equation iii.29}$$

Then, with the increase in temporal standard deviation this changes to:

$$Q_{SB,IN}(t) = \tilde{Q}e^{-\left(\frac{t}{c_{t,init}+\Delta c_t}\right)^2} \qquad \textit{equation iii.30}$$

In this equation $\tilde{Q}$ is the decreased maximum flood flow rate. The improper integral, i.e. interval (-∞, +∞), of both equations iii.29 and iii.30 must be equal because the amount of water [m^3] conveyed by the flood wave does not change. For a given initial temporal standard deviation $c_{t,init}$, a calculated change in temporal standard deviation Δc_t, a maximum flood flow rate $\hat{Q}$, the decreased maximum flood flow rate $\tilde{Q}$ can be calculated:

$$\begin{aligned}
&\int_{-\infty}^{+\infty} \hat{Q}e^{-\left(\frac{t}{c_{t,init}}\right)^2} = \int_{-\infty}^{+\infty} \tilde{Q}e^{-\left(\frac{t}{c_{t,init}+\Delta c_t}\right)^2} \\
&\Rightarrow c_{t,init}\sqrt{\pi}\hat{Q} = \left(c_{t,init} + \Delta c_t\right)\sqrt{\pi}\tilde{Q} \\
&\Rightarrow \tilde{Q} = \hat{Q} \times \frac{c_{t,init}}{c_{t,init} + \Delta c_t}
\end{aligned} \qquad \textit{equation iii.31}$$

Now the decrease in maximum flood flow rate can be calculated for all the trajectories. The initial temporal standard deviations at Lobith and Borgharen were calculated in §III.5.2 and are 3,1 × 10^5 and 3,3 × 10^5 seconds respectively, the change in temporal standard deviation is shown in Table iii.5.3. Figure iii.5.4 on the next page shows the relative flood flow rates $\tilde{Q}_{R,F}$ and $\tilde{Q}_{M,F}$ for the Rhine and Meuse respectively for some.

At bifurcation points, the flood flow rate is distributed in accordance with Figure iii.4.4. However, at downstream confluence points, e.g. at the Oude Maas where trajectories 2 and 3 meet, these flow rates are not re-added because they have become asynchronous. Instead, they are super positioned in the calculations, as shown in equation iii.23, with different values of b_t. For this reason, Figure iii.5.4 shows the trajectories bifurcated. This asynchrony is addressed in the next section, §III.5.5.

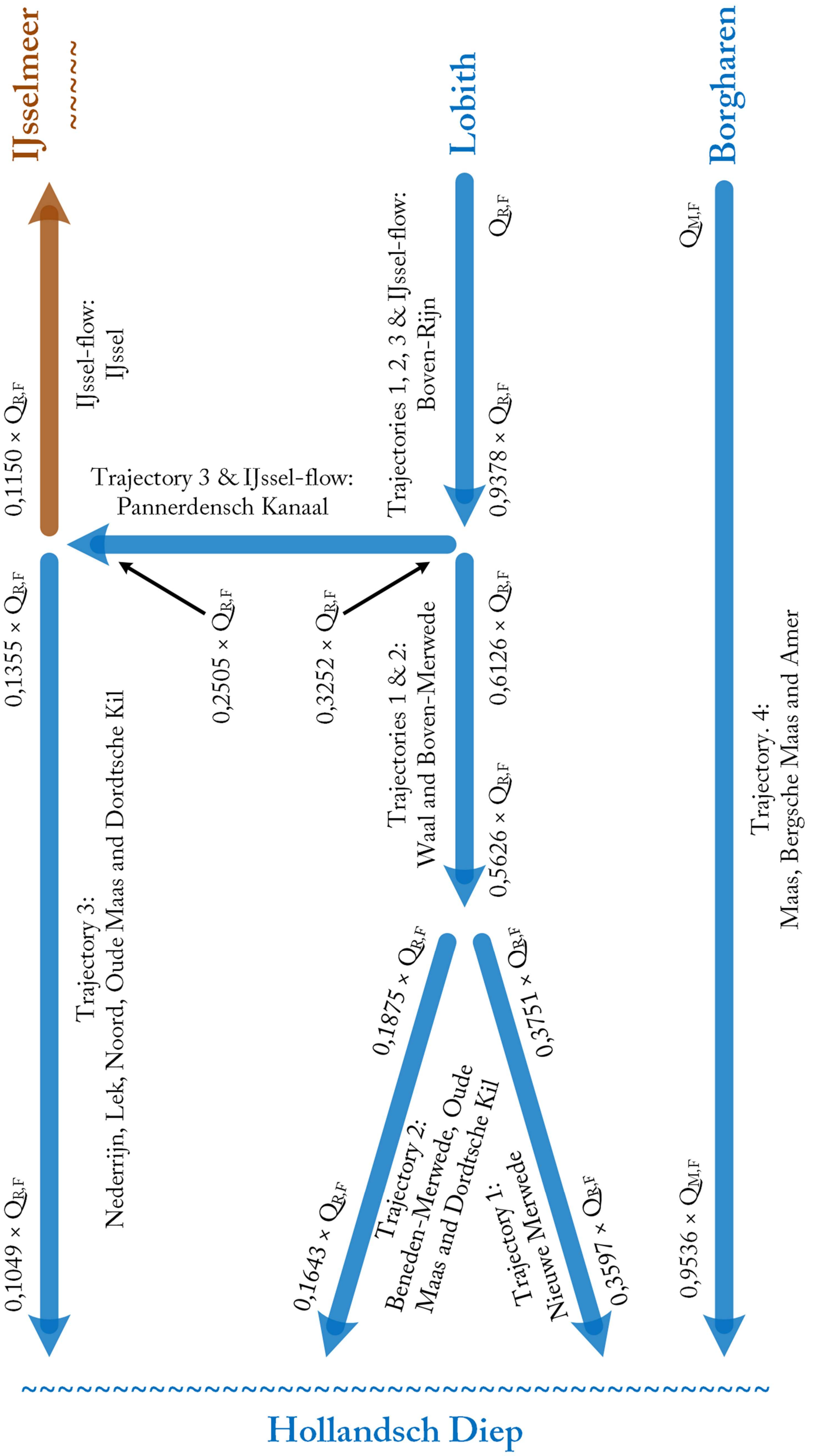

Figure iii.5.4 The flood flow rate for the four trajectories. $\hat{Q}_{R,F}$ and $\hat{Q}_{M,F}$ are the maximum flood flow rates at Lobith and Borgharen respectively.

For the maximum flood flow rates at Lobith and Borgharen from Table iii.3.5, the trajectory maximum flood flow rates $\tilde{Q}_i$ are calculated with help of Figure iii.5.4. See the table below.

Table iii.5.5 Flood flow rates of the four trajectories at the storage basin inlet as function of maximum flood flow rate at Lobith and Borgharen. Final flood flow rate calculated by subtracting the mean flow from the maximum flood flow rate and subsequently multiplying with the values from Figure iii.5.4.

Rhine maximum flood flow rate at Lobith $\hat{Q}_{R,FLOOD}$ [m^3s^{-1}]	$\tilde{Q}_1$ [m^3s^{-1}]	$\tilde{Q}_2$ [m^3s^{-1}]	$\tilde{Q}_3$ [m^3s^{-1}]	**Meuse maximum flood flow rate Borgharen** $\hat{Q}_{M,FLOOD}$ [m^3s^{-1}]	$\tilde{Q}_4$ [m^3s^{-1}]
4.000	1.439	657	420	1.000	954
6.000	2.158	986	629	1.500	1.430
8.000	2.878	1.314	839	2.000	1.907
10.000	3.597	1.643	1.049	2.500	2.384
12.000	4.316	1.972	1.259	3.000	2.861
12.900	4.640	2.119	1.353	3.082	2.939
14.000	5.036	2.300	1.469	3.500	3.338
16.000	5.755	2.629	1.678	4.000	3.814
18.000	6.475	2.957	1.888	4.600	4.387

§III.5.5 Flood wave travel time

In this section, the travel times of the four trajectories are calculated. For the three Rhine trajectories, see the table below. The travel time for flood wave on the Meuse, trajectory 4, is more straightforward: 12,0/1,25 + 24,5/2,40 + 196,0/2,40 = 101 × 10^3 seconds or 28,2 hours.

Table iii.5.6 Travel times of the three Rhine trajectories between Lobith and the storage basin.

River	Length [km]		Wave velocity [ms^{-1}]		Travel time [× 10^3 s]	Trajectories 1	2	3
Beneden-Merwede	14,8	/	1,23	=	12,0			
Boven-Merwede	8,8	/	1,14	=	7,72			
Boven-Rijn	6,0	/	1,00		6,0			
Dordtsche Kil & Oude Maas	13,2	/	0,93	=	14,2			
Lek	62	/	1,07	=	57,9			
Nieuwe Merwede	21	/	1,08	=	19,4			
Noord	8,6	/	1,29	=	6,67			
Nederrijn	54	/	0,99	=	54,5			
Pannerdensch Kanaal	11,0	/	0,60	=	18,3			
Waal	85	/	1,14	=	74,6			
					Σ [× 10^3 s]	108	115	158

The peak of trajectory 1 arrives the earliest. The peaks of trajectories 2 and 3 arrive respectively 7 × 10^3 and 50 × 10^3 seconds or 1,94 and 13,9 hours later at the storage basin. The gaussian temporal mean b_t for trajectories 1 and 4 should be set at t = 20 hours so that the integral is maximised; the storm surge is present at 0 < t < 40 hours. From this follows that b_t is 21,94 and 33,9 hours for trajectories 2 and 3 respectively.

In §III.5.2 it was concluded that for an offset larger than 50 hours, the gaussian model becomes inaccurate. The largest offset is 33,9 hours. This is well within the domain of [-50, +50 hours] thus the gaussian functions can be used.

§III.5.6 Flood wave time period

With all parameters determined for the mathematical model of inflow, equation iii.23 can now be written with the appropriate constants:

$$Q_{SB,IN}(t) = Meuse(t) + Rhine(t) + 2.350 \ [m^3 s^{-1}]$$

$$Meuse(t) = 0{,}9536 \times \hat{Q}_{Borgharen} e^{-\left(\frac{t}{3{,}3\times10^5+16{,}04\times10^3}\right)^2} \qquad \textit{equation iii.32}$$

$$Rhine(t) = \hat{Q}_{Lobith} \begin{Bmatrix} 0{,}3597 e^{-\left(\frac{t}{3{,}1\times10^5+65{,}29\times10^3}\right)^2} \\ +0{,}1643 e^{-\left(\frac{t-7\times10^3}{3{,}1\times10^5+100{,}75\times10^3}\right)^2} \\ +0{,}1049 e^{-\left(\frac{t-50\times10^3}{3{,}1\times10^5+244{,}32\times10^3}\right)^2} \end{Bmatrix}$$

With this equation, all effects of the flood wave propagation can be illustrated: increase in temporal standard deviation (or wavelength if analysed spatially), decrease in maximum flood flow rate and the travel time. See Figure iii.5.7. For Rhine flood flow, the individual trajectories are shown as well. Both figures show flood waves departing at t = 0 hours from Lobith or Borgharen.

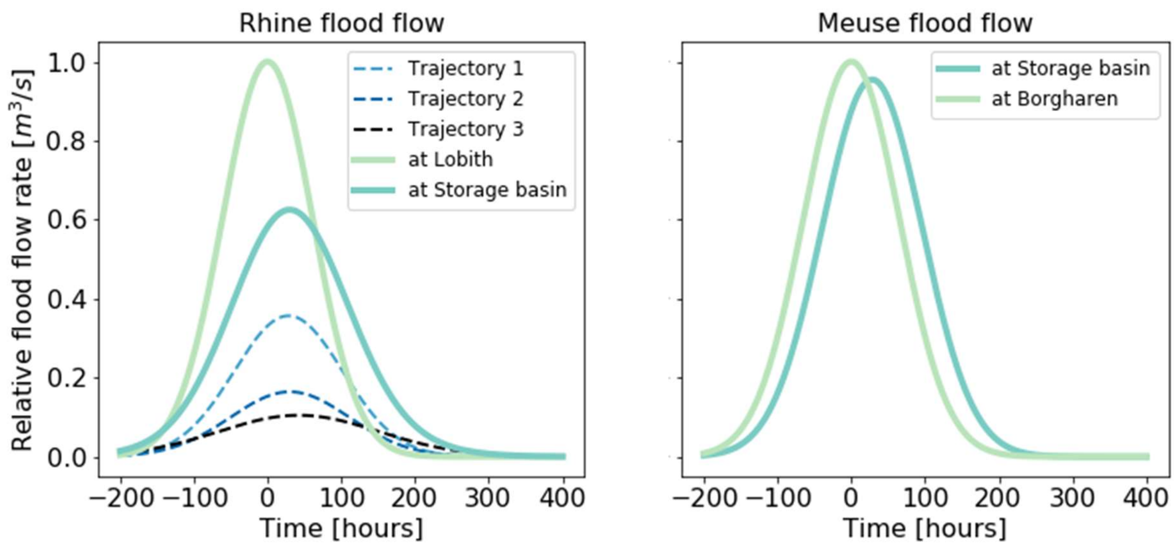

Figure iii.5.7 Relative flood flow rates for the storage basin and at Lobith and Borgharen respectively. Rhine flood flow rate at the storage basin is the sum of trajectories 1 to 3.

From the figure above it can be derived that for Meuse flood flow, the decrease in maximum flood flow rate is minimal; both gaussians are almost equal in height. Concerning Rhine flood flow, the decrease in maximum flood flow rate is significant: a ratio of 0,6.

The determination of the flood wave time period is straightforward for the Meuse as this concerns a single Gaussian function. This period can be retrieved from the Gaussian temporal standard deviation multiplied with some constant *A*: $\left(c_{t,init} + \Delta c_t\right) \times A$ as the time period of a Gaussian function is actually infinite. This is in contrary to the Rhine flood wave, which is a combination of three Gaussian functions with each its own temporal mean and standard deviation; it doesn't have a single temporal standard deviation to derive the time period from.

In light of that, let's introduce the term „practical time period" T_{PRAC}. Let this be the time period of a Gaussian flood wave symmetrically centred around its maximum, so that it covers 95% of the total conveyed water volume. The total conveyed water volume can be determined by summing the improper integrals (-∞, +∞) of each trajectory. See **Figure iii.5.8** for this calculation model of the scenario with Rhine flood flow from **Figure iii.5.7**.

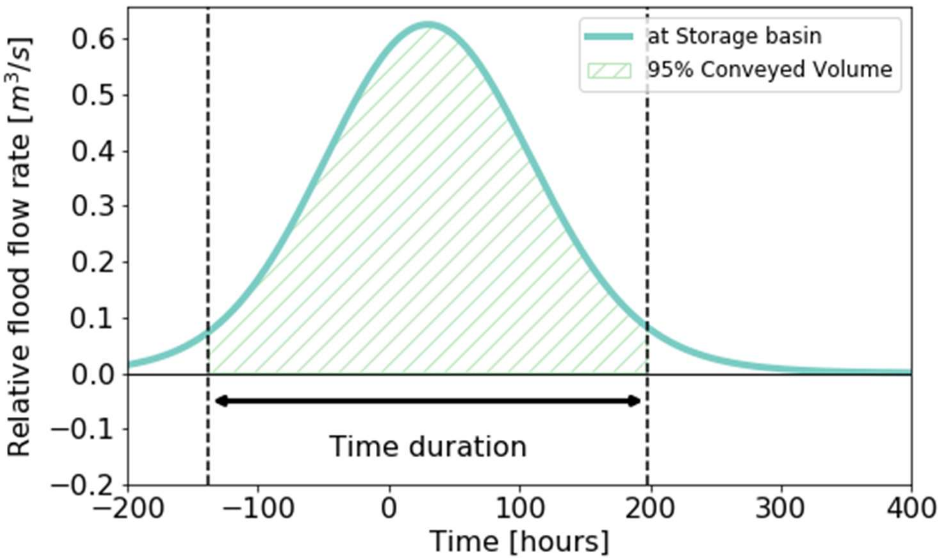

Figure iii.5.8 Practical time period for Rhine flood flow. The time period in this graph is 335 hours.

This calculation is performed for all three flood scenarios: Rhine flood, Meuse flood and Rhine and Meuse flood. The practical time periods T_{PRAC} are shown in the table below. As elaborated in **§III.5.2**, the practical time period is independent of the maximum discharge $\hat{Q}$.

Table iii.5.9 Practical time period for the flood scenarios.

Flood scenario	Practical time period in hours	Practical time period in days
Rhine flood	335 hours	14 days
Meuse flood	266 hours	11 days
Rhine and Meuse flood	298 hours	12,5 days

§III.6 Simulation of the fluvial flood scenarios

With all variables known for the storage basin model, iteration can commence through equations iii.12 to iii.16 with the boundary conditions, the initial conditions, the described operations in pseudo-code form from §III.2.9, the storage basin configurations from Table iii.1.4 and the fluvial flood scenarios presented in Table iii.3.6. For this iteration, a Python (version 3.6.5) program was written in a Jupyter Notebook (version 6.0.3) called „Rijn-Maasdelta overstromingsscenariomodel".

§III.6.1 Fluvial flood scenario Python simulation

In this simulation, the following variables must be manually entered to make calculations:

$\hat{Q}_{LOBITH}$	Maximum flood flow rate at Lobith	[2.200 – 18.000] m^3s^{-1}
$\hat{Q}_{BORGHAREN}$	Maximum flood flow rate at Borgharen	[500 – 4.600] m^3s^{-1}
$A_{SL,VD}$	Volkerakdam sluices effective area	[570; 1.200; 1.350; 2.000] m^2
$A_{SL,GD}$	Grevelingendam sluices effective area	[540; 1.350] m^2
t_{START}	Start of the numerical iteration	Default: -150 hours
t_{STOP}	End of the numerical iteration	Default: +150 hours
Δt	Numerical resolution	Default: 10 seconds
Concept	Storage concept of the storage basin model	GR/ZO/VO, ZO/VO or no storage

The program then returns an informative graph containing plots of all water levels from Figure iii.2.1, the variables from the box above and the (theoretical) highest water level.

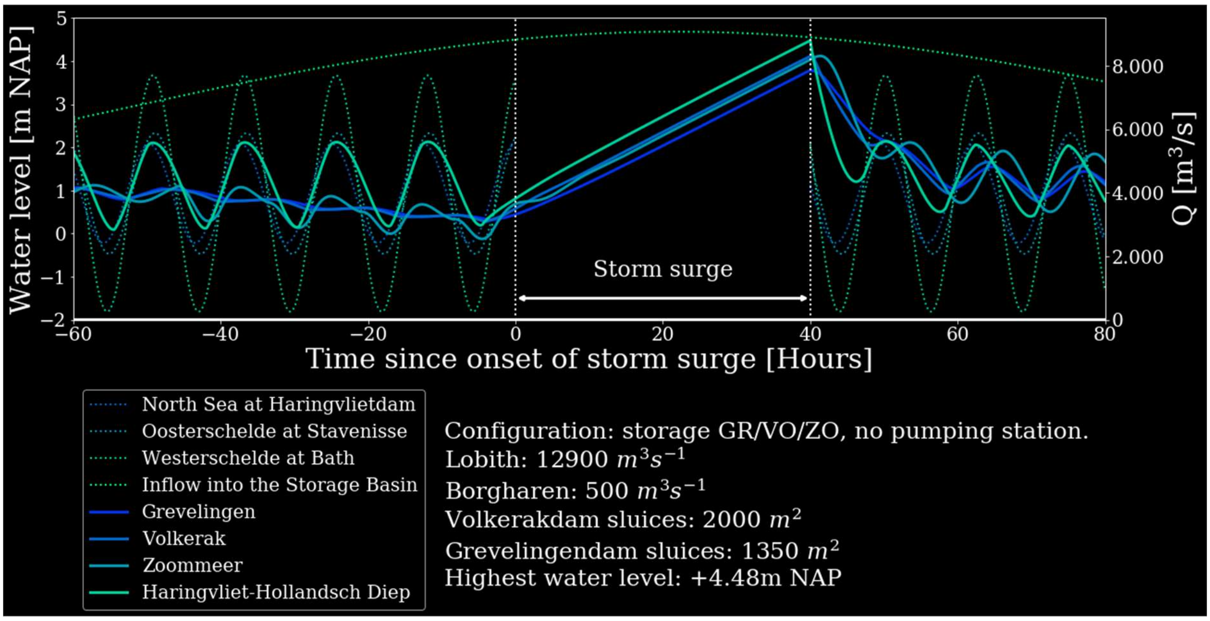

Figure iii.6.1 Example of the informative graph created with the Rhine-Meuse delta flooding scenarios simulation.

§III.6.2 Effects of pre-draining

The solid lines from Figure iii.6.1 are those of the storage basin whilst the dotted lines are those of the boundary conditions: North Sea, Oosterschelde and Westerschelde. These are included to illustrate the pre-draining window. The figure below shows the effects of pre-drainage for the same configuration as in Figure iii.6.1. When water levels in the Oosterschelde and Westerschelde are lower than those of the Grevelingen, Volkerak and Zoommeer, pre-drainage happens; in this period a drop in water level is visible. Outside the pre-draining windows, water levels in the Grevelingen and Volkerak are constant whilst the Zoommeer, due to the long and narrow tidal channels, oscillates.

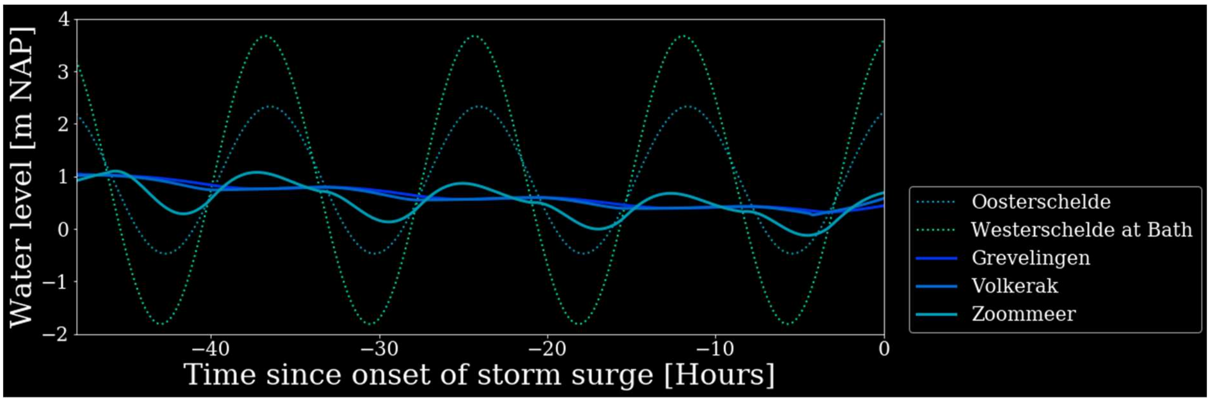

Figure iii.6.2 Example of the effect of pre-draining

The pre-draining depends only on the initial and boundary conditions which don't change within the simulation model. Therefore, the following calculation is applicable to every storage basin configuration and river inflow. In Figure iii.6.2, the water levels of the Zoommeer, Grevelingen and Volkerak dropped 114, 70 and 72 cm respectively. Averaged over the entire storage basin this is 40 cm: quite significant!

§III.6.3 Critical flood flow rates

In §III.3.4 the decisive flood scenario for an exceedance probability of 1/2.000 annum^{-1} was determined to be 12.900 m^3s^{-1} flood flow rate at Lobith coinciding with Meuse flow of 500 m^3s^{-1}. Now, to answer to second sub-question, for each of configurations from Table iii.1.4, the theoretical highest water level, i.e. infinitely high dykes, is calculated with the program. See the table below for the results.

Table iii.6.3 Maximum theoretical water levels [m NAP] for the twelve storage basin configurations for a Lobith flood flow rate of 12.900 m^3s^{-1} and Meuse mean flow with a +2,5 m NAP design water level in the storage basin.

		Volkerak sluices			
		570 m^2	1.350 m^2	1.500 m^2	2.000 m^2
No storage in Grevelingen		+6,73	+6,33	+6,31	+6,26
Storage in Grevelingen,	540 m^2	+6,29	+5,26	+5,17	+4,97
Grevelingen sluices	1.350 m^2	+6,12	+4,85	+4,73	+4,48

The hydraulic boundary condition, equation iii.8, requires water levels to not exceed +2,5 m NAP. From the results in Table iii.6.3 it can be derived that water levels have indeed exceeded the design water levels.

This is however not a good formulation of the necessity of the pumping station, as it doesn't show probabilities or return periods; it only shows theoretical water levels, which is a pointless notion. Therefore, let's introduce the concept of critical flood flow rates. This means the Lobith flood flow rate for which the pumping station is required to be in operation—or the Lobith flood flow rate for which, without a pumping station, flooding will occur during the 40-hour storm surge. See the table below for these critical flood flow rates and its corresponding return period.

Table iii.6.4 For the given 12 storage basin configurations, the critical Lobith flood flow rates $\hat{Q}$ [m^{3}s^{-1}] and its return period T when coinciding with a +2,5 m NAP storm surge [annum] for which the storage basin floods.

		Volkerak sluices							
		570 m^2		1.350 m^2		1.500 m^2		2.000 m^2	
		T	$\hat{Q}$	T	$\hat{Q}$	T	$\hat{Q}$	T	$\hat{Q}$
No storage in Grevelingen		*86*	*4.450*	88	4.600	88	4.600	88	4.600
Storage in Grevelingen, Grevelingen sluices	**540 m^2**	92	4.500	102	5.800	111	5.850	117	6.050
	1.350 m^2	95	5.100	124	6.250	127	6.350	137	6.600

For the current situation, the design water levels in the Rhine-Meuse delta are exceeded every 86 years. Even for the most extreme proposed storage basin configuration from §III.1, this will happen once every 137 years. The acceptable risk is only once every 2.000 years so the answer to the second sub-question,

> ” *Is a large pumping station required in the Rhine-Meuse delta before the year 2100?*

is: If the current design water levels of the storage basin remain unchanged, a large pumping station is urgently required because the acceptable risk of 1/2.000 annum^{-1} is compromised.

With this conclusion, some boundary conditions of the pumping station need to be investigated. See next page.

§III.6.4 Pumping station boundary conditions

Three parameters for the design of the pumping station are missing. These can now be derived:

- → Minimum required pump capacity
- → Maximum storm surge water levels
- → Minimum operational water level of the basin

The first parameter, the minimum required pump capacity will be derived from running the simulation with 12.900 m^3s^{-1} Lobith flood flow rate and Meuse mean flow, as this has a 1/2.000 $annum^{-1}$ probability; the acceptable risk. Then by introducing a factor $Q_{PUMP}(\Delta h)$, depending on the location of the pumping station, in one of the mass balances of equation iii.15, the minimum required pumping capacity can be derived. This is performed in §IX.1.

The second parameter is an important parameter for the pumping station as it describes a situation where the pumping station requires operation (critical flood flow rate), but the storm surge water level, is at its highest. These maximum storm surge water levels can be found by analysing the return periods associated with the critical flood flow rates from Table iii.6.4. For example, no Grevelingen storage and 570 m^2 Volkerak sluices:

- ⇒ For +2,5 m NAP storm surge coinciding with a 4.450 m^3s^{-1} Lobith flood flow rate: T = 86
- ⇒ Removing the return period of the +2,5 m NAP storm surge: 86 / 3 = 28,7
- ⇒ Finding the allowable return period of the maximum storm surge: 2.000 / 28,7 = 69,8
- ⇒ Finding the Gumbel variate $y = -\ln(-\ln(1-1/69,8)$ = 4,24
- ⇒ Using Figure iii.3.1 with its corresponding linear relation (h = 1,4 + 0,225×y) to find the water level h: 1,4 + 0,225 × 4,24 = +2,35 m NAP.
- ⇒ Adding the rise in sea-level by the year 2100: 2,35 + 0,85 = +3,20 m NAP.

See the table below for all results.

Table iii.6.5 For the 12 storage basin configurations the maximum storm surge water level coinciding with critical flood flow rates with a total probability of 1/2.000.

	Volkerak sluices			
	570 m^2	1.350 m^2	1.500 m^2	2.000 m^2
No storage in Grevelingen	+3,20	+3,20	+3,20	+3,20
540 m^2	+3,20	+3,16	+3,14	+3,13

Storage in Grevelingen, Grevelingen sluices	1.350 m²	+3,18	+3,12	+3,12	+3,10

From the table above it can be derived that the maximum storm surge levels are almost all equal. Therefore, for all twelve configurations the pumping station, the maximum storm surge level of +3,20 m NAP will be used. This greatly eases calculations.

The third and final parameters is relevant because, as mentioned in the basis of design, the Deltapump should be fully submerged when it is in operation. In the simulation, at the start of the storm surge, the Haringvliet-Hollandsch Diep have low water levels because the Haringvlietdam has closed at low tide and the Grevelingen and Volkerak-Zoommeer because of pre-draining. With the simulation this was derived for the critical flood flow rates, as these yields to lowest water level:

→ Haringvliet-Hollandsch Diep: -0,02 m NAP
→ Grevelingen: +0,36 m NAP
→ Volkerak: +0,27 m NAP
→ Zoommeer: -0,13 m NAP

§III.7 Validity of the calculation model

In this model the small-basin approximation was used. This approximation is valid when the wavelength is at least twenty times the largest dimension of the basin. The largest dimension of the basin is about 56 km (Zoom Earth, n.d.). Because the flood wave is modelled as a gaussian function, in theory its period is infinite. Therefore, in section §III.5.6, the term practical time period T_{PRAC} was introduced. If this time period is multiplied with the flood wave propagation velocity, its practical wavelength is obtained. See the table below. The flood wave propagation velocity at the confluence point in the Hollandsch Diep is calculated per flood scenario, by taking the weighted average flood wave propagation velocities of the adjacent rivers in which flood is flowing (Dordtsche Kil, Nieuwe Merwede and Amer).

Table iii.7.1 Practical wavelength for the flood scenarios.

Flood scenario	Time period in hours	Flood wave propagation velocity	Wavelength
Rhine flood	335 hours	1,01 m s^{-1}	1.218 km
Meuse flood	266 hours	1,25 m s^{-1}	1.197 km
Rhine and Meuse flood	298 hours	1,09 m s^{-1}	1.169 km

The smallest practical wavelength is thus 1.169 km. The ratio between largest dimension and wavelength is then approximately 20. Quite miraculously this is the minimum ratio for the small-basin approximation to be true.

For the equations for the Bathse Spuikanaal and the Schelde-Rijnkanaal, inertia had to be significant for the equations to be applicable. Inertia can be neglected for the following condition (Battjes & Labeur, 2017, p. 104):

$$\frac{\omega_{M_2}{}^2 L}{g} \frac{A_{ZO}}{B_C d_C} \ll 1 \qquad \textit{equation iii.33}$$

For the Bathse Spuikanaal and Schelde-Rijnkanaal, the lengths are respectively 8 and 15 km, the widths 180 and 270 m and the depth 6 m for both canals. The surface area of the Zoommeer is 18 km^2. The left hand-side of the equation above is then respectively 0,27 and 0,34. The condition is not satisfied so inertia can't be neglected. Therefore, the equations used for the two canals are valid.

Appendix IV // Pumping station stakeholder analysis

To gain insight in the parties that should be kept informed and/or satisfied, this stakeholder analysis is performed. The stakeholders are shown in Figure iv.1 and are categorised by two criteria: influence and interest, ranging from least (--) to most (++).

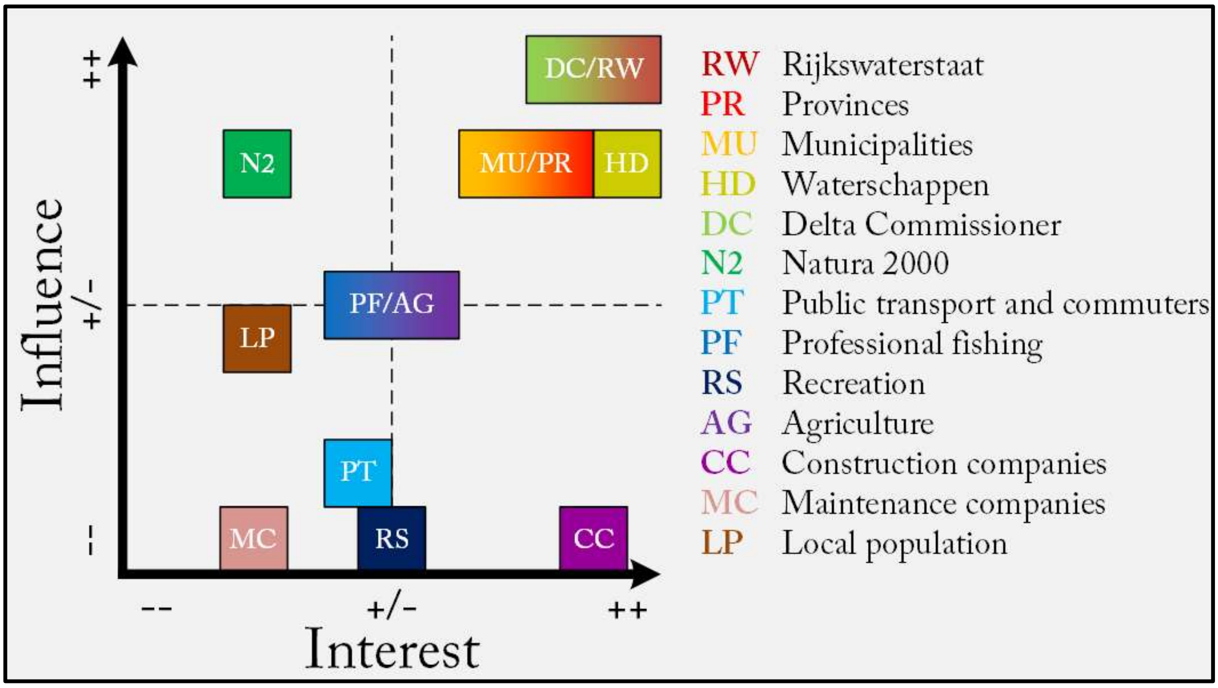

Figure iv.1 Influence-interest graph of the stakeholders involved with the pumping station project

Rijkswaterstaat (and the Department of Infrastructure and Water Management)

The Rijkswaterstaat, which is an agency under the Department of Infrastructure and Water Management, would be the project initiator. Therefore, their influence and interest of the project is the greatest of all. Their wishes are directly translated into the basis of design. Rijkswaterstaat's wishes could be that the project has low costs and a low as possible impact on the environment.

Provinces of South-Holland, Zeeland and North Brabant

The storage basin is located in the provinces of South-Holland, Zeeland and North Brabant. Their influence and interest are also significant. The Provinces want their inhabitants to be protected from flooding dangers. Moreover, the provincial road N57, located along the coast of the storage basin, will be affected by the work so South-Holland and Zeeland will be involved in the planning. The Provinces wish that the project has low costs and a low as possible impact on the environment. Furthermore, since the project is innovative, it could attract awareness from the engineering world towards the provinces, so the project is encouraged to look aesthetically pleasing.

Municipalities surround in the storage basin

The influence and interest of the municipalities surrounding the storage basin is significant, slightly smaller than the province. The municipalities want their inhabitants to be protected from flooding. The inhabitants of the municipalities are fairly likely to be affected by the works, so the wish of the municipalities is to keep their inhabitants informed. Moreover, the municipalities are also the governmental institutions that grant the building permits.

Waterschappen

The storage basin is located within the Waterschappen (water agencies) of the Hollandsche Delta, Scheldestromen and Brabantse Delta (Waterschappen, n.d.). The Waterschap are directly responsible for the water management and the dykes in the area. Fluvial floods will manipulate the water levels thus decreasing the loads on the dykes. Furthermore, one of the options is strengthening the dykes. The Waterschappen should therefore be greatly involved.

Delta Commissioner

The Delta Commissioner is part of the Department of Infrastructure and Water Management. This commissioner creates a works programme and stimulates cooperation between governments and companies (Deltacommissaris, n.d.). Its influence and interest in the project are therefore equally as significant as the Rijkswaterstaat.

Natura 2000

In the Haringvliet nature is protected by European law. Natura 2000 (n.d.) states that its population of birds, animals and fish should be maintained and not be harmed during and after the project is finished. Some fishes like the sea lamprey, European river lamprey, allis shad, twait shad, salmon and sea trout should be able to migrate between the Haringvliet and the North Sea without obstruction (Rijkswaterstaat Oost-Nederland, 2017, pp. 82-84).

Public transport and commuters

Works along the coast of the storage basin could obstruct the daily traffic along the N57 provincial road. Commuters need to be kept informed when the N57 will be closed and what alternative routes will be available. It is possible that they file a protest, but chances are slim it succeeds.

Public transport concerns both the companies and the users. They are not interested in the project as a whole, but they are interested in the project timeline. Therefore, the public transport companies need to be kept informed when they can't run their buses. Moreover, they would want to receive financial compensation for loss of income during closure. It is also possible that they will file a protest, but chances are slim it succeeds.

Professional fishing

The construction of sluices in the Grevelingendam and Brouwersdam will stimulate shellfish farming and professional fishing in the Grevelingen and Volkerak-Zoommeer (Lammers, 2014, p. 29). These parties are therefore very much interested in the project and its consequences.

Recreation

The construction of sluices in the Grevelingendam and Brouwersdam will re-introduce tidal dynamics into the Grevelingen and the Volkerak-Zoommeer. Lammers (2014, p. 28) states that this will allow more locations for recreational diving in the Volkerak-Zoommeer. Moreover, due to the tidal dynamics, forces of nature are returned to the Rhine-Meuse delta which will enhance the experience. The salinification of the Volkerak-Zoommeer and Grevelingen will terminate the local occurrence of blue algae (Lammers, 2014, p. 53), so that the water is always safe for swimming.

Agriculture

The construction of sluices in the Grevelingendam and Brouwersdam will salify the Grevelingen and the Volkerak-Zoommeer. This has negative consequences for agriculture as there farmland will possibly salify as well and they will need to extract their water from somewhere else (Lammers, 2014, p. 28).

Construction companies

Construction companies are very interested in the project as the project is one-of-a-kind, ambitious and large. For these companies this means worldwide exposure and a large sum of money.

Maintenance companies

Maintenance companies are relatively interested in the project as they can draft a long-term contracts for the maintenance of the pumping stations and its attributes.

Local population

The local population is not really interested in the project as a whole, as it doesn’t affect their daily lives. Notwithstanding, they always have the right to protest any decision made for the pumping station or storage basin, so their influence is not insignificant.

Appendix V // Process, operational and functional analyses

In this appendix chapter the process, operational and functional analyses of the Haringvlietdam pumping station project are given.

§V.1 Process analysis

The process analysis describes the processes from the following categories:

→ Users: vessels and maintenance
→ Natural: water

§V.1.1 Usage processes

Vessels

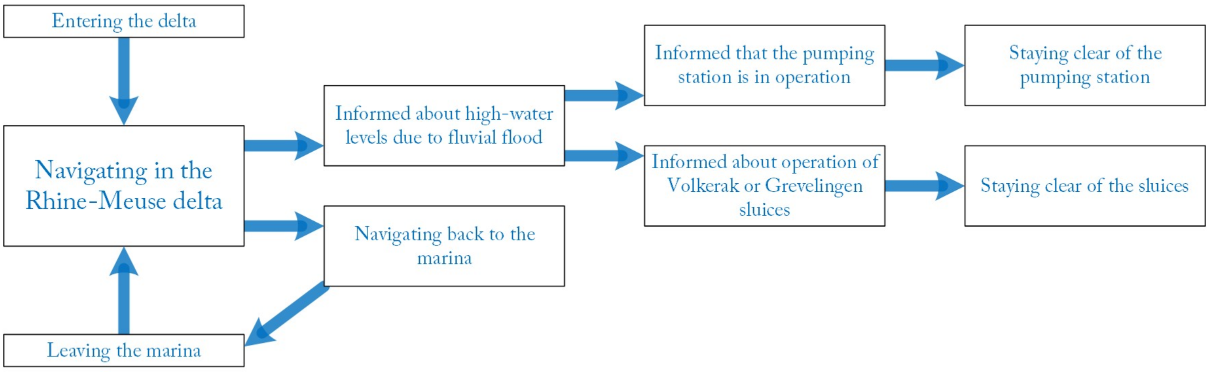

Figure v.1 Process analysis of vessels

Employees and maintenance crew

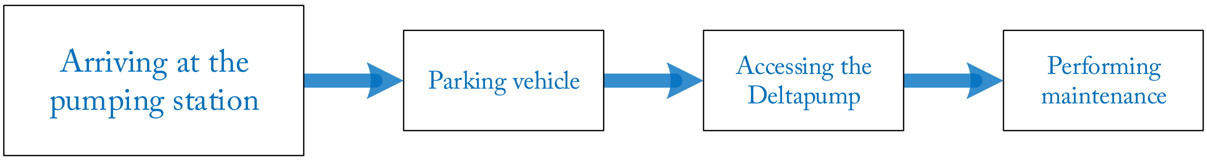

Figure v.2 Process analysis of employees and maintenance crew

§V.1.2 Natural processes

A water particle

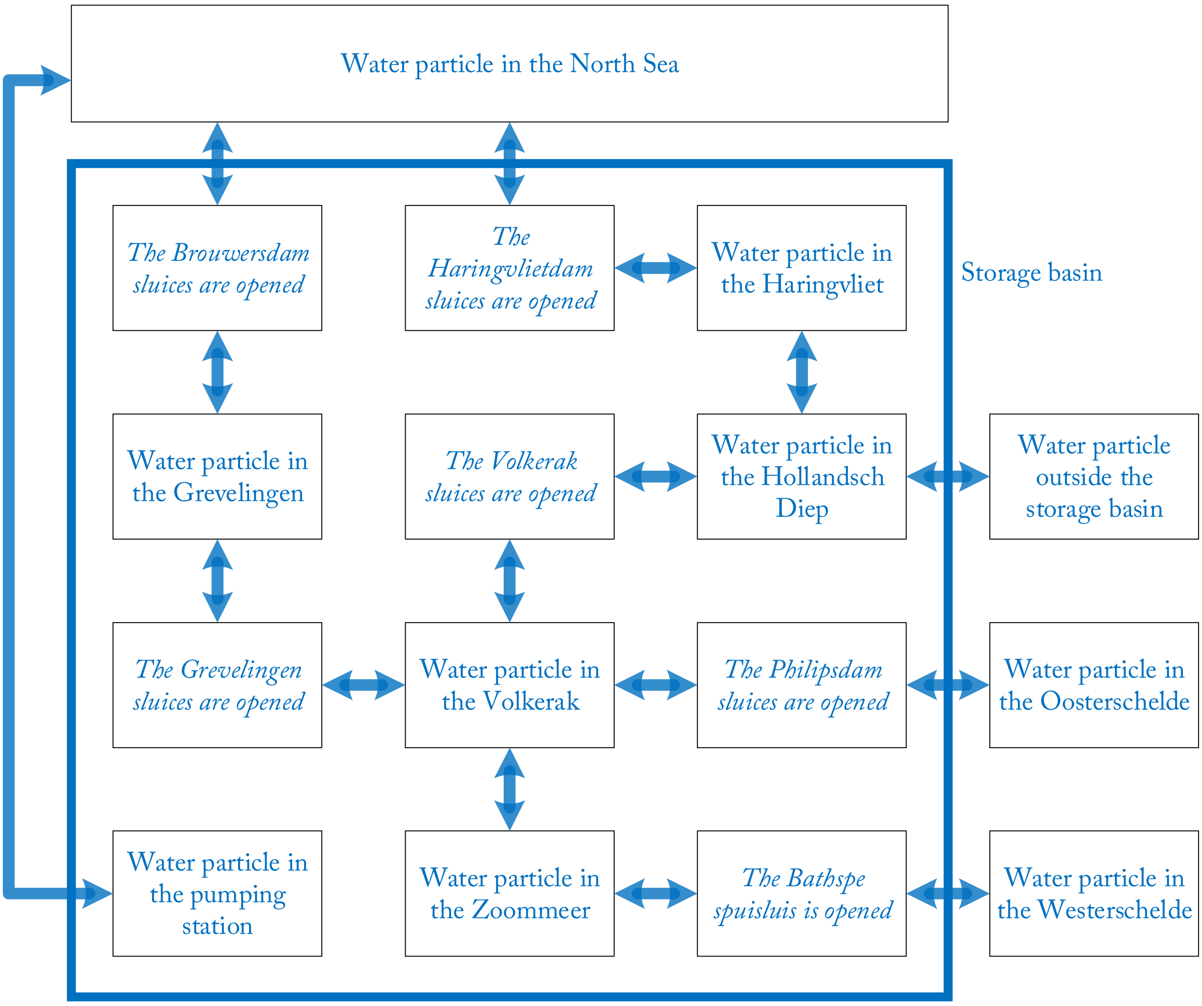

Figure v.3 Process analysis of water particles within the storage basin (large box).

§V.2 Function analysis

The functions are categorised into three groups: the principal function, the preserving functions and the additional functions.

Principal function

→ Transfer excessive river water of fluvial floods from the Rhine-Meuse delta to the North Sea during storm surges

Preservering functions

→ Limit the penetration of tides in the hinterland

→ Obstruct water flow from the North Sea to the Haringvliet during storm surges

→ Prevent the lands surrounding the Haringvliet from flooding by the North Sea

→ Allow fish migration from the Rhine-Meuse delta to the North Sea

→ Acts as a thoroughfare for vehicular and bike traffic

Additional functions

→ Allow maintenance vehicles access to the pumping stations without impeding traffic

§V.3 Operational analysis

This operational analysis is a flowchart describing how to system should function under varying circumstances. The circumstances for this operational analysis are dependent on two parameters: the discharge at Lobith and if the water level at the North Sea has exceeded +2,50 m NAP. The operations are shown in Figures v.4 and v.5. The operations are derived from section §III.2.9.

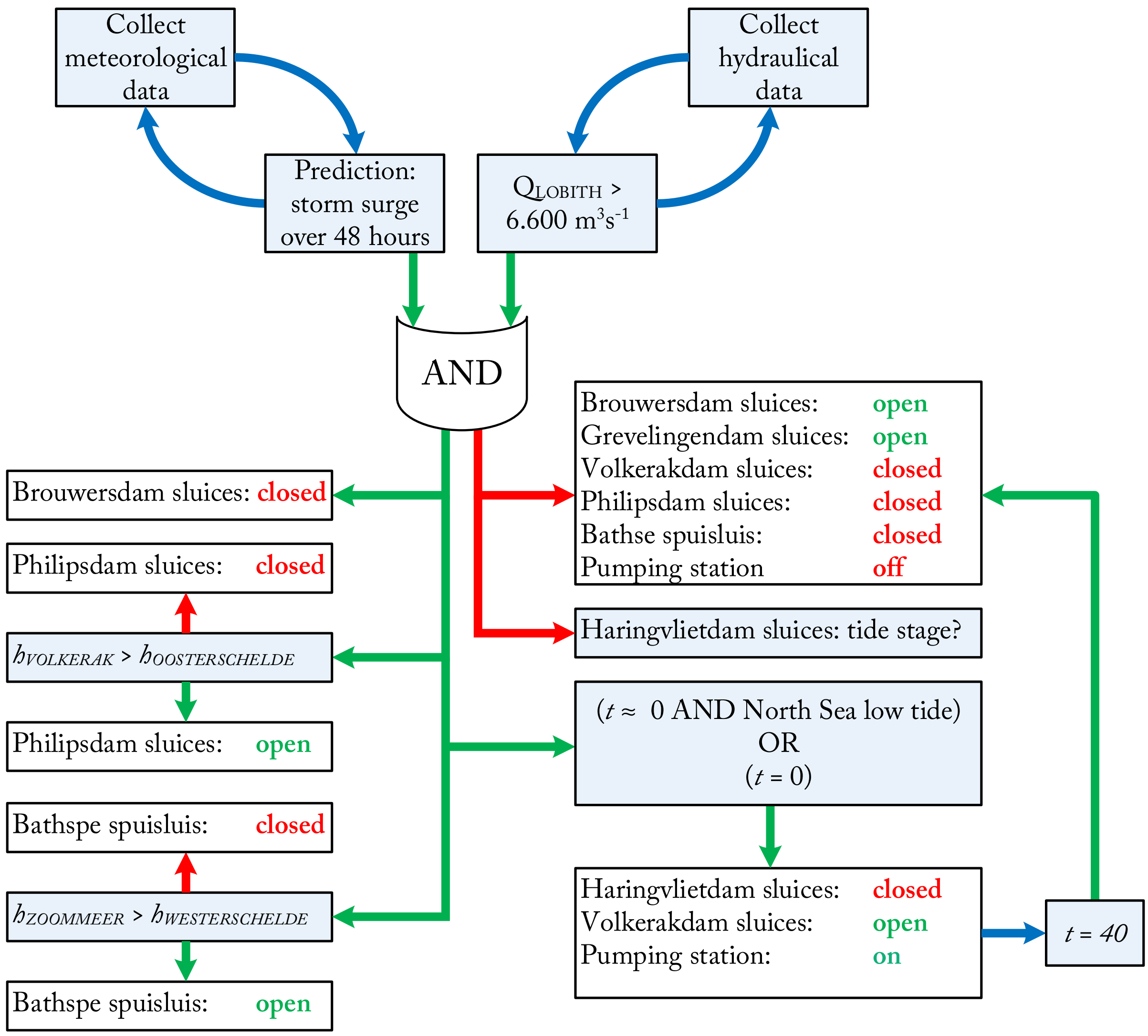

Figure v.4 Operational analysis of the Rhine-Meuse delta flood defences. „Haringvlietdam sluices: tide stage" continued in Figure v.5. Green implies TRUE and red implies FALSE.

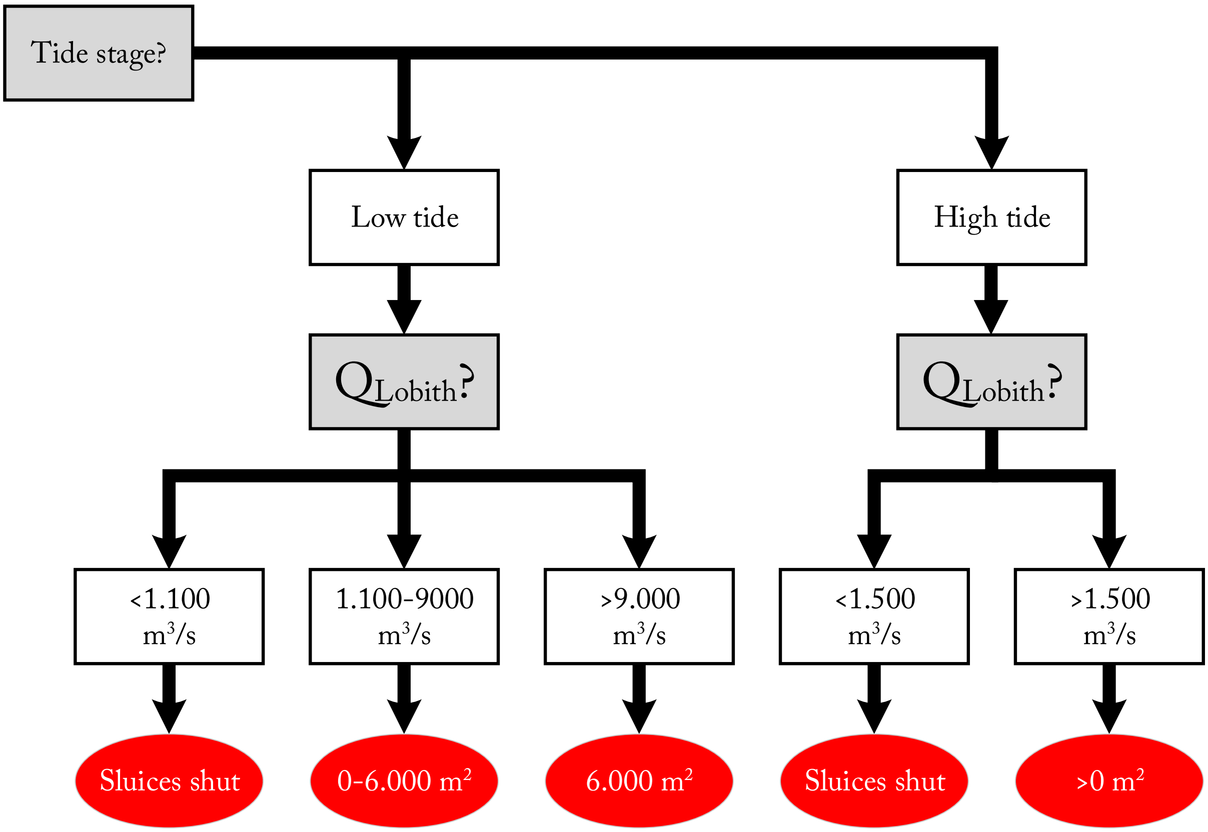

Figure v.5 Operational flowchart of the Haringvliet pumping station. The grey boxes imply questions, the white imply answers and the red boxes imply actions. Continuation from Figure v.4. Operations derived from Leeuwen et al. (2004, p. 9) and Rijkswaterstaat (2011a, pp. 8–9)

In Figure v.5 the operations during high tide are shown greatly simplified. This is because the precise workings of the Haringvliet sluices, when the discharge in Lobith is bigger than 1.500 m^3s^{-1}, could not be found in publicly accessible literature.

In practice, this flowchart should be continuously looped through by a computer. That computer should be connected to the monitoring services that determine the flow rate at Lobith and whether a storm surge is present. This is illustrated in Figure v.4.

Appendix VI // Basis of design for the Deltapump pumping station

In this appendix chapter a full description of the basis of design is given. First the design objective is presented. Next, the design assumptions, design requirements, boundary conditions and the design wishes are presented. Last, the evaluation criteria are given.

§VI.1 Design objective

The design objective is as follows:

→ Designing the civil structure of a pumping station in the Rhine-Meuse delta to transfer excessive river water from the Rhine and Meuse to the North Sea under the acceptable flooding risk of 1/2.000 annum^{-1} for the Hoeksche Waard.

§VI.2 Starting points and assumptions

The starting point of the pumping station is that the pump type used is that of a Deltapump. Furthermore, its specifications are:

- diameter: 10 m
- height: 6 m (variable)
- central axis diameter: 120 cm
- helical slope (at the circumference): 10%
- angle of inclination: 25%
- spout width: 1 m
- spout height: 1 m
- rotational velocity: 60 rpm

In addition, three assumptions are given for the Deltapump.

- The thrust bearing resists all of the vertical loads from the Deltapump.
- The forces subjected to the structure and environment are derived from a hydrostatical force distribution
- The thrust bearing is outfitted with hydrodynamic lubrication at a pressure of 10–20 bar.

This means that the Deltapump will not subject other structures to vertical loads, only the thrust bearing. It will subject other structures, besides the thrust bearing, to horizontal loads.

It is out of the scope of this thesis to consider the hydrodynamical forces that arise when the Deltapump is in operation. Its forces are therefore determined from a hydrostatical force distribution.

It out of the scope to determine the dimensions and precise workings of the thrust bearing. However, it is in the interest of foundation design, spatial design and the cost estimates to know what type of thrust bearing is used.

§VI.3 Design requirements

Functional requirements of the pumping station:

- → transfer excess river water from the Rhine-Meuse delta to the North Sea
- → preserve the flood protection function of the location

Structural requirements of the pumping station:

- → the structure must withstand a 1/4.000-year storm surge from the North Sea and 1/2.000-year water levels in the storage basin[1]
- → the structure must be designed to last 80 years
- → the structure must withstand the impact of a CEMT-VIa class ship (Openstreetmap, 2020).
- → the structure must suffice in stability, of which the following failing mechanisms must be prevented:
  - → slope instability
  - → internal erosion or piping
  - → scour
  - → overtopping
  - → micro instability
  - → floatation
  - → horizontal instability
  - → rotational instability
  - → buckling

[1] Whilst the pumping station only requires functioning with storm surge levels coinciding with fluvial floods, for a total probability of 1/2.000 annum^{-1}, the structure itselfs requires to withstand, when there is no coincidence with fluvial events, 1/4.000 annum^{-1} occurences (Ministerie van Verkeer en Rijkswaterstaat, 2006, p. 62).

§VI.4 Boundary conditions

These boundary conditions are determined by the local environment and legal restrictions. Four categories of boundary conditions are considered: hydraulic, meteorological, geotechnical and legal.

§VI.4.1 Hydraulic boundary conditions

Hydraulic boundary conditions are provided for the North Sea, the storage basin and the Deltapump.

North Sea

The water levels are expected to change due to climate change. Considering the most extreme scenario before 2100, factors have to be included. These factors can be seen in Tables vi.1 and vi.2.

Table vi.1 Design values of the North Sea corresponding to a flood frequency of 1/4.000 years (V&W, 2006, p. 241 & Technische Adviescommissie voor de Waterkeringen, 2002, p. 142)

Parameter	Present value	Difference	2100 value
Design water level	+5,2 m NAP	+0,85 m	+6,05 m NAP
Wave height (H_S)	2,25 m	+5%	2,36 m
Wave period ($T_{m-1.0}$)	6,2 s		
Wave angle of inclination (β)	10 °		

Table vi.2 Mean water level and lowest astronomical tide and their 2100 values (Leeuwen et al., 2004, p. 14 & Technische Adviescommissie voor de Waterkeringen, 2002, p. 142 & Rijkswaterstaat, 2019)

Parameter	Present value	Difference	2100 value
Lowest astronomical tide	-1,15 m NAP	+0,85 m	-0,30 m NAP
Mean water level	+0,08 m NAP	+0,85 m	+0,93 m NAP

Storage basin

For the Haringvliet, Rijkswaterstaat (2011a, p. 8) reports two values for low water levels: -0,35 m NAP and -0,20 m NAP for 1/10 and 1/1 years respectively. This value is extrapolated to -0,60 m NAP to account for extreme droughts. The highest water level is +2,50 m NAP, as this is the lowest design water level along all dykes of the storage basin (Ministerie van Verkeer en Rijkswaterstaat, 2006, pp. 122–165), see also §III.1.2. The mean water level is equal to the mean sea level, +0,93 m NAP.

These values for the Haringvliet are assumed for the entire storage basin, with the exception that the Grevelingen, if there are no sluices in the Brouwersdam and Grevelingendam present, has an average water level of +0,03 m NAP (Rijkswaterstaat, 2020).

Table vi.3 Extreme water levels in the Haringvliet at Hellevoetsluis.

Extreme high water (EHW)	+2,50 m NAP
Extreme low water (ELW)	-0,60 m NAP
Mean water level (MWL)	+0,93 m NAP

Deltapump and pumping station

→ The intake of the Deltapump should be fully submerged so that backflow is significantly reduced.

→ The maximum storm surge water level for which the pumping station is required to operate is +3,20 m NAP.

§VI.4.2 Meteorological boundary conditions

Data was analysed between 2000-2020 (KNMI, 2020) of the Hoek van Holland weather station, the closest weather station. From this data it can be concluded that the average hourly wind speed is 9,9 ms^{-1}, rounded up to 10 ms^{-1}, and the maximum hourly wind speed is 30 ms^{-1}. The average direction is 192° clockwise with respect to the north, say south-southwest.

Wind set-up is already incorporated in the design water levels for the North Sea, but not in those of the storage basin. It should be noted that under storm surge circumstances, wind set-up cannot be added to the water levels in the storage basin along the coast. This would be impossible as the storm surge is already implying that the wind direction is northwest whereas, for wind set-up in the storage basin at the coast, wind has to come from the southeast.

The wind set-up can be calculated with the following equation:

$$\frac{\partial h}{\partial x} = C_W \times \frac{u^2}{g \times d} \qquad \text{equation iii.34}$$

§VI.4.3 Geotechnical boundary conditions

Soil profile information

Soil profile information is gathered from the websites of the DINOLoket and BROLoket.

Bed level information

Bed level information is gathered from the nautical charts of Navionics (2020).

§VI.4.4 Legal boundary conditions

The Haringvliet is a Natura 2000 area. In practice this means that during and after construction, the local fish, bird and animal population must not be harmed or negatively affected. To be more precise, from Rijkswaterstaat Oost-Nederland (2017, pp. 82-84):

> Allow migration of the sea lamprey, European river lamprey, allis shad, twait shad, salmon and sea trout between the North Sea and the Haringvliet estuary.

Moreover, the area is not sensitive for nitrogen (Natura 2000, n.d.).

§VI.5 Design wishes

The design wishes are derived from the stakeholder analysis. These wishes are listed below.

From the Provinces, the following wish arises:

→ Create an architectural landmark of the pumping station to attract tourists and foreign interests.

From the Provinces, the municipalities, Natura 2000 and the Rijkswaterstaat, the following wish arises:

→ Create a sustainable and durable pumping station

From the Provinces, the municipalities and the Rijkswaterstaat, the following wish arises:

→ Keep the costs for the project as low as possible

From the public transport companies and the daily commuters, the following wish arises:

→ Obstruct vehicle and bike transport over the N57 provincial road as little as possible

§VI.6 Evaluation criteria

The evaluation criteria are used when deciding which concepts should be used. These criteria are listed below. These criteria are derived from the Stakeholder analysis in **App. IV**.

Environmental impact

Environmental impact means both sustainability and durability. Sustainability means how much the structure impacts the environmental during and after construction. Durability means how much the structure is impacted by the environment.

Aesthetical value

Aesthetical value means the extent to which the design is good-looking and could attract tourists.

Construction hindrance

Construction hindrance means the extent to which commuters, public transport companies and the resort are negatively impacted by the project. This can be either noise pollution or the temporary closure of the provincial road.

Constructability

Constructability means the relative ease at which the project can be constructed.

Accessibility

Accessibility means how relatively easy components of the structure are accessed after and during construction.

Integration

Integration means whether the structure fits within the environment/surroundings.

Fish migration

Fish friendliness means the extent to which the project, both after and during construction, does not negatively impact the migration an of fishes.

Safety

To what extent does this concept preserve or guarantee safety?

Morphodynamics

The morphodynamics entail the effect of the project on the sediments in the Rhine-Meuse delta.

Recreation

This merit expresses the extent to which the project enhances recreational activities in the Rhine-Meuse delta.

Professional fishing

This merit expresses the extent to which the project provides opportunities for professional fishing in the Rhine-Meuse delta.

It is important to have the evaluation criteria sorted on basis of relative importance. First, all criteria are compared to each other; is one important than the other? This is done in Table vi.4.

Table vi.4 Relative importance of the evaluation criteria. The rows are compared with the columns: 1 meaning it is more important and 0 meaning it is less important

Criterium		EI	AV	CH	CO	AC	IN	FM	SF	MD	RE	PF	Σ
Env. impact	EI		1	1	0	0	1	1	0	1	1	1	7
Aesthetical value	AV	0		0	0	0	1	0	0	0	0	0	1
Const. hindrance	CH	0	1		0	0	1	0	0	0	0	0	2
Constructability	CO	1	1	1		1	1	1	0	1	1	1	9
Accessibility	AC	1	1	1	0		1	1	0	1	1	1	8
Integration	IN	0	0	0	0	0		0	0	0	0	0	0
Fish migration	FM	0	1	1	0	0	1		0	1	1	1	6
Flooding safety	FS	1	1	1	1	1	1	1		1	1	1	10
Morphodynamics	MD	0	1	1	0	0	1	0	0		0	0	3
Recreation	RE	0	1	1	0	0	1	0	0	1		0	4
Professional fishing	PF	0	1	1	0	0	1	0	0	1	1		5

Now for these criteria the weighing factors can be formulated, see Table vi.5.

Table vi.5 Formulation of the weigh factors.

Criterium		Relative importance	Weigh factor
Flooding safety	FS	20	18 %
Constructability	CO	18	16 %
Accessibility	AC	16	14 %
Environmental impact	EI	14	13 %
Fish migration	FF	12	11 %
Professional fishing	PF	10	9 %
Recreation	RE	8	7 %
Morphodynamics	MD	6	5 %
Construction hindrance	CH	4	4 %
Aesthetical value	AV	2	2 %
Integration	IN	1	1 %
	Σ	111	100 %

Appendix VII // Conceptual designs for the Deltapump pumping station

In this appendix a variety of conceptual designs are explored. First, all the possible configurations of the storage basin are presented, then preliminary concepts are presented for the general layout of the pumping station. Next, a variety of concepts are presented for different components of the pumping station.

§VII.1 Storage basin configurations

From the analysis of the storage basin model in section §III.1, a total of 12 different configurations of the storage basin were presented. Each of these configurations has different initial costs and each yield different required pumping station capacities, therefore all of these options are investigated to determine the most cost-effective method. The possible configurations are presented below in a flowchart below.

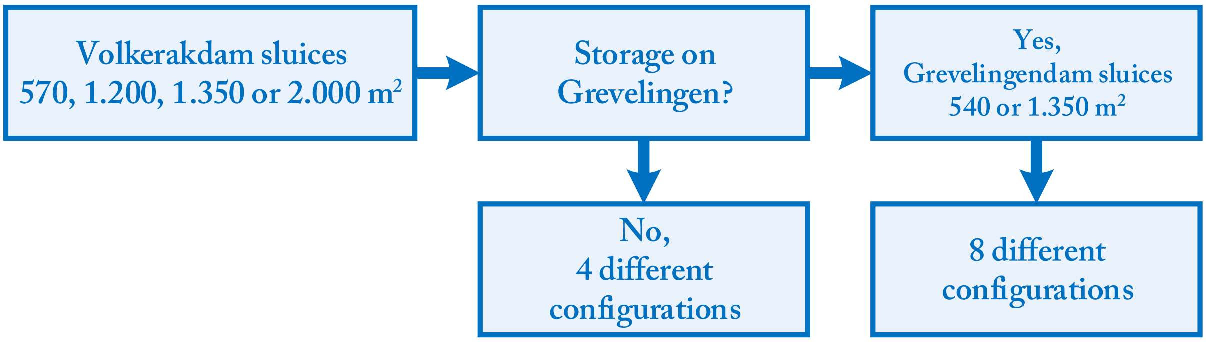

Figure vii.1 The 12 possible configurations for the storage basin.

§VII.2 Preliminary design of the pumping station layout

For the preliminary designs, the general layout of the pumping station is evaluated: where is the Deltapump placed with respect to the flood defences? How does water flow? In total three concepts are presented.

Concept 1: Schut's concept

This concept is analogue to the Haringvlietdam pumping station concept of Schut, as presented in the introduction. In this concept the Deltapump is placed within the storage basin, behind the flood defences. Water flows over a sharp-crested weir and enters a small stilling basin. It then goes through a culvert, which is located within the flood defence (dyke or dam), and enters the North Sea. The flood defence, dyke or dam, that is already in place prevents wave overtopping and the culvert attenuates waves from the ocean.

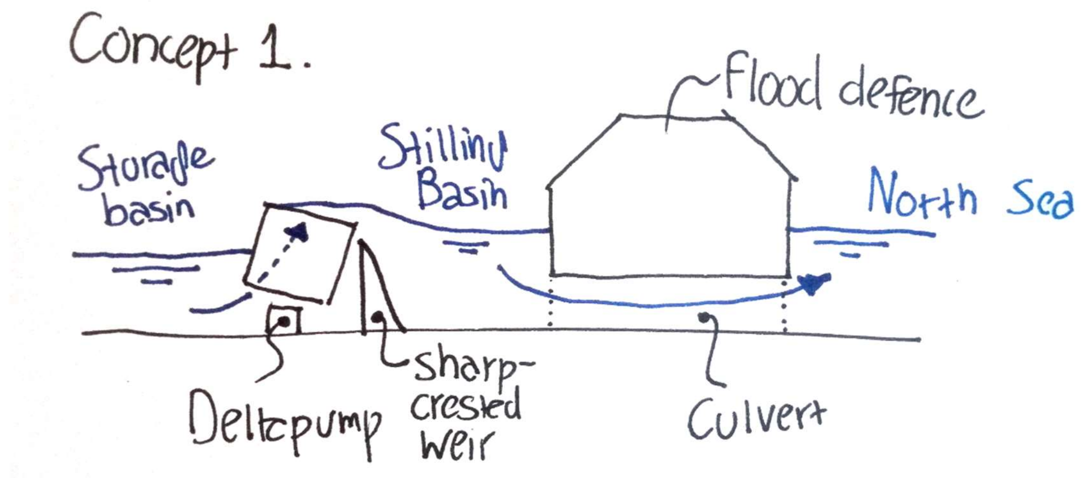

Figure vii.2 Preliminary design concept 1: Schut's concept

Concept 2: Reference projects

This concept is based on those of the reference projects (Chapter 2). In the Rijksgemaal IJmuiden and the West Closure Complex, flow enters a submerged culvert and consequently the pump which is located in the culvert. The pump increases the head of the water so that it can flow into the downstream basin, in this case the North Sea.

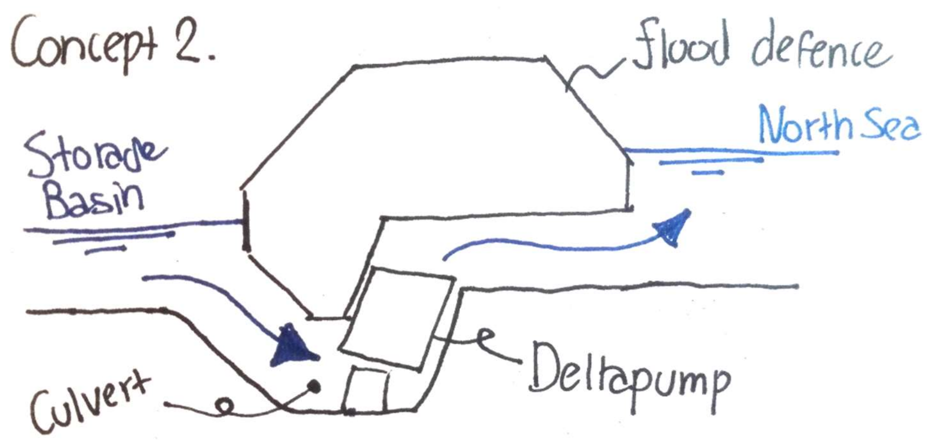

Figure vii.3 Preliminary design concept 2: Submerged Deltapump

Concept 3: Dyke integration

The third and final concept combines concepts 1 and 2: located within the dyke or dam but not submerged (located outside the dyke but submerged is also a combination of the two, albeit—very—impractical).

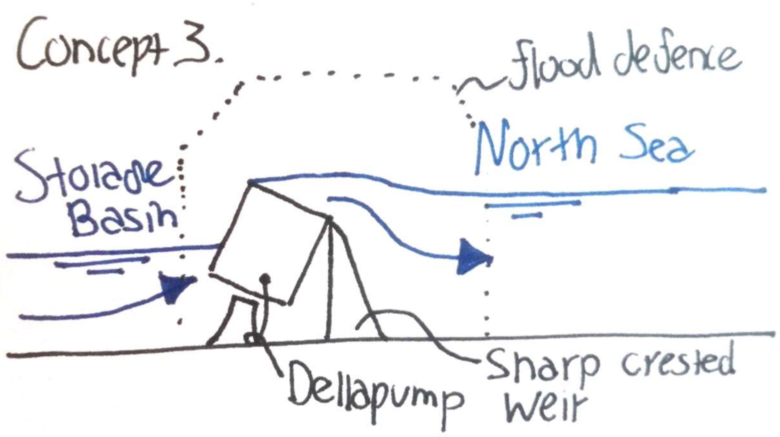

Figure vii.4 Preliminary design concept 3: Integration within flood defence system

Evaluation of the preliminary design concepts

Although it is convention to fully submerge pumps in (large) pumping stations, the Deltapump is not designed for submersion. As described in the introduction and App. I, the Deltapump is a so-called positive displacement pump; pumps that physically replace water. This is not practical if it is already fully submerged; kinetic pumps are then more suitable. Therefore, concept 2 is discarded.

For the other two concepts, the evaluation criteria from the basis of design, App. VI, are used. Not all criteria are relevant, like recreation, so they are left out. The scores are awarded relative to each other: one concept always scores a 10, whilst the other can range from 0 to 10. See Table vii.5.

Table vii.5 Evaluation of the preliminary designs

Criterium		Concept 1	Concept 3	Weigh factor
Flooding safety	SF	10	5	18 %
Constructability	CO	10	3	16 %
Accessibility	AC	10	0	14 %
Environmental impact	EI	8	10	13 %
Construction hindrance	CH	10	0	4 %
Aesthetical value	AV	3	10	2 %
Integration	IN	3	10	1 %
	Σ	6,33	2,98	100 %

For the third concept, the low score on constructability is due to the integration into the dyke or dam. It would have to be completely removed for a long period of time for the construction. As a result of that, the construction hindrance is very high. Moreover, due to its integration within the dyke, it's is barely accessible: maintenance work that requires large machinery is then impossible. The flooding safety criterium is also lower, because incoming waves are attenuated by the culvert in concept 1, which is not the case for the third concept.

In conclusion, concept 1 is the best concept for the layout of the pumping station. It is easily to construct, is easier to access and it is safer because it attenuates incoming waves.

§VII.3 Modular design method

The design of the pumping station will be considered per module: a modular design method. Each module covers one Deltapump and all other components, like weirs. To illustrate this design concept, see the figure below. The Deltapump is Ø 10 m so the centre-to-centre distance of each module will be set at 15 meters. This ensures enough room is left for structures between two adjacent Deltapumps.

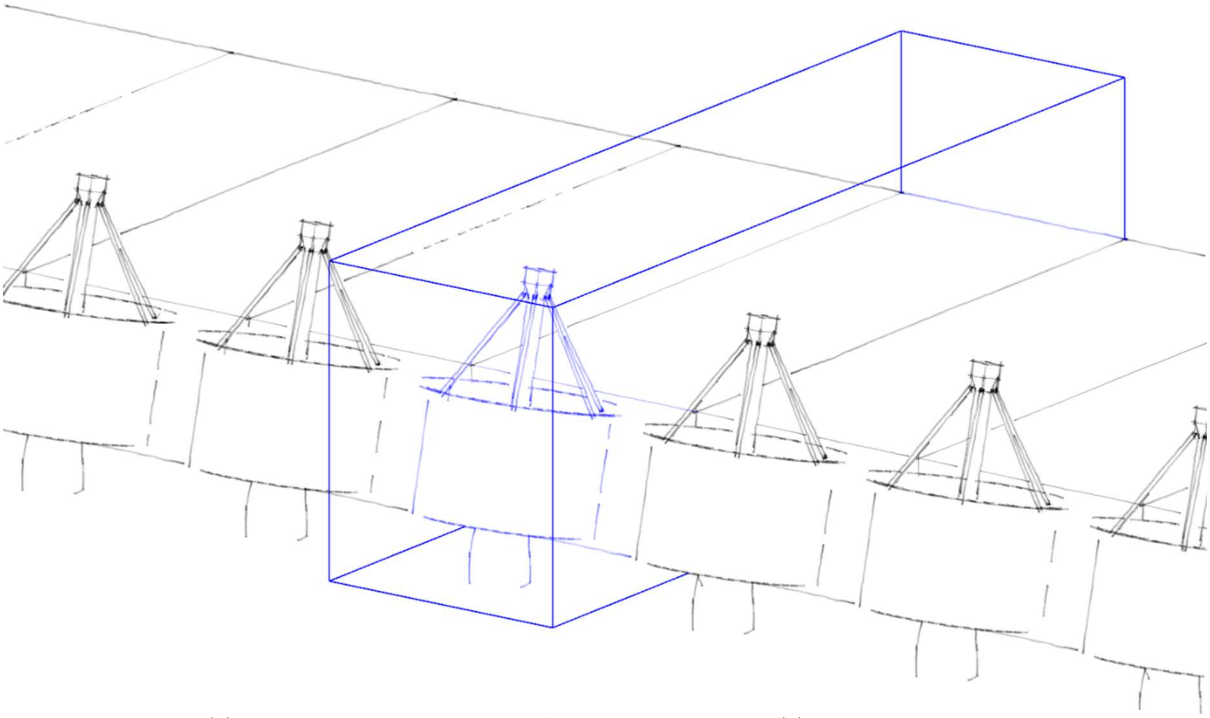

Figure vii.6 The modular design concept of the pumping station. The blue box is one module.

The reason for this design method is that, due the pumping characteristics of the Deltapump, the capacity of the pumping station is unknown—and so is the necessary number of Deltapumps. Once the modular design is finished, the pumping curve for the pumping station can be expressed as a function of storage basin water level (either Haringvliet-Hollandsch Diep or Grevelingen). For each of the storage basin configurations, with the help of the simulation program from §III.6, the necessary number of Deltapumps can then be calculated.

Moreover, designing the pumping station modularly significantly eases calculations. With one exception (supporting structure), all components can be calculated by only considering one module. Furthermore, it is then easily expandable if larger capacities are required in the future.

§VII.4 Conceptual design of components

Based on the stakeholders, functional, operational and process analyses, the basis of design and the conceptual design by Schut, a list of necessary components can be derived for the pumping station. Each of these components is consequently verified in App. VIII per module as well. The components are:

→ Intake canal
→ Deltapump
→ Overspill protection
→ Deltapump thrust bearing
→ Deltapump supporting structure
→ Weir
→ Inner basin
→ Culvert
→ Service road

Next, each of these components are elaborated: why is it necessary, what is its function? Moreover, for each of these components a few concepts are presented as possible solutions.

§VII.4.1 Intake canal

The intake is defined as the part of the structure from the point where flow is such that bed protection is required to the point where water enters the Deltapump. Within the intake canal, a number of components can be defined.

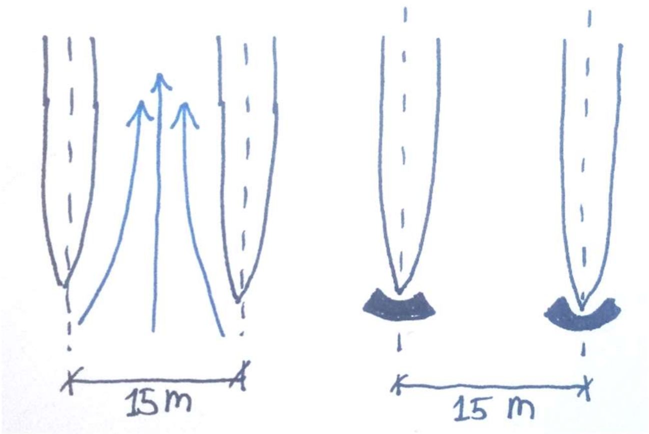

Figure vii.7 Concepts for the intake shape (left) and vessel collision prevention (right)

Shape of the intake

The shape of the intake will be a funnel-shaped concrete wall. Its width increases from 0 to about 1,0 m. This guarantees it's wide enough to mount other components on top of it. Only this concept is presented because it's rather conventional to have a funnel-shaped intake for high flow rates. The funnel-shape guarantees minimal friction and guides flow towards the Deltapump.

Trash and fish screens

It is not known whether the Deltapump is fish-friendly or how it operates when trash or driftwood enters the system. Three concepts are derived.

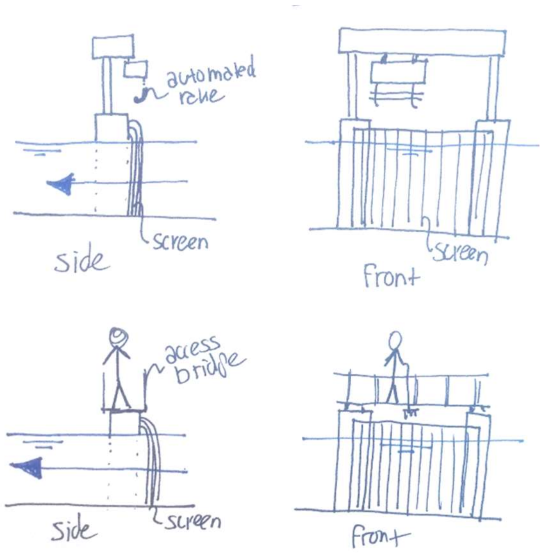

Figure vii.8 Concepts for trash and fish screens. Automated concept (above) and manual concept (below)

1. Automated trash screen. A trash screen is placed with an automated motorised rake that cleans it under a time interval. Its length can span multiple modules. This self-cleaning trash screen requires a location to drop off the trash that is easily accessible with a truck or wheelbarrow. The screen should be made such that fish can't pass; they remain unharmed by the Deltapump
2. Manual trash screen. In this concept the trash screen is cleaned by a person with a rake. It requires an access bridge of some sorts. Fish should not be able to pass through the screen.
3. No trash screens. All fish and trash are free to flow into the Deltapump.

Vessel collision prevention

The basis of design states that the pumping station must withstand an impact force of a CEMT class VI-a vessel. One concept is created, see Figure vii.7. The concept features circular steel protection around the intake walls.

§VII.4.2 Deltapump and weir

For the Deltapump, the following specifications will be used as stated by the basis of design (App. VI).

→ diameter: 10 m
→ central axis diameter: 120 cm
→ helical slope (at the circumference): 10%
→ angle of inclination: 25%
→ spout width: 1 m
→ spout height: 1 m
→ rotational velocity: 60 rpm

Since the pumping curve was derived in App. I, it is possible deviate from the standard height of 7 m. Three concepts are proposed: single default-spec Deltapump, two default-spec Deltapumps in series and a longer-spec Deltapump. See the figure below. The second and third concept are introduced because the head difference might be too big for the default-spec Deltapump.

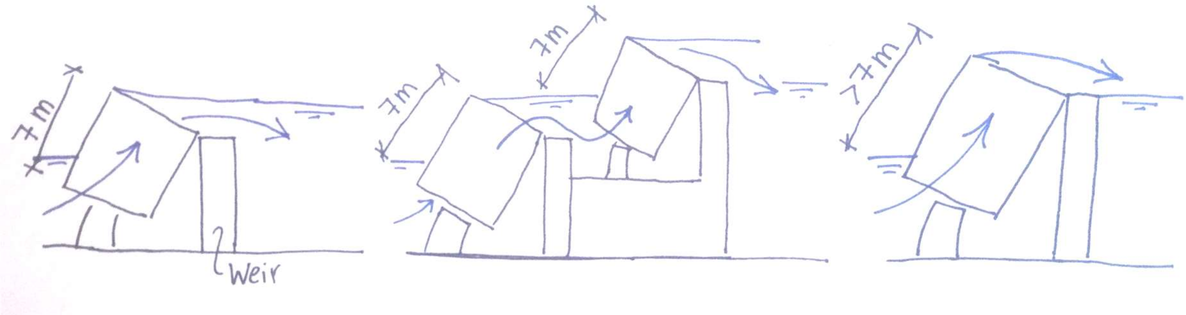

Figure vii.9 Concepts for the Deltapump and weir layout. Left: single default-spec Deltapump, middle: two default-spec Deltapumps in series and right: single longer-spec Deltapump.

For the weir a sharp-crested design will be used. The weir concept corresponding to the first Deltapump concept is called submerged flow. This means that downstream water levels are higher than the weir. It also means that, as the name states, the Deltapump is effectively partially submerged.

The second weir concept corresponds to the second and third Deltapump concept. This concept is called free flow as downstream water levels are lower than the weir.

§VII.4.3 Deltapump overspill protection

Due to the large discharge out of the top of the Deltapump, it is likely that overspill protection is required. This overspill protection ensures that water flows to the weir instead back down or over the back side. Figure vii.10 shows how this could look like. It's basically an open rectangular box with one side missing and a circular hole in the bottom. Moreover, it is tilted in the direction of the Deltapump.

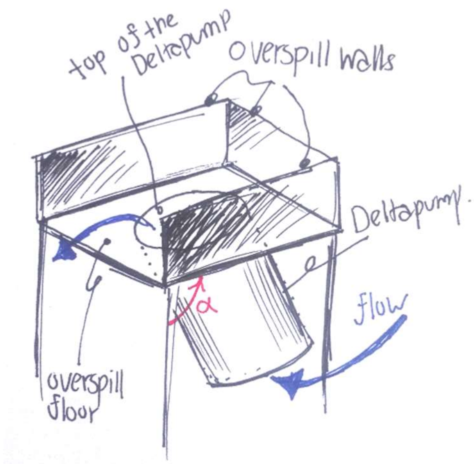

Figure vii.10 Concept for the Deltapump overspill protection.

§VII.4.4 Deltapump thrust bearing

As stated by the basis of design, for the Deltapump thrust bearing, a single concept is proposed: hydrodynamic lubrication with glycol at a pressure ranging from 10–20 bar.

§VII.4.5 Deltapump supporting structure

As stated by the basis of design, all vertical forces are transferred directly to the thrust bearing. The horizontal forces, caused by the tilt of the Deltapump, are transferred to the ground with this supporting structure. One concept is proposed: a steel truss. This truss structure will span multiple modules to save materials.

§VII.4.6 Inner basin

For the inner basin, one concept is presented: a concrete bed. The dimensions of this inner basin will be derived later.

§VII.4.7 Culvert

The culvert will be made out of (reinforced) concrete and it will be placed under mean sea level to attenuate possible effects of incoming waves.

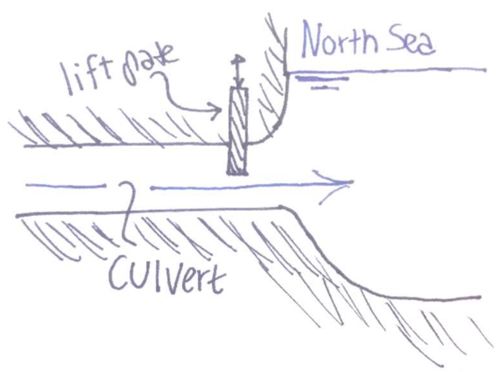

Figure vii.11 Concept for the culvert: a submerged culvert and a lift gate to protect the hinterland during storm surges when it is not in operation.

During high-tide or storm surge conditions without fluvial floods, water should not just flow back into the storage basin, as stated within the basis of design. Furthermore, from the perspective of safety, the addition of sluices gates is very beneficial. The concept presented for this sluice gate is a vertical lift gate, see the figure below.

§VII.4.8 Service road

For the service road one concept is presented: a service road that is placed on the intake walls of the canal. That way, it guarantees good accessibility to the Deltapump and the fish and trash screens for maintenance and construction. The service road will be made out prestressed concrete slabs and are 15 meters wide, the width of one module.

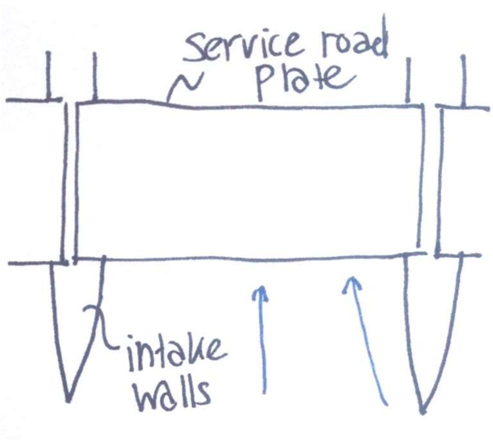

Figure vii.12 Concept for the service road.

§VII.5 Structural design

1. Constructability

To ensure constructability, a temporary earthen construction pit will be created. In this construction pit a pump will dewater the pit so that construction is done in the dry.

2. Stability

In the basis of design, the following failure mechanisms are defined:

- → slope instability
- → internal erosion or piping
- → scour
- → overtopping
- → micro instability
- → floatation

- → horizontal instability
- → rotational instability
- → buckling

All of these failure mechanisms need to be check during the verification phase. A short explanation of each failure mechanism follows with possible solutions.

Slope instability
This is applicable to the flood defence, that is already in place. The construction of the culvert might possibly compromise the slope stability. The maximal slope angle will have to be investigated for this failure mechanism.

Internal erosion or piping
The maximum water difference levels and their duration need to be investigated so it can be determined whether this failure mechanism occurs. If it occurs a piping screen will need to be installed.

Scour
Scour can occur at the intake and at the outlet of the culvert. This can both be caused by waves and by the water flow. If it occurs, bed protection like concrete or coarse gravel will need to be placed.

Overtopping
It should be calculated how high waves reach (run-up height). If that exceeds the height of the flood defence, it should be calculated how much the overtopping discharge is. This should be limited.

Micro instability
Micro instability is applicable to the flood defence. It occurs when flow removes soil particles from the dyke. The dyke needs to be designed in such a way that water doesn't reach the soil or it is made from other materials.

Floatation
Floatation occurs when the ground water pressure pushes a submerged structure upwards. It should be calculated whether this occurs and if it occurs, for example tensile piles need to be installed or the weight needs to be increased.

Horizontal instability
This failure mechanisms occurs when the horizontal loads to a component are bigger than the resistance provided by the ground. If from calculations this appears to happen, the weight of the structure can be increased, or tensile piles can be installed.

Rotational instability
Rotation instability occurs when the horizontal forces create a moment that the ground can't resist.

Buckling

Buckling occurs when the normal load on column has exceeded the buckling force.

§VII.6 Sequence of design

The dimensioning and placement of certain components of the pumping station are dependent on those of others. For example, you can't design a foundation first and then the structure it will support. Therefore, the sequence of design is now elaborated.

First, the vertical placement of the Deltapump and weir have to determined according to the boundary conditions and workings of the Deltapump. Next, the procedure is basically from top to bottom: the supporting structure and the service road are calculated. Then, calculations can be performed on the intake, the weir and the culvert. Consequently, the foundations can be calculated. Lastly, global stability checks like piping can be performed.

Appendix VIII // Verification of the conceptual design components

In this appendix chapter, all concepts from App. VII are verified through means of engineering calculations. First, the choice of location is presented. Then, all calculations are performed on the following components, in order of appearance:

- → Deltapump and weir: vertical integration
- → Deltapump thrust bearing and foundation
- → Deltapump overspill protection
- → Deltapump supporting structure
- → Service road
- → Intake canal
- → Weir
- → Inner basin
- → Culvert

§VIII.1 Choice of location

The storage basin configurations as presented in §VII.1 allow two possible locations for the pumping station. The figure below (from §III.1) shows the storage basin in the Rhine-Meuse delta. Along this storage basin there are only two locations where water can be discharged into the North Sea: The Haringvlietdam and the Brouwersdam. Both of these locations are considered, and are later evaluated.

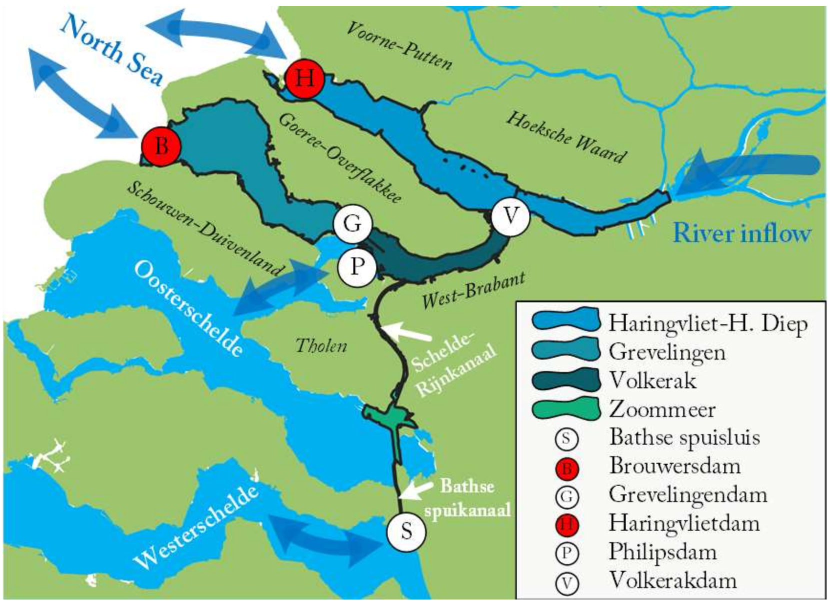

Figure viii.1.1 Two possible choices of location: Haringvlietdam and the Brouwersdam. Created with open-source data from Openstreetmap (2020).

§VIII.2 Vertical integration of the Deltapump

In this section the vertical integration of the Deltapump and the weir are derived from the boundary conditions. Three concepts were presented, they are each elaborated separately. Because the rest of the pumping station depends on the vertical integration of the Deltapump—its most important component, evaluation is performed at the end of this section.

§VIII.2.1 Concept 1: Single default-spec Deltapump with submerged weir flow

This concept uses the default-spec Deltapump. That is, Ø 10 m and height 7 m (including its spout). Two hydraulic boundary conditions from the basis of design are applicable to this concept

→ The intake of the Deltapump must always be submerged
→ The pumping station must operate at a North Sea storm surge level of +3,20 m NAP

See the figure below of a cross-section corresponding to this concept and calculations.

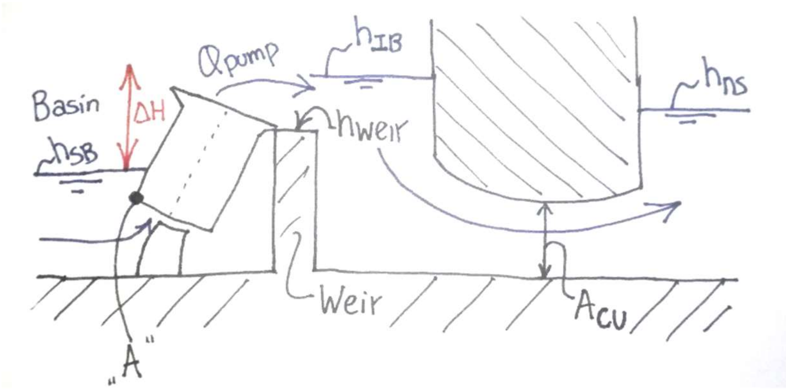

Figure viii.2.1 Overview of relevant parameters for the first concept for vertical integration.

To solve the vertical integration, five equations are necessary. These are:

1. Equation for the first boundary condition: intake of Deltapump always submerged
2. Relation between the location of the weir and intake of the Deltapump
3. Equation for discharge over a submerged weir
4. Equation for discharge through the culvert
5. Pumping performance equation from App. I.

For the first condition/equation, the initial water levels $h_{SB,0}$ in the Grevelingen or Haringvliet are +0,36 m NAP and -0,02 m NAP respectively (§III.6.4). When the pumping station is in operation, the hydraulic head in the intake canal drops due to the flow velocity. This can be approximated with:

$$\Delta h_{SB} = -\frac{\left(\frac{Q_{PUMP}(\Delta h)}{A_{PUMP}}\right)^2}{2g} \Rightarrow h_{SB} = h_{SB,0} - \frac{\left(\frac{Q_{PUMP}(\Delta h)}{A_{PUMP}}\right)^2}{2g} \qquad \textit{Equation viii.1}$$

Point A from **Figure viii.2.1** must always be submerged, so $h_{SB} \approx A$ from the previous equation. Then with goniometrical relations, the height of the weir h_{WEIR} can be calculated from point A or h_{SB}:

$$h_{WEIR} = h_{SB} + 7\cos(\tan^{-1}(0,25)) - 11\sin(\tan^{-1}(0,25)) \approx h_{SB} + 4,123 \quad \textit{Equation viii.2}$$

For the third equation, discharge over a submerged weir, the method from Bansal (2005, pp. 375–376) is used:

$$\begin{aligned} &Q_{WEIR} = Q_1 + Q_2 \\ &\Rightarrow Q_1 = \frac{2}{3} C_D \times B_{WEIR} \times \sqrt{2g}\left(h_{DP} - h_{IB}\right)^{1,5} \\ &\Rightarrow Q_2 = C_D \times B \times (h_{IB} - h_{WEIR})\sqrt{2g\left(h_{DP} - h_{IB}\right)} \\ &\Rightarrow C_D = 0,611 \end{aligned} \quad \textit{Equation viii.3}$$

In this equation $h_{DP,WEIR}$ is the head in the Deltapump with respect to the weir, $h_{IB,WEIR}$ is the head in the inner basin with respect to the weir and C_D is a discharge coefficient. Q_1 in the equation is the free-flow part and Q_2 is the submerged part. The fourth required equation is for the discharge through the culvert:

$$\begin{aligned} &Q_{CU} = A_{CU}\sqrt{2g\left(h_{IB} - h_{NS}\right)} \\ &\Rightarrow h_{IB} = \frac{\left(\frac{Q_{CU}}{A_{CU}}\right)^2}{2g} + h_{NS} \end{aligned} \quad \textit{Equation viii.4}$$

In this equation h_{NS} is the head in the North Sea, which s +3,20 m NAP and A_{CU} is the cross-sectional area of the culvert. For the undefined constants in all the equations, A_{PUMP} is 24,64π m^2, B_{WEIR} is 14 meter (little smaller than one module) and A_{CU} is for now assumed as 60 m^2. The last equation is the pumping capacity, from **App. I**, with the following head difference:

$$\Delta h = h_{DP} - h_{SB} \quad \textit{Equation viii.5}$$

Due to volume balance, the pump capacity should be equal to the discharge over the weir and through the culvert: $Q_{PUMP}(\Delta h) = Q_{CU} = Q_{WEIR}$. As the equations depend on one other, iteration is therefore required. The algorithm to solve this problem is as follows:

1. Take an initial pump capacity, e.g. 200 m^{3}s^{-1}
2. Calculate with equations viii.1 and viii.2 the height of the weir.
3. Calculate with equation viii.4 the head in the inner basin
4. Equation viii.3 has only one unknown now that can be solved: h_{DP}
5. With this h_{DP} find the head Δh and calculate the pump capacity, then repeat until convergence.

The iteration of both the Haringvlietdam and Brouwersdam resulted that, as a matter of fact, flow over the weir is not submerged. The iteration converged at a weir height of +4,24 m NAP whilst the inner basin water level was +3,62 m NAP: the weir is 62 cm higher than water levels in the inner basin. Therefore, the equations are invalid and the concept can be discarded. Moreover, the second and third concept can also be discarded because the fact that flow over the weir is indeed free, proves that the default-spec Deltapump is large enough for the head difference. A longer Deltapump or two default-spec Deltapumps are thus not required. A new concept is introduced in the next section.

NB It is possible to have submerged flow over the weir, but that would require the Deltapump to be sunk deeper within the storage basin (Grevelingen or Haringvliet). This is impractical as it is harder to build, maintain and above all, it absolutely poses no advantages.

§VIII.2.2 Concept 4: Single default-spec Deltapump with free weir flow

With this new concept, downstream conditions, i.e. the North Sea, have no effect on the vertical integration of the Deltapump, as long as, of course, the weir is higher than the water levels in the inner basin. Therefore, only one boundary condition needs to be satisfied:

→ The intake of the Deltapump must always be submerged

See the figure below for an overview of this concept

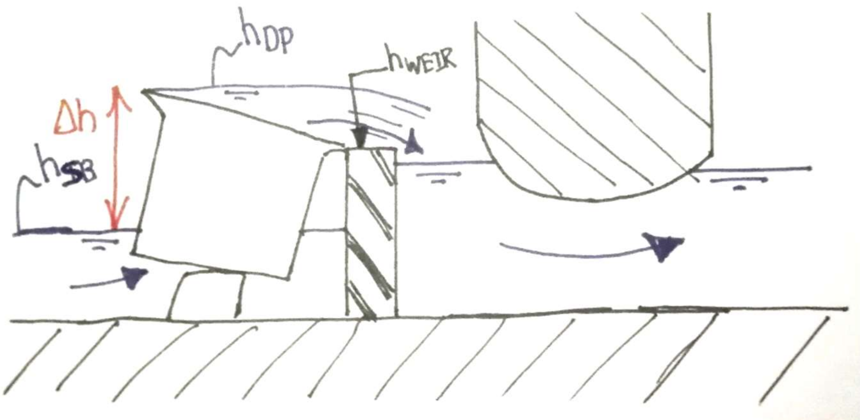

Figure viii.2.2 Overview of relevant parameters for the fourth concept for vertical integration.

Now, only four equations are required. For the boundary condition at the Deltapump intake, the following equation is still valid:

$$h_{SB} = h_{SB,0} - \frac{\left(\frac{Q_{PUMP}(\Delta h)}{A_{PUMP}}\right)^2}{2g} \qquad \textit{Equation viii.6}$$

Then from this boundary conditions, with the known dimensions of the Deltapump, the vertical location of the top of the weir can be calculated:

$$h_{WEIR} = h_{SB} + 7\cos(\arctan(0,25)) - 11\sin(\arctan(0,25)) \qquad \textit{Equation viii.7}$$

For the discharge over the weir, a new equation will be used. This equation is from Bansal (2005, p. 375):

$$Q = \frac{2}{3} C_D \times B_{WEIR} \times \sqrt{2g} H_{DP,WEIR}^{\frac{3}{2}} \qquad \textit{Equation viii.8}$$

In this equation C_D is the discharge coefficient, which is 0,611, B_{WEIR} is the width of the weir, which is still 14 m, and $H_{DP,WEIR}$ is the energy head in the Deltapump with respect to the top of the weir. The last equation is the total head difference:

$$\Delta h = H_{DP} - h_{SB,0} = H_{DP,WEIR} + h_{WEIR} - h_{SB,0} \qquad \textit{Equation viii.9}$$

From this head difference the pump capacity can be calculated. The algorithm to solve this:

1. Take an initial pump capacity
2. Calculate the height of the weir with equations viii.6 and viii.7
3. With the initial capacity, calculate the required head in the Deltapump with equation viii.8
4. Calculate the new pump capacity with the head difference of equation viii.9 and repeat

The execution of this algorithm is shown below for both the Haringvlietdam and the Brouwersdam.

Table viii.2.3 Iteration of the boundary condition to determine the vertical integration of the Deltapump

	Symbol	Haringvlietdam	Brouwersdam	Unit
1	Q_{PUMP}	200	200	m^3s^{-1}
	h_{WEIR}	3,763	4,143	m NAP
	H_{DP}	7,686	8,116	m NAP
	Δh	7,755	7,755	m
		↓	↓	
∞	Q_{PUMP}	176,1	176,1	m^3s^{-1}
	h_{WEIR}	3,839	4,219	m NAP
	H_{DP}	7,489	7,869	m Weir
	Δh	7,509	7,509	m

As downstream conditions have no influence, it is not a surprise that the only difference between the two concepts is the relative weir placement. The difference between the top of the weir is 38 cm, which is also the difference between the lowest operational water levels of them: 36 + 2 = 38 cm.

This observation is vital, as it simplifies further calculations. For both the Haringvlietdam and Brouwersdam, almost the same design can be used with the difference that the pumping station at the Haringvlietdam will be 38 cm lower than that of the Brouwersdam. The only difference in the calculations occurs when working with water levels (floatation, effective stress, piping, etc.) and ground properties (foundation, settlement). All above-ground structural design: overspill-protection, supporting structure and service road are equal.

As stated at the beginning, this concept requires downstream water levels (the inner basin h_{IB}) to be lower than the height of the weir. This must be check for the situation when the highest pump capacity is reached: when the head difference is the lowest. This occurs when storage basin water levels are at their maximum: +2,50 m NAP. Re-iterating through the equations viii.8 and viii.9, now with known dimensions, it can be found that this is 189 m^3s^{-1} for Haringvlietdam 187 m^3s^{-1} for the Brouwersdam. The differences are due to that the Brouwersdam Deltapump is located lower. With equation viii.4 it can be found that the inner basin water levels are then +3,71 m NAP at its highest; this is below the weir.

§VIII.2.3 Conclusion

The figure below shows a cross-section of the vertical integration. The five hydraulic or energy heads and the points of the Deltapump A to F' are listed in Table viii.2.5 for both locations.

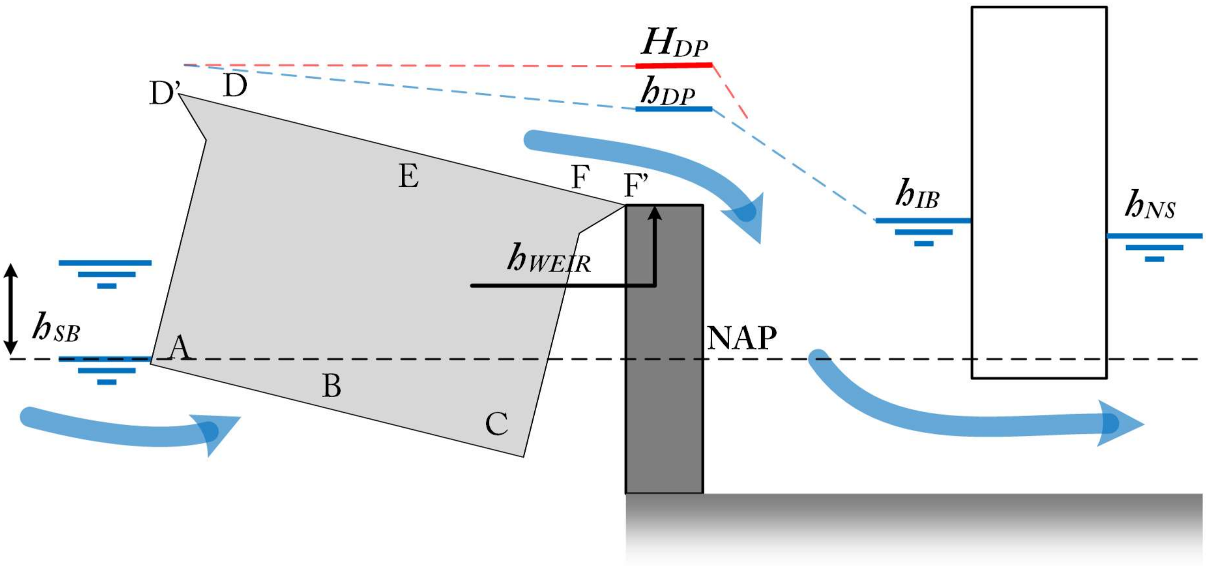

Figure viii.2.4 Schematic cross-section of concept 1. Ranges of water levels, energy heads and hydraulic heads shown. Suggestive lines shown dashed. Length of outlet and dyke **not** to scale.

Table viii.2.5 Vertical locations of characteristic points of the Deltapump, as shown in Figure viii.2.4

Symbol	Elaboration	Haringvlietdam [m NAP]	Brouwersdam [m NAP]
A	Bottom intake high	-0,284	+0,096
B	Bottom central axis	-1,496	-1,116
C	Bottom intake low	-2,709	-2,329
D'	Spout high	+6,750	+7,130
D	Top high	+6,507	+6,887
E	Top central axis	+5,295	+5,675
F	Top low	+4,082	+4,462
F'/h_{WEIR}	Spout low	+3,839	+4,219
h_{SB}	Storage basin head	-0,020 to +2,500	+0,360 to +2,500
H_{DP}	Deltapump energy head	+7,489 to +7,665	+7,868 to +8,017
h_{DP}	Deltapump hydraulic. head	+6,272 to +6,389	+6,652 to +6,751
h_{IB}	Inner basin head	+2,939 to +3,006	+2,939 to +2,995
h_{NS}	North Sea head	+2,500 to +3,200	+2,500 to +3,200

With this table and the figure, the need for overspill protection can be proven. Due to zero flow velocities, the hydraulic head will equal the energy head at the back of the Deltapump, above point D'. This energy head H_{DP} is higher than point D' as can be derived from the table. Therefore, water can flow back down over the Deltapump: overspill protection is required.

Furthermore, when the Deltapump is in operation, water levels should not dive below those of point A so that the intake of the Deltapump is always submerged.

§VIII.3 Deltapump thrust bearing and foundation design

First the force distribution of the Deltapump is calculated. Then the pile foundations are calculated for the Haringvlietdam and for the Brouwersdam. Finally, a summary is shown.

§VIII.3.1 Determining the forces subjected to the foundation

The forces are determined from a hydrostatical force distribution, as assumed by the basis of design, see Figure viii.18. The centroid is assumed to be at 1/2 of the height of the Deltapump which is at 1/4 of the height of the central axis. This seems reasonable for an assumption as almost all mass is centred here: the helical blades, the cylinder and the water are centred here.

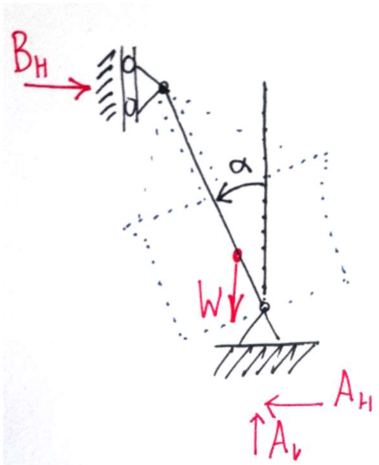

Figure viii.3.1 Hydrostatical force distribution

From the hydrostatical force distribution follows:

$$A_v = W \qquad \textit{equation viii.10}$$

$$B_H = A_H = \frac{W}{4}\tan(\alpha) = \frac{W}{16} \qquad \textit{equation viii.11}$$

The angle α is 25%. The total weight W can be approximated. The water level directly above point E from Figure viii.2.4 and Table viii.2.5 is 1,709 and 1,732 m for the Brouwersdam and Haringvlietdam respectively. Since this difference is small, 1,732 m is used for both. This means that, with the total Deltapump length of 7 m, a cylindrical water column of 8,732 m needs to be resisted by the foundation. The load of this water column is: 8,732 × 9,81 × 1.000 × π × 5^2 = 6,73 MN.

For the weight of the Deltapump itself, assumptions have to be made. For now, let's assume a material with a density of steel: 7.800 kgm^{-3}. Furthermore, let's assume the following:

> Thickness of cylinder shell: 10 cm
>
> Thickness of the helical blade: 5 cm
>
> Thickness of central axis: 10 cm
>
> Weights of tensile rods disregarded
>
> Extension of spouts disregarded (so a Ø10 m, 7,0 m high cylinder)

The circumference of the Deltapump is 31,4 m. With a helical slope of 10% this means that every 360° the blades rise 3,14 m, approximately 1/2 of the entire height. Therefore, by approximation every blade rotates 720° in total around the central axis. So, with two separate blades, the surface area of a single 360° helix has to be multiplied by four.

The total volume of steel can now be calculated:

$$\begin{aligned}&\text{Cylinder: } 10\times\pi\times0{,}1\times9{,}3=22{,}0\ \text{m}^2\\&\text{Helix: } 4\times5^2\times\pi\times0{,}05=15{,}7\ \text{m}^2\\&\text{Central axis: } 14\times1{,}2\times\pi\times0{,}1=5{,}3\ \text{m}^2\end{aligned} \qquad \textit{equation viii.12}$$

Multiplied with the density of steel this adds another 3,29 MN. For the thrust bearing and other missing components at the bottom of the Deltapump, a total weight of 300 kN is assumed. The table below summarises the loads with their safety factors.

Table viii.3.2 Summary of the characteristic and design loads.

Load	Characteristic load	γ	Design load
Deltapump self-weight, vertical	3.290	1,2	3.950
Deltapump water, vertical	6.730	1,5	10.100
Deltapump self-weight, horizontal	206	1,2	247
Deltapump water, horizontal	421	1,5	631
Thrust bearing, vertical	300	1,2	360
		Σ_V	14.410
		Σ_H	878

§VIII.3.2 Pile foundation design: Haringvlietdam

Due to the enormous loads and the high rotational velocities, for which the effects are yet to investigated, pile foundations will be designed instead of shallow foundations. This section describes the pile foundations for the Haringvlietdam

The CPT figure shows a strong layer is located between -17,0 and -20,0 m NAP and -10,0 and -13,0 m NAP. For the first iteration, the upper layer will be investigated.

Let's use 300×300 mm² prefabricated concrete foundation piles, to be driven into the ground. The bearing capacity of compression piles can be calculated:

$$R_{\max} = R_{Tip} + R_{Shaft} \qquad \textit{equation viii.13}$$

Pile foundation design: iteration 1

For the first iteration, the higher level is used. The bottom of the pile is chosen to be at -11,0 m NAP. The top of the pile is located at -5,0 m NAP, underneath a slab (poer). The calculation method used is Koppejan (NEN9997, p.162), for tip resistance the following equation is used:

$$q_{b;\max} = \frac{1}{2} \times \alpha_p \times \beta \times s \left(\frac{q_{c;I;avg} + q_{c;II;avg}}{2} + q_{c;III;avg} \right) \qquad \textit{equation viii.14}$$

The factor α_p is found to be 0,7 for driven prefabricated piles (NEN9997, p. 163). The factor β is found to be 1,0 if the tip is left unchanged. Factor *s* is also 1,0 due to the square dimensions. The results of the CPT can be found in **Figure viii.3.6** which yields the following values:

$$q_{c;I;avg} = 9{,}0 \text{ MPa}$$
$$q_{c;II;avg} = 5{,}2 \text{ MPa}$$
$$q_{c;III;avg} = 3{,}5 \text{ MPa}$$

With equation viii.14 a total tip resistance stress of 3,71 MPa is found. Multiplied with the cross-sectional area of the pile: 3,71 × 300² = 333,9 kN. The shaft resistance is then the average CPT-value over the length of the pile, this is approximately 4 MPa. Multiplied by pile installation factor of 0,010 this yields a total resistance of 288 kN: 4 × 300 × (11.000 – 5.000) × 4 × 0,01.

The total capacity of this 300×300 mm² pile from -5,00 to -11,00 m NAP is 621,9 kN. With a total design load of 14,4 MN, this means 24 of these are necessary. This is too much.

Pile foundation design: iteration 2

For the second iteration, the piles are placed up to -17,00 m NAP. In Figure viii.3.7 the CPT figure can be found. This yields the following values of q-trajectories:

$$q_{c;I;avg} = 16,5 \text{ MPa}$$
$$q_{c;II;avg} = 16,5 \text{ MPa}$$
$$q_{c;III;avg} = 4,0 \text{ MPa}$$

With equation viii.14 the total tip resistance stress is then 14,35 MPa which yields a total tip resistance of 1,292 MN. The average shaft resistance along the pile is approximately 7,5 MPa which adds another 1,08 MN: 7,5 × 4 × 300 × (17.000-5.000) × 0,01. In total, the resistance is than 2,372 MN. This requires a total of 7 piles.

Quick observation of the CPT profiles shows that it is not beneficial to go deeper than -17,0 m NAP as the values of trajectories I and II would decrease rapidly. As seven piles is not practical for installation, instead the width of the foundation piles is increased to 350 × 350 mm^2. This yields a total resistance of 3,02 MN which would require 5 of these piles: this is O.K.

Pile group distance and slab

In Molenaar & Voorendt ([Lecture notes], p. 282) that it is preferred that piles are placed at least eight times their diameter from each other. This means 8 × 350 = 2.800 mm. A pile plan that satisfies this criterium is featured in the figure below. A 6.000×6.000 mm^2 1 m thick reinforced concrete slab will transfer the loads from the thrust bearing to the five piles.

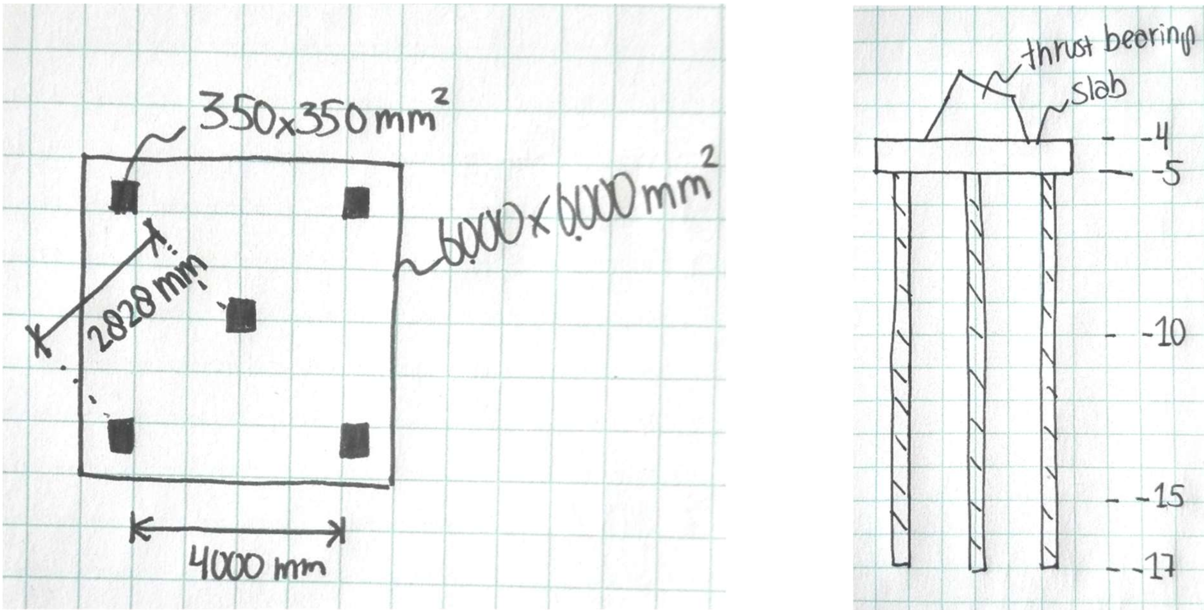

Figure viii.3.3 Pile foundation plan. Left: top view and right: vertical cross-section

Concrete strength class and pile shortening

For the given maximum vertical load of 14,4 MN, the stress in the concrete piles becomes: 14,4 × 10^6/(5×350×350) = 23,5 MPa. This means concrete class C25/30 suffices, which has a characteristic compressive strength of 30 MPa (as it's a cube). Moreover, this concrete class has an elasticity modulus of 31 GPa (Braam & Lagendijk, 2011, p. 28). For the 12-meter long compression pile, its shortening can be calculated: 23,5 / 31.000 × 12.000 = 9 mm. This is an acceptable shortening.

Horizontal loads

The limit state horizontal loads were determined to be 878 MN, see Table viii.3.2. For the calculation of horizontal resistance, the following in equations are used (Molenaar & Voorendt [lectures notes], 2020, p. 211):

$$R_{Hor} = \gamma' \times K_P \times \frac{t_0^{\,3}}{24} \times \frac{t_0 + 4 \times b}{t_0 + h}$$

$$K_P = \frac{\cos^2(\varphi)}{\left(1 - \sqrt{\frac{\sin(\varphi - \delta) \times \sin(\varphi)}{\cos(-\delta)}}\right)} \qquad \textit{equation viii.15}$$

$$t_0 = \frac{t}{1,2}$$

$$\delta = -\frac{2}{3}\varphi$$

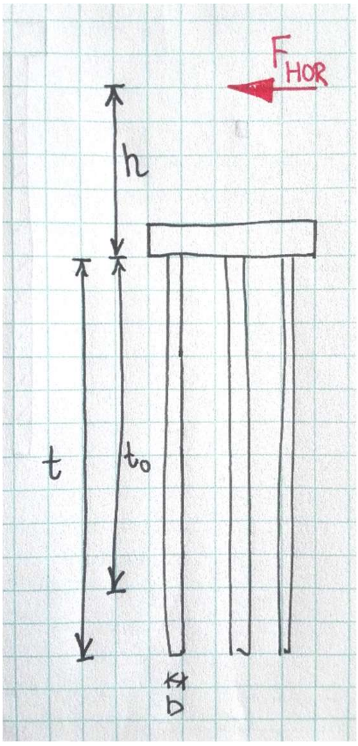

See Figure viii.3.4 corresponding to these calculations. For the effective density, soil cross-sections from DINOLoket (n.d.) is used. At the location of the Haringvlietdam, the ground between -5,0 m NAP and -17,0 m NAP consists for 95% out of sand [„Zand midden categorie"]. With NEN9997 (p. 54) the corresponding effective stress γ' is then found to be 10 kNm^{-3}, for „Zand, schoon, matig".

The practical length t is 12 m, the width b is 0,35 m, internal friction φ is 32,5° (NEN9997, p. 54). From Table viii.2.5 it can be calculated that the centroid is located at +3,80 m NAP, which is 8,80 m from the top of the foundation, this is the parameter h. With all parameters determined, the equation yields a total resistance of 570 kN per pile. The total resistance for the five piles is then 2,85 MN. This is much larger than the horizontal load of 878 kN so this criterium is satisfied.

Figure viii.3.4 Calculation of the horizontal resistance

§VIII.3.3 Pile foundation design: Brouwersdam

The process as described for the Haringvlietdam is repeated for the Brouwersdam. The only difference is that the foundations are located 38 cm higher and that the ground has a different CPT. Only the results are shown.

Cross-sectional area: 350×350 mm². From ~-5,0 m NAP to -15,0 m NAP. See Figure viii.3.8,

$$q_{c;I;avg} = 15 \text{ MPa}$$
$$q_{c;II;avg} = 15 \text{ MPa}$$
$$q_{c;III;avg} = 6 \text{ MPa}$$
$$q_{s;avg} = 10 \text{ MPa}$$
$$R_{Tip} = 0,7 \times 1 \times 1 \times \left(\frac{15+15}{2} + 6 \right) \times 350^2 = 1{,}8 \text{ MN}$$
$$R_{Shaft} = 0,010 \times (15000 - 5000) \times 10 \times 4 \times 350 = 1{,}4 \text{ MN}$$

Total resistance: 3,2 MN so in total five piles required. Same pile group layout as for the Haringvlietdam. Concrete class also C25/30.

Ground fully consists of sand („zand midden categorie") at the Brouwersdam, with equation viii.15 the horizontal resistance is found to be 309 kN per pile, in total 1.548 kN. This satisfies the 878 kN horizontal load.

§VIII.3.4 Summary

Table viii.3.5 Summary of the compression piles for the Haringvlietdam and Brouwersdam.

	Haringvlietdam	Brouwersdam	
Design vertical load	14.400		kN
Number of piles	5		
Concrete class	C25/30		
Pile shortening	9	8	mm
Pile dimensions	350×350		mm²
Pile length	12.000	10.000	mm
Pile top	-5,0	-4,62	m NAP

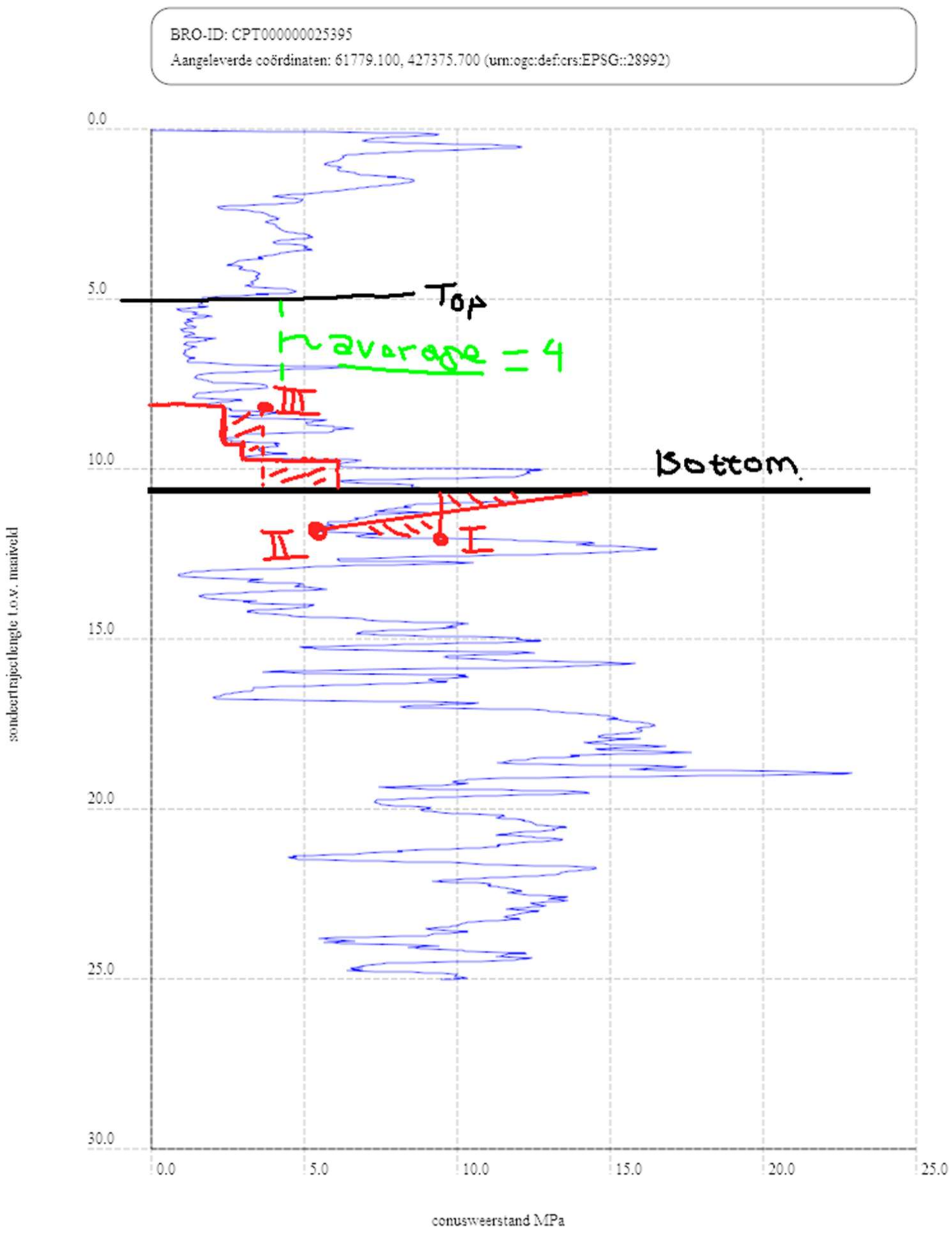

Figure viii.3.6 Calculation of cone stress for the first iteration of the Haringvlietdam. Cone penetration profile #CPT000000025395 (Haringvlietdam), from DINOLoket (2009).

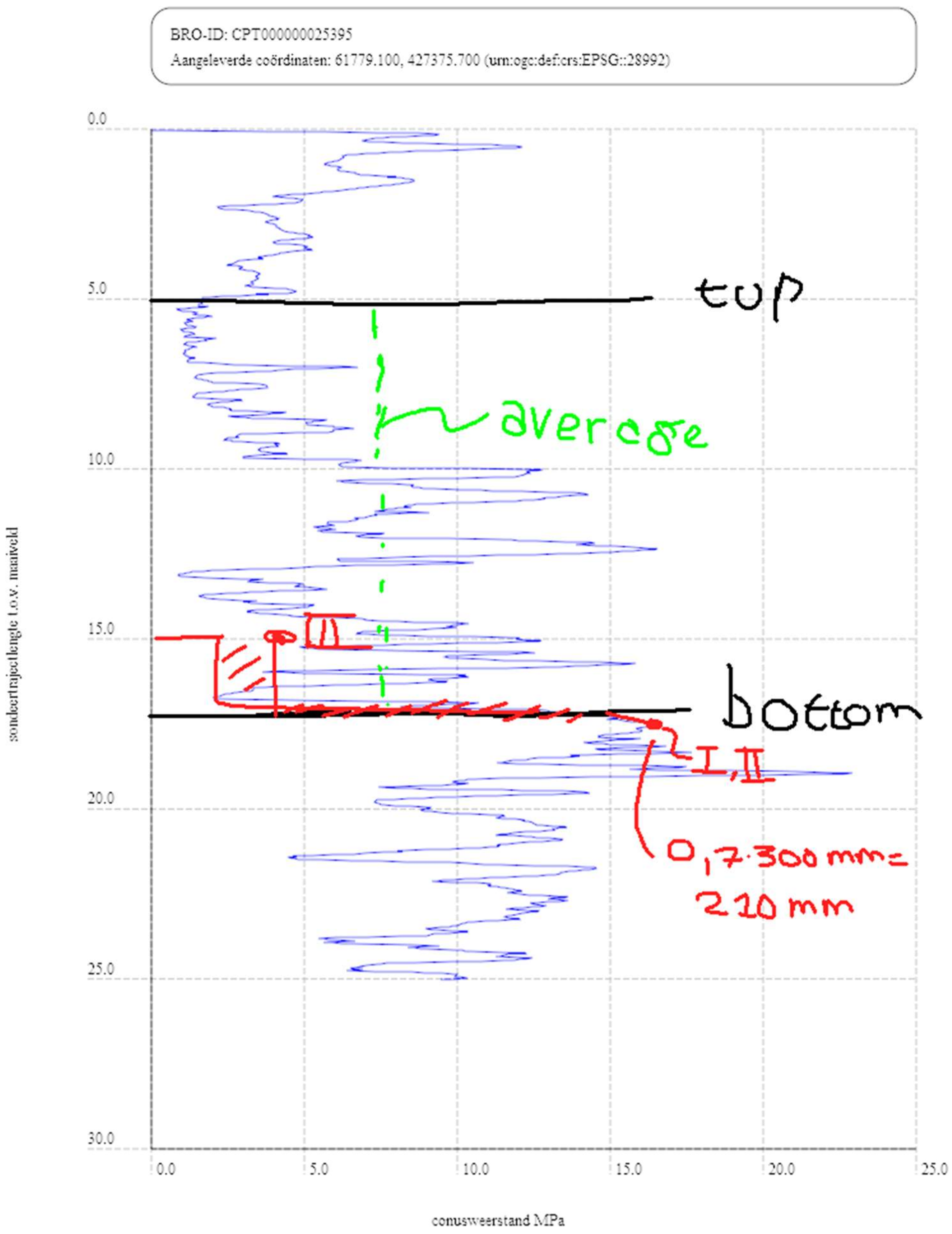

Figure viii.3.7 Calculation of cone stress for the second iteration of the Haringvlietdam. Cone penetration profile #CPT000000025395 (Haringvlietdam), from DINOLoket (2009).

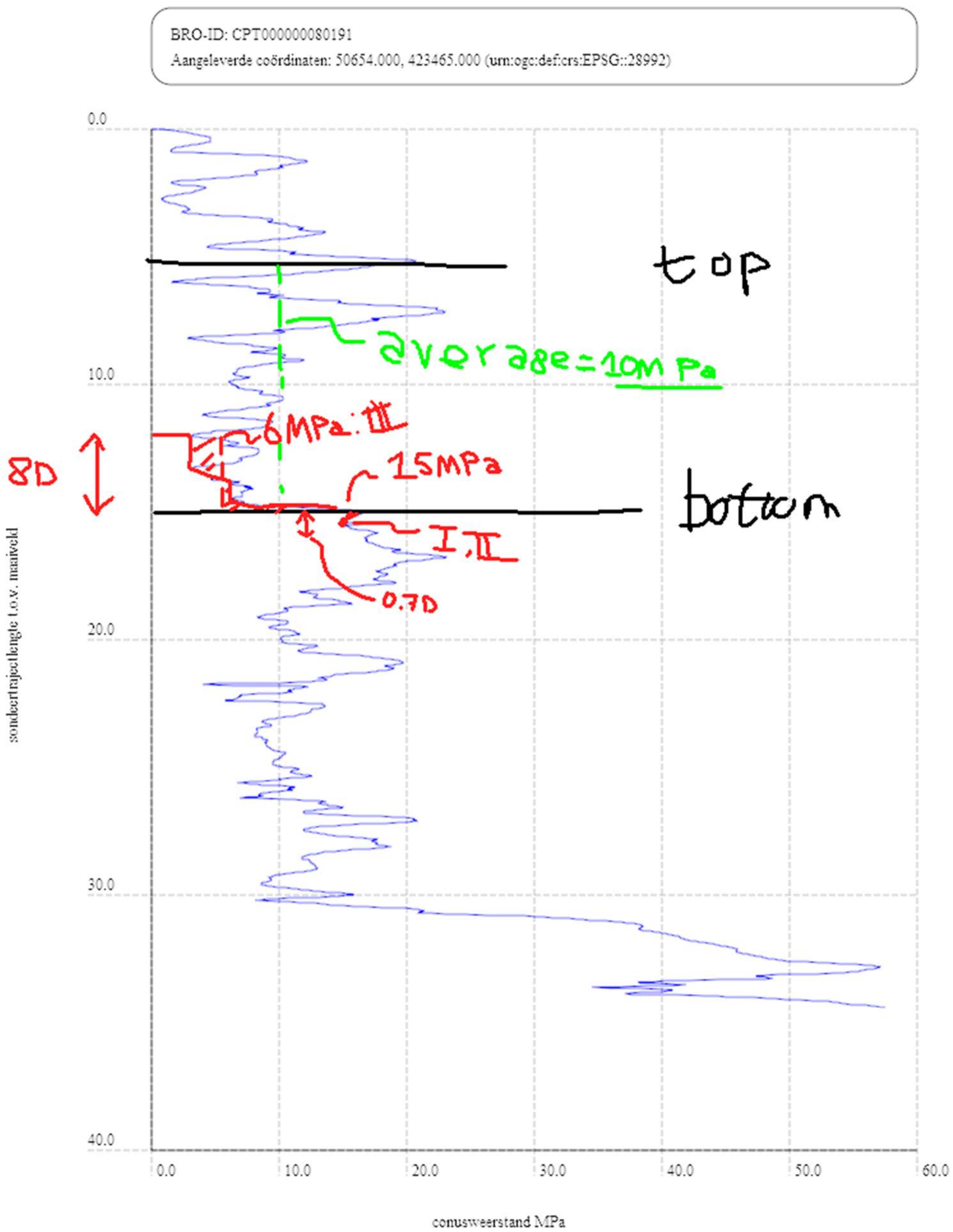

Figure viii.3.8 Calculation of cone stress for the first iteration of the Brouwersdam. Cone penetration profile #CPT000000080191 (Brouwersdam), from DINOLoket (2017).

§VIII.4 Overspill protection

To derive the necessary heights for the overspill protection, Table viii.2.5 and Figure viii.2.4 are used. Below the relevant portions of each are shown below

Table viii.4.1 Relevant vertical locations of the top of the Deltapump [m NAP].

		Haringvlietdam	Brouwersdam
D’	Spout high	+6,750	+7,130
E	Top central axis	+5,295	+5,675
F’/h_{WEIR}	Spout low	+3,839	+4,219
H_{DP}	Deltapump energy head	+7,489 to +7,665	+7,868 to +8,017
h_{DP}	Deltapump hydraulic. head	+6,272 to +6,389	+6,652 to +6,751

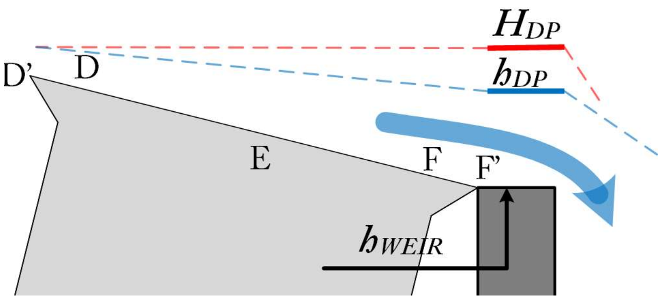

Figure viii.4.2 Relevant vertical locations of the top of the Deltapump

See Figure viii.4.5, let’s construct concrete walls on either side and a steel plate on the back and bottom to stop overspill. The water level above the weir is for Haringvlietdam and Brouwersdam is (6,389 – 3,839 =) 2,550 m and (6,751 – 4,219 =) 2,532 m respectively. For both, let’s raise the concrete wall to 3 meter above the weir for safety. At the back, point *D’* in Figure viii.4.2, the water levels are (7,665 – 6750 =) 0,915 m and (8,017 – 7,130 =) 0,887 m respectively. Point *D’* is located 2,91 m higher than the weir (12 × sin (arctan (0,25))), so these values are 3,83 and 3,80 m above the weir respectively. For safety, let’s raise both concrete walls at the back to 4,50 m above the weir. For the result, see the figure below. The width of the concrete wall is 1 meter and its length 12 m.

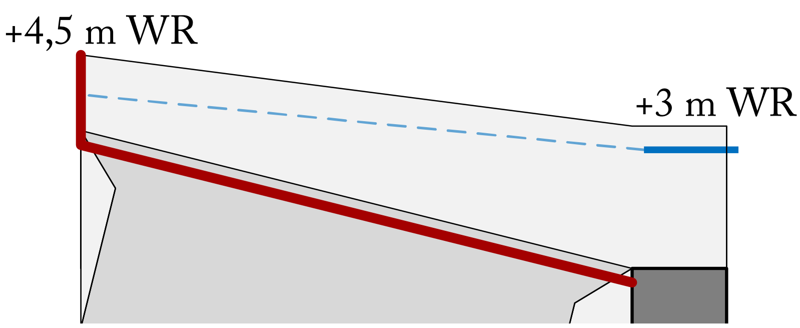

Figure viii.4.3 Dimensions of the overspill concrete walls. Heights shown with respect to the weir, or [m WR]

For the overspill protection around the Deltapump, a steel plate is introduced. See **Figure viii.4.5** and **Figure viii.4.3** (the red line). This plate is place 300 mm below the top of the Deltapump, so that it can be better attached to the weir and so that leakage is minimised. Of course, a small gap between the steel plate and the Deltapump will arise, but this can be filled with a watertight, near-frictionless material.

For the steel plate, a thickness of 40 mm is used and S355 steel. Because the concrete walls are 1 meter wide, the steel plate becomes 15 – 1 = 14 m wide. To calculate the stresses in the plate, the average water level over the plate is used. As the steel plate is located 300 mm below the spout of the Deltapump, the average water level is 300 + (0,5 × (7.665 + 6.389)) – 5.295 ≈ 2.050 mm. This is increased to 2.500 mm for safety.

To calculate whether this steel plate can hold the loads of this water, an overestimate is presented here, as plates like these require more complex calculations.

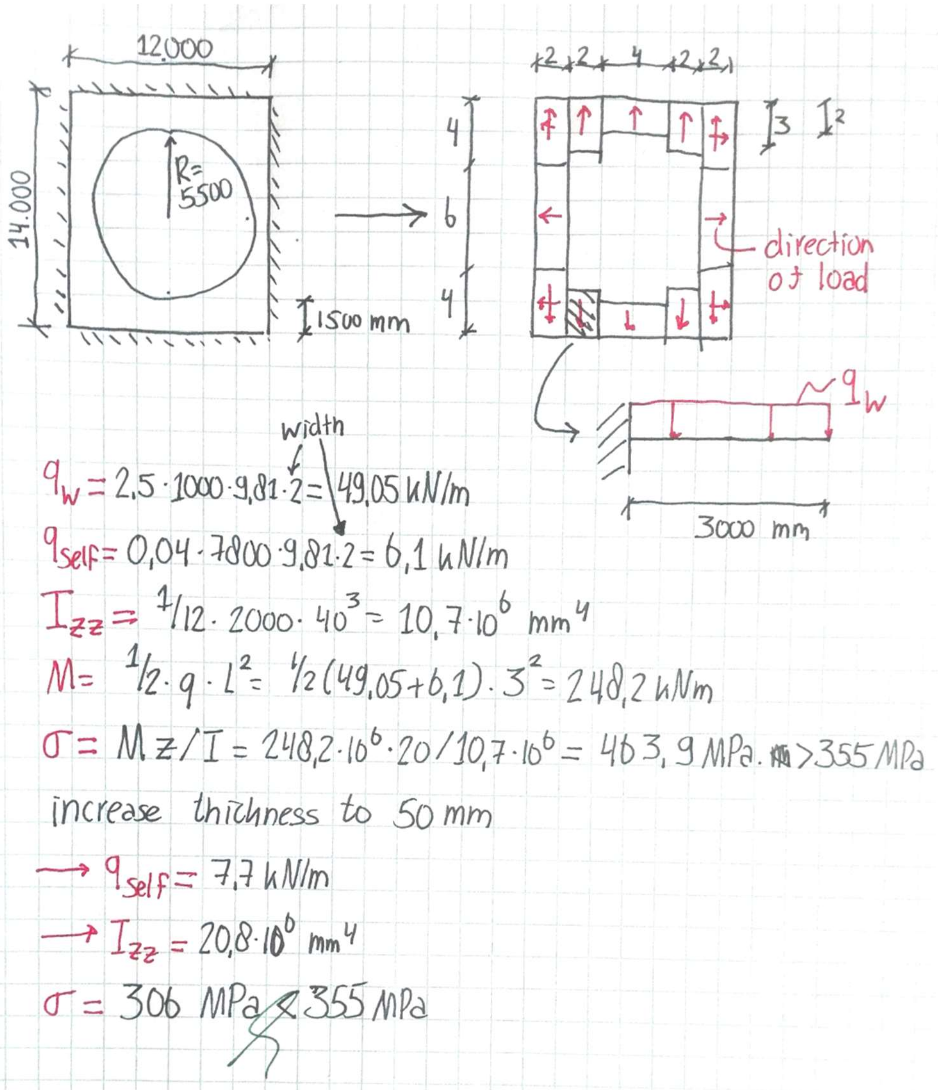

Figure viii.4.4 Calculations for the overspill plate strength.

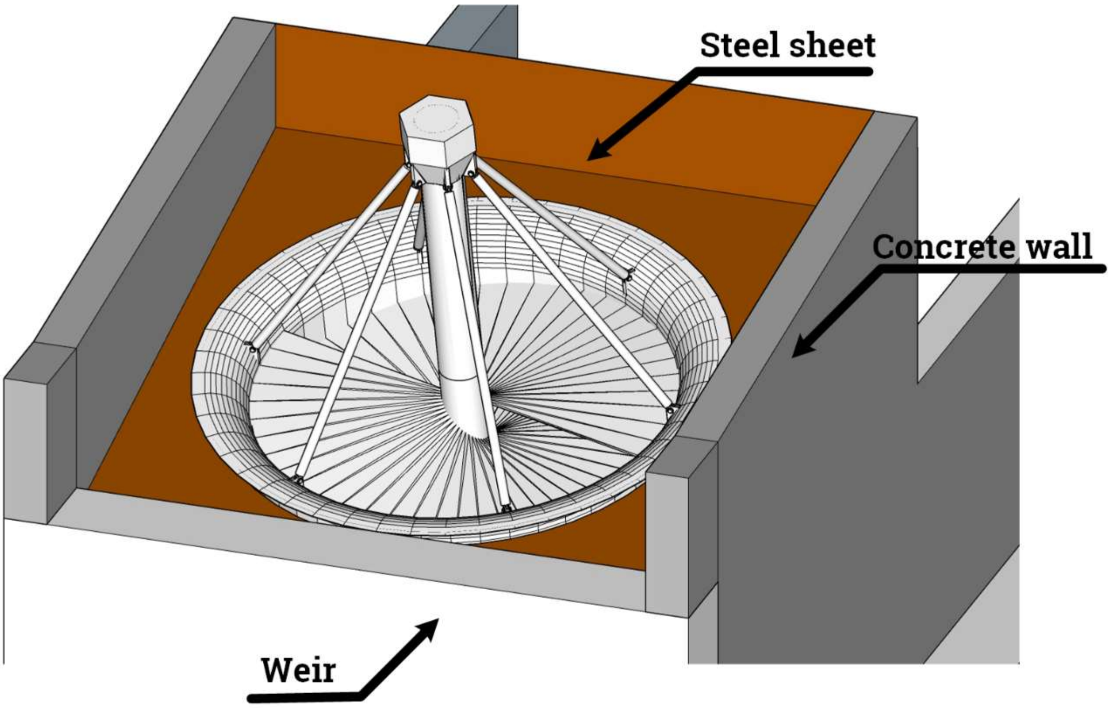

Figure viii.4.5 Three-dimensional overview of the overspill components: concrete walls and steel plate.

§VIII.5 Supporting structure

In this section the dimensions of the supporting structure are determined. This structure is placed upon the concrete separation walls that were created for the overspill. The length of these walls is 12 meter, their width 1 meter and they are placed 15 meters centre-to-centre. The height difference between the front and the end of the concrete wall is 1,50 m, see Figure viii.4.3.

This supporting structure is continuous; it spans multiple modules, because it is placed on the shared separation walls. The figure below shows the design for the supporting structure, a steel truss. The points *B* and *C* are 10 meter apart and consequent points *B* or *C* are 15 meters apart.

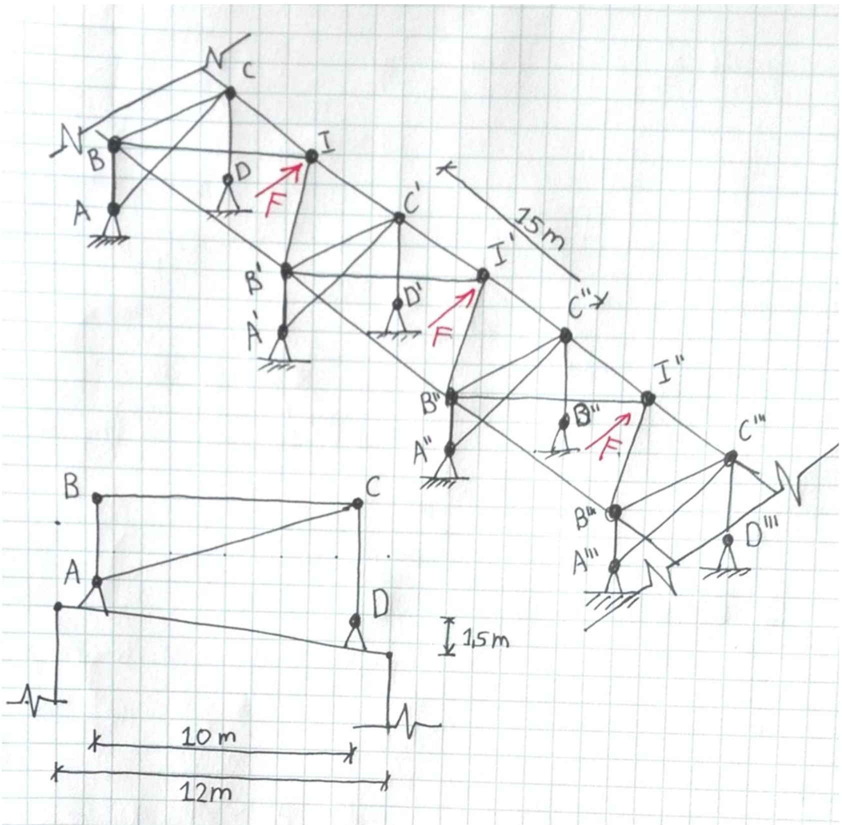

Figure viii.5.1 Overview of the supporting structure

The top of the driving mechanism of the Deltapump is located 7cos(arctan(0,25)) = 6,8 m above point *E* from Figure viii.2.4, which is 6,8 + 6sin(arctan(0,25)) = 8,26 m above the weir. Support *D* from the figure above is located 3 meters above the weir, see Figure viii.4.3. So, the length of rod CD is then 8,26 – 3 = 5,25 m. Support A is located 1,5 m higher than support D, so the length of rod AB is 3,75 m.

The horizontal force is 878 kN as determined in §VIII.3.1. The force distribution is as follows. The force subjects point *I* and is then equally distributed over *IB* and *IB'*. From there, the force is transferred in rod BC and B'C' and is then split into AC/DC and A'C'/D'C' respectively before reaching the concrete separation walls.

Furthermore, it should be noted that for segments at the edges, the forces activate rod BB'. See the figure below. The green encircled rods keep each other in equilibrium, whilst the red encircled don't. They activate the rods BB' in which a compressive force arises.

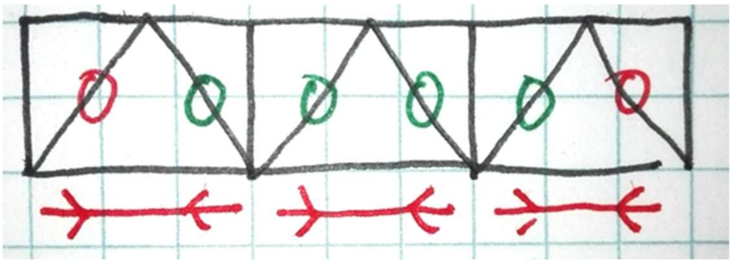

Figure viii.5.2 Top view for explanation of compressive forces in rods BB'

The last thing to be mentioned before the dimensioning can commence, are the vertical forces. Let's assume a permanent distributed load of 3 kNm^{-2} for machinery over the entire plane BCB'C' and a variable load of 1 kNm^{-2} corresponding to roughly 1 person. With the safety factors this becomes: 1,2 × 3 + 1,5 × 1 = 5,1 kNm^{-2}, without: kNm^{-2}. Let the structure be built such, that these forces act on rods BB' and CC' directly, see Figure viii.5.3.

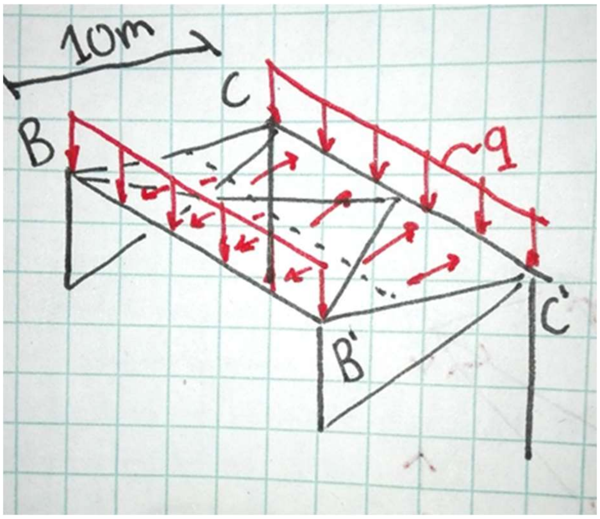

Figure viii.5.3 Distributed vertical loads in the structure

Rods BB' and CC' are 10 meters apart, so the distributed load becomes: 5 × 5,1 = 25,5 kN/m in ULS and 20 kN/m in SLS.

Now all forces that act on the structure are known, suitable profiles can be found for the requirements:

→ Strength requirement: $\sigma \leq 355$ MPa ; all loads with safety factors

→ Stiffness requirement: $w_{MAX} \leq 0,004 \times L$; no safety factors

The profiles are found by analysing the structure top to bottom, starting with rods IB and IB'. All cross-sectional parameters are shown in Table viii.5.4. These include self-weight *G*, cross-sectional area *A*, section modulus W_{ZZ} and second moment of inertia I_{YY} and I_{ZZ}.

Rods IB and IB'

The length of these rods is: $L = \sqrt{\left(\frac{15}{2}\right)^2 + (10)^2}$ = 12,5 m

The Deltapump ULS force of 878 kN is distributed equally over both rods: +439 kN. Due to the angle, the force in the rods is +549 kN. For the strength requirement, a cross-sectional area of 1.548 mm^2 is necessary. Let's choose profile HE 120 AA. Due to the self-weight, a moment is generated that causes extra stresses. The rod is simply supported, so the moment, with a safety factor of 1,2, is: 0,125 × 0,146 × 1,2 × 12,5^2 = 3,42 kNm. The maximum tensile stress is then: $\frac{549 \times 10^3}{18,6 \times 10^2} + \frac{3,42 \times 10^6}{75,8 \times 10^3} = 340$ MPa. This satisfies the strength requirement. Let's now check the stiffness requirement with the following equation:

$$w = \frac{5}{384} \times \frac{q \times L^4}{EI_{ZZ}} \qquad \textit{equation viii.16}$$

The distributed load is now without safety factors: 0,146 kN/m. The maximum deflection yields 54 mm. The allowed deflection is 0,004 × 12.500 = 50 mm. Let's choose HE 140 AA. With the same method the tensile stress becomes 277 MPa and the deflection 38 mm. This satisfies both criteria.

Rod BB'

The length of these rods is 15 m. The rod is subjected to:

→ Self-weight

→ Deltapump compressive force: -329 kN (= 0,75 × -439)

→ Vertical distributed load: 25,5 kN/m (ULS) and 20 kN/m (SLS)

Let's choose a profile HE 450 M. The moments caused by self-weight and the vertical distributed load are 0,125 × 1,2 × 2,6 × 15^2 + 0,125 × 25,5 × 15^2 = 804,9 kNm. The maximum compressive stress is then:

$$-\frac{329 \times 10^3}{335 \times 10^2} - \frac{804,9 \times 10^6}{5.501 \times 10^3} = \text{-156 MPa}.$$

Let's first check the stiffness requirement:

$$\frac{5}{384}\times\frac{(2,6+20)\times 15.000^4}{210\times 10^3\times 131.500\times 10^4} = \ 54\ \text{mm}$$

The maximum allowed deflection is 0,004 × 15.000 = 60 mm, so this profile suffices. Choosing lower profiles is not possible as the deflection will exceed the limit.

Rod CC'

The length of these rods is 15 m. The rod is subjected to:

- → Self-weight
- → Self-weight from rods IB and IB'
- → Vertical distributed load: 25,5 kN/m (ULS) and 20 kN/m (SLS)

The self-weight from the rods IB and IB' is subjected to rod CC' as a point load. This point load is 2 × 0,5 × 12,5 × 1,2 × 0,181 = 2,715 kN (ULS) and 2 × 0,5 × 12,5 × 0,181 = 2,26 kN (SLS) for both rods.

Let's also use profile HE 450 M. The moment caused by the self-weight is equal to that of Rod BB': 804,9 kNm. The moment caused by the point loads is: 0,25 × 2,715 × 15 = 10,2 kNm (ULS). The maximum stress is then:

$$\frac{(804,9+10,2)\times 10^6}{5.501\times 10^3} = 148\ \text{MPa}$$

The maximum deflection is:

$$\frac{5}{384}\times\frac{(2,6+20)\times 15.000^4}{210\times 10^3\times 131.500\times 10^4}+\frac{1}{48}\times\frac{2,26\times 10^3\times 15.000^3}{210\times 10^3\times 131.500\times 10^4} = \ 55\ \text{mm}$$

The maximum allowed deflection is 60 mm, so this profile suffices.

Rods BC and B'C'

The length of these rods is 10 m. These rods are subjected to:

- → Self-weight
- → Deltapump compressive force: -878 kN (ULS)

For the compressive force, a cross-sectional area of 2475 mm^2 is required. Let's choose HE 160 AA. The moment caused by self-weight is: 0,125 × 1,2 × 0,238 × 10^2 = 3,57 kNm. The maximum compressive stress becomes:

$$-\frac{878\times 10^3}{30,4\times 10^2}-\frac{3,57\times 10^6}{173\times 10^3} = \text{-}309\ \text{MPa}$$

Let's check the stiffness requirement:

$$\frac{5}{384} \times \frac{0,238 \times 10.000^4}{210 \times 10^3 \times 1.283 \times 10^4} = 11,5 \text{ mm}$$

The maximum allowed deflection is 0,004 × 10.000 = 40 mm. Both criteria are satisfied.

Rods AC and A'C'

The length of these rods is: $\sqrt{10^2 + 4^2} \approx 10,8 \text{ m}$. The forces subjected on these rods are:

- → Self-weight
- → Deltapump tensile force: 878 × 10,8/10 = +948 kN

For this tensile force, a cross-sectional surface area of 2.680 mm^2 is required. Let's choose the same profile as rods BC and B'C': HE 180 AA. The moment caused by self-weight is: 0,125 × 1,2 × 0,287 × 10,8^2 = 5,02 kNm. The maximum tensile stresses are then:

$$\frac{948 \times 10^3}{36,5 \times 10^2} + \frac{5,02 \times 10^6}{236 \times 10^3} = +281 \text{ MPa}$$

Let's check the stiffness requirement:

$$\frac{5}{384} \times \frac{0,287 \times 10.800^4}{210 \times 10^3 \times 1967 \times 10^4} = 12 \text{ mm}$$

where 43 mm is allowed. Both criteria are satisfied.

Rods AB and A'B'

These rods are 3,75 meter long and are subjected to:

- → Self-weight
- → Self-weight from rod BB': 46,8 kN (ULS) and 39 kN (SLS)
- → Self-weight from rod BC and B'C': 1,72 kN (ULS) and 1,44 kN (SLS)
- → Self-weight from rod IB and IB': 2,72 kN (ULS) and 2,26 kN (SLS)
- → Vertical distributed load: 382,5 kN (ULS) and 300 kN (SLS)

The total ULS compressive loads are 433,7 kN. A total cross-sectional area of 1.222 mm^2 is required, let's choose profile HE 120 AA. This gives a maximum compressive force (including self-weight) of 230 N/mm^2.

As this profile is loaded axially, its buckling force needs to be verified. The method is derived from Abspoel et al. ([Lecture notes], 2014, pp. 60-71).

Let's first check buckling over the y-y axis. The buckling length ℓ_{buc} of a simply supported beam is equal to its length, which is 3,75 m. The radius of gyration is:

$$i = \sqrt{\frac{I}{A}} = \sqrt{\frac{413 \times 10^4}{1.860}} = 47{,}1 \text{ mm} \qquad \textit{equation viii.17}$$

The slenderness is then calculated as:

$$\lambda = \frac{\ell_{buc}}{i} = \frac{3.750}{47{,}1} = 79{,}6 \qquad \textit{equation viii.18}$$

The limit slenderness is calculated as:

$$\lambda_e = \pi\sqrt{\frac{E}{f_y}} = \pi\sqrt{\frac{210.000}{355}} = 76{,}4 \qquad \textit{equation viii.19}$$

The slenderness ratio $\bar{\lambda}$ is then the slenderness divided by the limit slenderness, which yields 1,04.

For the profile, an imperfection parameter α of 0,34 is found. The buckling factor χ is then found to be 0,571. The buckling force is then found with:

$$N_{b,Rd} = \chi \times A \times f_y \qquad \textit{equation viii.20}$$

Which yields 377 kN. This is less than the load (433,7 kN) so it doesn't not satisfy the buckling criterium.

Let's choose profile HE 160 AA. The buckling force around the y-y axis is found to be 811 kN and around the z-z axis 450 kN. This satisfies now all criteria.

Rods DC and D'C'

These rods are 5,25 meter long and are subjected to:

- → Self-weight
- → Self-weight from rod CC': 46,8 kN (ULS) and 39 kN (SLS)
- → Self-weight from rod BC and B'C': 1,72 kN (ULS) and 1,44 kN (SLS)
- → Self-weight from rod IB and IB': 2,72 kN (ULS) and 2,26 kN (SLS)
- → Self-weight from rod AC and A'C': 1,86 kN (ULS) and 1,55 kN (SLS)
- → Vertical distributed load: 382,5 kN (ULS) and 300 kN (SLS)
- → Deltapump compressive force: 878 × 3,75/10 = 329 kN.

The total ULS compressive loads are 765 kN. This requires a cross-sectional area of 2.155 mm^2. Let's try HE 200 B. The buckling force over the z-z axis is the lowest, so let's check that.

The radius of gyration is:

$$i = \sqrt{\frac{I}{A}} = \sqrt{\frac{2.003 \times 10^4}{7.810}} = 50,6 \text{ mm} \qquad \textit{equation viii.21}$$

The slenderness is then calculated as:

$$\lambda = \frac{\ell_{buc}}{i} = \frac{5250}{50,6} = 103,7 \qquad \textit{equation viii.22}$$

The limit slenderness is calculated as:

$$\lambda_e = \pi \sqrt{\frac{E}{f_y}} = \pi \sqrt{\frac{210.000}{355}} = 76,4 \qquad \textit{equation viii.23}$$

The slenderness ratio $\bar{\lambda}$ is then the slenderness divided by the limit slenderness, which yields 1,357.

For the profile, an imperfection parameter α of 0,49 is found. The buckling factor χ is then found to be 0,366. The buckling force is then found with:

$$N_{b,Rd} = \chi \times A \times f_y \qquad \textit{equation viii.24}$$

This yields 1.014 kN. This satisfies the buckling criterium. Lower, more economical profiles could not be found.

Table viii.5.4 Cross-sectional parameters of steel profiles used in this section. From TU Delft supplemental material (2016).

Profile	Self-weight G [N/m]	Area A [×10^2 mm^2]	Section modulus W_{ZZ} [×10^3 mm^3]	Second area moment I_{ZZ} [×10^4 mm^4]	Second area moment I_{YY} [×10^4 mm^4]
HE 120 AA	146	18,6	75,8	413	159
HE 140 AA	181	23	112	719	275
HE 160 AA	238	30,4	173	1.283	479
HE 180 AA	287	36,5	236	1.967	730
HE 200 A	423	53,8	389	3.692	1.336
HE 200 B	613	78,1	570	5.696	2.003
HE 450 M	2.600	335	5.501	131.500	19.340

Support reactions (SLS)

- → A: vertical: +108 kN, horizontal: +878 kN
- → D: vertical: +765 kN

Summary of all the profiles

The figure below shows three segments of the supporting structure; the profiles used and the hinges.

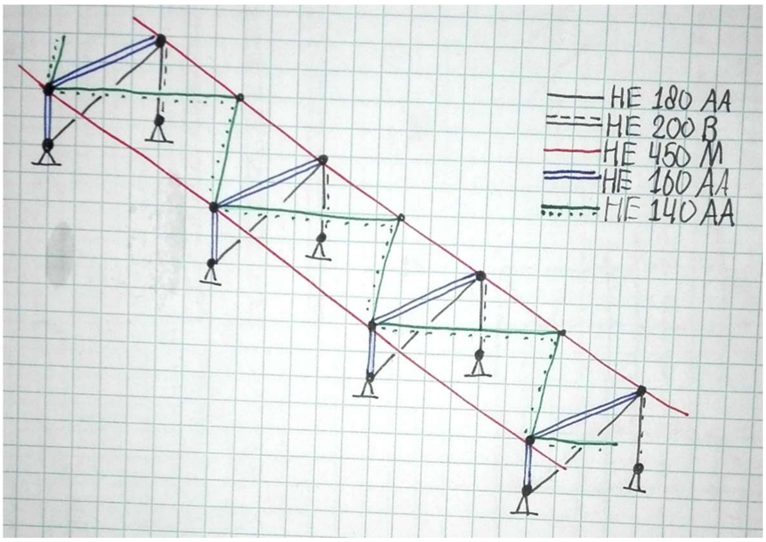

Figure viii.5.5 Summary of all profiles

Stability

The structure as shown in Figure viii.5.5 is a mechanism; it can move in its longitudinal direction. To provide stability, diagonal stability struts are added to one every five segments, see the figure below.

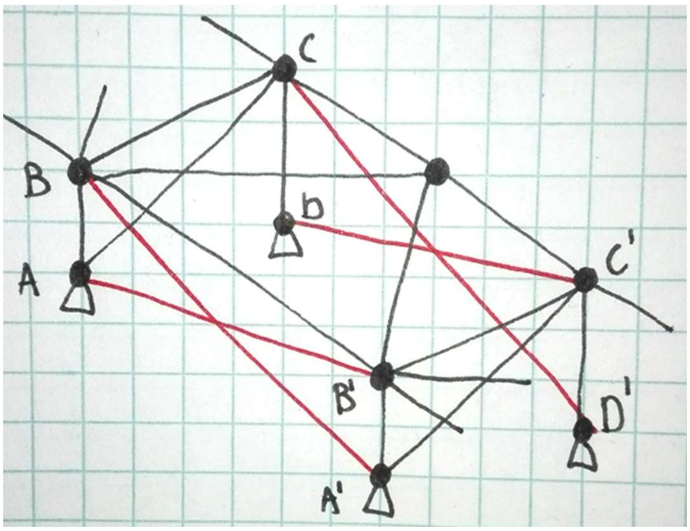

Figure viii.5.6 Stability struts to prevent the structure turning to a mechanism

§VIII.6 Service road slab

In this section the slab for the service road is designed that will be placed upon the walls in the intake canal. A summary of the results is presented at the end.

Loads and load cases

To start, let's identify the forces that act on the service road. In section §VIII.3.1 it was calculated that the Deltapump weights approximately 3,3 MN or 330 ton. To be on the safe side, a crane with a 500 ton lifting capacity is required. This means that the service road has to support such a crane. According to Nederhoff (n.d., p.1), the weight of such a crane is 257 tons. Furthermore, weight is transferred to the road with four outriggers with a surface area of 4 × 2,5 m^2 each. The total width of the crane is 12 meters when the outriggers are fully extended. The distance between the outriggers is 12 meter, see the figure below.

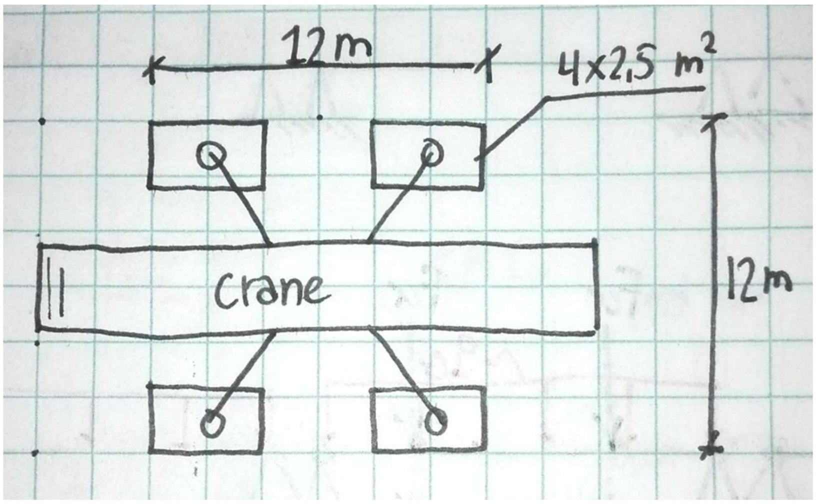

Figure viii.6.1 Layout of the crane outriggers when it is in operation.

The service road will be made out of multiple prefabricated prestressed concrete slabs with a centre-to-centre distance of 15 meters, just like the modules of the design. In practice, the length is a little less than 15 meters to allow thermal expansion and to ease installations, so let's downsize this to 14,8 meters. From Figure viii.6.1 it can be derived that the required width is at least 12 meters in order to allow a crane. Let's increase this with a margin; 15 meter wide road. To enhance the constructability the road will be made out of five separate 3-meter-wide concrete slabs.

The concrete slabs will be simply supported and they are not continuous. Furthermore, in these calculations the slab will be analysed one-dimensionally, just like shown in Figure viii.6.2. This means that only one out of the five parallel slabs are analysed for the load cases. The resulting dimensioning and prestressing will be applied to the other four slabs as well. See the figure below

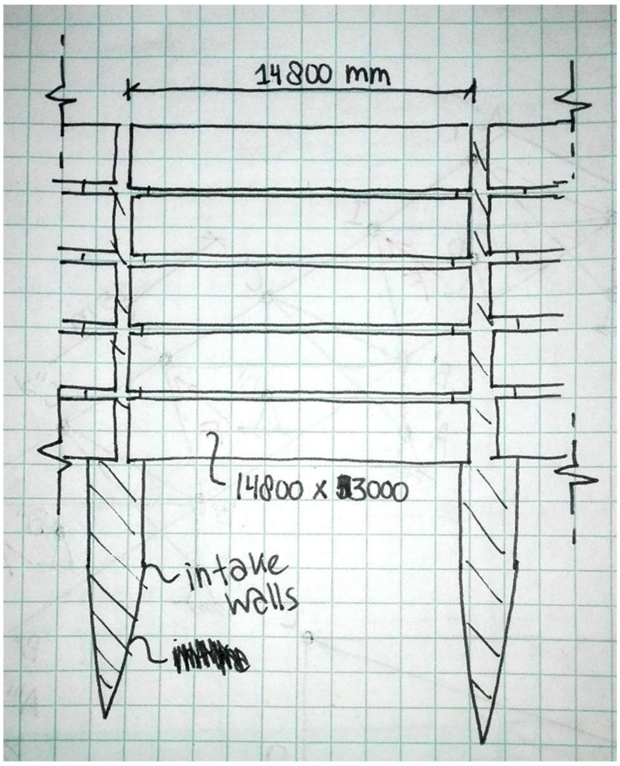

Figure viii.6.2 Top view the five service road slabs, place upon the intake walls.

In order to find appropriate dimensioning, the load cases have to be examined. For this one-dimensional analysis, we analyse a concrete slab on which crane outriggers are placed upon. Let's model the loads on the outriggers as point loads. Maximum two point loads from the outriggers can occupy a single 3.000×14.800 mm^2 road slab, more is geometrically impossible. These loads are than 8 meters apart (12 – 2 × 0,5 × 4,0) in longitudinal direction, derived from Figure viii.6.1.

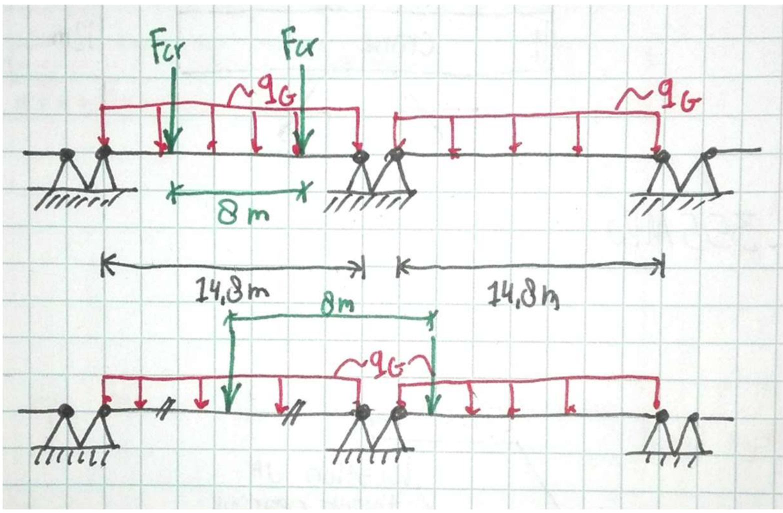

Figure viii.6.3 Two ULS load scenarios. Above: load case for maximum shear force, bottom: load case for maximum bending moment.

See Figure viii.6.3, two ULS load cases have been defined. In the first load case, the point loads are centred around the middle of a single concrete slab so that the vertical loads are maximised on a single concrete slabs. In the second load case, one point load is exactly in the middle of a concrete slab; this will maximise the bending moment.

Material characteristics

The prestressed steel will be Y1860C with a characteristic strength value of 1.860 MPa. The concrete class is C30/37 when it is prestressed and increases to C50/60 after 28 days of curing. Furthermore, a few requirements need to be met.

For the concrete in the cross-section:

→ When fully loaded, no tensile stresses in concrete

→ During stressing, bottom concrete compressive stress: $\left|\sigma_{\text{C, BOTTOM}}\right| \leq 0,7 \times f_{CK}$

→ During stressing, top concrete tensile stress: $\sigma_{\text{C,TOP}} \leq \max\left\{(1,6 - {}^{h}\!/_{1.000}) \times f_{CTM}; f_{CTM}\right\}$

For the prestressing steel in the cross-section:

→ After stressing, maximum stress: $\sigma_P \leq 0,75 f_{PK}$

→ During stressing, maximum stress: $\sigma_P \leq 0,8 f_{PK}$

Service road slab dimensions

For the first calculations, let's use a slab height h of 600 mm and an eccentricity e of 200 mm. Thee self-weight G of the concrete is: 1.800 × 9,81 × 3 × 0,6 = 31,8 kN/m. This gives a mid-span moment M of 0,125 × 31,8 × 14,8^2 = 870 kNm. The section modulus W is: 1/6 × 3.000 × 600^2 = 1,8 × 10^8 mm^3. During stressing, the compressive force may not exceed 0,7 × 30 = 21 MPa. The mean tensile strength f_{CTM} of C30/37 is 2,9 MPa (Braam & Lagendijk, 2011, p. 28). The concrete tensile stress requirement then yields it must not exceed 2,9 MPa.

The prestressing causes a constant upward bending moment of $P_0 \times e$ and a compressive normal force of P_0, see Figure viii.6.4.

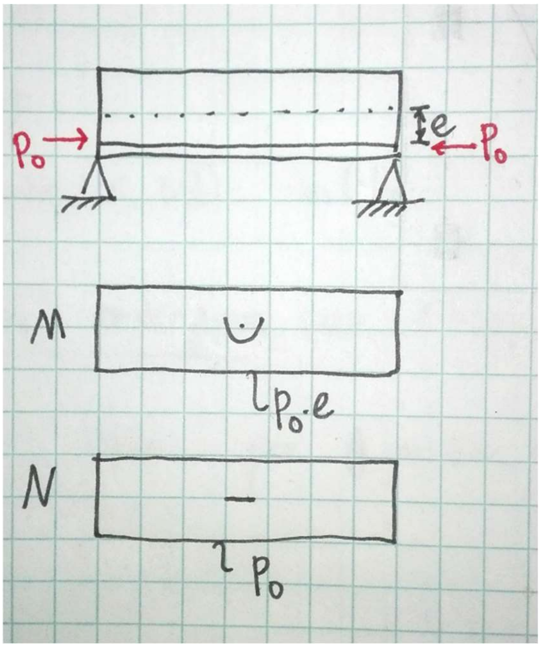

Figure viii.6.4 Bending moments and normal forces during pre-stressing of the service road slab.

During prestressing, the stresses can be calculated at the top and at the bottom for the requirements:

$$\sigma_{C,Top} = -\frac{P_0}{A_C} + \frac{P_0 \times e}{W_{ZZ,Top}} - \frac{M_G}{W_{ZZ,Top}} \leq 2{,}9 \text{ MPa}$$

$$\sigma_{C,Bot} = -\frac{P_0}{A_C} - \frac{P_0 \times e}{W_{ZZ,Bot}} + \frac{M_G}{W_{ZZ,Bot}} \geq -21 \text{ MPa}$$

In these equations A_C is the cross-sectional area of the slab 600 × 3.000 = 18 × 10^5 mm^2 and M_G is the moment caused by self-weight: 870 kNm. The first condition gives a maximum prestressing force of 13,92 MN. The second condition gives a maximum prestressing force of 15,5 MN. This is larger than the first condition, so 13,92 MN is the decisive maximum prestressing force. To find the minimum prestressing force, we need to look at the load cases. Let's assume that due to losses the prestressing capacity has decreased by $P_\infty = 0{,}8 \times P_0$.

Load case 1

The force F_{CR} from Figure viii.6.3 is one-fourth of the weight of the crane and the lifted Deltapump: 0,25 × (3,3 + 2,57) = 1,47 MN. This is not multiplied by safety factors, as this concerns SLS. The mid-span moment due to the crane can be calculated: 1,47 × (14,8 – 8,0) × 0,5 = 4,99 MNm. Let's find the minimum required prestressing force to not have tensile forces:

$$\sigma_{C,Bot} = -\frac{P_\infty}{A_C} - \frac{P_\infty \times e}{W_{ZZ,Bot}} + \frac{M_G + M_{Pr}}{W_{ZZ,Bot}} \leq 0 \text{ MPa}$$

This gives a minimum P_∞ of 19,5 MN, which gives a minimum P_0 of 24,4 MN. This is higher than the maximum prestressing force of 13,95 MN. Since the difference is large between the minimum and maximum prestressing forces, another cross-section is proposed, see the figure below.

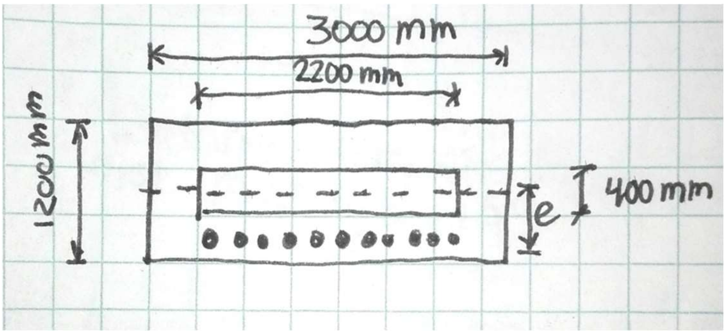

Figure viii.6.5 Hollow cross-sectional concept for the service road.

For this hollow profile, the section modulus W is: $1/6 \times 3.000 \times 1.200^2 - 1/6 \times 2.200 \times 400^2 = 661 \times 10^6$ mm^3. The cross-sectional surface area A is $3.000 \times 1.200 - 2.200 \times 400 = 27,2 \times 10^5$ mm^2. The self-weight G is 48 kN/m which causes a bending moment M_G of 1,314 MNm. The eccentricity is 400 mm. With the equations described earlier, the maximum prestressing force P_0 can be calculated for the tensile condition at the top:

$$\sigma_{C,Top} = -\frac{P_0}{A_C} + \frac{P_0 \times e}{W_{ZZ,Top}} - \frac{M_G}{W_{ZZ,Top}} \leq 2,9 \text{ MPa}$$

$$\Rightarrow P_0 \leq \frac{2,9 + \frac{M_G}{W_{ZZ,Top}}}{\frac{e}{W_{ZZ,Top}} - \frac{1}{A_C}}$$

$$\Rightarrow P_0 \leq \frac{2,9 + \frac{1,314 \times 10^9}{661 \times 10^6}}{\frac{400}{661 \times 10^6} - \frac{1}{2,72 \times 10^6}} = 20,6 \text{ MN}$$

The same goes for the compressive condition at the bottom of the slab:

$$\sigma_{C,Bot} = -\frac{P_0}{A_C} - \frac{P_0 \times e}{W_{ZZ,Bot}} + \frac{M_G}{W_{ZZ,Bot}} \geq -21 \text{ MPa}$$

$$\Rightarrow \text{P}_0 \leq \frac{21 + \frac{1,314 \times 10^9}{661 \times 10^6}}{\frac{1}{27,2 \times 10^5} + \frac{400}{661 \times 10^6}} = 23,6 \text{ MN}$$

This is larger than the first condition, so 20,6 MN is the maximum prestressing force. Let's now first investigate the second load case.

Load case 2

The mid-span moment caused by the crane can be calculated: 0,25 × 1,47 × 14,8 = 5,44 MNm. For this load case, the minimum required prestressing force P_0 is:

$$\sigma_{C,Bot} = -\frac{P_\infty}{A_C} - \frac{P_\infty \times e}{W_{ZZ,Bot}} + \frac{M_G + M_{Pr}}{W_{ZZ,Bot}} \leq 0 \text{ MPa}$$

$$\Rightarrow P_\infty \geq \frac{\dfrac{M_G + M_{Pr}}{W_{ZZ,Bot}}}{\dfrac{1}{A_C} + \dfrac{e}{W_{ZZ,Bot}}}$$

$$\Rightarrow P_\infty \geq \frac{\dfrac{(1{,}314 + 5{,}44) \times 10^9}{661 \times 10^6}}{\dfrac{1}{27{,}2 \times 10^5} + \dfrac{400}{661 \times 10^6}} = 10{,}5 \text{ MPa}$$

With the relation $P_\infty = 0{,}8 \times P_0$ this means P_0 equals 13,1 MN where a maximum of 20,6 MN is allowed. This criterium is satisfied. It is however not extremely economical, but since this is only the SLS check, let's check the SLS now.

Ultimate limit state check

Second load case yields the highest bending moments, so this case determines the dimensions of the prestressing steel. The minimum prestressing force was determined as 13,1 MN. With Y1860C steel, its characteristic strength is 1.860 MPa, however the requirements stated earlier that it should not be higher than three-quarters of that: 1.395 MPa. The required prestressing steel cross-sectional area is then 13,1 × 10^6/1.395 = 9.400 mm^2.

To check the moment the cross-section can resist mid-span, the cross-section needs to be analysed.

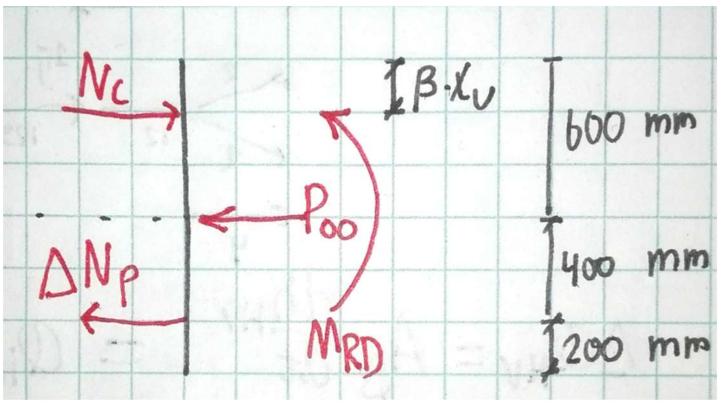

Figure viii.6.6 Concrete cross-section force balance.

The force balance is shown in Figure viii.6.6 is:

$$N_C = \Delta N_P + P_\infty$$

$$\alpha \times x_u \times b \times f_{CD} = A_P \times \frac{f_{PD} + \frac{f_{PK}}{\gamma_S}}{2}$$

In this equation α is a shape factor, x_u is the compression zone height, b is the width and f_{CD} is the design value of concrete compressive strength. As concrete has cured by now, the concrete class has increased from C30/37 to C50/60. For C50/60 α is 0,75 and f_{CD} is 33,3 MPa (Braam & Lagendijk, 2011, p. 28; p. 49). Assuming that the concrete compressive zone is located in the top flange:

$$\alpha \times x_u \times b \times f_{CD} = A_P \times \frac{f_{PD} + \frac{f_{PK}}{\gamma_S}}{2}$$

$$\Rightarrow x_u = \frac{A_P \times \frac{f_{PD} + \frac{f_{PK}}{\gamma_S}}{2}}{\alpha \times b \times f_{CD}} = \frac{9.400 \times \frac{1.395 + 1.691}{2}}{0,75 \times 3.000 \times 33,3} = 193 \text{ mm}$$

The assumption is true as the compression zone is indeed within the top flange.

The resisting moment M_{RD} as shown in Figure viii.6.6 is:

$$(\alpha \times x_u \times b \times f_{CD}) \times (1.000 - \frac{7}{18} x_u) - 13,1 \times 10^6 \times 400 = 8,173 \text{ MNm}$$

The ULS bending moment for load case 2 is: 1,5 × 4,99 × 1,2 × 1,314 = 9,06 MNm. This is a little more than the slab can resist.

Let's increase the prestressing force from 13,1 MN to the maximum 20,6 MN. The cross-sectional area of the prestressing steel tendons is now required to be: $20{,}6 \times 10^6 / 1.395 = 14.800$ mm^2. Repeating the previous equations yields a compression zone height of 304 mm and a resisting moment of 11,9 MNm. This satisfies the ULS bending moment.

Summary

A 3.000 × 1.200 mm² hollow prestressed concrete slab with a hole of 2.200 × 400 mm² and 14.800 mm² of prestressed Y1860C steel can resist a mid-span bending moment of 11.900 kNm where 9.060 kNm is the maximum determined bending moment for different load cases. This maximum moment originates from the loads of a 500-ton lifting the Deltapump, placed in the middle of the road so that the loads are maximal. In the figure below a cross-section is shown of the road.

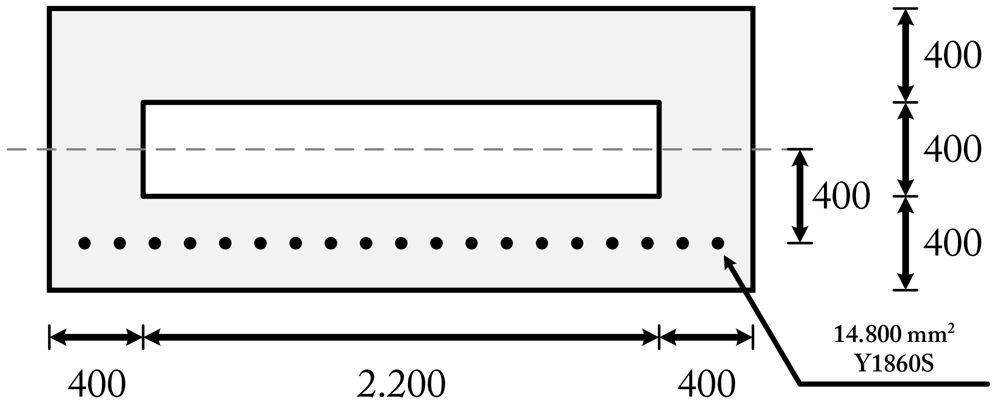

Figure viii.6.7 Cross-section of the service road hollow slab

These concrete prestressed slabs are 14.800 mm long and are place in groups of five over the intake walls, see the figure below.

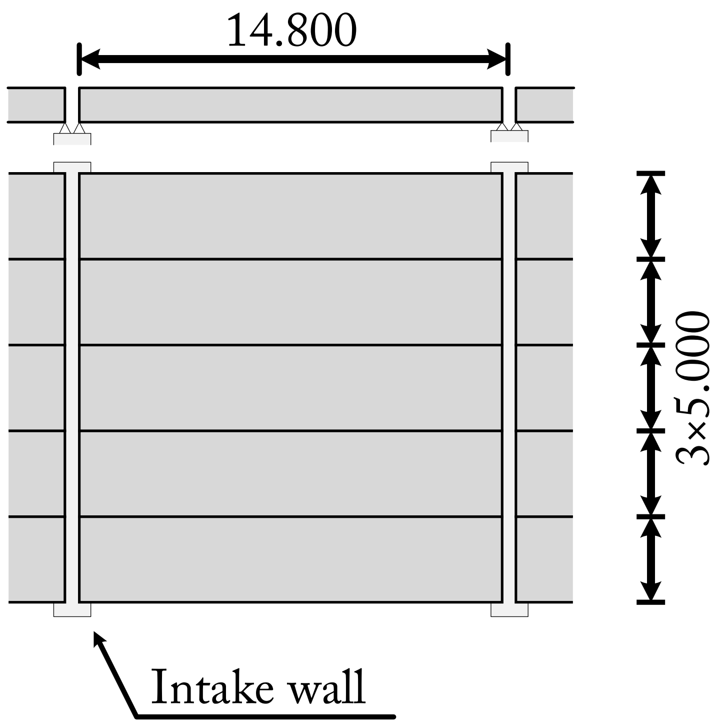

Figure viii.6.8 Top and side view of the service road. The service road is made out of five slabs.

§VIII.7 Intake canal and inner basin

§VIII.7.1 Intake walls

To support the supporting structure, the overspill protection, the service road, the fish-trash screens and to guide the water towards the Deltapump, the intake walls are created. See the figure below for the solution that is created.

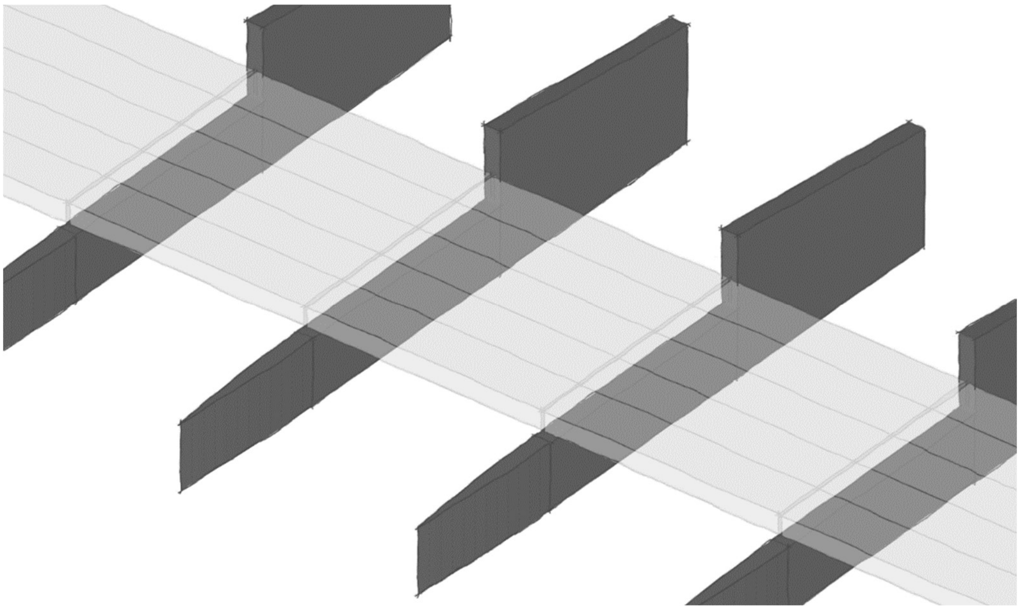

Figure viii.7.1 Intake walls with the service road shown semi-transparent.

Load and dimensions of the intake walls

The intake walls are 1 meter wide except at the funnel, were it converges to zero width. The figure below shows a side view with all relevant loads and dimensions.

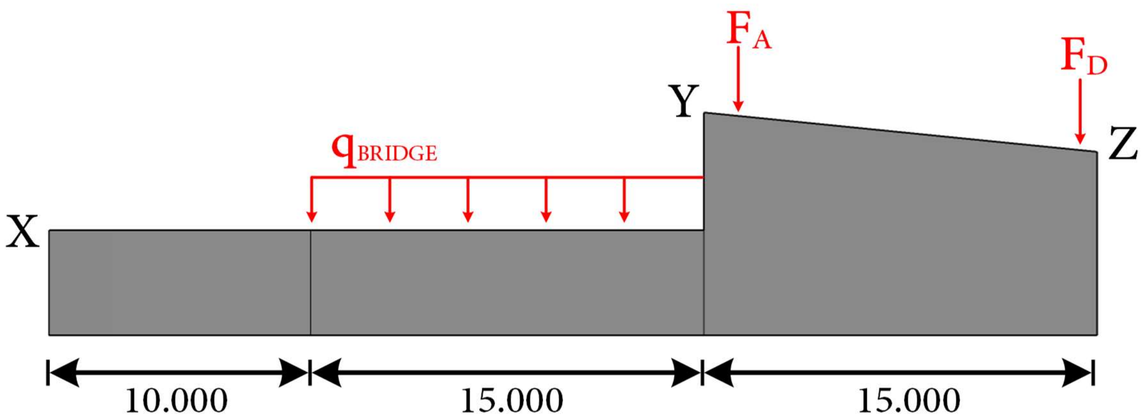

Figure viii.7.2 Side view of the intake walls with relevant loads and dimensions

The height X is for both locations +4,00 m NAP, which is 1,5 m above the highest water level. This ensure that water is at a safe distance underneath the service road. The heights Y and Z are situated respectively 4,5 and 3,0 m above the weir. See **Table viii.2.5**, for the Haringvlietdam these locations are therefore at +8,34 and +6,84 m NAP and for the Brouwersdam +8,72 and +7,22 m NAP respectively.

The self-weight of one 3-meter-wide bridge slab is: 48 × 14,8 = 710,4 kN. This force is distributed over the full 3 meters of the intake wall so this causes a distributed load of 710,4 / 3 = 237 kNm^{-1}. For the variable distributed load of the crane, see **Figure viii.6.3**, the first load case is assumed to be effective on two adjacent bridge decks, that is two cranes, each on one bridge deck, next to each other. This is a total load of 3,3 + 2,57 = 5,9 MN per bridge deck. As each bridge deck transfer the loads to two intake walls equally for that load case, the total load from two bridge decks on a single intake wall becomes: 5,9 × 0,5 × 2,0 = 5,9 MN. For simplification, this is divided by its length so that is becomes a distributed load: 5,9 / 15 = 393 kNm^{-1}.

Strength requirement

With safety factors, the distributed load q_{BRIDGE} becomes: 1,2 × 237 + 1,5 × 393 = 874 kNm^{-1}. As the intake wall is 1 meter wide, this subjects a 1×1 m^2 section of the intake wall to: 874.000 / 1.000^2 = 0,87 MPa. The lowest conventional concrete class, C20/25, has a design compressive stress of 13,3 MPa so the strength criterium of the intake wall is very well satisfied.

The points loads F_A and F_D were determined in **§III.5** and these are 108 and 765 kN respectively. This is lower than the loads of the bridge, so these are also satisfied with a C20.25 class.

Concrete environment class

Because the intake walls are exposed to brackish water, a non-conventional environment class is required for the intake walls. A suitable environmental class is *XS* as this also including flowing water (Braam & Lagendijk, 2011, pp. 39–40).

§VIII.7.2 Bed protection and inner basin

To prevent local scour and to protect the structure on a long-term basis, a 50 cm thick concrete layer will be placed with its top at -4,0 m NAP for both locations (Haringvlietdam and Brouwersdam). This is placed at the intake canal and at the inner basin. The inner basin will be 25 m in length.

§VIII.8 Sharp-crested weir

For the design of the weir, a 1-meter-wide section of the weir will be analysed. For the loads, two extreme load cases are distinguished. See the figure below. For the first load case, the water level in the inner basin is the largest, for the second load case in the storage basin is the largest. The forces caused by advection of water flowing over the weir is not included.

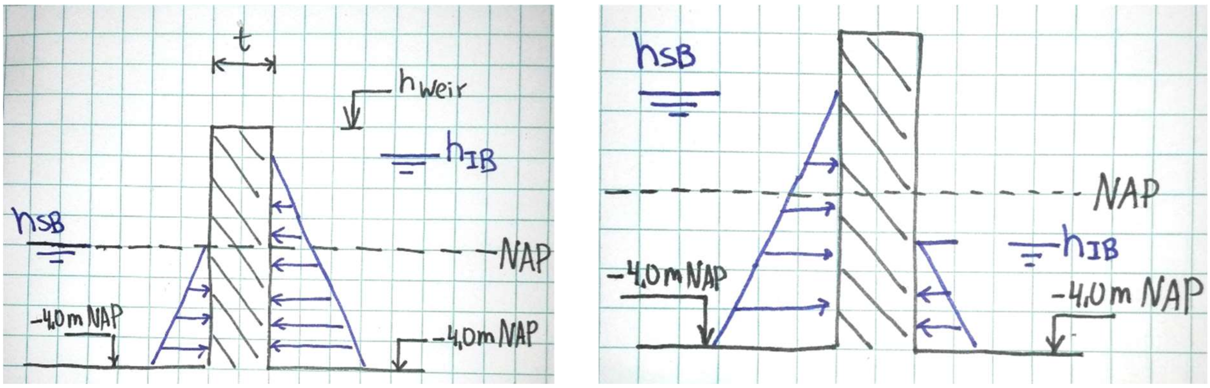

Figure viii.8.1 Two load cases. Left: inner basin high water levels, right: storage basin high water levels. Water levels not to scale; only showing that one is higher than the other.

In the table below, the bending moments caused by the load cases are shown for both the Haringvlietdam and Brouwersdam. The water levels are from **Table viii.2.5** and basis of design. NB for the second load case, the water levels are equal for both locations. The total design bending moments are calculated with 1,5 × M_1 + 0,9 × M_2 where M_2 is favourable.

Table viii.8.2 Calculations for net bending moments on the weir for both locations and both extremes.

		Brouwersdam	Haringvlietdam	
Load case 1	h_{SB}	+0,36	-0,02	m NAP
	h_{IB}	+2,995	+3,006	m NAP
	M_{SB}	+31,1	+25,9	kNm
	M_{IB}	-80,0	-80,3	kNm
	$M_{D,TOT}$	-92,0	-143,3	kNm
Load case 2	h_{SB}	+2,50		m NAP
	h_{IB}	+0,93		m NAP
	M_{SB}	+69,1		kNm
	M_{IB}	-39,7		kNm
	$M_{D,TOT}$	67,9		kNm

From these calculations the highest bending moment is -143,3 kNm counter-clockwise and 67,9 kNm clockwise: 143,3 kNm is decisive. Moreover, the weir is subjected to a normal load from the water that is flowing over the weir. In §VIII.4 these water levels were calculated. The largest of the two is 2,55 m water level above the weir. This causes the following design (with safety factor) normal load: 1,5 × 2,55 × 1.000 × 9,81 = 37,5 kN. Let's use concrete strength class C20/25, just like the intake walls. First, let's calculate whether reinforcement is required.

For the first iteration, let's use a thickness t of 500 mm. The section modulus W is then, for the 1-meter-wide section, $1/6 \times 1000 \times 500^2 = 41{,}7 \times 10^6$ mm^3. The cross-sectional area A is then 5×10^5 mm^2. The maximum tensile stress in the cross-section is then: $143{,}3 \times 10^6 / 41{,}7 \times 10^6 + 37.500 / 5 \times 10^5 = 3{,}5$ MPa. The maximum tensile stress of C20/25 is +2,56 MPa. If the thickness is increased to 600 mm, the tensile stress becomes +2,45 MPa. Reinforcement is then not required.

§VIII.9 Culvert

Within the calculations of vertical Deltapump integration, a cross-sectional area of 60 m^2 was used for the tunnel. Let's preserve that value. Below a front-view of the culvert design is shown.

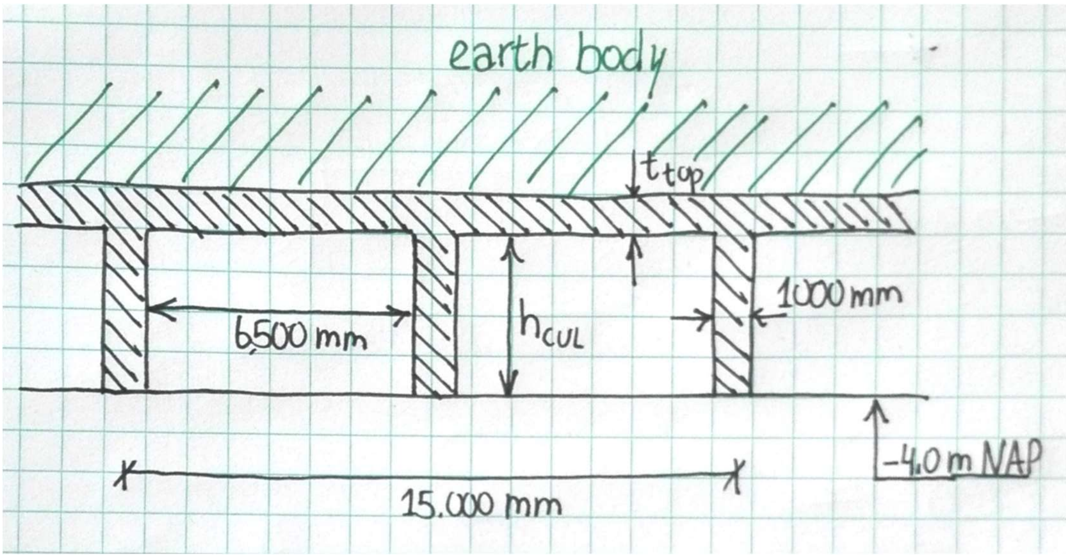

Figure viii.9.1 Front-view of the culvert.

In total, two smaller culverts cover the module-width of 15 meters. This will decrease bending moments by four times. The walls between the culvert openings are 1 meter wide so that each culvert will be 6,5 m wide. With the required 60 m^2, the height of the culverts become: 60 / (2×6,5) = 4,6 m. As determined in §VIII.7.2 the bed level in the inner basin is located at -4,0 m NAP so this means that the ceiling of the culvert is at +0,6 m NAP. With a North Sea water level of at least +2,50 m NAP when the pumping station is in operation, the culvert will be submerged by 1,9 meters which is assumed to be enough to attenuate the propagation of waves.

The vertical loads subjected to the culvert are from the soil lying above it. See the figures below.

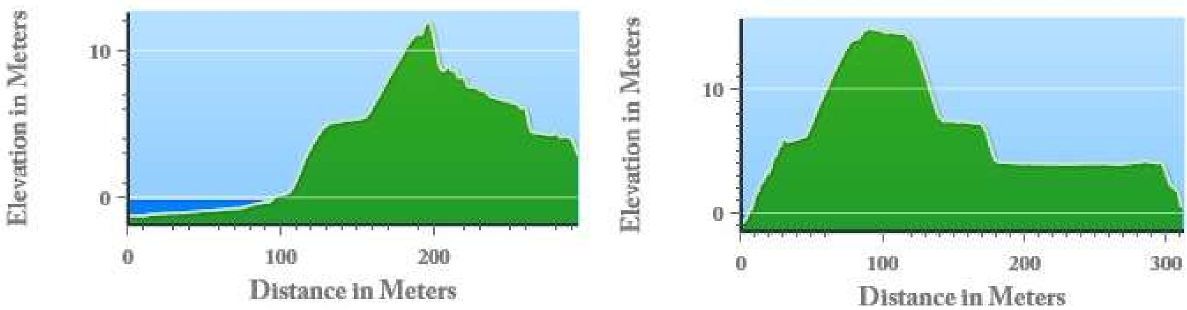

Figure viii.9.2 Elevation profiles of the Brouwersdam (left) and Haringvlietdam (right). From AHN (2020).

For the Brouwersdam the highest section is +11,0 m NAP and for the Haringvlietdam +15,0 m NAP. For the design of the culvert ceiling, let's consider a 1-meter-wide section, that is a slab of 1.000 × 6.500

mm^2. The static scheme corresponding to the culvert is a double-clamped beam, as the ceiling of the culvert is continuous.

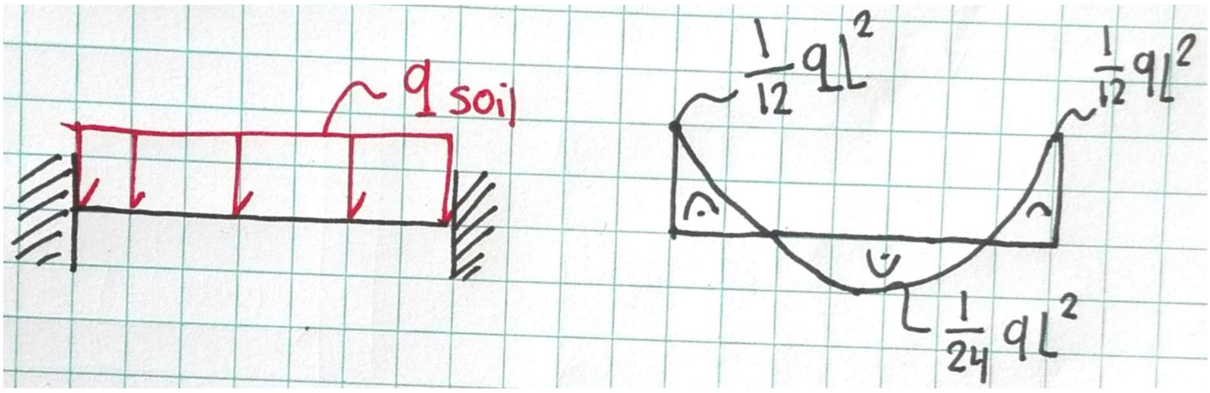

Figure viii.9.3 Static scheme corresponding to the culvert

For the first iteration, let's use a concrete slab of 500 mm thickness and let's look at the Haringvlietdam, as its soil pocket is larger. The thickness of the soil pocket above the culvert is 15 – 0,5 – 0,6 = 13,9 m. With a soil density of 20 kNm^{-3}, the stress exerted on the culvert is 13,9 × 20 = 278 kPa. For the 1-meter-wide section, this gives a distributed load of 278 kN/m.

First let's look at the reinforcement midspan. The midspan moment is then 1/24 × 278 × 6,5^2 = 489 kNm. Let's use reinforcement of 0,5% of B500B steel and concrete C20/25. Calculations are shown below for the resisting bending moment (Braam & Lagendijk, 2011, pp. 51–52).

Horizontal force equilibrium:

$$A_S f_{yd} = 0,75 x_u f_{cd} b$$

$$x_u = \frac{A_S f_{yd}}{0,75 f_{cd} b} = \frac{0,005 \times 1000 \times 500 \times 435}{0,75 \times 13,3 \times 1000} = 109 \text{ mm}$$

Resisting bending moment:

$$d \approx 0,9h$$

$$z = d - \frac{7}{18} x_u = 0,9 \times 500 - \frac{7}{18} \times 109 = 408 \text{ mm}$$

$$\mathrm{M}_{RD} = A_S f_{yd} z = 0,005 \times 1000 \times 500 \times 435 \times 408 = 443 \text{ kNm}$$

This does not meet the required bending moment. Increasing the reinforcement percentage to 0,60% will yield a resisting bending moment of 521 kNm. This is satisfactory.

The same equations can be repeated for reinforcement at the upward clamped moment. A reinforcement percentage of 1,4% is enough to resist the clamped moment of 979 kNm.

The minimum length of the culvert depends on the road that lies on top of both dams and on the slope of the dam. The minimum culvert length is then calculated by: (road width + bicycle path width) + 2 ×

(vertical position of the road – top of the culvert) / slope. The slopes of the dams were measured with AHN (2020) and were approximately 1:3.

Table viii.9.4 Calculations for minimum culvert length. Heights and slopes from AHN (2020).

	Haringvlietdam	Brouwersdam
Road width	30	10
Bicycle path width	5	5
Road vertical location	+15,0 m NAP	+11,0 m NAP
Top of the culvert	+1,1 m NAP	+1,1 m NAP
Slope of the dam	1:3	1:3
Minimum culvert length	120	65

Appendix IX // Evaluation of the pumping station concepts

In this appendix chapter, all alternatives are evaluated so that one definite design can be chosen. First, for all storage basin configurations, the required number of Deltapumps is calculated with the simulation. Then, all configurations are evaluated by relative merit and costs.

§IX.1 Required number of Deltapumps per storage basin configuration

In App. VIII, two locations were found suitable for a pumping station: the Haringvlietdam and the Brouwersdam. The latter can only be included if storage is expanded to include the Grevelingen which requires the construction of sluices in the Grevelingendam. In total, this expands to possible number of storage basin configurations to twenty.

To simulate the number of Deltapumps necessary per concept, equation iii.15 from App. III will have to be modified. The modified equation is shown below:

$$\frac{dh_{GR,N}}{dt} = \frac{1}{A_{GR}}\left(-\underbrace{Q_{BD,N}}_{\text{If Brouwersdam == Open}} - \underbrace{Q_{GD,N}}_{\text{If Grevelingendam == Open}} - \underbrace{Q_{STATION}}_{\text{If BrouwersdamHasPump == True}} \right)$$

$$\frac{dh_{HH,N}}{dt} = \frac{1}{A_{HH}}\left(Q_{SB\_IN,N} - \underbrace{Q_{HD,N}}_{\text{If Haringvlietdam == Open}} - \underbrace{Q_{VD,N}}_{\text{If Volkerakdam == Open}} - \underbrace{Q_{STATION}}_{\text{If HaringvlietdamHasPump == True}} \right)$$

Equation viii.25

The pumping station discharge $Q_{STATION}$ has been introduced to both the Grevelingen and the Haringvliet-Hollandsch Diep, as the pumping station is either built on the Brouwersdam of the Haringvlietdam. The pumping station discharge is calculated with the following equations, adapted from equation i.9:

$$Q_{DELTAPUMP}\left(\Delta h\right) = 0,9 \times (24,64\pi^2 - 5,28\sqrt{19,62 \times \Delta h}) \times \left(1 - \frac{\Delta h}{\Delta H_{DP,MAX}}\right) + 0,1 \times (24,64\pi^2)$$

Equation viii.26

$$Q_{STATION}\left(\Delta h\right) = n_{PUMP} \times Q_{DELTAPUMP}\left(\Delta h\right)$$

Equation viii.27

In this equation Δh is the head difference and n_{PUMP} is the number of Deltapumps. The head difference depends on the energy head in the Deltapump, which depends again on the current discharge. Therefore, iteration must take place. The iteration takes place with the following two equations:

$$H_{DP,WEIR} = \left(\frac{Q_{DELTAPUMP}\left(\Delta h\right)}{\frac{2}{3} C_D \times B_{WEIR} \times \sqrt{2g}} \right)^{\frac{2}{3}}$$ *Equation viii.28*

$$\Delta h = \begin{cases} \text{Haringvlietdam,} & H_{DP,WEIR} + 3{,}839 - h_{HH} \\ \text{Brouwersdam,} & H_{DP,WEIR} + 4{,}219 - h_{GR} \end{cases}$$ *Equation viii.29*

For the iteration, first an initial value for $Q_{DELTAPUMP}\left(\Delta h\right)$ has to be filled in, e.g. 200 m^3s^{-1}, in equation ix.4. From that follows the energy head $H_{DP,WEIR}$ in the Deltapump with respect to the weir. With equation ix.5, the head difference can then be calculated. The numbers 3,839 and 4,219 are the heights of the weirs with respect to NAP, as determined in §III.2. With this head difference, the Deltapump discharge can be calculated with equation ix.2. Then, the iteration can start again at equation ix.4. This process is repeated about five times, as by then convergence has taken place.

This procedure has been implemented in the Python program to solve the required number of Deltapumps or modules, for all twenty storage basin configurations. The results are shown in the table below.

Table ix.1 Required number of Deltapumps for the pumping station, per storage basin configuration for the decisive flood scenario of 12.900 m^3s^{-1} Rhine flood flow at Lobith and 500 m^3s^{-1} Meuse mean flow.

			Volkerak sluices			
Location	Grevelingen storage?	Grevelingen sluices	570 m²	1.200 m²	1.350 m²	2.000 m²
Haringvlietdam	No	N/A	30	30	30	30
	Yes	540 m²	28	25	25	25
		1.350 m²	28	24	23	23
Brouwersdam	Yes	540 m²	-	-	-	-
		1.350 m²	-	-	-	-

As the simulations turn out, it is impossible to operate a pumping station at the Brouwersdam: a number of Deltapumps n_{PUMP} could not be found for which the design water level was not exceeded. The reason for this is relatively simple. The boundary conditions state that the Deltapump should be fully submerged to work. In §VIII.2.3 this was quantified as +0,096 m NAP for the Brouwersdam. This means that when the pumping station is in operation, water levels may not dive below +0,096 m NAP.

The maximum discharge through the bottleneck, the Grevelingendam sluices, is then: $1.350\sqrt{2\times 9{,}81\times(2{,}5-0{,}096)} = 9.270\ m^3s^{-1}$. The maximum flow rate into the storage basin is just a little lower for the decisive scenario: 9.071 m^3s^{-1}. However, as there is already an initial water level difference between the Haringvliet-Hollandsch Diep and Grevelingen, as the Grevelingen was pre-drained, equilibrium is not found. Below the figure of the simulation is shown.

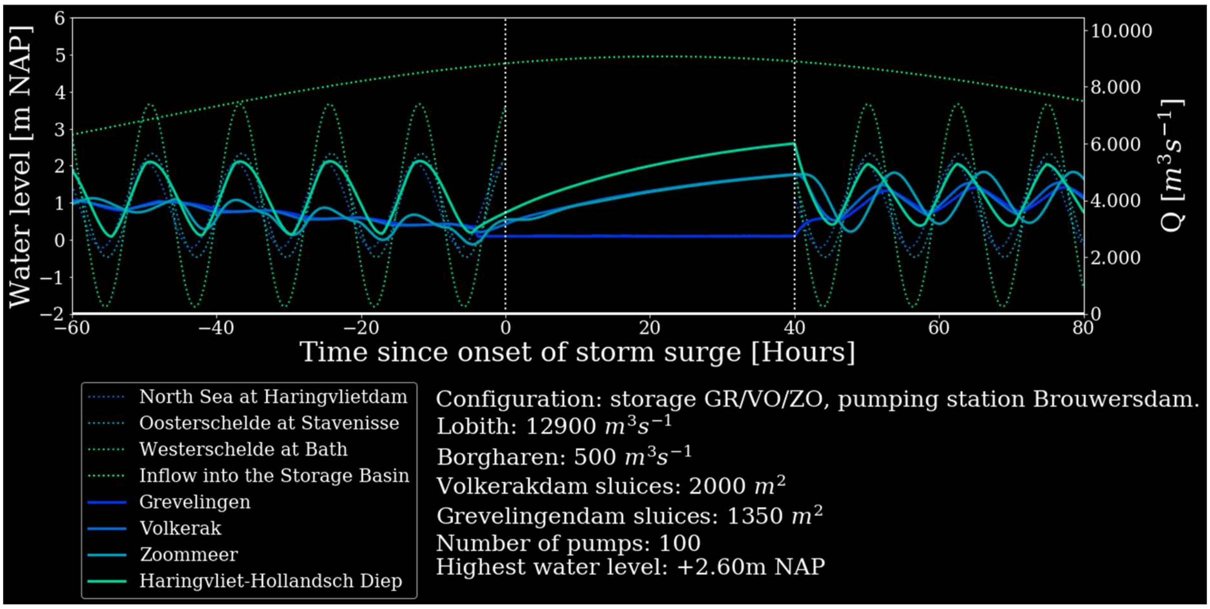

Figure ix.2 Simulation graph of the decisive flood scenario with a pumping station at the Brouwersdam.

Even with 100 pumps, as shown in the figure above, the highest water level only dropped to +2,60 m NAP, which is 10 cm above the limit. In comparison, the maximum number of pumps necessary for the Haringvlietdam pumping station is 30 (see Table ix.1). When only 30 pumps are used for the Brouwersdam, the highest water level increases to +2,85 m NAP. The Brouwersdam concept is therefore discarded completely.

§IX.2 Multi-criteria analysis of the storage basin configurations

With the Brouwersdam pumping station location being discarded, only twelve alternatives are left. All these twelve alternatives meet the hydraulic requirement of maximum +2,5 m NAP water level in the storage basin. Therefore, all these twelve configurations are equally viable and can now be evaluated based on relative merit, that is, at least one concept always scores a 10. This is done in accordance with the evaluation criteria as presented in the basis of design. Since not all evaluation criteria are relevant, some are left out. These include aesthetic value and accessibility, as these are applicable to the pumping station only. The following reports were consulted for grading the concepts: Lammers (2014), Rijkswaterstaat (2011b), Slootjes et al. (2010) and Slootjes (2013).

Table ix.3 Evaluation of the storage basin configurations for the Haringvlietdam pumping station. Abbreviations: GR: Grevelingenmeer; GD: Grevelingendam; VD: Volkerakdam.

Criterium		Weigh factor	GR: No storage VD: 570 m^2	GR: No storage VD: 1.200 m^2	GR: No storage VD: 1.350 m^2	GR: No storage VD: 2.000 m^2	GD: 540 m^2 VD: 570 m^2	GD: 540 m^2 VD: 1.200 m^2	GD: 540 m^2 VD: 1.350 m^2	GD: 540 m^2 VD: 2.000 m^2	GD: 1.350 m^2 VD: 570 m^2	GD: 1.350 m^2 VD: 1.200 m^2	GD: 1.350 m^2 VD: 1.350 m^2	GD: 1.350 m^2 VD: 2.000 m^2
Configuration nr. →			**1**	**2**	**3**	**4**	**5**	**6**	**7**	**8**	**9**	**10**	**11**	**12**
Flooding safety	FS	18 %	7	7	7	7	9	9	9	9	10	10	10	10
Constructability	CO	16 %	10	7	7	5	7	5	5	3	5	3	3	1
Environmental impact	EI	13 %	8	7	7	6	10	9	9	8	9	8	8	7
Fish migration	FF	11 %	3	3	3	3	10	10	10	10	10	10	10	10
Professional fishing	PF	9 %	5	5	5	5	10	10	10	10	10	10	10	10
Recreation	RE	7 %	6	6	6	8	8	10	8	10	8	10	8	10
Morphodynamics	MD	5 %	3	3	3	3	10	10	10	10	10	10	10	10
Construction hindrance	CH	4 %	10	7	7	5	7	5	5	3	5	3	3	1
Integration	IN	1 %	3	3	3	3	10	10	10	10	10	10	10	10
Total score			5,7	5,0	5,0	4,6	7,5	7,1	7,0	6,6	7,1	6,7	6,6	6,2

From the evaluation table above, it can be derived that the best concept by merit is the concept without any upgrades to the Volkerakdam sluices and the construction of 540 m^2 Grevelingendam sluices. However, this concept includes 28 Deltapumps whereas other concepts include only 23. Therefore, the next step is to compare the merit with their costs.

The costs per module have been calculated in App. X and can be multiplied with the number of Deltapumps from Table ix.1. Besides the costs per module, additional costs from the storage basin configurations need to be added to the calculations as well, so that a clear picture is formed of the overall costs. All these costs can be found in Table ix.4. When the opex is not provided in literature, the following estimates are used:

- → Civil works: 1% of initial costs per year
- → Mechanical works: 10% of initial costs per year

Table ix.4 Inventory of the capital expenditures (capex), operational expenditures (opex) and the net present value (npv) by the year 2100. Shown up to three significant digits. [1] from Lammers (2014, p. 32) and [2] from Slootjes (2013, pp. D-1–D-5).

		Capex [€]	Opex [€ annum^{-1}]	NPV 2100 [€]
A	Pumping station module: civil	6.750.000	67.500	7.960.000
B	Pumping station module: mechanical	6.320.000	632.000	17.700.000
C	Global pumping station costs	29.400.000	N/A	29.400.000
D	[1]Brouwersdam sluices	130.000.000	1.300.000	153.000.000
E	[1]Philipsdam sluices	47.400.000	474.000	55.900.000
F	[2]VD sluice upgrade: 1.200 m^2	150.000.000	2.100.000	187.700.000
G	[2]VD sluice upgrade: 1.350 m^2	134.000.000	1.060.000	153.000.000
H	[2]VD sluice upgrade: 2.000 m^2	284.000.000	3.160.000	341.000.000
I	[2]GD sluice construction: 540 m^2	56.000.000	170.000	59.000.000
J	[2]GD sluice construction: 1.350 m^2	92.000.000	280.000	97.000.000

In order to express the operational costs in today's exchange rates, the Net Present Value (NPV) is calculated. This is done with the following equation:

$$NPV(n) = F_0 + \sum_{1}^{n} \frac{F_n}{(1+r)^n} \qquad \textit{Equation viii.30}$$

This equation calculates the NPV for the year n. In this equation, F_N means the cash flow, the opex, in year n and r means the discount rate. The initial costs, the capex, are included within the factor F_0. The discount rate is assumed to be 5,5%, just like in reports of Lammers (2014) and Slootjes (2013).

For the calculations of the NPV, the year 2100 is considered or n = 80. The results of the NPV value by the year 2100 are shown in the right column of Table ix.4.

Now, with the NPV determined, the total costs of all twelve configurations can be calculated. This is presented in Table ix.5. The twelve different configurations are marked with numbers 1 to 12, as shown in Table ix.3, and the 10 different NPVs are marked with letters A to J, as shown in Table ix.4.

Table ix.5 Total net present value for each of the twelve storage basin configurations.

Storage basin configuration	Net present value A	B	C	D	E	F	G	H	I	J	TOTAL
1	30	30	1	0	1	0	0	0	0	0	€ 855.100.000
2	30	30	1	0	1	1	0	0	0	0	€ 1.042.800.000
3	30	30	1	0	1	0	1	0	0	0	€ 1.008.100.000
4	30	30	1	0	1	0	0	1	0	0	€ 1.196.100.000
5	28	28	1	1	1	0	0	0	1	0	€ 1.015.780.000
6	25	25	1	1	1	1	0	0	1	0	€ 1.126.500.000
7	25	25	1	1	1	0	1	0	1	0	€ 1.091.800.000
8	25	25	1	1	1	0	0	1	1	0	€ 1.279.800.000
9	28	28	1	1	1	0	0	0	0	1	€ 1.053.780.000
10	24	24	1	1	1	1	0	0	0	1	€ 1.138.840.000
11	23	23	1	1	1	0	1	0	0	1	€ 1.078.480.000
12	23	23	1	1	1	0	0	1	0	1	€ 1.266.480.000

Now, the last step in the Multi-criteria analysis is calculating the merit-to-cost ratio. This is presented in the table below.

Table ix.6 Merit-to-cost ratio of all twelve storage basin configurations. NVP shown in thousand million €.

	1	2	3	4	5	6
Merit	5,7	5,0	5,0	4,6	**7,5**	7,1
NPV	0,855	1,043	1,008	1,196	**1,016**	1,127
Merit-to-NPV	6,6	4,7	4,9	3,8	**7,4**	6,3

	7	8	9	10	11	12
Merit	7,0	6,6	7,1	6,7	6,6	6,2
NPV	1,092	1,280	1,054	1,139	1,078	1,266
Merit-to-NPV	6,4	5,1	6,8	5,9	6,1	4,9

From this table it can be concluded that the fifth configuration is the relatively best configuration. Therefore, this configuration is chosen as the definite storage basin configuration. This implies the pumping station will be outfitted with 28 Deltapumps or modules.

Appendix X // Cost estimates of the pumping station modules

In this appendix chapter, the costs of a single pumping station module are calculated. The table containing all the costs is listed on the next page. A list of assumptions and sources is presented below.

Earth moving costs

To calculate the costs of earth moving, the elevation maps of AHN (2020) were consulted, see the figure below. Over the entire width of the Haringvlietdam, the average height is approximately +10,0 m NAP. As excavation takes place down to -4,5 m NAP, on which the 50 cm concrete floors are laid, the total height of soil that needs to be removed is 14,5 m; this is rounded up to 15 m. The total width of the Haringvlietdam is approximately 240 m. With the module being 15 meters wide, the total volume of soil then becomes 240 × 15 × 15 = 54.000 m^3.

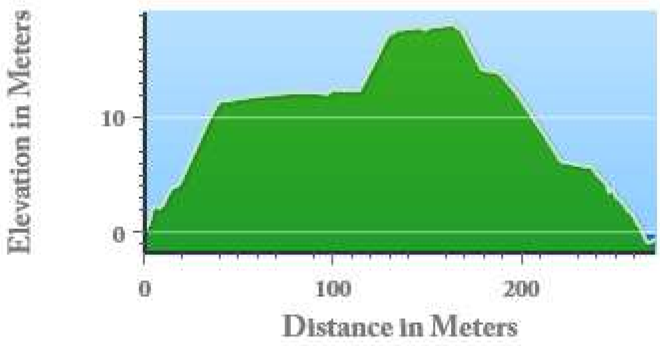

Figure x.1 Elevation cross-section of the Haringvlietdam (AHN, 2020).

It is assumed 50% of the total volume is excavated and later returned, and the other 50% is excavated and dumped elsewhere. The costs of these both are €5 and €3 per square cube respectively (Grondverzet, n.d.).

Cofferdam

The cofferdam will be erected on either side of a module: the Haringvliet and the North Sea. In total this is then 30 meters. Here, the design and costs of the cofferdam from Heemskerk (2016, pp. 223–224) are used. His project was also located in the Haringvliet, so are therefore applicable.

Sources for costs

Denoted with 1 and 2 are from: 1, from ArcelorMittal (2018); 2, from Dukers (2003). All other costs are either from Schut, from the aforementioned sources or rough estimates.

Table x.2 Total costs of one pumping station module. Costs include materials, labour, earth moving and temporary structures.

Concrete (incl. labour)	Quantity	Price
Intake canal	360 m^3	€350/m^3
Weir	70 m^3	€350/m^3
Concrete bed	1400 m^3	€350/m^3
Culvert wall	1110 m^3	€350/m^3
Foundation slab	40 m^3	€350/m^3
Culvert roof	900 m^3	€450/m^3
Service road	210 m^3	€450/m^3
	subtotal	**€ 1.542.500**

Steel	Quantity	Price
HE140AA[1]	452,5 kg	€1.240/ton
HE160AA[1]	327,3 kg	€1.240/ton
HE180AA[1]	310 kg	€1.240/ton
HE200B[1]	375,4 kg	€1.245/ton
HE450M[1]	7899 kg	€1.460/ton
Nodes and supports	5	€500/unit
Overspill plate	1	€1.000/unit
Service road traffic barrier	30	€60/m
Service road supports	10	€2.000/unit
	subtotal	**€ 38.651**

Mechanical	Quantity	Costs
Trash rake	1	€75.000/unit
Deltapump and thrust bearin	1	€1.100.000/unit
Driving mechanism	1	€700.000/unit
Electrical wiring	1	€1.200.000/unit
Deltapump misc.	1	€300.000/unit
Vertical lift door	2	€500.000/unit
	subtotal	**€ 3.875.000**

Earth	Quantity	Costs
Excavated and dumped	27.000 m^3	€3/m^3
Excavated and returned	27.000 m^3	€5/m^3
	subtotal	**€ 216.000**

Miscellaneous	Quantity	Costs
Service road traffic lights	1	€2.000/unit
Watertight overspill	1	€2.000/unit
Crane hire	5	€ 5.000/day
	subtotal	**€ 29.000**

Foundation	Quantity	Costs
Foundation piles[2]	60	€30/m
Digging[2]	5	€24/pile
	subtotal	**€ 1.920**

Cofferdam	Quantity	Costs
Retaining wall	420 ton	€850/ton
Tension rings	30	€1.000/m
Labour: pressure	600	€45/m^2
Labour: burning	30	€60/m
Labour: welding	30	€50/m
Coating	300	€50/m^2
	subtotal	**€ 432.300**

Labour		
Mechanical	1	€ 640.000
Electrical	1	€ 160.000
Transport	1	€ 400.000
Civil	1	€ 2.000.000
	subtotal	**€ 3.200.000**

Global pumping station costs		
Management	1	€ 12.000.000
Design	1	€ 5.000.000
Detail design	1	€ 4.000.000
	Global costs total	**€ 21.000.000**

Civil works per module	**€ 4.820.371**
Mechanical works per module	**€ 4.515.000**
Total costs per module	**€ 9.335.371**

All costs shown are per module, that is per single Deltapump. The only exception are the global pumping station costs, these are **not** multiplied with the number of pumps. As these costs only include the direct costs and not indirect costs like insurance, site facilities, the values are multiplied with a factor 1,4. This gives the following three values:

→ Global pumping station costs: **€ 29.400.000**
→ Civil works per module: **€ 6.750.000**
→ Mechanical works per module: **€ 6.320.000**